



Internal components of continuous quantum thermal machines

Javier Onam González López

PhD Thesis
Departamento de Física
Universidad de La Laguna
La Laguna, July 2019

Supervisor: Daniel Alonso Ramírez
Co-supervisor: José Pascual Palao González

Este documento incorpora firma electrónica, y es copia auténtica de un documento electrónico archivado por la ULL según la Ley 39/2015.
Su autenticidad puede ser contrastada en la siguiente dirección <https://sede.ull.es/validacion/>

Identificador del documento: 2111210 Código de verificación: lZvvKBaU

Firmado por: Javier Onam González López
UNIVERSIDAD DE LA LAGUNA

Fecha: 09/09/2019 11:04:42

Daniel Alonso Ramírez
UNIVERSIDAD DE LA LAGUNA

11/09/2019 14:53:47

1

Este documento incorpora firma electrónica, y es copia auténtica de un documento electrónico archivado por la ULL según la Ley 39/2015.
Su autenticidad puede ser contrastada en la siguiente dirección <https://sede.ull.es/validacion/>

Identificador del documento: 2111210 Código de verificación: lZvvKBaU

Firmado por: Javier Onam González López
UNIVERSIDAD DE LA LAGUNA

Fecha: 09/09/2019 11:04:42

Daniel Alonso Ramírez
UNIVERSIDAD DE LA LAGUNA

11/09/2019 14:53:47

Preface

This thesis is the result of four consecutive years of research at Universidad de La Laguna. During this period, the Spanish Ministry of Education, Culture and Sport (MECD) has provided financial support, through a Formación de Profesorado Universitario (FPU) fellowship. We also acknowledge financial support by the Spanish Ministerio de Economía y Competitividad (MINECO), Grants FIS2013-41352-P and FIS2017-82855-P. The work has been done under the supervision of Dr. Daniel Alonso Ramírez and Dr. José Pascual Palao González.

We present here an unified and pedagogical revision of some of the main results included in the following four scientific publications:

- J. Onam González, Daniel Alonso, and José P. Palao. Performance of continuous quantum thermal devices indirectly connected to environments. *Entropy*, 18(5):166, 2016.
- J. Onam González, Luis A. Correa, Giorgio Nocerino, José P. Palao, Daniel Alonso, and Gerardo Adesso. Testing the validity of the local and global gkls master equations on an exactly solvable model. *Open Syst. Inf. Dyn.*, 24(04):1740010, 2017.
- J. Onam González, José P. Palao, and Daniel Alonso. Relation between topology and heat currents in multilevel absorption machines. *New J. Phys.*, 19(11):113037, 2017.
- J. Onam González, José P. Palao, Daniel Alonso, and Luis A. Correa. Classical emulation of quantum-coherent thermal machines. *Phys. Rev. E*, 99:062102, 2019.

The compendium with these articles is included in the last part of this document. The third article in the compendium was carried out in collaboration with Luis Correa, Giorgio Nocerino and Gerardo Adesso, during an academic visit of three months to the Quantum Correlation Group in the University of Nottingham. This thesis also benefits from a short visit to Queen's University in Belfast to collaborate with Adam Hewgill and Gabrielle de Chiara. Javier Onam González López, the author of this thesis, has significantly contributed to the conceptual development, calculations, composition and illustration of the publications included in the compendium.

Este documento incorpora firma electrónica, y es copia auténtica de un documento electrónico archivado por la ULL según la Ley 39/2015.
Su autenticidad puede ser contrastada en la siguiente dirección <https://sede.ull.es/validacion/>

Identificador del documento: 2111210 Código de verificación: lZvvKBaU

Firmado por: Javier Onam González López
UNIVERSIDAD DE LA LAGUNA

Fecha: 09/09/2019 11:04:42

Daniel Alonso Ramírez
UNIVERSIDAD DE LA LAGUNA

11/09/2019 14:53:47

Abstract

The dynamics of continuous quantum machines weakly coupled to thermal reservoirs is described by master equations when the bath temperatures are high enough. If, in addition, the bare frequency gaps are much larger than the thermal couplings, the steady state or limit cycle of the device coincides with the stationary solution of a set of balance equations. This solution can be analyzed by using Graph Theory. Within this framework, the balance equations are represented by a graph. We employ a circuit decomposition of this graph to calculate and, most importantly, interpret the stationary thermodynamic properties of different continuous devices. We show that each circuit can be associated with a thermodynamically consistent mechanism. This follows from the consistency of the corresponding master equations with the Laws of Thermodynamics for a proper definition of the energy currents. As a consequence, these circuits can be thought of as internal components of the corresponding machine. Thus, the overall steady state functioning of the device is the result of the contributions of its internal components and the interplay between them.

We study two types of continuous devices. On one hand, we analyze absorption machines including only thermal baths. We show here that not only the total number of constituents circuits affects the device performance, but also the specific structure of the graph containing these circuits. Crucially, we find that the *device connectivity* has a major role in the design of optimal absorption machines. On the other hand, we consider periodically driven devices with a cyclic pattern of transitions. These machines are connected to thermal baths and also to a sinusoidal laser field. We study both the strong and the weak driving limits by using Global and Local master equations respectively. We compare these approaches with the Redfield master equation. A circuit decomposition can be used to describe the stationary thermodynamic quantities in both limits. Interestingly, given an arbitrary basis, the device needs coherences to operate in the weak driving limit. However, an incoherent stochastic-thermodynamic model may replicate the same stationary functioning.

We conclude that the steady state thermodynamic operation in all the models under consideration can be described without invoking any quantum feature. Along these lines, the graph approach may be useful for identifying genuinely quantum effects in other continuous machines. For example, devices with non-cyclic pattern of transitions and degenerate states.

Este documento incorpora firma electrónica, y es copia auténtica de un documento electrónico archivado por la ULL según la Ley 39/2015.
Su autenticidad puede ser contrastada en la siguiente dirección <https://sede.ull.es/validacion/>

Identificador del documento: 2111210 Código de verificación: lZvvKBaU

Firmado por: Javier Onam González López
UNIVERSIDAD DE LA LAGUNA

Fecha: 09/09/2019 11:04:42

Daniel Alonso Ramírez
UNIVERSIDAD DE LA LAGUNA

11/09/2019 14:53:47

Contents

1	Introduction	6
1.1	Motivation	7
1.1.1	Identification of thermodynamic mechanisms	8
1.1.2	Scaling up thermal devices	8
1.1.3	Comparison between master equation approaches	9
1.1.4	Quantumness in Quantum Thermodynamics	9
1.2	Outline	11
2	Absorption machines	12
2.1	Four-level absorption machine	12
2.2	Master equation approach	13
2.3	Graph representation	18
2.3.1	Graph objects	19
2.4	Circuit decomposition	21
2.5	Classification of internal components	22
2.6	Graph topology and heat currents	25
2.6.1	Graph \mathcal{J}	27
2.6.2	Graph \mathcal{I}	27
2.6.3	Graph \mathcal{H}	29
3	Periodically driven machines	30
3.1	Periodically driven three-level machine	30
3.2	Redfield approach	32
3.3	Global approach	34
3.3.1	Internal components	35
3.4	Local approach	37
3.4.1	Internal component	38
3.4.2	Classicality criteria	39
4	Conclusions	40

Este documento incorpora firma electrónica, y es copia auténtica de un documento electrónico archivado por la ULL según la Ley 39/2015.
 Su autenticidad puede ser contrastada en la siguiente dirección <https://sede.ull.es/validacion/>

Identificador del documento: 2111210 Código de verificación: lZvvKBaU

Firmado por: Javier Onam González López
 UNIVERSIDAD DE LA LAGUNA

Fecha: 09/09/2019 11:04:42

Daniel Alonso Ramírez
 UNIVERSIDAD DE LA LAGUNA

11/09/2019 14:53:47

5	Compendium	42
5.1	Performance of Continuous Quantum Thermal Devices Indirectly Connected to Environments	43
5.2	Testing the Validity of the ‘Local’ and ‘Global’ GKLS Master Equations on an Exactly Solvable Model	59
5.3	Relation between topology and heat currents in multilevel absorption machines	85
5.4	Classical emulation of quantum-coherent thermal machines . . .	107
A	Master equations	121
A.1	Redfield master equation	122
A.1.1	Energy currents	124
A.2	Global master equation	125
A.3	Local master equation	125

Este documento incorpora firma electrónica, y es copia auténtica de un documento electrónico archivado por la ULL según la Ley 39/2015.
Su autenticidad puede ser contrastada en la siguiente dirección <https://sede.ull.es/validacion/>

Identificador del documento: 2111210 Código de verificación: lZvvKBaU

Firmado por: Javier Onam González López
UNIVERSIDAD DE LA LAGUNA

Fecha: 09/09/2019 11:04:42

Daniel Alonso Ramírez
UNIVERSIDAD DE LA LAGUNA

11/09/2019 14:53:47

Chapter 1

Introduction

Quantum Thermodynamics is a field that lies somewhere between Thermodynamics and the Theory of Open Quantum Systems [1, 2, 3]. A typical quantum thermodynamic setup consists of a quantum system in contact with one or several environments. Such device can be analyzed by using the “toolbox” provided by the Theory of Open Quantum Systems [4, 5]. When using this approach, one observes the emergence of thermodynamic-like relations describing the energy exchanges between the quantum system and the environments [6]. Paradigmatic examples of these relations are based on microscopic derivations of the Laws of Thermodynamics [7, 8, 9, 10]. The formal structure of this sort of expressions is completely equivalent to those we employ in the context of macroscopic Thermodynamics. This test of thermodynamic consistency is required to interpret the behavior of some open quantum system from a purely thermodynamic perspective.

As in the classical case, a major issue in Quantum Thermodynamics is the analysis of thermal machines. A conventional scheme of a quantum thermal machine is composed of a quantum N -level system connected to a work source and coupled with two thermal baths at different temperatures [11, 12, 13]. Quantum thermal machines are either continuous (see [14] and references therein) or discrete, for example four stroke [15, 16, 17, 18, 19, 20, 21] and two strokes [22, 23, 24] engines. Namely, we focus on the study of continuous quantum thermal machines that are permanently coupled to these environments. Several proposals and, even, physical realizations of this kind of machines have been reported recently [25, 26, 27, 28, 29]. After a transient regime, these continuous devices reach some non equilibrium steady state, or limit cycle, with non vanishing energy currents between the environments and the system. We are interested in characterizing this stationary energy transfer process for two different choices of the work source. We consider either a thermal bath or a sinusoidal laser field acting as the work source,

Este documento incorpora firma electrónica, y es copia auténtica de un documento electrónico archivado por la ULL según la Ley 39/2015.
Su autenticidad puede ser contrastada en la siguiente dirección <https://sede.ull.es/validacion/>

Identificador del documento: 2111210 Código de verificación: lZvvKBaU

Firmado por: Javier Onam González López
UNIVERSIDAD DE LA LAGUNA

Fecha: 09/09/2019 11:04:42

Daniel Alonso Ramírez
UNIVERSIDAD DE LA LAGUNA

11/09/2019 14:53:47

which corresponds to absorption machines [30, 31, 32] or periodically driven devices [33, 34].

The exact characterization of the functioning of a continuous quantum thermal machine is not a trivial task. In principle, one has to deal not only with the coordinates of the quantum system, but also with a very large number of degrees of freedom related to the environments. The full Hamiltonian corresponding to this setup also includes the interactions between system and environments. This many particle problem is greatly simplified when the coupling to the baths is very weak. In this work we assume that the weak coupling approximation is valid. Within this regime, the correlations between the baths and the system are negligible and the baths remain approximately in a thermal state with a well defined temperature. This allows us to take a reduce description of the quantum system and derive a master equation for the system density matrix [4]. The thermodynamic quantities describing the functioning of the machine can be inferred from such equation.

The system density matrix of a thermal device is composed of populations and coherences in a given basis. Therefore, in this weak coupling limit, a complete characterization of a device necessarily requires knowledge of the corresponding population and coherence dynamics. In general, these dynamics are not decoupled. However, clever choices of a preferred basis may lead to simplified descriptions involving only the population dynamics. In these cases, the populations follow balance equations widely employed in the context of stochastic-thermodynamic models. Thus, we can employ the tools of balance equations systems to characterize our quantum-thermodynamic setup. One paradigmatic example of these tools is the use of decompositions of the stationary thermodynamic quantities based on Graph Theory [35, 36, 37, 38, 39]. These techniques facilitate either the calculation or the interpretation of the steady state properties of the device. Namely, we employ a circuit decomposition attributed to Hill whose strong point is mainly related to interpretation purposes [36]. In order to simplify calculations, the choice of a Schnakenberg decomposition is more convenient [35].

1.1 Motivation

In this work we employ circuit decompositions of stationary thermodynamic quantities to address some issues that are of interest in the context of Quantum Thermodynamics. Interestingly, these techniques are also applicable for others balance equation systems whose physical realizations are not necessarily quantum, for instance, chemical reaction systems [35, 36].

Este documento incorpora firma electrónica, y es copia auténtica de un documento electrónico archivado por la ULL según la Ley 39/2015.
Su autenticidad puede ser contrastada en la siguiente dirección <https://sede.ull.es/validacion/>

Identificador del documento: 2111210 Código de verificación: lZvvKBaU

Firmado por: Javier Onam González López
UNIVERSIDAD DE LA LAGUNA

Fecha: 09/09/2019 11:04:42

Daniel Alonso Ramírez
UNIVERSIDAD DE LA LAGUNA

11/09/2019 14:53:47

1.1.1 Identification of thermodynamic mechanisms

Continuous quantum thermal machines show a wide variety of properties when looking at their functioning. Pretty similar implementations can be associated with different performances or, conversely, different implementations may lead to similar results [40, 41]. For example, some machines can attain the reversible limit and some others not, some can operate as refrigerators and many others cannot. In order to compare different implementations we can resort to the conventional master equation calculations. However, although this approach is effective from a quantitative point of view, it does not provide a deep understanding on the fundamental differences between the implementations. Overcoming this limitation is not only important from a fundamental perspective, but also it is crucial for a clever design of continuous devices. In summary, a combined quantitative and qualitative approach is required to provide a complete description of the stationary functioning of the machines. With this goal in mind, we employ a circuit decomposition of the stationary thermodynamic magnitudes. Within this approach, the stationary functioning of a given device is decomposed into thermodynamically consistent internal components. Each component is associated with a thermodynamic mechanism. Thus, the combined operation and interplay between these components enable us to interpret the particularities of a machine. In the article included in Sec. 5.1, we describe the thermodynamic mechanisms resulting from the stationary functioning of absorption and periodically driven devices. The processes that prevents the machine from achieving the reversible limit are also discussed in this article. Throughout this work, we provide an illustrative explanation of these concepts by studying different benchmark models and, most importantly, we use such concepts to interpret particular results in an intuitive way, see Secs. 2.5, 3.3.1 and 3.4.1.

1.1.2 Scaling up thermal devices

The search for optimal designs of continuous machines has attracted considerable interest within the field of Quantum Thermodynamics [41, 42, 43]. There exist two main ways of boosting the performance of a thermal device. First, one can include exotic properties in the environments to improve the operation of the machine. A paradigmatic example of this is, amongst others, the consideration of non equilibrium baths [44, 45, 46, 47, 48, 49]. Second, one can include modifications in the quantum system by scaling up both its number of levels and the connections with the environments. Although considerable effort has been devoted to this scaling up procedure [50, 51, 24],

Este documento incorpora firma electrónica, y es copia auténtica de un documento electrónico archivado por la ULL según la Ley 39/2015.
Su autenticidad puede ser contrastada en la siguiente dirección <https://sede.ull.es/validacion/>

Identificador del documento: 2111210 Código de verificación: lZvvKBaU

Firmado por: Javier Onam González López
UNIVERSIDAD DE LA LAGUNA

Fecha: 09/09/2019 11:04:42

Daniel Alonso Ramírez
UNIVERSIDAD DE LA LAGUNA

11/09/2019 14:53:47

drawing model-independent conclusions turns out to be difficult. In the paper included in Sec. 5.3, this issue is addressed by making use of circuit decompositions based on Graph Theory. Namely, the analysis is focused on scaling up schemes for absorption machines although the same procedure can be applied to periodically driven devices, leading to equivalent conclusions. The Sec. 2.6 of the present work is dedicated to review the main result of such publication, which concerns the impact of the graph topology on the device functioning.

1.1.3 Comparison between master equation approaches

Continuous quantum machines admit a reduced description in terms of master equations when the couplings between the quantum system and the baths are very weak. There are different master equation approaches whose validity depends on internal parameters of the quantum system. In the article included in Sec. 5.2 we discuss the validity of Local and Global master equations for an exactly solvable absorption device. Instead, we analyze in the present work the Local and Global approaches for a periodically driven machine. Both of them are thermodynamically consistent when using proper definitions for the energy currents. In order to explore the range of applicability of each approach, we compare them with the Redfield master equation. The thermodynamic consistency and positivity of the density matrix is not guaranteed in the Redfield approach. However, the corresponding violations are found in very specific limits [52] and, in most cases, it has been shown that the Redfield equation reproduces the exact dynamics [53, 54]. We show that the coupling with the driving field determines which is the appropriate master equation approach. Namely, a Local master equation is valid when this coupling is weak, while a Global approach may be used in the opposite regime. The same machine shows very different characteristics in these two limits. Interestingly, we find that circuit decompositions can be built to describe the stationary functioning associated with the Local and Global master equations. Our aim is to compare these two approaches by examining the properties of the internal components that play a role in the stationary functioning.

1.1.4 Quantumness in Quantum Thermodynamics

As the name suggests, the search for quantum effects in Quantum Thermodynamics is a topic of major importance [55, 56, 57, 47, 58, 59, 60, 3, 61, 62, 63]. A possible approach to identify quantum signatures is to add a strong enough dephasing to the master equation describing the machine. This leads to a

Este documento incorpora firma electrónica, y es copia auténtica de un documento electrónico archivado por la ULL según la Ley 39/2015.
Su autenticidad puede ser contrastada en la siguiente dirección <https://sede.ull.es/validacion/>

Identificador del documento: 2111210 Código de verificación: lZvvKBaU

Firmado por: Javier Onam González López
UNIVERSIDAD DE LA LAGUNA

Fecha: 09/09/2019 11:04:42

Daniel Alonso Ramírez
UNIVERSIDAD DE LA LAGUNA

11/09/2019 14:53:47

(classical) stochastic counterpart of the device [58]. Any difference between the quantum and the stochastic description may be then associated with quantum effects. However, this approach does not consider the possibility that some other stochastic model could provide the same thermodynamic magnitudes by using similar resources. Inspired by the fact that the stationary behavior of many quantum machines is often similar to some stochastic-thermodynamic model [64, 65], we propose a different approach: *No thermal machine should be classified as quantum from a thermodynamic perspective if its relevant quantities, such as energy currents and performance, can be replicated by an incoherent emulator.* This classical emulator has the same number of discrete states and frequency gaps than the original device. Besides, the emulator is built with the same thermal couplings. In the paper attached in Sec. 5.4, we show that cyclic periodically driven devices can be classically emulated in the weak driving limit. In this case, the quantum properties of the device, such as coherences, should not be considered essential to emulate the machine functioning. Device and emulator are indistinguishable from a thermodynamic viewpoint, i.e., without knowing specific details of their Hamiltonians. Conversely, given a quantum machine, the absence of an emulator can be considered a necessary requirement in the search for truly quantum effects. In Chapter 3, we analyze the concept of classical emulator for a periodically driven machine in the strong and weak driving regime.

Este documento incorpora firma electrónica, y es copia auténtica de un documento electrónico archivado por la ULL según la Ley 39/2015.
Su autenticidad puede ser contrastada en la siguiente dirección <https://sede.ull.es/validacion/>

Identificador del documento: 2111210 Código de verificación: lZvvKBaU

Firmado por: Javier Onam González López
UNIVERSIDAD DE LA LAGUNA

Fecha: 09/09/2019 11:04:42

Daniel Alonso Ramírez
UNIVERSIDAD DE LA LAGUNA

11/09/2019 14:53:47

1.2 Outline

In the following chapters we illustrate the previous issues in a pedagogical way by studying some benchmark models. The document is organized as follows: In Chapter 2 we analyze the steady state functioning of absorption machines by using a circuit decomposition of the thermodynamic quantities. Here, we provide a classification of the different internal components. Besides, we analyze the impact of adding new levels and couplings to absorption machines. In Chapter 3 we study a periodically driven device in the regimes of weak and strong coupling with the laser field. We analyze the differences between these two limits. We also examine whether equivalent results can be obtained from a classical stochastic-thermodynamic picture. In Chapter 4 we present our conclusions and discuss their implications. The compendium of publications is included in Chapter 5. In Appendix A, we briefly describe the microscopic derivations of Redfield, Global and Local master equations.

Este documento incorpora firma electrónica, y es copia auténtica de un documento electrónico archivado por la ULL según la Ley 39/2015.
Su autenticidad puede ser contrastada en la siguiente dirección <https://sede.ull.es/validacion/>

Identificador del documento: 2111210 Código de verificación: lZvvKBaU

Firmado por: Javier Onam González López
UNIVERSIDAD DE LA LAGUNA

Fecha: 09/09/2019 11:04:42

Daniel Alonso Ramírez
UNIVERSIDAD DE LA LAGUNA

11/09/2019 14:53:47

Chapter 2

Absorption machines

2.1 Four-level absorption machine

In this chapter we analyze the stationary functioning of absorption devices. For the sake of simplicity, we consider the four-level machine depicted in Fig. 2.1 as a benchmark model. The device consists of a quantum system S in contact with three thermal baths B_c , B_h and B_w at temperatures T_c , T_h and $T_w > T_h > T_c$. Therefore, B_c and B_h are respectively a cold and a hot bath, while B_w is a thermal reservoir playing a role similar to a work source.

We consider that the thermal reservoirs B_α are infinite collections of bosonic modes. The Hamiltonians of these baths read

$$\hat{H}_{B_\alpha} = \sum_{\mu} \hbar \omega_{\mu,\alpha} \hat{b}_{\mu,\alpha}^\dagger \hat{b}_{\mu,\alpha}, \quad (\alpha = c, h, w), \quad (2.1)$$

being $\hat{b}_{\mu,\alpha}^\dagger$ and $\hat{b}_{\mu,\alpha}$ the creation and annihilation operators corresponding to the mode with frequency $\omega_{\mu,\alpha}$. On the other hand, the system Hamiltonian can be written as

$$\hat{H}_S = \sum_{n=1}^4 E_n |n\rangle\langle n|, \quad (2.2)$$

where $E_1 = 0$, $E_2 = \hbar \omega_c$, $E_3 = \hbar \omega_h$, $E_4 = \hbar(\omega_h + \omega_c + \Delta)$ and \hbar is the Planck constant. The system is permanently coupled to the baths through the following interaction Hamiltonians

$$\hat{H}_{SB_\alpha} = \hat{A}^\alpha \otimes \hat{B}^\alpha, \quad (2.3)$$

with

$$\begin{aligned} \hat{A}^c &= |1\rangle\langle 2| + |3\rangle\langle 4| + |2\rangle\langle 1| + |4\rangle\langle 3|, \\ \hat{A}^h &= |1\rangle\langle 3| + |2\rangle\langle 4| + |3\rangle\langle 1| + |4\rangle\langle 2|, \\ \hat{A}^w &= |2\rangle\langle 3| + |3\rangle\langle 2|, \end{aligned} \quad (2.4)$$

Este documento incorpora firma electrónica, y es copia auténtica de un documento electrónico archivado por la ULL según la Ley 39/2015.
 Su autenticidad puede ser contrastada en la siguiente dirección <https://sede.ull.es/validacion/>

Identificador del documento: 2111210 Código de verificación: lZvvKBaU

Firmado por: Javier Onam González López
 UNIVERSIDAD DE LA LAGUNA

Fecha: 09/09/2019 11:04:42

Daniel Alonso Ramírez
 UNIVERSIDAD DE LA LAGUNA

11/09/2019 14:53:47

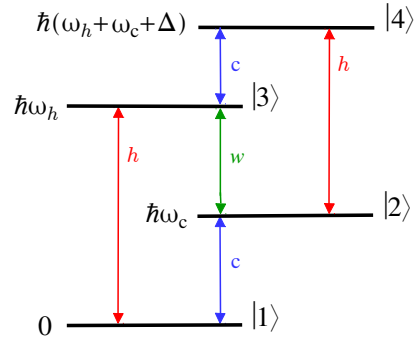


Figure 2.1: Schematic illustration of the four-level absorption device. The vertical arrows indicate the transitions coupled to the cold (c), work (w) and hot (h) baths. For example, the four-level system can undergo an absorption, $|2\rangle \rightarrow |3\rangle$, or an emission, $|3\rangle \rightarrow |2\rangle$, both mediated by the work reservoir B_w .

and

$$\hat{B}^\alpha = \hbar \sqrt{\gamma_\alpha} \sum_{\mu} g_{\mu,\alpha} (\hat{b}_{\mu,\alpha} + \hat{b}_{\mu,\alpha}^\dagger). \quad (2.5)$$

The parameter γ_α is the coupling constant in the interaction between S and B_α and $g_{\mu,\alpha} \propto \sqrt{\omega_{\mu,\alpha}}$. The total Hamiltonian of the machine is

$$\hat{H} = \hat{H}_S + \hat{H}_{B_c} + \hat{H}_{B_h} + \hat{H}_{B_w} + \hat{H}_{SB_c} + \hat{H}_{SB_h} + \hat{H}_{SB_w}. \quad (2.6)$$

2.2 Master equation approach

The stationary functioning of the four-level machine is the result of the combination of different time scales. According to the Hamiltonian (2.6), we can distinguish three different time scales: the characteristic time of the baths $\tau_B \sim \hbar/k_B T_c$, where k_B is the Boltzmann constant, the intrinsic time of the quantum system $\tau_S \sim \max\{|\omega_c|^{-1}, |\omega_h|^{-1}, |\omega_h - \omega_c|^{-1}, |\omega_h + \Delta|^{-1}, |\omega_c + \Delta|^{-1}\}$ and the scale corresponding to the system-baths interaction $\tau_{SB} \sim \min\{\gamma_c^{-1}, \gamma_h^{-1}, \gamma_w^{-1}\}$. A master equation approach can be used when the interaction between the quantum system and the baths determines the

largest time scale in the device, i. e. $\tau_{SB} \gg \tau_S$ and $\tau_{SB} \gg \tau_B$. This corresponds to a very weak coupling with the thermal baths. In such a parameter regime, the Born-Markov approximation can be applied to derive a Secular (also referred as Global) master equation describing the time evolution of the system density matrix. In the Appendix A we describe in detail how to obtain this Secular master equation for a general setup. Following this standard procedure [4], we get

$$\frac{d\hat{\rho}_S}{dt} = -\frac{i}{\hbar}[\hat{H}_S, \hat{\rho}_S] + \mathcal{L}_c\{\hat{\rho}_S\} + \mathcal{L}_h\{\hat{\rho}_S\} + \mathcal{L}_w\{\hat{\rho}_S\}, \quad (2.7)$$

where $\hat{\rho}_S$ is the system density matrix. Note that we have neglected the small Lamb shift term in the unitary evolution. The Lindblad super-operators $\mathcal{L}_\alpha\{\hat{\rho}_S\}$ that describe the influence of the baths on the system are given by [66, 4]

$$\begin{aligned} \mathcal{L}_c\{\hat{\rho}_S\} &= \Gamma_{\omega_c}^c \left(|1\rangle\langle 2|\hat{\rho}_S|2\rangle\langle 1| - \frac{1}{2}|2\rangle\langle 2|\hat{\rho}_S - \frac{1}{2}\hat{\rho}_S|2\rangle\langle 2| \right) \\ &+ \Gamma_{-\omega_c}^c \left(|2\rangle\langle 1|\hat{\rho}_S|1\rangle\langle 2| - \frac{1}{2}|1\rangle\langle 1|\hat{\rho}_S - \frac{1}{2}\hat{\rho}_S|1\rangle\langle 1| \right) \\ &+ \Gamma_{\omega_c+\Delta}^c \left(|3\rangle\langle 4|\hat{\rho}_S|4\rangle\langle 3| - \frac{1}{2}|4\rangle\langle 4|\hat{\rho}_S - \frac{1}{2}\hat{\rho}_S|4\rangle\langle 4| \right) \\ &+ \Gamma_{-(\omega_c+\Delta)}^c \left(|4\rangle\langle 3|\hat{\rho}_S|3\rangle\langle 4| - \frac{1}{2}|3\rangle\langle 3|\hat{\rho}_S - \frac{1}{2}\hat{\rho}_S|3\rangle\langle 3| \right), \quad (2.8) \end{aligned}$$

$$\begin{aligned} \mathcal{L}_h\{\hat{\rho}_S\} &= \Gamma_{\omega_h}^h \left(|1\rangle\langle 3|\hat{\rho}_S|3\rangle\langle 1| - \frac{1}{2}|3\rangle\langle 3|\hat{\rho}_S - \frac{1}{2}\hat{\rho}_S|3\rangle\langle 3| \right) \\ &+ \Gamma_{-\omega_h}^h \left(|3\rangle\langle 1|\hat{\rho}_S|1\rangle\langle 3| - \frac{1}{2}|1\rangle\langle 1|\hat{\rho}_S - \frac{1}{2}\hat{\rho}_S|1\rangle\langle 1| \right) \\ &+ \Gamma_{\omega_h+\Delta}^h \left(|2\rangle\langle 4|\hat{\rho}_S|4\rangle\langle 2| - \frac{1}{2}|4\rangle\langle 4|\hat{\rho}_S - \frac{1}{2}\hat{\rho}_S|4\rangle\langle 4| \right) \\ &+ \Gamma_{-(\omega_h+\Delta)}^h \left(|4\rangle\langle 2|\hat{\rho}_S|2\rangle\langle 4| - \frac{1}{2}|2\rangle\langle 2|\hat{\rho}_S - \frac{1}{2}\hat{\rho}_S|2\rangle\langle 2| \right) \quad (2.9) \end{aligned}$$

and

$$\begin{aligned} \mathcal{L}_w\{\hat{\rho}_S\} &= \Gamma_{\omega_h-\omega_c}^w \left(|2\rangle\langle 3|\hat{\rho}_S|3\rangle\langle 2| - \frac{1}{2}|3\rangle\langle 3|\hat{\rho}_S - \frac{1}{2}\hat{\rho}_S|3\rangle\langle 3| \right) \\ &+ \Gamma_{-(\omega_h-\omega_c)}^w \left(|3\rangle\langle 2|\hat{\rho}_S|2\rangle\langle 3| - \frac{1}{2}|2\rangle\langle 2|\hat{\rho}_S - \frac{1}{2}\hat{\rho}_S|2\rangle\langle 2| \right). \quad (2.10) \end{aligned}$$

Este documento incorpora firma electrónica, y es copia auténtica de un documento electrónico archivado por la ULL según la Ley 39/2015.
 Su autenticidad puede ser contrastada en la siguiente dirección <https://sede.ull.es/validacion/>

Identificador del documento: 2111210 Código de verificación: lZvvKBaU

Firmado por: Javier Onam González López
 UNIVERSIDAD DE LA LAGUNA

Fecha: 09/09/2019 11:04:42

Daniel Alonso Ramírez
 UNIVERSIDAD DE LA LAGUNA

11/09/2019 14:53:47

For our choice of bosonic baths with an infinite cutoff, the functions Γ_ω^α read [4],

$$\begin{aligned}\Gamma_\omega^\alpha &= \gamma_\alpha (\omega/\omega_0)^{d_\alpha} \left(1 + \frac{1}{\exp(\hbar\omega/k_B T_\alpha) - 1} \right), \\ \Gamma_{-\omega}^\alpha &= \exp(-\hbar\omega/k_B T_\alpha) \Gamma_\omega^\alpha,\end{aligned}\quad (2.11)$$

with $\omega > 0$. ω_0 is a frequency depending on the physical realization of the coupling with the baths and d_α is the physical dimension of B_α .

Within this reduced description approach, the expectation value $\langle \hat{A} \rangle$ of an arbitrary system operator \hat{A} is written as

$$\langle \hat{A} \rangle = \text{Tr}\{\hat{A} \hat{\rho}_S\}, \quad (2.12)$$

where $\text{Tr}\{\}$ denotes the trace. From the previous equation it is possible to determine the thermodynamically relevant quantities of the four-level machine, see Appendix A. In particular, considering $\hat{A} = \hat{H}_S$ and using Eq. (2.7), we obtain the time evolution of the system energy

$$\frac{d}{dt} \langle \hat{H}_S \rangle = \dot{Q}_c(t) + \dot{Q}_h(t) + \dot{Q}_w(t), \quad (2.13)$$

being

$$\dot{Q}_\alpha(t) = \text{Tr}\{\hat{H}_S \mathcal{L}_\alpha\{\hat{\rho}_S\}\} \quad (2.14)$$

the heat current from the bath B_α into the system S . In the long time limit, the system reaches an stationary state and Eq. (2.13) becomes

$$\dot{Q}_c + \dot{Q}_h + \dot{Q}_w = 0, \quad (2.15)$$

where $\dot{Q}_\alpha \equiv \dot{Q}_\alpha(t \rightarrow \infty)$ is the steady state heat current between B_α and S . The previous expression plays the role of the First Law of Thermodynamics [7, 6]. Besides, the structure of the super-operators (2.8), (2.9) and (2.10) ensures that the stationary entropy production rate \dot{S} defined in terms of such heat currents is positive definite [67, 66, 9]

$$\dot{S} = -\frac{\dot{Q}_c}{T_c} - \frac{\dot{Q}_h}{T_h} - \frac{\dot{Q}_w}{T_w} \geq 0, \quad (2.16)$$

which, in turn, implies consistency with the Second Law of Thermodynamics.

In order to characterize the stationary functioning of the device, we first have to obtain the steady state solution of Eq. (2.7) and, secondly, we introduce this in Eq. (2.14) to determine the corresponding heat currents. The magnitude and sign of these steady state currents define the operation

Este documento incorpora firma electrónica, y es copia auténtica de un documento electrónico archivado por la ULL según la Ley 39/2015.
 Su autenticidad puede ser contrastada en la siguiente dirección <https://sede.ull.es/validacion/>

Identificador del documento: 2111210 Código de verificación: lZvvKBaU

Firmado por: Javier Onam González López
 UNIVERSIDAD DE LA LAGUNA

Fecha: 09/09/2019 11:04:42

Daniel Alonso Ramírez
 UNIVERSIDAD DE LA LAGUNA

11/09/2019 14:53:47

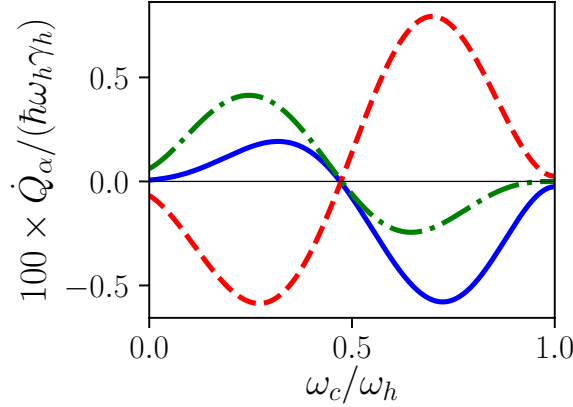


Figure 2.2: Heat currents \dot{Q}_α as functions of ω_c . The solid, dashed and dotted-dashed lines correspond to $\alpha = c, h$ and w respectively. The set of parameters is: $\omega_h = 1, \Delta = 0.1, T_c = 2, T_h = 3, T_w = 6, d_c = d_h = d_w = 3, \gamma_c = \gamma_h = \gamma_w = 10^{-6}$ and $\omega_c \in [0, \omega_h]$. We have taken natural units: $\hbar = k_B = \omega_0 = 1$.

mode of the machine for a given set of parameters. In Fig. 2.2 we show the currents \dot{Q}_α versus the frequency ω_c . We observe two different operation modes in the figure. In the interval $\omega_c \lesssim 0.5\omega_h$, energy is extracted from the cold bath at the expense of the energy supplied from the work reservoir. The surplus energy is conducted to the hot bath. In this operation mode, $\{\dot{Q}_c > 0, \dot{Q}_h < 0, \dot{Q}_w > 0\}$, the device acts as a refrigerator. The set of values of ω_c for which this cooling task is achieved is denoted the cooling window of the machine. Conversely, in the regime $\omega_c \gtrsim 0.5\omega_h$ a heat transformer operation mode is observed, $\{\dot{Q}_c < 0, \dot{Q}_h > 0, \dot{Q}_w < 0\}$. In this case, energy is pumped into the highest temperature bath. To fix ideas, in this chapter we focus on the cooling operation mode. There exist two main figures of merit characterizing the operation of a refrigerator: the amount of energy per unit of time extracted from the cold bath, i. e. the cooling power \dot{Q}_c , and the coefficient of performance

$$\varepsilon = \frac{\dot{Q}_c}{\dot{Q}_w}, \quad (2.17)$$

which also takes into account the input energy coming from B_w . Characteristic curves combining the information of these two relevant quantities are

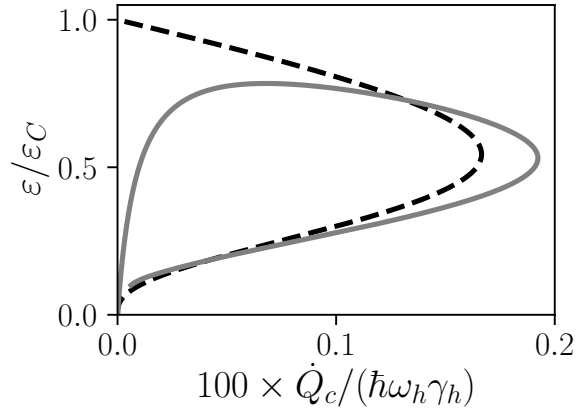


Figure 2.3: Coefficient of performance ε against the cooling power \dot{Q}_c within the cooling window of the four-level device shown in Fig. 2.1. For $\Delta = 0$ (dashed line) we obtain an open characteristic curve, while for $\Delta = 0.1$ (solid line) the reversible limit of maximum efficiency is unattainable. The other parameters are the same as in Fig. 2.2.

shown in Fig. 2.3 for two different values of the parameter Δ . For $\Delta = 0$ the reversible limit of maximum efficiency and vanishing currents is achieved. Using Eqs. (2.15) and (2.16), this upper bound for ε is nothing but the Carnot coefficient of performance of an absorption refrigerator

$$\varepsilon_C = \varepsilon|_{\dot{s}=0} = \frac{T_c(T_w - T_h)}{T_w(T_h - T_c)}. \quad (2.18)$$

Remarkably, any other non zero value of Δ prevents the machine from reaching this reversible limit.

As has been shown, the master equation approach provides a full description of the overall stationary functioning of the four-level absorption device. However, interpreting the results within this framework is not straightforward. The dependence of the cooling window with the parameters, the mechanisms that precludes the device from achieving the maximum coefficient of performance, the contributions of the different processes that take place in the device and contribute to its overall currents, etc. These are some examples of issues that requires either a deep understanding of the device functioning, or tedious analytical calculations concerning the particular master equation. As an alternative to this standard method, we adopt a different

Este documento incorpora firma electrónica, y es copia auténtica de un documento electrónico archivado por la ULL según la Ley 39/2015.
 Su autenticidad puede ser contrastada en la siguiente dirección <https://sede.ull.es/validacion/>

Identificador del documento: 2111210 Código de verificación: lZvvKBaU

Firmado por: Javier Onam González López
 UNIVERSIDAD DE LA LAGUNA

Fecha: 09/09/2019 11:04:42

Daniel Alonso Ramírez
 UNIVERSIDAD DE LA LAGUNA

11/09/2019 14:53:47

perspective in the following. Our aim is to built a representation based on the internal processes that play a role in the stationary functioning of the machine. This will facilitates the interpretation of the previous results.

2.3 Graph representation

Taking diagonal projections in the master equation (2.7), we get the time evolution of the populations $p_n \equiv \langle n | \hat{\rho}_S | n \rangle$ in the four-level device

$$\frac{d}{dt} \begin{bmatrix} p_1 \\ p_2 \\ p_3 \\ p_4 \end{bmatrix} = \mathbf{W} \begin{bmatrix} p_1 \\ p_2 \\ p_3 \\ p_4 \end{bmatrix}. \quad (2.19)$$

\mathbf{W} is the matrix of rates whose non diagonal elements, $W_{nm} \equiv W_{nm}^{\alpha_{nm}}$, are given by

$$\begin{aligned} W_{12}^c &= \Gamma_{\omega_c}^c; & W_{21}^c &= \Gamma_{-\omega_c}^c; & W_{34}^c &= \Gamma_{\omega_c+\Delta}^c; & W_{43}^c &= \Gamma_{-(\omega_c+\Delta)}^c; \\ W_{13}^h &= \Gamma_{\omega_h}^h; & W_{31}^h &= \Gamma_{-\omega_h}^h; & W_{24}^h &= \Gamma_{\omega_h+\Delta}^h; & W_{42}^h &= \Gamma_{-(\omega_h+\Delta)}^h; \\ W_{23}^w &= \Gamma_{\omega_h-\omega_c}^w; & W_{32}^w &= \Gamma_{-(\omega_h-\omega_c)}^w. \end{aligned} \quad (2.20)$$

The levels $|1\rangle$ and $|4\rangle$ are not directly connected, hence $W_{14} = W_{41} = 0$. The label $\alpha_{nm} = c, h$ or w indicates that the transition $|m\rangle \rightarrow |n\rangle$ is connected to the bath B_c, B_h or B_w . Thus, $W_{nm}^{\alpha_{nm}}$ can be interpreted as the transition probability rate from state $|m\rangle$ to $|n\rangle$ mediated by the bath α_{nm} . Note that $\alpha_{nm} = \alpha_{mn}$, i. e. the same bath induces simultaneously absorptions and emissions between the states $|n\rangle$ and $|m\rangle$. According to Eqs. (2.20), (2.11) and (2.2), the rates fulfill detailed balance relations

$$W_{mn}^{\alpha_{mn}} = W_{nm}^{\alpha_{nm}} \exp[-(E_m - E_n)/k_B T_{\alpha_{nm}}], \quad (n \neq m). \quad (2.21)$$

Besides, the diagonal elements W_{nn} can be easily expressed in terms of the non diagonal rates

$$W_{nn} = - \sum_{m \neq n}^4 W_{mn}^{\alpha_{mn}}. \quad (2.22)$$

We do not use a superscript α_{nn} for the diagonal rates since they are not associated with a single bath.

The population dynamics (2.19) does not depend on coherences $\langle n | \hat{\rho}_S | m \rangle$, $n \neq m$. Interestingly, the matrix of rates fulfills the properties needed to claim that Eqs. (2.19) are a proper set of balance equations: the non diagonal rates are positive ensuring their interpretation in terms of transition

Este documento incorpora firma electrónica, y es copia auténtica de un documento electrónico archivado por la ULL según la Ley 39/2015.
 Su autenticidad puede ser contrastada en la siguiente dirección <https://sede.ull.es/validacion/>

Identificador del documento: 2111210 Código de verificación: lZvvKBaU

Firmado por: Javier Onam González López
 UNIVERSIDAD DE LA LAGUNA

Fecha: 09/09/2019 11:04:42

Daniel Alonso Ramírez
 UNIVERSIDAD DE LA LAGUNA

11/09/2019 14:53:47

probabilities, see Eqs. (2.20) and (2.11), and additionally, the matrix \mathbf{W} is singular leading to the conservation of the probability, see Eq. (2.22). The same type of balance equations describe the behavior of thermal devices [68, 69, 70, 71] within the framework of Stochastic Thermodynamics [65, 72]. Hence, the thermodynamic stationary functioning of this device can be described classically without invoking any quantum feature. This connection with a stochastic-thermodynamic picture allows us to employ the conventional procedures in this field. Namely, we define a graph representation of the set of balance equations in the following way: each state $|n\rangle$ becomes a vertex n of the graph \mathcal{G} representing the balance equations and each non zero pair of rates, $\{W_{nm}^{\alpha nm}, W_{mn}^{\alpha mn}\}_{n \neq m}$, becomes an edge of \mathcal{G} connecting the vertices n and m . The number of edges and vertices is denoted by E and V respectively. In Fig. 2.4(a) we show the graph representing the Eqs. (2.19) of the four-level absorption device.

2.3.1 Graph objects

To proceed further, we have to introduce some basic concepts of Graph Theory. A maximal tree \mathcal{T}_μ is a subgraph of \mathcal{G} containing all the V vertices without forming a closed path. Such closed path is called a circuit \mathcal{C}_ν . The circuit \mathcal{C}_ν can be oriented in two possible directions leading the cycles $\vec{\mathcal{C}}_\nu$ and $-\vec{\mathcal{C}}_\nu$. Cycles are associated with opposite thermodynamic processes in the machine. For instance, when performing the cycle $\vec{\mathcal{C}}_1$ shown in Fig. 2.4(c), the system absorbs energy from the cold and work baths (transitions $|1\rangle \rightarrow |2\rangle$ and $|2\rangle \rightarrow |3\rangle$ respectively). To complete the process, energy is rejected into the hot bath (transition $|3\rangle \rightarrow |1\rangle$). Thus, $\vec{\mathcal{C}}_1$ is related to a process that promotes the cooling task. On the contrary, the cycle $-\vec{\mathcal{C}}_1$ is associated with an energy intake from the hot bath (transition $|1\rangle \rightarrow |3\rangle$) and rejection of energy into the work and cold reservoirs (transitions $|3\rangle \rightarrow |2\rangle$ and $|2\rangle \rightarrow |1\rangle$ respectively). Hence, $-\vec{\mathcal{C}}_1$ favours the heat transformer operation mode, which is contrary to the cooling task. As the circuits can be oriented to get the corresponding cycles, the information about the competition between two opposite thermodynamic processes can be associated with circuit currents, see Sec. 2.4. On the other hand, maximal trees can also be directed towards a particular vertex. Namely, when orienting the maximal tree \mathcal{T}_μ towards n , an oriented maximal tree $\vec{\mathcal{T}}_\mu^n$ is found. Each one of the $E - V + 1$ edges not belonging to the maximal tree \mathcal{T}_μ is a chord. By definition, the addition of a chord to the maximal tree results in a subgraph with a circuit \mathcal{C}_ν and, eventually, some additional edges. When orienting these additional edges towards the circuit, a forest $\vec{\mathcal{F}}_\beta(\mathcal{C}_\nu)$ of the circuit is found.

Este documento incorpora firma electrónica, y es copia auténtica de un documento electrónico archivado por la ULL según la Ley 39/2015.
 Su autenticidad puede ser contrastada en la siguiente dirección <https://sede.ull.es/validacion/>

Identificador del documento: 2111210 Código de verificación: lZvvKBaU

Firmado por: Javier Onam González López
 UNIVERSIDAD DE LA LAGUNA

Fecha: 09/09/2019 11:04:42

Daniel Alonso Ramírez
 UNIVERSIDAD DE LA LAGUNA

11/09/2019 14:53:47

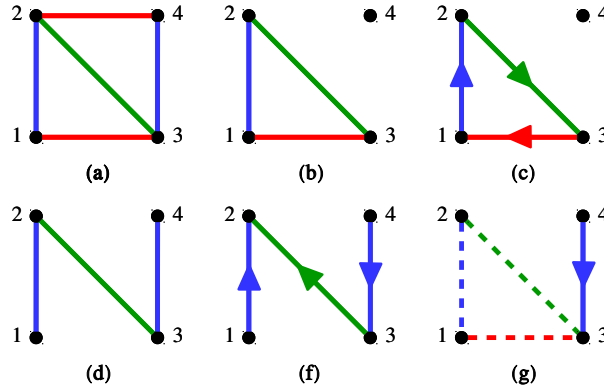


Figure 2.4: (a) Graph \mathcal{G} representing the balance equations (2.19) of the four-level device depicted in Fig. 2.1. The graph has $V = 4$ vertices and $E = 5$ edges. The colors blue, red and green indicate a coupling with the cold, hot or work bath. (b) Circuit \mathcal{C}_1 of \mathcal{G} . (c) When orienting \mathcal{C}_1 clockwise the cycle $\vec{\mathcal{C}}_1$ is obtained. The algebraic value of this cycle is $\mathcal{A}(\vec{\mathcal{C}}_1) = W_{21}^c W_{32}^w W_{13}^h$. (d) Maximal tree \mathcal{T}_1 of \mathcal{G} . (e) When orienting \mathcal{T}_1 towards the vertex $n = 2$ the oriented maximal tree $\vec{\mathcal{T}}_1^2$ is found. The corresponding algebraic value is $\mathcal{A}(\vec{\mathcal{T}}_1^2) = W_{21}^c W_{23}^w W_{34}^h$. (f) The edge connecting the vertices 1 and 3 is a chord of \mathcal{T}_1 . When adding this chord to \mathcal{T}_1 , we get the circuit \mathcal{C}_1 (dashed lines). The remaining edge oriented towards \mathcal{C}_1 is a forest $\vec{\mathcal{F}}_1(\mathcal{C}_1)$ of the circuit. The algebraic value of the forest is $\mathcal{A}(\vec{\mathcal{F}}_1(\mathcal{C}_1)) = W_{34}^c$.

The index β indicates that the same circuits may have different forests.

In order to perform numerical calculations with the graph representation, we need to establish a connection between the graph objects and the values of the rates. Thus, the directed edge from vertex n to m is related to the transition rate $W_{mn}^{\alpha mn}$. Finally, the algebraic value $\mathcal{A}(\vec{\mathcal{S}})$ of any directed subgraph $\vec{\mathcal{S}}$ of \mathcal{G} is given by the product of all the rates associated with the directed edges of $\vec{\mathcal{S}}$. In the Fig. 2.4, we show some directed graph objects with their corresponding algebraic values.

Este documento incorpora firma electrónica, y es copia auténtica de un documento electrónico archivado por la ULL según la Ley 39/2015.
 Su autenticidad puede ser contrastada en la siguiente dirección <https://sede.ull.es/validacion/>

Identificador del documento: 2111210 Código de verificación: lZvvKBaU

Firmado por: Javier Onam González López
 UNIVERSIDAD DE LA LAGUNA

Fecha: 09/09/2019 11:04:42

Daniel Alonso Ramírez
 UNIVERSIDAD DE LA LAGUNA

11/09/2019 14:53:47

2.4 Circuit decomposition

The graph representation can be employed to build a thermodynamically consistent circuit decomposition of the stationary heat currents. Within this approach, the overall steady state currents \dot{Q}_α read

$$\dot{Q}_\alpha \equiv \dot{Q}_\alpha(\mathcal{G}) = \sum_{\nu=1}^{N_C} \dot{q}_\alpha(\mathcal{C}_\nu), \quad (2.23)$$

with $\dot{q}_\alpha(\mathcal{C}_\nu)$ the heat current associated with the circuit \mathcal{C}_ν . N_C is the total number of circuits in \mathcal{G} . This number may grow very fast, even exponentially, when considering graphs with an increasing number of vertices and edges. Fortunately, the circuits can be identified by using efficient algorithms [73]. The circuits currents are, in turn,

$$\dot{q}_\alpha(\mathcal{C}_\nu) = -T_\alpha X^\alpha(\vec{\mathcal{C}}_\nu) \frac{\sum_{\beta=1}^{F_\nu} \mathcal{A}(\vec{\mathcal{F}}_\beta(\mathcal{C}_\nu))}{\sum_{\mu=1}^M \sum_{n=1}^V \mathcal{A}(\vec{\mathcal{T}}_\mu^n)} [\mathcal{A}(\vec{\mathcal{C}}_\nu) - \mathcal{A}(-\vec{\mathcal{C}}_\nu)]. \quad (2.24)$$

We denote by M the total number of maximal trees. F_ν is the number of forests of \mathcal{C}_ν . When \mathcal{C}_ν contains all the vertices in \mathcal{G} , the circuit has no forest and the algebraic value $\mathcal{A}(\vec{\mathcal{F}}_\beta(\mathcal{C}_\nu))$ is equal to 1. $X^\alpha(\vec{\mathcal{C}}_\nu)$ is the circuit affinity given by

$$X^\alpha(\vec{\mathcal{C}}_\nu) = k_B \ln \left(\frac{\mathcal{A}^\alpha(\vec{\mathcal{C}}_\nu)}{\mathcal{A}^\alpha(-\vec{\mathcal{C}}_\nu)} \right), \quad (2.25)$$

where $\mathcal{A}^\alpha(\pm\vec{\mathcal{C}}_\nu)$ is the algebraic value of the cycle $\pm\vec{\mathcal{C}}_\nu$ related to the bath B_α . This quantity returns the product of the rates corresponding to the directed edges, $n \rightarrow m$, of $\pm\vec{\mathcal{C}}_\nu$ such that $\alpha_{mn} = \alpha$. If the circuit \mathcal{C}_ν has no edges related to the bath B_α , the value of \mathcal{A}^α is 1.

The expression (2.24) for the circuit current is a central result of the paper included in Sec. 5.3, since it provides a complete understanding on the different processes that can take place in the steady state functioning. These currents do not depend on the cycle orientations. Besides, each term in (2.24) has a clear interpretation. The quantity $-T_\alpha X^\alpha(\vec{\mathcal{C}}_\nu)$ is just the amount of energy resulting from the interaction between S and B_α when performing the cycle $\vec{\mathcal{C}}_\nu$. Therefore, energy conservation implies $\sum_\alpha T_\alpha X^\alpha(\vec{\mathcal{C}}_\nu) = 0$. The factor $\mathcal{A}(\vec{\mathcal{C}}_\nu) - \mathcal{A}(-\vec{\mathcal{C}}_\nu)$ highlights the importance of the cycle asymmetry on the magnitude of the currents. This factor is related to the competition between opposite cycles. The winner of this competition, either $\vec{\mathcal{C}}_\nu$ or $-\vec{\mathcal{C}}_\nu$, determines the thermodynamic operation of the circuit. This circuit contribution can involve the three baths, in the case of cooling and heat transformer operation

Este documento incorpora firma electrónica, y es copia auténtica de un documento electrónico archivado por la ULL según la Ley 39/2015.
 Su autenticidad puede ser contrastada en la siguiente dirección <https://sede.ull.es/validacion/>

Identificador del documento: 2111210 Código de verificación: lZvvKBaU

Firmado por: Javier Onam González López
 UNIVERSIDAD DE LA LAGUNA

Fecha: 09/09/2019 11:04:42

Daniel Alonso Ramírez
 UNIVERSIDAD DE LA LAGUNA

11/09/2019 14:53:47

modes, or two baths which is simply related to heat transport between them. The term of the forests $\sum_{\beta=1}^{F_\nu} \mathcal{A}(\vec{\mathcal{F}}_\beta(\mathcal{C}_\nu))$ accounts for external contributions coming from edges and vertices not belonging to \mathcal{C}_ν . Therefore, circuits with a small number of vertices (with respect to V) have a large number of forests and, as a consequence, their contribution to the overall currents is generally greater than the one associated with circuits containing many vertices. Finally, the factor $\sum_{\mu=1}^M \sum_{n=1}^V \mathcal{A}(\vec{\mathcal{T}}_\mu^n)$, which is the same for all the circuits, increases exponentially with the complexity of the graph, i.e. with both the number of vertices and edges. In summary, clever designs of absorption machines should include as many small circuits with high cycle asymmetry as possible. Besides, the contribution of the circuits should overcome the contribution of the maximall trees, since the later appears in the denominator of Eq. (2.24).

Remarkably, the stationary circuit decomposition (2.23) is valid for any non-degenerate N -level absorption device in the weak coupling limit. Besides, this decomposition is also applicable to the study of any balance equation system whose matrix of rates satisfies expressions analogous to (2.21) and (2.22). Using Eqs. (2.24) and (2.25), it is easy to verify that the circuit currents are consistent with the First and Second Law of Thermodynamics

$$\begin{aligned}
 \dot{q}_c(\mathcal{C}_\nu) + \dot{q}_h(\mathcal{C}_\nu) + \dot{q}_w(\mathcal{C}_\nu) &= 0, \\
 -\frac{\dot{q}_c(\mathcal{C}_\nu)}{T_c} - \frac{\dot{q}_h(\mathcal{C}_\nu)}{T_h} - \frac{\dot{q}_w(\mathcal{C}_\nu)}{T_w} &\geq 0.
 \end{aligned} \tag{2.26}$$

The previous expressions settle the basis for the interpretation of the stationary functioning of the device. Each circuit can be thought as an internal component that is directly linked with a thermodynamically consistent mechanism. In the following, the terms circuit and internal component are used interchangeably. The stationary device operation is the result of the contributions and interplay between its internal components.

2.5 Classification of internal components

The classification of internal components \mathcal{C}_ν is based on the values of their affinities $X^c(\vec{\mathcal{C}}_\nu)$, $X^h(\vec{\mathcal{C}}_\nu)$ and $X^w(\vec{\mathcal{C}}_\nu)$. Within the context of absorption machines, there exist three categories of internal components

- $X^\alpha(\vec{\mathcal{C}}_\nu) = 0, \forall \alpha \Rightarrow \mathcal{C}_\nu$ is a trivial circuit since $\dot{q}_\alpha(\vec{\mathcal{C}}_\nu) = 0$.
- $X^{\alpha_1}(\vec{\mathcal{C}}_\nu), X^{\alpha_2}(\vec{\mathcal{C}}_\nu) \neq 0$ and $X^{\alpha_3}(\vec{\mathcal{C}}_\nu) = 0 \Rightarrow \mathcal{C}_\nu$ is always a non useful component related to energy transport between the baths B_{α_1} and B_{α_2} .

Este documento incorpora firma electrónica, y es copia auténtica de un documento electrónico archivado por la ULL según la Ley 39/2015.
 Su autenticidad puede ser contrastada en la siguiente dirección <https://sede.ull.es/validacion/>

Identificador del documento: 2111210 Código de verificación: lZvvKBaU

Firmado por: Javier Onam González López
 UNIVERSIDAD DE LA LAGUNA

Fecha: 09/09/2019 11:04:42

Daniel Alonso Ramírez
 UNIVERSIDAD DE LA LAGUNA

11/09/2019 14:53:47

The energy flows directly from the hottest to the coldest reservoir. Within the context of absorption machines, these circuit currents are associated with undesired heat leaks.

- $X^\alpha(\vec{C}_\nu) \neq 0, \forall \alpha \Rightarrow \mathcal{C}_\nu$ is a three-bath circuit. This category includes the useful components that can operate as refrigerators or heat transformers, at least in some parameter regimes.

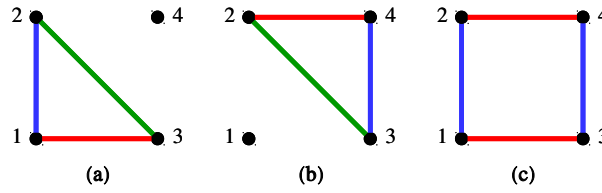


Figure 2.5: The graph shown in 2.4(a) contain three different circuits. We denote them by \mathcal{C}_1 (a), \mathcal{C}_2 (b) and \mathcal{C}_3 (c).

Circuit	Affinities: (X^c, X^h, X^w)	Category
\mathcal{C}_1	$(-\hbar\omega_c/T_c, \hbar\omega_h/T_h, -\hbar\omega_w/T_w)$	Useful component
\mathcal{C}_2	$(-\hbar(\omega_c + \Delta)/T_c, \hbar(\omega_h + \Delta)/T_h, -\hbar\omega_w/T_w)$	Useful component
\mathcal{C}_3	$(\hbar\Delta/T_c, -\hbar\Delta/T_h, 0)$	Non useful or trivial circuit

Table 2.1: Classification of the components of the four-level absorption device. The affinities (2.25) has been obtained by taking a clockwise orientation in the circuits depicted in Fig. 2.5. We have denoted $\omega_w \equiv \omega_h - \omega_c$.

The components describing the stationary functioning of the four-level device are depicted in figure 2.5. We present the classification of these circuits in the Table 2.1. The circuits \mathcal{C}_1 and \mathcal{C}_2 are associated with thermodynamic mechanisms involving the three baths and, as a result, they can operate either as refrigerators or heat transformers. Considering Eq. (2.24) and imposing $\dot{q}_c(\mathcal{C}_\nu) > 0$ for $\nu = 1, 2$, it is straightforward to show that \mathcal{C}_1 and \mathcal{C}_2 perform the cooling task within the cooling windows $\omega_c < \omega_h \frac{T_c(T_w - T_h)}{T_h(T_w - T_c)} \equiv \omega_c^{max}(\mathcal{C}_1)$ and $\omega_c < \omega_c^{max}(\mathcal{C}_1) - \Delta \frac{T_w(T_h - T_c)}{T_h(T_w - T_c)} \equiv \omega_c^{max}(\mathcal{C}_2)$ respectively. However, \mathcal{C}_3 involves only two baths. For $\Delta = 0$, see Tab. 2.1, the affinities of this circuit are

Este documento incorpora firma electrónica, y es copia auténtica de un documento electrónico archivado por la ULL según la Ley 39/2015.
 Su autenticidad puede ser contrastada en la siguiente dirección <https://sede.ull.es/validacion/>

Identificador del documento: 2111210 Código de verificación: lZvvKBaU

Firmado por: Javier Onam González López
 UNIVERSIDAD DE LA LAGUNA

Fecha: 09/09/2019 11:04:42

Daniel Alonso Ramírez
 UNIVERSIDAD DE LA LAGUNA

11/09/2019 14:53:47

zero and, as a consequence, \mathcal{C}_3 is a trivial component with zero currents. For $\Delta \neq 0$, \mathcal{C}_3 is a heat leak between the bath B_c and B_h . As $T_h > T_c$, this heat leak transports energy from the hot to the cold bath.

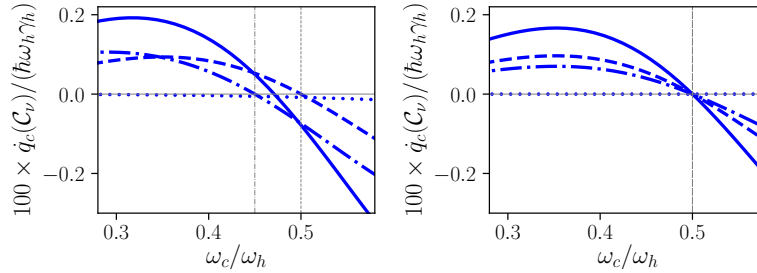


Figure 2.6: Circuit cold heat currents against ω_c for $\Delta = 0.1$ (left) and 0 (right). The dashed, dashed-dotted and dotted lines corresponds to $\nu = 1, 2$ and 3 respectively. The solid line shows the sum of the circuit contributions which is the total stationary cooling power. The vertical dashed and dashed-dotted lines are respectively located at $\omega_c^{\max}(\mathcal{C}_1)$ and $\omega_c^{\max}(\mathcal{C}_2)$.

In the figure 2.6, we plot the circuit contributions to the overall steady state cooling power. For $\Delta = 0$, \mathcal{C}_1 and \mathcal{C}_2 have the same cooling window since $\omega_c^{\max}(\mathcal{C}_1) = \omega_c^{\max}(\mathcal{C}_2)$ and, as a result, these useful circuits always follow the same operation mode. Besides, \mathcal{C}_3 is a trivial component with no contribution to the current. Therefore, the reversible limit of maximum coefficient of performance and vanishing currents is achieved at $\omega_c = \omega_c^{\max}(\mathcal{C}_1)$. However, for $\Delta \neq 0$, $\omega_c^{\max}(\mathcal{C}_1) > \omega_c^{\max}(\mathcal{C}_2)$. Thus, when $\omega_c < \omega_c^{\max}(\mathcal{C}_1)$, both \mathcal{C}_1 and \mathcal{C}_2 operate as refrigerators, while for $\omega_c^{\max}(\mathcal{C}_1) < \omega_c < \omega_c^{\max}(\mathcal{C}_2)$, \mathcal{C}_2 works as a heat transformer. This competition between opposite operation modes in useful circuits prevents the device from achieving the reversible limit. The contribution of \mathcal{C}_3 is an additional mechanism responsible for the unattainability of the Carnot performance in this device. The undesired currents of this non useful circuit does not vanish for $\Delta \neq 0$. In general, these are the two mechanisms that make it impossible to reach the reversible limit: the competition between useful circuits and the contributions of non useful components [74, 40]. As we have seen, the interpretation of the figures 2.2 and 2.3 becomes much more clear when dealing with the internal components of the four-level machine.

Este documento incorpora firma electrónica, y es copia auténtica de un documento electrónico archivado por la ULL según la Ley 39/2015.
 Su autenticidad puede ser contrastada en la siguiente dirección <https://sede.ull.es/validacion/>

Identificador del documento: 2111210 Código de verificación: lZvvKBaU

Firmado por: Javier Onam González López
 UNIVERSIDAD DE LA LAGUNA

Fecha: 09/09/2019 11:04:42

Daniel Alonso Ramírez
 UNIVERSIDAD DE LA LAGUNA

11/09/2019 14:53:47

2.6 Graph topology and heat currents

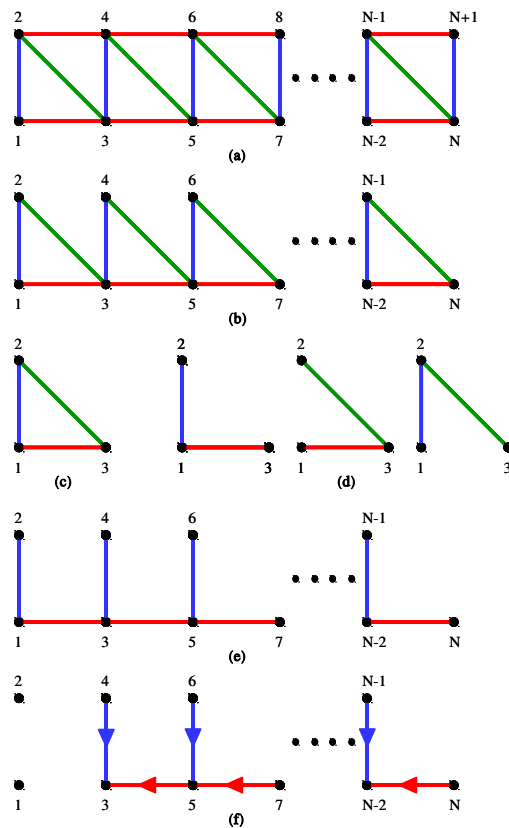


Figure 2.7: (a) Graph \mathcal{H} obtained by using the graph \mathcal{G} of Fig. 2.4(a) as a building unit. (b) Graph \mathcal{I} obtained from \mathcal{H} by removing the hot edges connecting even vertices. (c) Circuit graph \mathcal{J} . (d) Maximal trees of \mathcal{J} . The graph objects of \mathcal{I} are determined in terms of those for the graph \mathcal{J} . For example, in (e) we show a maximal tree of \mathcal{I} that has been obtained by considering a maximal tree of \mathcal{J} in each triangle of \mathcal{I} . In (f) a forest of the first triangle in \mathcal{I} is depicted.

We have analyzed the graph \mathcal{G} of Fig. 2.4(a) representing the balance equations (2.19) of the four-level absorption device depicted in Fig. 2.1. This graph contains only three circuits, see Fig. 2.5. The addition of new circuits to the graph has a direct effect on the machine performance. For example, one can include non useful components diminishing the useful currents and removing the possibility of reaching the Carnot limit. This causes a negative impact on the device operation. Therefore, an important question is whether the addition of useful and, eventually, trivial components without introducing non useful circuits may be beneficial for the device functioning. In the following we deal with this issue.

Let us consider the graph \mathcal{H} shown in Fig. 2.7(a). This graph is built by merging copies of the graph \mathcal{G} , see Fig. 2.4(a), that share a vertical cold edge. We assume $\Delta = 0$ to ensure that the graph does not contain non useful circuits. The balance equations corresponding to \mathcal{H} read $\frac{d\mathbf{p}}{dt} = \mathbf{W}\mathbf{p}$, where \mathbf{p} is a probability vector $\mathbf{p} = [p_1, p_2, \dots, p_N, p_{N+1}]$ and \mathbf{W} the matrix of rates. The non diagonal rates $W_{nm} = W_{nm}^{\alpha}$ of \mathbf{W} are

$$\begin{aligned}
 W_{ll+1}^c &= \Gamma_{\omega_c}^c; W_{l+1l}^c = \Gamma_{-\omega_c}^c; (l = 1, 3, \dots, N); \\
 W_{ll+2}^h &= \Gamma_{\omega_h}^h; W_{l+2l}^h = \Gamma_{-\omega_h}^h; (l = 1, 2, \dots, N-1); \\
 W_{ll+1}^w &= \Gamma_{\omega_h - \omega_c}^w; W_{l+1l}^w = \Gamma_{-(\omega_h - \omega_c)}^w; (l = 2, 4, \dots, N-1); \quad (2.27)
 \end{aligned}$$

and zero for any other pair of indexes. According to Eq. (2.27), all the transitions with the bath B_α , $\alpha = c, h, w$, share the same pair of rates. This is a preferred scheme to understand the impact of the graph topology on the device performance. Additionally, the diagonal elements of \mathbf{W} fulfill the condition analogous to (2.22). The physical implementation corresponding to this matrix of rates is the multistage quantum-absorption device studied in [50]. For comparison purposes, we also consider a graph \mathcal{I} which is a subgraph of \mathcal{H} . Namely, removing from \mathcal{H} the hot edges connecting vertices l and $l+2$, $l = 2, 4, \dots, N-1$, leads to \mathcal{I} . Both \mathcal{H} and \mathcal{I} contain a triangle graph \mathcal{J} depicted in Fig. 2.7(c). We use \mathcal{J} as a reference to determine possible increments in the magnitude of the heat currents. The physical realization related to \mathcal{J} is nothing but the well known three-level quantum absorption refrigerator [30, 31]. As the affinities \mathcal{X}^α are the same for all the useful circuits in \mathcal{H} , \mathcal{I} and \mathcal{J} , the associated devices show the same coefficient of performance, see the paper included in Sec. 5.3. In the following, we focus on the cooling power. Remarkably, in a low temperature regime the three graphs provide the same currents. Hence, we consider a regime from moderate to high temperatures. Thus, the levels with high energies will have non vanishing populations and, as a consequence, contribute to the device functioning.

Este documento incorpora firma electrónica, y es copia auténtica de un documento electrónico archivado por la ULL según la Ley 39/2015.
 Su autenticidad puede ser contrastada en la siguiente dirección <https://sede.ull.es/validacion/>

Identificador del documento: 2111210 Código de verificación: lZvvKBaU

Firmado por: Javier Onam González López
 UNIVERSIDAD DE LA LAGUNA

Fecha: 09/09/2019 11:04:42

Daniel Alonso Ramírez
 UNIVERSIDAD DE LA LAGUNA

11/09/2019 14:53:47

2.6.1 Graph \mathcal{J}

The circuit graph \mathcal{J} is composed of $V = 3$ vertices and $E = 3$ edges. This graph is characterized by a single internal component which, in this case, is a triangle. Using Eqs. (2.24), (2.25), (2.27) and (2.11) it is straightforward to find the following expression for the cooling power of the triangle

$$\dot{Q}_c(\mathcal{J}) = \hbar \omega_c \Gamma_{\omega_c}^c \Gamma_{\omega_h}^h \Gamma_{\omega_h - \omega_c}^w \frac{\exp\left[-\frac{\hbar \omega_c}{k_B T_c} - \frac{\hbar(\omega_h - \omega_c)}{k_B T_w}\right] - \exp\left[-\frac{\hbar \omega_h}{k_B T_h}\right]}{\sum_{\mu=1}^3 \sum_{n=1}^3 \mathcal{A}(\vec{\mathcal{T}}_{\mu}^n; \mathcal{J})}, \quad (2.28)$$

where the three maximal trees of \mathcal{J} are shown in Fig. 2.7(d). The dependence of the maximal trees with the graph under consideration has been made explicit in the corresponding algebraic value.

2.6.2 Graph \mathcal{I}

The graph \mathcal{I} is obtained by merging copies of the triangle \mathcal{J} . \mathcal{I} has $V = N$ vertices and $E = 3\left(1 + \frac{N-3}{2}\right)$ edges with $N = 3, 5, 7, \dots$. The graph contains $N_C = 1 + \frac{N-3}{2}$ circuits. All these triangle circuits are useful components. \mathcal{I} has neither non useful nor trivial components. Using Eq. (2.23) for $\alpha = c$, we obtain the steady state cooling power corresponding to this graph

$$\dot{Q}_c(\mathcal{I}) = \hbar \omega_c \Gamma_{\omega_c}^c \Gamma_{\omega_h}^h \Gamma_{\omega_h - \omega_c}^w \left(\exp\left[-\frac{\hbar \omega_c}{k_B T_c} - \frac{\hbar(\omega_h - \omega_c)}{k_B T_w}\right] - \exp\left[-\frac{\hbar \omega_h}{k_B T_h}\right] \right) \times \frac{\sum_{\nu=1}^{N_C} \sum_{\beta=1}^{F_{\nu}} \mathcal{A}(\vec{\mathcal{F}}_{\beta}(\mathcal{C}_{\nu}; \mathcal{I}))}{\sum_{\mu=1}^M \sum_{n=1}^N \mathcal{A}(\vec{\mathcal{T}}_{\mu}^n; \mathcal{I})}. \quad (2.29)$$

Again, we make the label corresponding to the graph explicit in the algebraic values of forests and maximal trees. The number of maximal trees and forests, M and F_{ν} , are 3^{N_C} and 3^{N_C-1} respectively. Note that these graph objects of \mathcal{I} can be easily obtained by considering adequate products of maximal trees of the reference graph \mathcal{J} , see Fig. 2.7(e) and (f). We consider the ratio between Eq. (2.29) and Eq. (2.28)

$$\frac{\dot{Q}_c(\mathcal{I})}{\dot{Q}_c(\mathcal{J})} = \frac{\sum_{\nu=1}^{N_C} \sum_{\beta=1}^{F_{\nu}} \mathcal{A}(\vec{\mathcal{F}}_{\beta}(\mathcal{C}_{\nu}; \mathcal{I})) \sum_{\mu=1}^3 \sum_{n=1}^3 \mathcal{A}(\vec{\mathcal{T}}_{\mu}^n; \mathcal{J})}{\sum_{\mu=1}^M \sum_{n=1}^N \mathcal{A}(\vec{\mathcal{T}}_{\mu}^n; \mathcal{I})}. \quad (2.30)$$

The numerator in the previous expression is the sum of all the maximal trees in the graph \mathcal{I} oriented to the vertices of the corresponding circuits. The vertices $\{3, 5, 7, \dots, N-2\}$ belong simultaneously to two circuits, see Fig.

Este documento incorpora firma electrónica, y es copia auténtica de un documento electrónico archivado por la ULL según la Ley 39/2015.
 Su autenticidad puede ser contrastada en la siguiente dirección <https://sede.ull.es/validacion/>

Identificador del documento: 2111210 Código de verificación: lZvvKBaU

Firmado por: Javier Onam González López
 UNIVERSIDAD DE LA LAGUNA

Fecha: 09/09/2019 11:04:42

Daniel Alonso Ramírez
 UNIVERSIDAD DE LA LAGUNA

11/09/2019 14:53:47

2.7(b), and, as a result, they have a double contribution in the sum

$$\begin{aligned}
 \sum_{\nu=1}^{N_C} \sum_{\beta=1}^{F_\nu} \mathcal{A}(\vec{\mathcal{T}}_\beta(\mathcal{C}_\nu; \mathcal{I})) \sum_{\mu=1}^3 \sum_{n=1}^3 \mathcal{A}(\vec{\mathcal{T}}_\mu^n; \mathcal{J}) = \\
 \sum_{\mu=1}^M \sum_{n=1}^N \mathcal{A}(\vec{\mathcal{T}}_\mu^n; \mathcal{I}) + \sum_{\mu=1}^M \sum_{l=1}^{N_C-1} \mathcal{A}(\vec{\mathcal{T}}_\mu^{2l+1}; \mathcal{I}). \quad (2.31)
 \end{aligned}$$

Inserting this into Eq. (2.30), we get

$$\frac{\dot{Q}_c(\mathcal{I})}{\dot{Q}_c(\mathcal{J})} = 1 + \frac{\sum_{\mu=1}^M \sum_{l=1}^{N_C-1} \mathcal{A}(\vec{\mathcal{T}}_\mu^{2l+1}; \mathcal{I})}{\sum_{\mu=1}^M \sum_{n=1}^N \mathcal{A}(\vec{\mathcal{T}}_\mu^n; \mathcal{I})}. \quad (2.32)$$

As the quotient in the previous equation is lower or equal than 1 (since $N_C < N$), the ratio between heat currents fulfill the following inequality

$$1 \leq \frac{\dot{Q}_c(\mathcal{I})}{\dot{Q}_c(\mathcal{J})} \leq 2. \quad (2.33)$$

Hence, the addition of triangle circuits results in an increment of the cooling power. Interestingly, this boosting is not unlimited since the ratio (2.33) is upper bounded.

In order to understand in simple terms the Eq. (2.33), we consider the limit of vanishing circuit affinities (2.25). Within this regime, the rates do not depend on the orientation $W_{nm}^{\alpha nm} = W_{mn}^{\alpha mn}$ and, as a consequence, a maximal tree oriented to different vertices corresponds to the same algebraic value: $\mathcal{A}(\vec{\mathcal{T}}_\mu^n; \mathcal{I}) \equiv \mathcal{A}(\vec{\mathcal{T}}_\mu; \mathcal{I})$, $\forall n$. Assuming this, Eq. (2.32) can be written as $\dot{Q}_c(\mathcal{I})/\dot{Q}_c(\mathcal{J}) = 1 + (N_C - 1)/N = (3N - 3)/(2N) = 3N_C/V$. Note that $N_C = N_3$ for this graph, where N_3 is the total number of triangles. The topological parameter $\tau_3 = N_3/V$ indicates on average the number of triangles whereby each state participates. Such parameter describes the *device connectivity*. In the graph \mathcal{I} , it reaches a constant value in the large V limit and, consequently, the heat current enhancement also saturates in the regime under consideration.

In the article included in Sec. 5.3 we analyze more general settings built by using triangles with fixed rates for each bath. It is shown that the heat current boosting is also described by the parameter τ_3 . Such schemes do not contain non useful circuits. Given a number of vertices, increasing the number of triangles is equivalent to the addition of new edges which, in turn, leads to an increment in the *device connectivity*. Therefore, it is a key factor to take into account when designing optimal machines.

Este documento incorpora firma electrónica, y es copia auténtica de un documento electrónico archivado por la ULL según la Ley 39/2015.
 Su autenticidad puede ser contrastada en la siguiente dirección <https://sede.ull.es/validacion/>

Identificador del documento: 2111210 Código de verificación: lZvvKBaU

Firmado por: Javier Onam González López
 UNIVERSIDAD DE LA LAGUNA

Fecha: 09/09/2019 11:04:42

Daniel Alonso Ramírez
 UNIVERSIDAD DE LA LAGUNA

11/09/2019 14:53:47

2.6.3 Graph \mathcal{H}

The graph \mathcal{H} , see Fig. 2.7(a), contains trivial components, for example the four-edge circuit shown in Fig. 2.5(c), and useful components such as the triangle depicted in Fig. 2.5(a). Remarkably, the graph also contains useful circuits with more than three edges. In principle, from a conventional master equation perspective it is not straightforward to find out whether \mathcal{H} provides generally a larger cooling power than \mathcal{I} . However, the graph approach gives a direct answer: \mathcal{H} has more number of triangles per vertex than \mathcal{I} and, as a result, the choice of \mathcal{H} is more convenient to obtain larger currents. Note that \mathcal{H} has also a limited connectivity which leads to a saturation of this enhancement. Machines with non limited connectivity are studied in the paper included in Sec. 5.3. As shown in Fig. 2.8, the behavior of the heat currents is well described by τ_3 in typical regimes of the parameters.

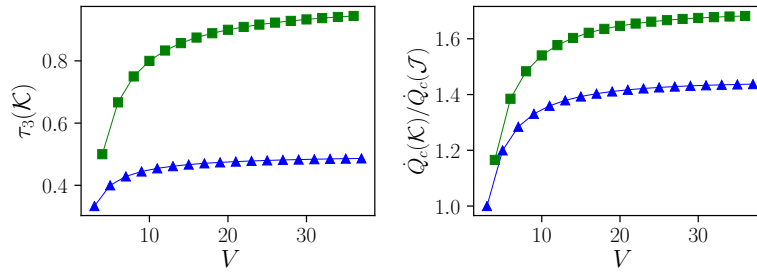


Figure 2.8: Parameter τ_3 and cooling power \dot{Q}_c as functions of the number of vertices V . The blue triangles and green squares correspond to $\mathcal{K} = \mathcal{I}, \mathcal{H}$ respectively. The topological parameters have simple analytical expressions: $\tau_3(\mathcal{I}) = (V - 1)/(2V)$ with $V = 3, 5, 7, \dots$ and $\tau_3(\mathcal{H}) = (V - 2)/V$ with $V = 4, 6, 8, \dots$. The set of parameters is: $\omega_h = 1$, $\omega_c = 0.5$, $\Delta = 0$, $T_c = 5$, $T_h = 6$, $T_w = 7$, $d_c = d_h = d_w = 1$, $\gamma_c = \gamma_h = \gamma_w = 10^{-6}$ and $\hbar = k_B = \omega_0 = 1$.

Este documento incorpora firma electrónica, y es copia auténtica de un documento electrónico archivado por la ULL según la Ley 39/2015.
 Su autenticidad puede ser contrastada en la siguiente dirección <https://sede.ull.es/validacion/>

Identificador del documento: 2111210 Código de verificación: lZvvKBaU

Firmado por: Javier Onam González López
 UNIVERSIDAD DE LA LAGUNA

Fecha: 09/09/2019 11:04:42

Daniel Alonso Ramírez
 UNIVERSIDAD DE LA LAGUNA

11/09/2019 14:53:47

Chapter 3

Periodically driven machines

3.1 Periodically driven three-level machine

In this chapter we use the well known periodically driven three-level device [75, 11], see Fig. 3.1, as a benchmark model to compare different master equation approaches. The system S consists of three states $|1\rangle$, $|2\rangle$ and $|3\rangle$. The bare system Hamiltonian is $\hat{H}_S^0 = \sum_{n=1}^3 E_n |n\rangle\langle n|$, with energies $E_1 = 0$, $E_2 = \hbar\omega_c$ and $E_3 = \hbar\omega_h$. S is coupled to a cold and a hot bath, B_c and B_h , at temperatures T_c and $T_h > T_c$ respectively. The bath Hamiltonians \hat{H}_{B_α} ($\alpha = c, h$) are given by Eq. (2.1). Besides, the system-bath interactions are $\hat{H}_{SB_\alpha} = \hat{A}^\alpha \otimes \hat{B}^\alpha$, with coupling operators $\hat{A}^c = |1\rangle\langle 2| + |2\rangle\langle 1|$ and $\hat{A}^h = |1\rangle\langle 3| + |3\rangle\langle 1|$. The bath operators \hat{B}^α are given in Eq. (2.5). The system is coupled to a laser field that acts as a work source. This time-dependent coupling is described by the following Hamiltonian

$$\hat{H}_S^w(t) = \hbar\lambda [|2\rangle\langle 3| e^{i\omega_L t} + |3\rangle\langle 2| e^{-i\omega_L t}], \quad (3.1)$$

where ω_L is the laser frequency. We consider the resonant case, i.e. $\omega_L = \omega_h - \omega_c$. The coupling constant λ is associated with the interaction between the driving field and the system. Thus, the system Hamiltonian $H_S(t)$ becomes

$$\hat{H}_S(t) = \hat{H}_S^0 + \hat{H}_S^w(t). \quad (3.2)$$

The total Hamiltonian \hat{H} of the machine has five contributions

$$\hat{H} = \hat{H}_S(t) + \hat{H}_{B_c} + \hat{H}_{B_h} + \hat{H}_{SB_c} + \hat{H}_{SB_h}. \quad (3.3)$$

Este documento incorpora firma electrónica, y es copia auténtica de un documento electrónico archivado por la ULL según la Ley 39/2015.
 Su autenticidad puede ser contrastada en la siguiente dirección <https://sede.ull.es/validacion/>

Identificador del documento: 2111210 Código de verificación: lZvvKBaU

Firmado por: Javier Onam González López
 UNIVERSIDAD DE LA LAGUNA

Fecha: 09/09/2019 11:04:42

Daniel Alonso Ramírez
 UNIVERSIDAD DE LA LAGUNA

11/09/2019 14:53:47

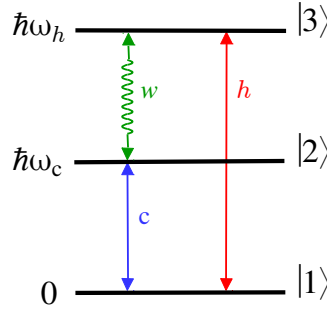


Figure 3.1: Schematic representation of the periodically driven three-level device. The vertical blue and red arrows correspond to the transitions coupled with the cold (c) and hot (h) baths. The curly green arrow indicates that the level $|3\rangle$ is coupled with the state $|2\rangle$ through a periodic laser field labeled with w .

Four different time scales play a role in the evolution of the Hamiltonian (3.3): the scale related to the bare system $\tau_S^0 \sim |\omega_\alpha|^{-1}$, the characteristic time of the baths $\tau_B \sim \hbar/k_B T_\alpha$, the time scale of the interaction between system and baths $\tau_{SB} \sim \gamma_\alpha^{-1}$ and finally, the scale associated with the influence of the driving field $\tau_S^w \sim \lambda^{-1}$. We assume that the conditions $\tau_{SB} \gg \tau_S^0$ and $\tau_{SB} \gg \tau_B$ are valid. This guarantees the existence of a master equation to describe the steady state operation of the machine, see Appendix A. In this regime, the coupling constants γ_α are very small in comparison with the temperatures of the baths and the frequency gaps in the system. On the other hand, depending on the magnitude of the coupling strength λ the structure of this master equation can be different. In the following, we study both the strong and weak driving limit, $\lambda \gg \gamma_\alpha$ and $\lambda \ll \gamma_\alpha$. We use a Global or a Local approach to obtain the master equations in each case. The thermodynamic consistency of these two approaches is guaranteed. The corresponding stationary populations are described by proper balance equations. Thus, we can employ the consistent decomposition (2.23) to calculate the heat currents. The power can then be obtained by resorting energy conservation. For comparison purposes, we consider another approach based on the Redfield master equation. In this case, the consistency with the Laws of

Thermodynamics is not ensured.

3.2 Redfield approach

The Redfield master equation allows us to characterize the functioning of the device for any value of the strength with the driving field. In the Appendix A we briefly describe the procedure leading to such equation. We take advantage of the fact that the evolution operator for this system can be written as $\hat{U}_S(t) = e^{-i\hat{A}_1 t/\hbar} e^{-i\hat{A}_2 t/\hbar}$, with $\hat{A}_1 = \hat{H}_S^0$ and $\hat{A}_2 = \hat{H}_S^w(t=0)$. Note that this choice verifies the Schrodinger equation $i\hbar \frac{d\hat{U}_S(t)}{dt} = (\hat{H}_S^0 + \hat{H}_S^w(t)) \hat{U}_S(t)$. Thus, we can pick a rotating frame characterized by a master equation with no explicit time dependence [76, 77, 59, 41, 40]

$$\frac{d\hat{\rho}_S}{dt} = -\frac{i}{\hbar}[\hat{A}_2, \hat{\rho}_S] + \mathcal{R}_c\{\hat{\rho}_S\} + \mathcal{R}_h\{\hat{\rho}_S\}, \quad (3.4)$$

where $\hat{\rho}_S$ is the system density matrix in the rotating frame. The dissipative terms are given by

$$\mathcal{R}_\alpha\{\hat{\rho}_S\} = \mathcal{L}_\alpha\{\hat{\rho}_S\} + \mathcal{S}_\alpha\{\hat{\rho}_S\} \quad (3.5)$$

with

$$\begin{aligned} \mathcal{S}_\alpha\{\hat{\rho}_S\} = & \left(\frac{\Gamma_{\omega_\alpha+\lambda}^\alpha + \Gamma_{\omega_\alpha-\lambda}^\alpha}{4} \right) \left(|1\rangle\langle+|\hat{\rho}_S|-\rangle\langle 1| + |1\rangle\langle-|\hat{\rho}_S|+\rangle\langle 1| \right) \\ & + \left(\frac{\Gamma_{-(\omega_\alpha+\lambda)}^\alpha + \Gamma_{-(\omega_\alpha-\lambda)}^\alpha}{4} \right) \left(|+\rangle\langle 1|\hat{\rho}_S|1\rangle\langle-| + |-\rangle\langle 1|\hat{\rho}_S|1\rangle\langle+| \right) \\ & - \frac{\Gamma_{\omega_\alpha+\lambda}^\alpha}{4} \left(|-\rangle\langle+|\hat{\rho}_S + \hat{\rho}_S|+\rangle\langle-| \right) - \frac{\Gamma_{\omega_\alpha-\lambda}^\alpha}{4} \left(|+\rangle\langle-|\hat{\rho}_S + \hat{\rho}_S|-\rangle\langle+| \right) \end{aligned} \quad (3.6)$$

and

$$\begin{aligned} \mathcal{L}_\alpha\{\hat{\rho}_S\} = & \frac{\Gamma_{\omega_\alpha+\lambda}^\alpha}{2} \left(|1\rangle\langle+|\hat{\rho}_S|+\rangle\langle 1| - \frac{1}{2}|+\rangle\langle+|\hat{\rho}_S - \frac{1}{2}\hat{\rho}_S|+\rangle\langle+| \right) \\ & + \frac{\Gamma_{-(\omega_\alpha+\lambda)}^\alpha}{2} \left(|+\rangle\langle 1|\hat{\rho}_S|1\rangle\langle+| - \frac{1}{2}|1\rangle\langle 1|\hat{\rho}_S - \frac{1}{2}\hat{\rho}_S|1\rangle\langle 1| \right) \\ & + \frac{\Gamma_{\omega_\alpha-\lambda}^\alpha}{2} \left(|1\rangle\langle-|\hat{\rho}_S|-\rangle\langle 1| - \frac{1}{2}|-\rangle\langle-|\hat{\rho}_S - \frac{1}{2}\hat{\rho}_S|-\rangle\langle-| \right) \\ & + \frac{\Gamma_{-(\omega_\alpha-\lambda)}^\alpha}{2} \left(|-\rangle\langle 1|\hat{\rho}_S|1\rangle\langle-| - \frac{1}{2}|1\rangle\langle 1|\hat{\rho}_S - \frac{1}{2}\hat{\rho}_S|1\rangle\langle 1| \right). \end{aligned} \quad (3.7)$$

Este documento incorpora firma electrónica, y es copia auténtica de un documento electrónico archivado por la ULL según la Ley 39/2015.
 Su autenticidad puede ser contrastada en la siguiente dirección <https://sede.ull.es/validacion/>

Identificador del documento: 2111210 Código de verificación: lZvvKBaU

Firmado por: Javier Onam González López
 UNIVERSIDAD DE LA LAGUNA

Fecha: 09/09/2019 11:04:42

Daniel Alonso Ramírez
 UNIVERSIDAD DE LA LAGUNA

11/09/2019 14:53:47

The label α takes values c and h , the functions Γ_{ω}^{α} are given in Eq. (2.11) and $|\pm\rangle = \frac{1}{\sqrt{2}}(|2\rangle \pm |3\rangle)$ are the eigenstates of A_2 . Note that the super-operators \mathcal{S}_{α} include non secular terms, while \mathcal{L}_{α} are Lindblad or Secular super-operators. In the Appendix A we show the expressions for the heat currents and power corresponding to this approach. In the following Secs. 3.3 and 3.4 we describe the global and local approaches, which can be obtained from the Redfield equation (3.4). In Fig. 3.2 we plot the cooling power as a function of λ for the three different master equation approaches. As expected, the Global and Redfield equations coincide when the driving strength is strong enough. At $\lambda \sim \gamma_{\alpha}$, the differences between these approaches become significant. On the other hand, the Local and Redfield master approaches coincide in the weak driving regime and beyond. For example, when $\lambda \sim 1000\gamma_h$ both the Local and Global master equations reproduces the Redfield currents. Fig. 3.3 illustrates the regimes of applicability of the different master equation approaches.

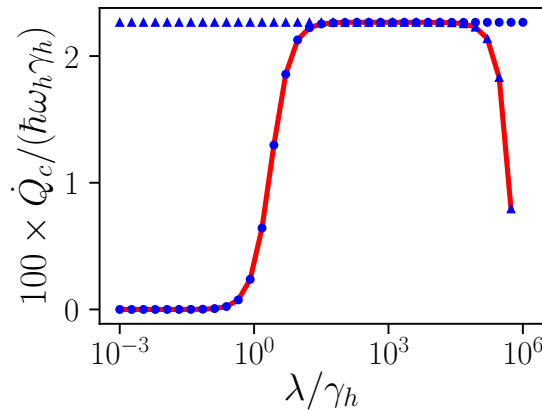


Figure 3.2: Cooling power against the coupling strength of the laser field. The blue triangles, blue dots and red solid line correspond to the Global, Local and Redfield approach. The parameters are $\omega_h = 1$, $\omega_c = 0.2$, $T_c = 4$, $T_h = 5$, $d_c = d_h = 1$, $\gamma_c = \gamma_h = 10^{-6}$ and $\hbar = k_B = \omega_0 = 1$.

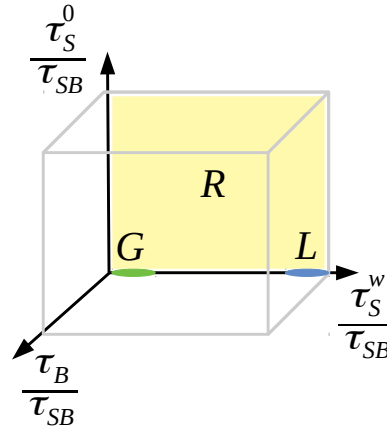


Figure 3.3: Schematic representation of the parameter regimes for which the different master equations can be employed to calculate the currents in the resonant three-level model. We represent a cube with sides of infinite length. The axes are τ_B/τ_{SB} , τ_S^w/τ_{SB} and τ_S^0/τ_{SB} with $\tau_{SB} \sim \gamma_\alpha^{-1}$, $\tau_B \sim \hbar/k_B T_\alpha$, $\tau_S^0 \sim |\omega_\alpha|^{-1}$ and $\tau_S^w \sim \lambda^{-1}$. The yellow, green and blue areas correspond to the regimes of validity of the Redfield, Global and Local approach (labelled by R , G and L).

3.3 Global approach

In this section we explore the strong coupling limit, $\lambda \gg \gamma_\alpha$. Within this regime, the use of a Global master equation is well justified [54, 53, 78]. In the Appendix A we discuss the procedure to find this master equation. The Global master equation for the three-level machine is obtained from Eq. (3.4) by removing the non secular terms

$$\frac{d\hat{\rho}_S}{dt} = -\frac{i}{\hbar}[\hat{A}_2, \hat{\rho}_S] + \mathcal{L}_e\{\hat{\rho}_S\} + \mathcal{L}_h\{\hat{\rho}_S\}. \quad (3.8)$$

The term global indicates that the Lindblad operators (3.7) are not only given in terms of parameters of the baths, since they also contain information about the driving field. The following population dynamics is obtained when taking

Este documento incorpora firma electrónica, y es copia auténtica de un documento electrónico archivado por la ULL según la Ley 39/2015.
 Su autenticidad puede ser contrastada en la siguiente dirección <https://sede.ull.es/validacion/>

Identificador del documento: 2111210 Código de verificación: lZvvKBaU

Firmado por: Javier Onam González López
 UNIVERSIDAD DE LA LAGUNA

Fecha: 09/09/2019 11:04:42

Daniel Alonso Ramírez
 UNIVERSIDAD DE LA LAGUNA

11/09/2019 14:53:47

diagonal projections in Eq. (3.8)

$$\frac{d}{dt} \begin{bmatrix} p_1 \\ p_+ \\ p_- \end{bmatrix} = \sum_{\alpha=c,h} \mathbf{W}^\alpha \begin{bmatrix} p_1 \\ p_+ \\ p_- \end{bmatrix}, \quad (3.9)$$

with $p_n = \langle n | \hat{\rho}_S | n \rangle$, $n = 1, +, -$. \mathbf{W}^α is a matrix of rates related to the bath B_α whose non diagonal elements W_{nm}^α are

$$W_{1\pm}^\alpha = \frac{\Gamma_{\omega_\alpha \pm \lambda}^\alpha}{2}, \quad W_{\pm 1}^\alpha = \frac{\Gamma_{-(\omega_\alpha \pm \lambda)}^\alpha}{2}, \quad W_{+-}^\alpha = W_{-+}^\alpha = 0. \quad (3.10)$$

Note that these rates fulfill detailed balance relations

$$\frac{W_{\pm 1}^\alpha}{W_{1\pm}^\alpha} = e^{-\frac{\hbar(\omega_\alpha \pm \lambda)}{k_B T_\alpha}}. \quad (3.11)$$

The diagonal elements of \mathbf{W}^α satisfy an expression analogous to Eq. (2.22).

3.3.1 Internal components

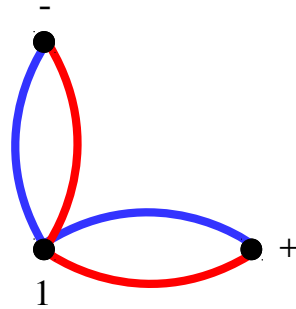


Figure 3.4: Graph \mathcal{K} representing the balance equations (3.9) corresponding to the three-level machine shown in Fig. 3.1. The blue and red edges are associated with B_c and B_h respectively.

The population dynamics (3.9) is a proper set of balance equations. This allows us to employ a graph representation to calculate the stationary thermodynamic magnitudes. In Fig. 3.4 we show the graph \mathcal{K} representing these balance equations. \mathcal{K} has two circuits \mathcal{C}_+ and \mathcal{C}_- , which connects vertices $\{1, +\}$ and $\{1, -\}$ respectively. We can use Eq. (2.24) to determine the stationary circuit currents

$$\dot{q}_\alpha(\mathcal{C}_\pm) = s_\alpha \frac{-T_\alpha X^\alpha(\vec{\mathcal{C}}_\pm)}{8} \frac{(\Gamma_{\omega_c \mp \lambda}^c + \Gamma_{\omega_h \mp \lambda}^h)}{D} \left[\Gamma_{-(\omega_c \pm \lambda)}^c \Gamma_{\omega_h \pm \lambda}^h - \Gamma_{-(\omega_h \pm \lambda)}^h \Gamma_{\omega_c \pm \lambda}^c \right], \quad (3.12)$$

where the factor D that contains the maximal trees of \mathcal{K} reads

$$D = \frac{1}{4} \left[\Gamma_{-(\omega_c - \lambda)}^c \Gamma_{\omega_c + \lambda}^c + \Gamma_{-(\omega_c - \lambda)}^c \Gamma_{\omega_h + \lambda}^h + \Gamma_{-(\omega_c + \lambda)}^c \Gamma_{\omega_c - \lambda}^c + \Gamma_{-(\omega_c + \lambda)}^c \Gamma_{\omega_h - \lambda}^h \right. \\ \left. + \Gamma_{\omega_c - \lambda}^c \Gamma_{\omega_c + \lambda}^c + \Gamma_{\omega_c - \lambda}^c \Gamma_{-(\omega_h - \lambda)}^h + \Gamma_{\omega_c - \lambda}^c \Gamma_{\omega_h + \lambda}^h + \Gamma_{\omega_c + \lambda}^c \Gamma_{-(\omega_h - \lambda)}^h \right. \\ \left. + \Gamma_{\omega_c + \lambda}^c \Gamma_{\omega_h - \lambda}^h + \Gamma_{-(\omega_h - \lambda)}^h \Gamma_{\omega_h - \lambda}^h + \Gamma_{-(\omega_h - \lambda)}^h \Gamma_{\omega_h + \lambda}^h + \Gamma_{\omega_h - \lambda}^h \Gamma_{\omega_h + \lambda}^h \right]. \quad (3.13)$$

The coefficients s_c and s_h are respectively 1 and -1 . The circuit affinities are $-T_\alpha X^\alpha(\vec{\mathcal{C}}_\pm) = \hbar(\omega_\alpha \pm \lambda)$. We can define the circuit power $p(\mathcal{C}_\pm)$ by invoking energy conservation

$$p(\mathcal{C}_\pm) = -\dot{q}_c(\mathcal{C}_\pm) - \dot{q}_h(\mathcal{C}_\pm). \quad (3.14)$$

Therefore, the total stationary heat currents and power performed by the field are $\dot{Q}_\alpha \equiv \dot{Q}_\alpha(\mathcal{K}) = \dot{q}_\alpha(\mathcal{C}_+) + \dot{q}_\alpha(\mathcal{C}_-)$ and $P \equiv P(\mathcal{K}) = p(\mathcal{C}_+) + p(\mathcal{C}_-)$. Remarkably, these currents coincide with those that are defined in the Appendix A.

According to Eq. (3.12), both \mathcal{C}_+ and \mathcal{C}_- can either work as refrigerators, $\{\dot{q}_c(\mathcal{C}_\pm) > 0, \dot{q}_h(\mathcal{C}_\pm) < 0, p(\mathcal{C}_\pm) > 0\}$, or engines, $\{\dot{q}_c(\mathcal{C}_\pm) < 0, \dot{q}_h(\mathcal{C}_\pm) > 0, p(\mathcal{C}_\pm) < 0\}$. The cooling window of \mathcal{C}_\pm is $\omega_c < \omega_h \frac{T_c}{T_h} \mp \lambda \frac{T_h - T_c}{T_h}$. Hence, \mathcal{C}_+ and \mathcal{C}_- can be classified as useful components associated with energy exchanges between the three environments, i. e. the two baths and the work source. Besides, they do not reach the reversible limit for the same parameters. This competition between useful components is the mechanism that prevents the device depicted in Fig. 3.1 from reaching the Carnot limit [14, 33].

More complicated schemes of periodically driven machines are described in the article included in Sec. 5.1. In general, we can distinguish four types of components:

- $X^\alpha(\vec{\mathcal{C}}_\nu) = 0, \forall \alpha \Rightarrow \mathcal{C}_\nu$ is a trivial circuit.

- $X^{\alpha_1}(\vec{C}_\nu) \neq 0$ and $X^{\alpha_2}(\vec{C}_\nu) = 0 \Rightarrow C_\nu$ is a non useful component related to power dissipation into the bath B_{α_1} .
- $X^c(\vec{C}_\nu), X^h(\vec{C}_\nu) \neq 0$ and $T_c X^c(\vec{C}_\nu) + T_h X^h(\vec{C}_\nu) = 0 \Rightarrow C_\nu$ is a non useful component corresponding to a heat leak from B_h into B_c .
- $X^\alpha(\vec{C}_\nu) \neq 0, \forall \alpha$ and $T_c X^c(\vec{C}_\nu) + T_h X^h(\vec{C}_\nu) \neq 0 \Rightarrow C_\nu$ is a three-environment component. This category includes the useful components that can operate as refrigerators or engines, at least in some parameter regimes.

Finally, it is important to stress that the balance equations (3.9) are completely analogous to those that arise naturally in the study of stochastic-thermodynamic models [65]. The rates in these expressions are positive and, therefore, they can be classically interpreted as transition probabilities. Thus, it is always possible to find a classical stochastic-thermodynamic emulator capable of replicating the steady state functioning of the device.

3.4 Local approach

We analyze here the three-level model shown in Fig. 3.1 in the weak driving regime, $\gamma_\alpha \gg \lambda$. In this limit the use of a local master equation is well justified [54, 53, 78]. The term local indicates that the dissipation is described without taking into account the influence of the driving field, see Appendix A. Such equation reads

$$\frac{d\hat{\rho}_S}{dt} = -\frac{i}{\hbar}[\hat{A}_2, \hat{\rho}_S] + \mathcal{L}_c^0\{\hat{\rho}_S\} + \mathcal{L}_h^0\{\hat{\rho}_S\}, \quad (3.15)$$

where the Lindblad super-operators are

$$\begin{aligned} \mathcal{L}_c^0\{\hat{\rho}_S\} &= \Gamma_{\omega_c}^c \left(|1\rangle\langle 2|\hat{\rho}_S|2\rangle\langle 1| - \frac{1}{2}|2\rangle\langle 2|\hat{\rho}_S - \frac{1}{2}\hat{\rho}_S|2\rangle\langle 2| \right) \\ &+ \Gamma_{-\omega_c}^c \left(|2\rangle\langle 1|\hat{\rho}_S|1\rangle\langle 2| - \frac{1}{2}|1\rangle\langle 1|\hat{\rho}_S - \frac{1}{2}\hat{\rho}_S|1\rangle\langle 1| \right) \end{aligned} \quad (3.16)$$

and

$$\begin{aligned} \mathcal{L}_h^0\{\hat{\rho}_S\} &= \Gamma_{\omega_h}^h \left(|1\rangle\langle 3|\hat{\rho}_S|3\rangle\langle 1| - \frac{1}{2}|3\rangle\langle 3|\hat{\rho}_S - \frac{1}{2}\hat{\rho}_S|3\rangle\langle 3| \right) \\ &+ \Gamma_{-\omega_h}^h \left(|3\rangle\langle 1|\hat{\rho}_S|1\rangle\langle 3| - \frac{1}{2}|1\rangle\langle 1|\hat{\rho}_S - \frac{1}{2}\hat{\rho}_S|1\rangle\langle 1| \right). \end{aligned} \quad (3.17)$$

Este documento incorpora firma electrónica, y es copia auténtica de un documento electrónico archivado por la ULL según la Ley 39/2015.
 Su autenticidad puede ser contrastada en la siguiente dirección <https://sede.ull.es/validacion/>

Identificador del documento: 2111210 Código de verificación: lZvvKBaU

Firmado por: Javier Onam González López
 UNIVERSIDAD DE LA LAGUNA

Fecha: 09/09/2019 11:04:42

Daniel Alonso Ramírez
 UNIVERSIDAD DE LA LAGUNA

11/09/2019 14:53:47

The functions Γ_ω^α are expressed in Eq. (2.11).

The population and coherence dynamics resulting from Eq. (3.15) are not decoupled. In fact, unlike in the strong driving limit, the population dynamics can not be interpreted as a set of balance equations at finite times. However, in the long time limit we can write the stationary coherences as functions of the populations. This procedure leads to a matrix equation $\mathbf{W} [p_1, p_2, p_3]^T = 0$. The non diagonal elements $W_{nm} = W_{nm}^{\alpha nm}$ of this matrix \mathbf{W} are

$$\begin{aligned}
 W_{12}^c &= \Gamma_{\omega_c}^c ; W_{21}^c = \Gamma_{-\omega_c}^c ; \\
 W_{13}^h &= \Gamma_{\omega_h}^h ; W_{31}^h = \Gamma_{-\omega_h}^h ; \\
 W_{23}^w &= W_{32}^w = \frac{4\lambda^2}{\Gamma_{\omega_c}^c + \Gamma_{\omega_h}^h} .
 \end{aligned} \tag{3.18}$$

The matrix \mathbf{W} is singular since it fulfills an expression analogous to Eq. (2.22). The rates associated with the driving field W_{23}^w and W_{32}^w satisfy a detailed balance relation with an effective infinite temperature.

3.4.1 Internal component

The structure of the matrix \mathbf{W} ensures the conservation of the probability. Besides, its non diagonal elements fulfill detailed balance relations with respect to the baths or the driving field. Therefore, we can build a graph representation corresponding to this matrix and, most importantly, use a circuit decomposition to describe the associated stationary functioning. In Fig. 3.5, we show the graph \mathcal{J} representing the matrix \mathbf{W} . \mathcal{J} consists of one circuit, the triangle \mathcal{C}_1 . Using Eq. (2.24) we can determine the corresponding heat currents. The same result can be obtained by using the definitions of currents provided in the Appendix A. The calculation of the circuit affinity (2.25) reveals that \mathcal{C}_1 is an useful component with cooling window $\omega_c < \omega_h \frac{T_c}{T_h}$.

In order to consider \mathbf{W} a matrix of rates that can be classically interpreted, we need to ensure that its non diagonal elements are positive definite. According to Eq. (3.18), all the rates are always positive. Thus, we can interpret the contribution of \mathcal{C}_1 within a classical stochastic-thermodynamic perspective, i.e. the device has a well defined classical emulator. Note that such emulator has the same thermal coupling than the original system. However, the coupling with the work source is weaker, see Eq. (3.18). In the article included in Sec. (5.4), a general scheme of a periodically driven device with a cyclic pattern of transitions is analyzed. The three-level is just a particular instance of this general configuration. It is shown that such kind

Este documento incorpora firma electrónica, y es copia auténtica de un documento electrónico archivado por la ULL según la Ley 39/2015.
 Su autenticidad puede ser contrastada en la siguiente dirección <https://sede.ull.es/validacion/>

Identificador del documento: 2111210 Código de verificación: lZvvKBaU

Firmado por: Javier Onam González López
 UNIVERSIDAD DE LA LAGUNA

Fecha: 09/09/2019 11:04:42

Daniel Alonso Ramírez
 UNIVERSIDAD DE LA LAGUNA

11/09/2019 14:53:47

of machine needs non-zero stationary coherences (between the levels coupled with the field) to provide non-zero currents. However, the presence of coherence should not be considered essential to replicate the same thermodynamic behavior since, as we have seen, the device is classically emulable.

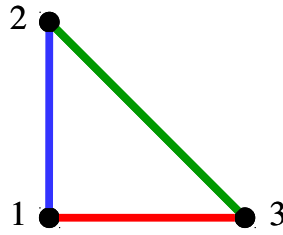


Figure 3.5: Graph \mathcal{J} resulting from the matrix \mathbf{W} with non diagonal elements given in Eq. (3.18). The colors blue, red and green correspond to a coupling with the cold bath, the hot reservoir and the laser field respectively.

3.4.2 Classicality criteria

Let us compare the dephasing criterion [58, 79] with the previous discussion about classical emulability. When adding a dephasing term $-k_d [\hat{H}_S^0, [\hat{H}_S^0, \hat{\rho}_S]]$ to Eq. (3.15), the rate related to the work source becomes

$$W_{23}^w = W_{32}^w = \frac{4\lambda^2}{\Gamma_{\omega_c}^c + \Gamma_{\omega_h}^h + \hbar^2(\omega_h - \omega_c)^2 k_d}, \quad (3.19)$$

while the other rates associated with the baths remain unaltered. In the limit of large enough k_d , W_{23}^w is vanishing and the graph 3.5 losses the connection between the vertices 2 and 3. The corresponding currents and power are then zero. Thus, the addition of strong dephasing precludes the machine from performing any useful thermodynamic task. The dephasing criterion indicates that stationary coherences between the states $|2\rangle$ and $|3\rangle$ are necessary for the device functioning. However, we have shown that a classical stochastic model can emulate the same steady state operation without using quantum features. Therefore, the dephasing criterion is capable of identifying quantum magnitudes that are essential in the operation, but these quantities do not lead to any advantage from a thermodynamic perspective.

Este documento incorpora firma electrónica, y es copia auténtica de un documento electrónico archivado por la ULL según la Ley 39/2015.
 Su autenticidad puede ser contrastada en la siguiente dirección <https://sede.ull.es/validacion/>

Identificador del documento: 2111210 Código de verificación: lZvvKBaU

Firmado por: Javier Onam González López
 UNIVERSIDAD DE LA LAGUNA

Fecha: 09/09/2019 11:04:42

Daniel Alonso Ramírez
 UNIVERSIDAD DE LA LAGUNA

11/09/2019 14:53:47

Chapter 4

Conclusions

We have studied the stationary functioning of absorption and periodically driven devices. In the limit of weak coupling with the thermal reservoirs, the thermodynamic relevant magnitudes of these machines can be analyzed by using circuit decompositions based on Graph Theory. Each circuit in such decompositions is consistent with the Laws of Thermodynamics. Thus, circuits could be view as internal components describing the device operation in the steady state. The strong point of this approach lies in its potential for interpreting results. This knowledge can be employed to build clever designs of thermal machines by avoiding contributions of non useful components.

Although we focus on the analysis of quantum thermodynamic devices, circuit decompositions can be used to describe the behavior of any other balance equation system, including stochastic-thermodynamic models. In fact, different physical implementations may lead to the same graph, which in turn implies equivalent equations for the population dynamics. The particularities of each implementation are then associated with the values of the rates and their dependence with the device parameters. Hence, the study of the properties of circuits decompositions in generic graphs becomes itself an interesting issue, since it allows for obtaining model independent results based on the topology of the graphs.

In the previous chapters, we have considered some benchmark models of continuous devices for readability and for pedagogical purposes. From this work, two main conclusions can be drawn. The first one is that, rather than the number of internal components, the *device connectivity* is a limiting factor for the magnitude of the stationary currents. In Chapter 2, we discuss this issue for absorption machines but the result is easily extensible to other setups, such as periodically driven devices. The second result concerns the interpretation of the processes that impede the attainment of the reversible limit in continuous devices, in terms of their internal components. Basically,

Este documento incorpora firma electrónica, y es copia auténtica de un documento electrónico archivado por la ULL según la Ley 39/2015.
Su autenticidad puede ser contrastada en la siguiente dirección <https://sede.ull.es/validacion/>

Identificador del documento: 2111210 Código de verificación: lZvvKBaU

Firmado por: Javier Onam González López
UNIVERSIDAD DE LA LAGUNA

Fecha: 09/09/2019 11:04:42

Daniel Alonso Ramírez
UNIVERSIDAD DE LA LAGUNA

11/09/2019 14:53:47

there are three kinds of internal components: trivial, useful and non useful components. The currents associated with the trivial components are zero. On the other hand, the operation mode of the useful components may be the same, at least in some parameter regimes, as the one in the overall device. Therefore, the useful components are related to thermodynamic mechanisms involving all the environments, i. e. baths and work source. Finally, the non useful components are related to undesired energy transport between only two environments, for example heat leaks between baths or dissipation of power into a bath. This classification enables us to distinguish two particular mechanisms: the competition of useful components with opposite operation modes and the undesired contributions of the non useful components. A machine presenting at least one of these mechanisms cannot achieve the reversible limit of maximum efficiency or coefficient of performance. As a corollary, designs with larger currents and capable of reaching the Carnot limit should be built by considering as many useful components as possible, without leading to the competition between them or to the emergence of non useful components.

We have taken advantage of the connection between the conventional master equation approach and a stochastic-thermodynamic perspective. We show that absorption and cyclic periodically driven devices, both with non-degenerate energy levels, are completely analogous to stochastic models when the coupling to the baths is weak enough. Both fulfill proper balance equations that can be interpreted from a classical stochastic picture, i. e. in term of positive transition probabilities. Hence, there exist classical emulators describing the stationary functioning of these devices. However, the existence of a classical emulator is not guaranteed in devices with a non-cyclic pattern of transitions that are weakly coupled to the driving field. The search for indicators of genuine quantumness in such machines is an interesting open issue.

Remarkably, the scope of the present work is limited to the regime of weak coupling to the baths. Under this assumption, some interesting concepts such as internal components have been defined. A subject of future work will be the search for alternative concepts when this coupling becomes stronger. These alternative concepts should be introduced within a thermodynamic consistent framework, which is a challenge in itself.

Este documento incorpora firma electrónica, y es copia auténtica de un documento electrónico archivado por la ULL según la Ley 39/2015.
Su autenticidad puede ser contrastada en la siguiente dirección <https://sede.ull.es/validacion/>

Identificador del documento: 2111210 Código de verificación: lZvvKBaU

Firmado por: Javier Onam González López
UNIVERSIDAD DE LA LAGUNA

Fecha: 09/09/2019 11:04:42

Daniel Alonso Ramírez
UNIVERSIDAD DE LA LAGUNA

11/09/2019 14:53:47

Chapter 5

Compendium

Este documento incorpora firma electrónica, y es copia auténtica de un documento electrónico archivado por la ULL según la Ley 39/2015.
Su autenticidad puede ser contrastada en la siguiente dirección <https://sede.ull.es/validacion/>

Identificador del documento: 2111210 Código de verificación: lZvvKBaU

Firmado por: Javier Onam González López
UNIVERSIDAD DE LA LAGUNA

Fecha: 09/09/2019 11:04:42

Daniel Alonso Ramírez
UNIVERSIDAD DE LA LAGUNA

11/09/2019 14:53:47

5.1 Performance of Continuous Quantum Thermal Devices Indirectly Connected to Environments

Entropy, 18(5):166, 2016

J. Onam González, Daniel Alonso and José P. Palao

Este documento incorpora firma electrónica, y es copia auténtica de un documento electrónico archivado por la ULL según la Ley 39/2015.
Su autenticidad puede ser contrastada en la siguiente dirección <https://sede.ull.es/validacion/>

Identificador del documento: 2111210 Código de verificación: lZvvKBaU

Firmado por: Javier Onam González López
UNIVERSIDAD DE LA LAGUNA

Fecha: 09/09/2019 11:04:42

Daniel Alonso Ramírez
UNIVERSIDAD DE LA LAGUNA

11/09/2019 14:53:47



Article

Performance of Continuous Quantum Thermal Devices Indirectly Connected to Environments

J. Onam González, Daniel Alonso * and José P. Palao

Departamento de Física and IUdEA, Universidad de La Laguna, La Laguna 38204, Spain;
jgonzall@ull.es (J.O.G); jppalao@ull.es (J.P.P)

* Correspondence: dalonso@ull.es; Tel.: +34-922-318-268

Academic Editor: Ronnie Kosloff

Received: 28 March 2016; Accepted: 20 April 2016; Published: 28 April 2016

Abstract: A general quantum thermodynamics network is composed of thermal devices connected to environments through quantum wires. The coupling between the devices and the wires may introduce additional decay channels which modify the system performance with respect to the directly-coupled device. We analyze this effect in a quantum three-level device connected to a heat bath or to a work source through a two-level wire. The steady state heat currents are decomposed into the contributions of the set of simple circuits in the graph representing the master equation. Each circuit is associated with a mechanism in the device operation and the system performance can be described by a small number of circuit representatives of those mechanisms. Although in the limit of weak coupling between the device and the wire the new irreversible contributions can become small, they prevent the system from reaching the Carnot efficiency.

Keywords: quantum thermodynamics; graph theory; thermodynamic performance

PACS: 05.30.-d; 05.70.Ln; 07.20.Pe

1. Introduction

Continuous quantum thermal devices are quantum systems connected to several baths at different temperatures and to work sources [1]. Their operation is necessarily irreversible when the heat currents are non-negligible. One of the possible irreversible processes is the ubiquitous finite-rate heat transfer effect considered in endoreversible models. In these models, the control parameters can be tuned to reach the reversible limit but at vanishing energy flows. Examples are the three-level and the two-qubit absorption refrigerators [2–5]. In other models, as the power-driven three-level maser [1,6] and the three-qubit absorption refrigerators [3,7], additional irreversible processes appear such as heat leaks and internal dissipation [1,8], which are detrimental to the device performance. Several experimental realizations of these continuous quantum thermal devices have been proposed—for example, nano-mechanical oscillators or atoms interacting with optical resonators [9,10], atoms interacting with nonequilibrium electromagnetic fields [11], superconducting quantum interference devices [12], and quantum dots [13]. Furthermore, the coupling between artificial atoms and harmonic oscillators is experimentally feasible nowadays [14], opening the possibility of connecting thermal devices to environments through quantum systems.

Although the most general design of a quantum thermal network is composed of thermal devices and wires [15], the device performance has been usually analyzed assuming a direct contact with the environments. The coupling between the device and a quantum probe has been suggested to characterize the device irreversible processes [16]. In this paper, we adopt a different perspective and study the additional irreversible processes induced by the coupling between the device and the wire. In particular, we will analyze in detail the performance of a system composed of a three-level device and a

Entropy 2016, 18, 166; doi:10.3390/e18050166

www.mdpi.com/journal/entropy

Este documento incorpora firma electrónica, y es copia auténtica de un documento electrónico archivado por la ULL según la Ley 39/2015.
Su autenticidad puede ser contrastada en la siguiente dirección <https://sede.ull.es/validacion/>

Identificador del documento: 2111210

Código de verificación: lZvvKBaU

Firmado por: Javier Onam González López
UNIVERSIDAD DE LA LAGUNA

Fecha: 09/09/2019 11:04:42

Daniel Alonso Ramírez
UNIVERSIDAD DE LA LAGUNA

11/09/2019 14:53:47

two-level wire connected to a work bath or source. When the system is weakly coupled to the baths, its evolution is described by a quantum master equation in which the dynamics of the populations can be decoupled from the coherences choosing an appropriate basis [17]. This property implies the positivity of the entropy production along the system evolution [18,19], and is broken when some uncontrolled approximations are considered in the derivation of the quantum master equation [20]. The Pauli master equation for the populations (in the following simply the master equation) is a particular example of the general master equations considered in stochastic thermodynamics for systems connected to multiple reservoirs [21]. For a long enough amount of time, the system reaches a non-equilibrium steady state where the heat currents \dot{Q}_α describe the energy transfer between the system and the baths, and the power \mathcal{P} characterizes the energy exchange with the work source [15]. Although the heat currents can be obtained directly from the steady solution of the master equation, identifying the different irreversible processes contributing to them is in general a very complicated task.

An alternative approach to analyze non-equilibrium processes is the decomposition of the steady state fluxes and the entropy production in the contribution due to simple circuits [22–24], fundamental circuits [25–27] or cycles [28] of the graph representation of the master equation. We will consider a decomposition in the full set of simple circuits that combined with the all minors matrix-tree theorem [29], which leads to very simple expressions for the steady state heat currents. More importantly, each circuit can be interpreted as a thermodynamically consistent unit and its contribution to the different irreversible processes can be easily identified [30]. Although the number of circuits may be very large, we will show that the system performance can be described by means of a reduced number of circuit representatives [31].

The paper is organized as follows: Section 2 presents a brief review of the derivation of the quantum master equation for a device coupled to a heat bath through a quantum wire. Next, the graph representation of the master equation and the decomposition in simple circuits is discussed, with special emphasis on the characterization of the steady state heat currents. Some procedures to determine the set of simple circuits are described in Appendix A. The absorption refrigerator composed of a three-level device connected to a work bath through a two-level wire is studied in Section 3 and some circuit representatives are suggested to describe the system performance. The same analysis is applied to a system driven by a periodic classical field in Section 4, which includes a brief discussion of the derivation of the master equation for the time dependent Hamiltonian. In this case, we study the performance operating as a refrigerator or as an engine. Finally, we draw our conclusions in Section 5.

2. Circuit Decomposition of the Steady State Heat Currents and Entropy Production

2.1. The Master Equation

We consider a system composed of a quantum thermal device with Hamiltonian \hat{H}_D directly coupled with a cold bath and a hot bath, at temperatures T_c and T_h , and a quantum wire with Hamiltonian \hat{H}_{wire} which connects the device to an additional bath at temperature T_w (work bath). The situation in which the system is driven instead by a work source will be discussed in Section 4. The total Hamiltonian reads

$$\hat{H} = \hat{H}_D + \hat{H}_{D,wire} + \hat{H}_{wire} + \hat{H}_{wire,w} + \hat{H}_w + \sum_{\alpha=c,h} (\hat{H}_{D,\alpha} + \hat{H}_\alpha), \quad (1)$$

where $\hat{H}_{D,wire}$ is the coupling between the device and the wire, $\hat{H}_{D,\alpha}$ and $\hat{H}_{wire,w}$ the coupling terms of the device and the wire with the baths, and \hat{H}_α the bath Hamiltonians. We assume that the coupling terms of the system with the baths are $\sqrt{\gamma_\alpha} \hbar \hat{S}^\alpha \otimes \hat{B}^\alpha$, where \hat{S}^α is a device or wire Hermitian operator, \hat{B}^α is a bath operator and γ_α characterizes the coupling strength.

If the system is weakly coupled with the baths and its relaxation time scale is slow compared with the correlation times of the baths, the system evolution can be described by a Markovian quantum master equation for its reduced density operator $\hat{\rho}$. The procedure to obtain this quantum

Este documento incorpora firma electrónica, y es copia auténtica de un documento electrónico archivado por la ULL según la Ley 39/2015.
 Su autenticidad puede ser contrastada en la siguiente dirección <https://sede.ull.es/validacion/>

Identificador del documento: 2111210

Código de verificación: lZvvKBaU

Firmado por: Javier Onam González López
 UNIVERSIDAD DE LA LAGUNA

Fecha: 09/09/2019 11:04:42

Daniel Alonso Ramírez
 UNIVERSIDAD DE LA LAGUNA

11/09/2019 14:53:47

master equation is described, for example, in [17]. Here, we just comment on the final result. Let $\hat{U}_S(t) = \exp(-i\hat{H}_S t/\hbar)$ denotes the evolution operator corresponding to the system Hamiltonian $\hat{H}_S = \hat{H}_D + \hat{H}_{D,wire} + \hat{H}_{wire}$. The essential elements in the quantum master equation can be identified from the following decomposition of the operators \hat{S}^α in interaction picture

$$\hat{U}_S^\dagger(t) \hat{S}^\alpha \hat{U}_S(t) = \sum_{\omega>0} \hat{S}_\omega^\alpha \exp(-i\omega t) + \hat{S}_\omega^{\alpha\dagger} \exp(i\omega t), \quad (2)$$

where $\sum_{\omega>0}$ denote the summation over the positive transition frequencies $\omega_{ij} = \omega_j - \omega_i$ between eigenstates of \hat{H}_S . The difference between the spectrum of \hat{H}_S and \hat{H}_D makes the frequencies and terms in the previous decomposition different from the one corresponding to the device directly coupled with the baths, and leads to new decay channels. This is the origin of the additional irreversible processes.

When system intrinsic dynamics are fast compared to the relaxation dynamics, the rotating wave approximation applies and the Lindblad–Gorini–Kossakovsky–Sudarshan (LGKS) generators of the irreversible dynamics associated with each bath can be written as:

$$\mathcal{L}_\alpha[\hat{\rho}(t)] = \sum_{\omega>0} \Gamma_\omega^\alpha \left(\hat{S}_\omega^\alpha \hat{\rho} \hat{S}_\omega^{\alpha\dagger} - \frac{1}{2} \{ \hat{S}_\omega^{\alpha\dagger} \hat{S}_\omega^\alpha, \hat{\rho} \} \right) + \Gamma_{-\omega}^\alpha \left(\hat{S}_\omega^{\alpha\dagger} \hat{\rho} \hat{S}_\omega^\alpha - \frac{1}{2} \{ \hat{S}_\omega^\alpha \hat{S}_\omega^{\alpha\dagger}, \hat{\rho} \} \right). \quad (3)$$

We have introduced the anticommutators $\{ \hat{S}^\dagger \hat{\rho}, \hat{\rho} \} = \hat{S}^\dagger \hat{\rho} + \hat{\rho} \hat{S}^\dagger$. In the following, we will consider bosonic baths of physical dimensions d_α and coupling operators $\hat{B}^\alpha \propto \sum_\mu \sqrt{\omega_\mu} (\hat{b}_\mu^\dagger + \hat{b}_\mu)$. The summation is over all the bath modes of frequencies ω_μ and annihilation operators \hat{b}_μ . With this choice, the rates $\Gamma_{\pm\omega}^\alpha$ are [17]

$$\begin{aligned} \Gamma_\omega^\alpha &= \gamma_\alpha (\omega/\omega_0)^{d_\alpha} [N^\alpha(\omega) + 1], \\ \Gamma_{-\omega}^\alpha &= \Gamma_\omega^\alpha \exp(-\omega\hbar/k_B T_\alpha), \end{aligned} \quad (4)$$

with $N^\alpha(\omega) = [\exp(\omega\hbar/k_B T_\alpha) - 1]^{-1}$, k_B , the Boltzmann constant, and the frequency, ω_0 , depending on the physical realization of the coupling with the bath. Finally, assuming that the Lamb shift of the unperturbed energy levels is small enough to be neglected, the quantum master equation in the Schrödinger picture is given by:

$$\frac{d}{dt} \hat{\rho}(t) = -\frac{i}{\hbar} [\hat{H}_S, \hat{\rho}(t)] + \sum_{\alpha=c,w,h} \mathcal{L}_\alpha[\hat{\rho}(t)]. \quad (5)$$

This quantum master equation is in the standard Lindblad form and defines a generator of a dynamical semigroup. If the spectrum of \hat{H}_S is non-degenerated, Equation (5) for the populations of the N eigenstates $|i\rangle$ of \hat{H}_S , $p_i = \langle i|\hat{\rho}|i\rangle$, reduces to [17]

$$\frac{d}{dt} p_i(t) = \sum_{j=1}^N \sum_{\alpha=c,w,h} W_{ij}^\alpha p_j(t) = \sum_{j=1}^N W_{ij} p_j(t), \quad (6)$$

where W_{ij}^α is the transition rate from the state j to the state i due to the coupling with the bath α . In the following, \mathbf{W} will denote the matrix with elements $W_{ij} = \sum_{\alpha=c,w,h} W_{ij}^\alpha$. The diagonal elements satisfy

$$W_{ii}^\alpha = -\sum_{j \neq i} W_{ji}^\alpha, \quad (7)$$

implying the conservation of the normalization. Furthermore, as a consequence of the Kubo–Martin–Schwinger condition in Equation (4), the forward and backward transition rates are related by

$$\frac{W_{ji}^\alpha}{W_{ij}^\alpha} = \exp\left(-\frac{\omega_{ij}\hbar}{k_B T_\alpha}\right). \quad (8)$$

Este documento incorpora firma electrónica, y es copia auténtica de un documento electrónico archivado por la ULL según la Ley 39/2015.
 Su autenticidad puede ser contrastada en la siguiente dirección <https://sede.ull.es/validacion/>

Identificador del documento: 2111210 Código de verificación: lZvvKBaU

Firmado por: Javier Onam González López
 UNIVERSIDAD DE LA LAGUNA

Fecha: 09/09/2019 11:04:42

Daniel Alonso Ramírez
 UNIVERSIDAD DE LA LAGUNA

11/09/2019 14:53:47

Equation (6) is the starting point of our analysis. When the system is driven by a work source, we will arrive to an equation with a similar structure, and the results described below will also apply to that case.

2.2. Circuit Fluxes and Affinities

Here, we describe how to determine the heat currents \dot{Q}_α and the entropy production \dot{S} in the steady state. In the following, we assume that the currents are positive when the energy flows towards the system. The method is based on the representation of the master Equation (6) by a connected graph $\mathcal{G}(V, E)$, being $|V| = N$ the number of vertices, representing the system states, and $|E|$ the number of undirected edges, representing the transitions between different states. A simple circuit C_v of \mathcal{G} is a closed path with no repetition of vertices or edges. Some procedures to determine the set of circuits in a graph are discussed in Appendix A. Each one of the two possible different orientations of a simple circuit, denoted by \vec{C}_v and $-\vec{C}_v$, is a cycle. A cycle then consists of a sequence of directed edges with transition rates W_{ij}^α , and it has an associated algebraic value [25]:

$$\mathcal{A}(\vec{C}_v) = \prod_{\alpha=c,w,h} \mathcal{A}^\alpha(\vec{C}_v), \quad (9)$$

with

$$\mathcal{A}^\alpha(\vec{C}_v) = \prod_{ij \in v} W_{ij}^\alpha, \quad (10)$$

where $\prod_{ij \in v}$ denotes the product of all the transition rates due to the bath α in the cycle \vec{C}_v . If the cycle does not involve the bath α , $\mathcal{A}^\alpha(\vec{C}_v) = 1$ for consistency.

The cycle affinity [25] is defined by:

$$X(\vec{C}_v) = \sum_{\alpha=c,w,h} X^\alpha(\vec{C}_v) = k_B \ln \left(\frac{\mathcal{A}(\vec{C}_v)}{\mathcal{A}(-\vec{C}_v)} \right), \quad (11)$$

where the affinity associated with each bath is $X^\alpha(\vec{C}_v) = k_B \ln[\mathcal{A}^\alpha(\vec{C}_v)/\mathcal{A}^\alpha(-\vec{C}_v)]$. When the system is only coupled with thermal baths, the same amount of energy is taken and transferred to them in a complete cycle, implying $\sum_\alpha T_\alpha X^\alpha(\vec{C}_v) = 0$. However, when the system is in addition coupled to a work source, the summation may differ from zero, indicating the net exchange of energy between the work source and the baths. The cycle flux is defined by [30]:

$$I(\vec{C}_v) = D^{-1} \det(-\mathbf{W}|_{C_v}) [\mathcal{A}(\vec{C}_v) - \mathcal{A}(-\vec{C}_v)], \quad (12)$$

where $D = |\det(\tilde{\mathbf{W}})|$. The matrix $\tilde{\mathbf{W}}$ is obtained from the rate matrix \mathbf{W} replacing the elements of an arbitrary row by ones, and $(-\mathbf{W}|_{C_v})$ denotes the matrix resulting from removing from $-\mathbf{W}$ all the rows and columns corresponding to the vertices of the circuit C_v . Considering the relation between the diagonal and non-diagonal elements of \mathbf{W} , the determinant of $(-\mathbf{W}|_{C_v})$ is always positive. The opposite cycle affinities and flux change according to $X^{(\alpha)}(-\vec{C}_v) = -X^{(\alpha)}(\vec{C}_v)$ and $I(-\vec{C}_v) = -I(\vec{C}_v)$.

Using these definitions, the steady state heat current between the system and a bath associated with a simple circuit is:

$$\dot{Q}_\alpha(C_v) = -T_\alpha I(\vec{C}_v) X^\alpha(\vec{C}_v), \quad (13)$$

and the steady state entropy production is given by $\dot{S}(C_v) = I(\vec{C}_v) X(\vec{C}_v)$. At this point, it is important to notice that, although the affinity and the flux are defined for each cycle, the steady state heat currents and entropy production are independent of the cycle orientation and can then be assigned to the circuit without any ambiguity. In addition, each circuit is consistent with the first and second law of thermodynamics as $\sum_{\alpha=c,w,h} \dot{Q}_\alpha(C_v) = 0$ and $\dot{S}(C_v) \geq 0$ [22–24,30]. Finally, the heat currents and the

Este documento incorpora firma electrónica, y es copia auténtica de un documento electrónico archivado por la ULL según la Ley 39/2015.
 Su autenticidad puede ser contrastada en la siguiente dirección <https://sede.ull.es/validacion/>

Identificador del documento: 2111210 Código de verificación: lZvvKBaU

Firmado por: Javier Onam González López
 UNIVERSIDAD DE LA LAGUNA

Fecha: 09/09/2019 11:04:42

Daniel Alonso Ramírez
 UNIVERSIDAD DE LA LAGUNA

11/09/2019 14:53:47

entropy production in the steady state can be obtained by adding the contribution of all the simple circuits of the graph, $\dot{Q}_\alpha = \sum_{C_\nu} \dot{Q}_\alpha(C_\nu)$ and $\dot{S} = \sum_{C_\nu} \dot{S}(C_\nu)$.

The relative importance of the contribution due to a simple circuit to the heat current Equation (13) is determined by both its affinity $X^\alpha(\vec{C}_\nu)$ and flux $I(\vec{C}_\nu)$ Equation (12). When the system is coupled with thermal baths, the circuits can be classified as trivial circuits (all the affinities $X^\alpha = 0$), circuits associated with heat leaks (one of the affinities is zero) and tricycles (the three affinities are different from zero) [30]. Trivial circuits do not contribute to the steady state heat currents or entropy production. Circuits associated with heat leaks only connect two baths, and the heat always flows from the higher to the lower temperature bath. Tricycles [15] are circuits connecting the three baths, independently of the number of edges involved. When the system is coupled instead with a work source, the circuits associated with heat leaks are identified from the condition $T_c X^c + T_h X^h = 0$ (as there is not net energy exchange with the source), and the tricycles from $T_c X^c + T_h X^h \neq 0$ [30].

The analysis of the circuit flux is more complicated as the term $\mathcal{A}(\vec{C}_\nu) - \mathcal{A}(-\vec{C}_\nu)$ strongly depends on the system parameters. In any case, the number of terms in the determinant of the matrix $(-W|C_\nu)$ decreases when the number of edges in the circuit increases. Then, the non-trivial circuits with a lower number of edges are the dominant contribution to the heat currents in a large range of the parameters, and the system operation as a thermal machine is mainly determined by tricycles with a low number of edges.

3. Quantum Three-Level Device Coupled through a Two-Level System to a Work Bath

An absorption refrigerator is a thermal device extracting heat from a cold bath and rejecting it to a hot bath at rates \dot{Q}_c and \dot{Q}_h , respectively. This process is assisted by the heat \dot{Q}_w extracted from a work bath at higher temperature. Its coefficient of performance (COP) is given by $\varepsilon = \dot{Q}_c / \dot{Q}_w$. The simplest model of quantum absorption refrigerator is a three-level system directly coupled with the heat baths [2,3]. When $T_c < T_h < T_w$, the refrigerator operates in the cooling window $\omega_c < \omega_{c,rev} = \omega_h T_c (T_w - T_h) / [T_h (T_w - T_c)]$, with ω_c , ω_h and $\omega_w = \omega_h - \omega_c$ the frequencies of the transitions coupled with the cold, hot and work baths, respectively. In the limit of ω_c approaching from below to $\omega_{c,rev}$, the COP reaches the Carnot limit $\varepsilon_C = T_c (T_w - T_h) / [T_w (T_h - T_c)]$, as the only source of irreversibility is the finite heat transfer rate through the thermal contacts. To analyze the effect of the indirect coupling, we consider a system consisting of the three-level device now connected through a two-level wire to the work bath, schematically shown in Figure 1a. The device and wire Hamiltonians read:

$$\hat{H}_D = \omega_c \hbar |2_D\rangle\langle 2_D| + \omega_h \hbar |3_D\rangle\langle 3_D|, \quad (14)$$

and

$$\hat{H}_{wire} = \omega_w \hbar |2_W\rangle\langle 2_W|. \quad (15)$$

The operators in the coupling terms with the baths are taken as $\hat{S}^\alpha = (\hat{S}_-^\alpha + \hat{S}_+^\alpha)$, with $\hat{S}_+^\alpha = \hat{S}_-^{\alpha\dagger}$ and

$$\hat{S}_-^c = |1_D\rangle\langle 2_D|; \hat{S}_-^h = |1_D\rangle\langle 3_D|; \hat{S}_-^w = |1_W\rangle\langle 2_W|. \quad (16)$$

The interaction between the device and the wire is described by:

$$\hat{H}_{D,wire} = g \hbar (|3_D 1_W\rangle\langle 2_D 2_W| + |2_D 2_W\rangle\langle 3_D 1_W|), \quad (17)$$

where the parameter g is the coupling strength. The eigenfrequencies of $\hat{H}_S = \hat{H}_D + \hat{H}_{D,wire} + \hat{H}_{wire}$ are $\omega_1 = 0$, $\omega_2 = \omega_w$, $\omega_3 = \omega_c$, $\omega_4 = [2\omega_h - \Delta - (\Delta^2 + 4g^2)^{1/2}] / 2$, $\omega_5 = [2\omega_h - \Delta + (\Delta^2 + 4g^2)^{1/2}] / 2$ and $\omega_6 = \omega_w + \omega_h$. We have introduced the detuning $\Delta = \omega_h - \omega_c - \omega_w$. Using the procedure of

Este documento incorpora firma electrónica, y es copia auténtica de un documento electrónico archivado por la ULL según la Ley 39/2015.
 Su autenticidad puede ser contrastada en la siguiente dirección <https://sede.ull.es/validacion/>

Identificador del documento: 2111210 Código de verificación: lZvvKBaU

Firmado por: Javier Onam González López
 UNIVERSIDAD DE LA LAGUNA

Fecha: 09/09/2019 11:04:42

Daniel Alonso Ramírez
 UNIVERSIDAD DE LA LAGUNA

11/09/2019 14:53:47

Section 2 to determine the master Equation (6), we obtain the following non-zero transition rates W_{ij}^{α} with indexes $j > i$,

$$\begin{aligned} W_{13}^c &= \Gamma_{\omega_c}^c, & W_{24}^c &= |c_-|^2 \Gamma_{\omega_4 - \omega_w}^c, & W_{25}^c &= |c_+|^2 \Gamma_{\omega_5 - \omega_w}^c, \\ W_{14}^h &= |c_-^h|^2 \Gamma_{\omega_4}^h, & W_{15}^h &= |c_+^h|^2 \Gamma_{\omega_5}^h, & W_{26}^h &= \Gamma_{\omega_h}^h, \\ W_{12}^w &= \Gamma_{\omega_w}^w, & W_{34}^w &= |c_-|^2 \Gamma_{\omega_4 - \omega_c}^w, & W_{35}^w &= |c_+|^2 \Gamma_{\omega_5 - \omega_c}^w, \\ W_{46}^w &= |c_-^w|^2 \Gamma_{\omega_w + \omega_h - \omega_4}^w, & W_{56}^w &= |c_+^w|^2 \Gamma_{\omega_w + \omega_h - \omega_5}^w, \end{aligned} \quad (18)$$

where the coefficients are given by

$$\begin{aligned} c_{\pm} &= \frac{[-\Delta \pm (\Delta^2 + 4g^2)^{1/2}] d_{\pm}}{4g(\Delta^2 + 4g^2)^{1/2}}, \\ c'_{\pm} &= \frac{d_{\pm}}{2(\Delta^2 + 4g^2)^{1/2}}, \end{aligned} \quad (19)$$

with $d_{\pm}^2 = 4g^2 + [\Delta \pm (\Delta^2 + 4g^2)^{1/2}]^2$. The remaining elements can be obtained using Equations (7) and (8). The graph representation of the master equation is shown in Figure 1b where we identified 38 simple circuits using the methods described in Appendix A. As each pair of vertices is connected by only one edge, the sequence of $E \leq 6$ vertices $\{i_1, i_2, \dots, i_E, i_1\}$ will denote in the following both a circuit containing these vertices and the corresponding cycle with orientation $i_1 \rightarrow i_2 \dots \rightarrow i_E \rightarrow i_1$. As we are interested in the system operating as a refrigerator, we will focus our analysis on the steady state heat current with the cold bath. Now, we will assume $\Delta = 0$, for which $\omega_4 = \omega_h - g$, $\omega_5 = \omega_h + g$ and $|c_{\pm}| = |c'_{\pm}|^2 = \frac{1}{2}$. The non-resonant case will be discussed later.

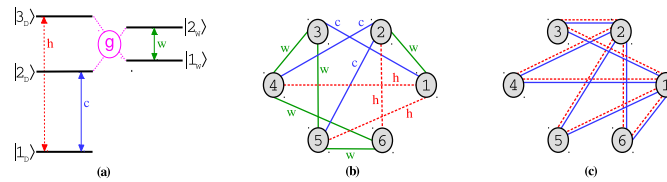


Figure 1. (a) schematic illustration of a three-level device coupled to a work bath or source through a two-level wire; (b) graph representation of the master equation when the wire connects a work bath. The six vertices represent the eigenstates of \hat{H}_5 and the eleven edges the transitions assisted by the cold (blue lines), work (green lines) and hot (dashed red lines) baths, labeled by c , w and h respectively; (c) graph representation of the master equation when the system is driven by a periodic classical field. Now the vertices correspond to the eigenstates of \hat{H}_2 , and there are eight pairs of parallel edges associated with the cold (solid lines) and hot (dashed lines) baths.

The simplest circuits in the graph are the three-edge tricycles $C_1 = \{1, 3, 4, 1\}$, $C_2 = \{1, 3, 5, 1\}$, $C_3 = \{1, 2, 5, 1\}$, $C_4 = \{1, 2, 4, 1\}$, $C_5 = \{2, 5, 6, 2\}$ and $C_6 = \{2, 4, 6, 2\}$, with affinities $X^c(\vec{C}_{1,2}) = -\omega_c \hbar / T_c$, $X^c(\vec{C}_{3,5}) = -(\omega_c + g) \hbar / T_c$ and $X^c(\vec{C}_{4,6}) = -(\omega_c - g) \hbar / T_c$. In all cases, the leading term of the affinity is proportional to the frequency of the transition coupled with the cold bath when $g \ll \omega_c$. From (13), we find that the upper limit of the cooling window ($\dot{Q}_c > 0$) for the circuits C_1 and C_2 is given by:

$$\omega_{c,rev}(C_v) = \omega_{c,rev} + (-1)^v g \frac{T_c(T_w - T_h)}{T_h(T_w - T_c)}. \quad (20)$$

A similar analysis gives $\omega_{c,rev}(C_\nu) = \omega_{c,rev} + (-1)^\nu g T_w (T_h - T_c) / T_h (T_w - T_c)$ for $\nu = 3, 4$ and $\omega_{c,rev}(C_\nu) = \omega_{c,rev} + (-1)^\nu g$ for $\nu = 5, 6$. The tricycles reach the Carnot COP when approaching $\omega_{c,rev}(C_\nu)$, but with vanishing circuit heat currents.

We identify 10 four-edge circuits associated with heat leaks, four involving the cold and work baths, four the work and hot baths and two the cold and hot baths. In all cases, the two non-zero affinities X^a are proportional to the coupling strength g . An example is the circuit $C_7 \equiv \{1, 4, 6, 5, 1\}$ shown in Figure 2a. In this case, the affinities are $X^h(\vec{C}_7) = 2g\hbar/T_h$ and $X^w(\vec{C}_7) = -2g\hbar/T_w$. From the circuit heat currents (13), the condition $T_h < T_w$ and the relation (8), one can easily determine that $\dot{Q}_h(C_7) < 0$ and $\dot{Q}_w(C_7) > 0$, resulting in a direct energy transfer from the work bath to the hot bath. There is also a trivial four-edge circuit involving only the edges associated with the work bath. We found 14 five-edge tricycles, as for example $C_8 = \{1, 4, 6, 2, 5, 1\}$ shown in Figure 2b. In this case, $X^c(\vec{C}_8) = -(\omega_c + g)\hbar/T_c$ and the circuit cooling window is given by the condition $\omega_c < \omega_{c,rev}(C_8) = \omega_{c,rev} + g(2T_c T_w - T_c T_h - T_w T_h) / (T_w T_h - T_h T_c)$. Finally, there are seven six-edge circuits, two tricycles and five associated to heat leaks. All the tricycles have affinities X^c with a leading term proportional to ω_c and cooling windows in the interval $\omega_c - g \leq \omega_{c,rev}(C_\lambda) \leq \omega_c + g$, whereas the non-zero affinities X^a of circuits associated with heat leaks are proportional to the coupling constant g .

For a given choice of the system parameters, the cooling power is determined by the positive contribution of the tricycles operating in their cooling window and the negative contribution of the other tricycles and the circuits associated with heat leaks. The optimal coupling constant g satisfies $\gamma_\alpha \ll g \ll \omega_c$, a regime where the contribution of the heat leaks is very small, the tricycles cooling windows approximately coincide and the rotating wave approximation is still valid. An example is shown in Figure 2c. As expected, the larger contributions correspond to the tricycles with a lower number of edges. The maximum cooling rate is slightly greater and displaced to higher frequencies when the device is connected through the two-level wire. This effect is the result of the evaluation of the rate functions Equation (4) at the displaced frequencies $\omega_\alpha \pm g$, and increases with the bath physical dimension d_α . However, it cannot be further exploited, as a larger g would increase the heat leaks, and, in any case, the COP would not improve.

If we examine the system performance characteristic (see Figure 2d) a closed curve is found for the indirectly-coupled three-level device indicating the existence of additional irreversible processes: heat leaks, with small influence for small g , and the internal dissipation appearing when approaching the upper limit of the cooling window. The internal dissipation results from the competition of positive and negative heat currents associated with tricycles having slightly different values of $\omega_{c,rev}(C_\nu)$ [8] and only works for very small ω_c (where the finite heat transfer rate effects dominate) and in the interval $\omega_{c,rev} - g < \omega_c < \omega_{c,rev} + g$. These irreversible contributions can be reduced decreasing the coupling strength g , but cannot be avoided, making the reversible limit unattainable for the device connected through a quantum wire.

For optimal coupling constant g , the main features of the system performance results from the tricycle contributions and can be described with a small number of circuit representatives. We choose as circuit representatives C_1 and C_2 , with $\omega_{c,rev}(C_{1,2})$ below and above $\omega_{c,rev}$ respectively, see Equation (20). Their fluxes are given by

$$\begin{aligned}
 I(\vec{C}_1) &= D^{-1} \det(-\mathbf{W}|C_1) \left(W_{31}^c W_{43}^w W_{14}^h - W_{13}^c W_{34}^w W_{41}^h \right), \\
 I(\vec{C}_2) &= D^{-1} \det(-\mathbf{W}|C_2) \left(W_{51}^c W_{33}^w W_{15}^h - W_{13}^c W_{35}^w W_{51}^h \right),
 \end{aligned} \tag{21}$$

from which the steady state heat currents of the circuit representatives $\dot{Q}_\alpha^R = \dot{Q}_\alpha(C_1) + \dot{Q}_\alpha(C_2)$ can be easily obtained. The currents \dot{Q}_α^R incorporate the main features of the system performance such as the frequency at which the maximum cooling rate is reached and the essential irreversible processes, and might be renormalized to account for the total heat currents [31]. Figure 2d compares the performance

Este documento incorpora firma electrónica, y es copia auténtica de un documento electrónico archivado por la ULL según la Ley 39/2015.
 Su autenticidad puede ser contrastada en la siguiente dirección <https://sede.ull.es/validacion/>

Identificador del documento: 2111210 Código de verificación: lZvvKBaU

Firmado por: Javier Onam González López
 UNIVERSIDAD DE LA LAGUNA

Fecha: 09/09/2019 11:04:42

Daniel Alonso Ramírez
 UNIVERSIDAD DE LA LAGUNA

11/09/2019 14:53:47

characteristic of the system and its circuit representatives. For a more accurate description, or for larger values of g , a larger number of circuit representatives, including, for example, heat leaks, might be needed.

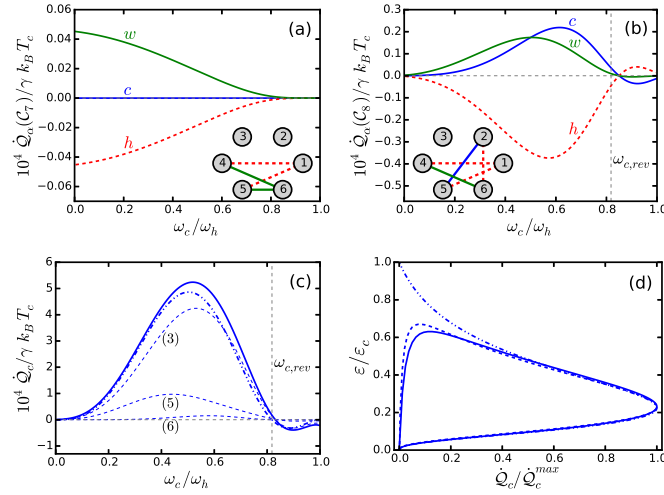


Figure 2. Steady state heat currents as a function of the frequency ω_c for (a) a circuit associated with a heat leak and (b) a five-edge tricycle. The circuits are shown in the insets; (c) heat current with the cold bath \dot{Q}_c for the three-level device connected through the two-level wire (solid line), the three-level directly coupled with the baths (dashed-dotted line). The labeled thin dashed lines show the contribution of tricycles with three, five and six edges. The vertical line indicates the frequency $\omega_{c,rev}$; (d) performance characteristics obtained from (c) in the cooling range. The dashed line depicts the performance characteristic of the circuit representatives C_1 and C_2 . Each curve has been normalized with respect to its maximum cooling rate. Parameters were chosen as $T_c = 9$, $T_h = 10$, $T_w = 20$, $\omega_h = 1$, $g = 0.05$, $d_a = 3$ and $\gamma_a = \gamma = 10^{-6}$ in units for which $h = k_B = \omega_0 = 1$.

The analysis of the non-resonant case leads to the same qualitative results, as the structure of the graph representation of the master equation is not modified and the same simple circuits and irreversible mechanisms are found. The main difference is the dependence of the transitions rates W_{ij}^0 on the detuning Δ . When $\gamma_a \ll g \ll \Delta$, the coefficients c_+ and c_- vanish and three circuits associated with heat leaks dominate the heat currents: $\{1, 2, 4, 3, 1\}$ (from the work bath to the cold one) $\{1, 5, 6, 2, 1\}$ (from the work to the hot) and $\{1, 3, 4, 2, 6, 5, 1\}$ (from the hot to the cold).

4. Quantum Three-Level Device Coupled through a Two-Level System to a Work Source

The three-level device coupled with a work source modeled by a periodic classical field is the simplest model of driven quantum thermal machines [1]. The engine efficiency is given by $\eta = -\mathcal{P} / \dot{Q}_h$ and the refrigerator COP by $\varepsilon = \dot{Q}_c / \mathcal{P}$. The operating mode of the device is determined by the frequency of the transition coupled with the cold bath. When $\omega_c < \omega_{c,max} - \lambda\eta_C$, the device works as a refrigerator, whereas for $\omega_c > \omega_{c,max} + \lambda\eta_C$, it works as an engine. Here, we have introduced the coupling strength with the field λ and the engine Carnot efficiency $\eta_C = 1 - T_c/T_h$. At the limit

frequency $\omega_{c,max} = \omega_h T_c / T_h$, an idealized device ($\lambda = 0$) would reach the engine Carnot efficiency or the refrigerator Carnot COP, $\epsilon_C = T_c / (T_h - T_c)$. However, when $\omega_{c,max} - \lambda \eta_C < \omega_c < \omega_{c,max} + \lambda \eta_C$ the operating mode of the three-level device is given by the competition between the heat currents associated with the two manifold resulting from the splitting of the system energy levels due to the field interaction. The competition of those heat currents is the origin of the internal dissipation preventing the system to reach the Carnot performance in any of the two working modes [1]. In this section, we will analyze the three-level device connected to a classical driving field through the two-level wire. The system Hamiltonian is:

$$\hat{H} = \hat{H}_D + \hat{H}_{D,wire} + \hat{H}_{wire} + \hat{H}_{wire,w}(t) + \sum_{\alpha=c,h} (\hat{H}_{D,\alpha} + \hat{H}_\alpha). \quad (22)$$

All these terms were already introduced in the previous section except for $\hat{H}_{wire,w}(t)$, which describes the coupling of the two-level system with the classical field,

$$\hat{H}_{wire,w}(t) = \lambda \hbar [|2_W\rangle\langle 1_W| \exp(-i\omega_w t) + |1_W\rangle\langle 2_W| \exp(i\omega_w t)]. \quad (23)$$

We will assume the resonant case in which the field frequency is equal to $\omega_w = \omega_h - \omega_c$. As the Hamiltonian (22) depends on time, the derivation of the quantum master equation described in Section 2 requires some modifications [4,32,33]. Let us define the operators $\hat{H}_1 = \hat{H}_D + \hat{H}_{wire}$ and

$$\hat{H}_2 = \hat{H}_{D,wire} + \lambda \hbar (|1_D 2_W\rangle\langle 1_D 1_W| + |2_D 2_W\rangle\langle 2_D 1_W| + |3_D 2_W\rangle\langle 3_D 1_W| + h.c.), \quad (24)$$

where *h.c.* stands for the Hermitian conjugate of the preceding terms. The eigenfrequencies of \hat{H}_2 , $\hat{H}_2|i\rangle = \omega_i \hbar|i\rangle$, are $\omega_1 = -\lambda$, $\omega_2 = \lambda$, $\omega_3 = -[g + (4\lambda^2 + g^2)^{1/2}]/2$, $\omega_4 = [g - (4\lambda^2 + g^2)^{1/2}]/2$, $\omega_5 = [-g + (4\lambda^2 + g^2)^{1/2}]/2$ and $\omega_6 = [g + (4\lambda^2 + g^2)^{1/2}]/2$. One can easily probe [33] that the propagator associated with $\hat{H}_5(t) = \hat{H}_D + \hat{H}_{D,wire} + \hat{H}_{wire} + \hat{H}_{wire,w}(t)$ is given by $\hat{U}_5(t) = \hat{U}_1(t)\hat{U}_2(t)$. In the following, we assume that the Lamb shifts of the energy levels of H_5 can be neglected. The coupling operators with the cold and hot baths (16) are then decomposed into

$$\hat{U}_5^\dagger(t) \hat{S}^\alpha \hat{U}_5(t) = \sum_{i=1}^5 \sum_{j>i} \hat{S}_{ij}^\alpha \exp[-i(\omega_\alpha + \omega_{ij})t] + \hat{S}_{ij}^{\alpha\dagger} \exp[i(\omega_\alpha + \omega_{ij})t], \quad (25)$$

where $\hat{S}_{ij}^\alpha = c_{ij}^\alpha|i\rangle\langle j|$ and $c_{ij}^\alpha = \langle i|\hat{S}^\alpha|i\rangle$. With these ingredients, the Lindblad–Gorini–Kossakovsky–Sudarshan (LGKS) generators for each bath (3) can be obtained as the summation of the terms corresponding to the frequencies $\omega_\alpha + \omega_{ij}$, leading to the following quantum master equation in the interaction picture under the unitary transformation associated with \hat{U}_5^\dagger ,

$$\frac{d}{dt} \hat{\rho}_I(t) = \sum_{\alpha=c,h} \mathcal{L}_\alpha[\hat{\rho}_I(t)]. \quad (26)$$

The steady state properties can then be derived from the diagonal part of the Equation (26) in the eigenbasis of \hat{H}_2 , which resembles Equation (6). Now, the steady state populations p_i and energy currents must be interpreted as the corresponding time-averaged quantities over a period $\tau = 2\pi/\omega_w$ of the driving. The transition rates with indexes $j > i$ are given by:

$$W_{ij}^\alpha = |c_{ij}^\alpha|^2 \Gamma_{\omega_\alpha + \omega_{ij}}, \quad (27)$$

where the non-zero coefficients are

$$\begin{aligned} |c_{13}|^2 &= |c_{26}|^2 = \frac{(1-u_-)^2}{4(1+u_-^2)}; & |c_{23}|^2 &= |c_{16}|^2 = \frac{(1+u_-)^2}{4(1+u_-^2)}; \\ |c_{14}|^2 &= |c_{25}|^2 = \frac{(1+u_+)^2}{4(1+u_+^2)}; & |c_{24}|^2 &= |c_{15}|^2 = \frac{(1-u_+)^2}{4(1+u_+^2)}, \end{aligned} \quad (28)$$

Este documento incorpora firma electrónica, y es copia auténtica de un documento electrónico archivado por la ULL según la Ley 39/2015.
 Su autenticidad puede ser contrastada en la siguiente dirección <https://sede.ull.es/validacion/>

Identificador del documento: 2111210 Código de verificación: lZvvKBaU

Firmado por: Javier Onam González López
 UNIVERSIDAD DE LA LAGUNA

Fecha: 09/09/2019 11:04:42

Daniel Alonso Ramírez
 UNIVERSIDAD DE LA LAGUNA

11/09/2019 14:53:47

with $u_{\pm} = 2\lambda/[g \pm (4\lambda^2 + g^2)^{1/2}]$. The remaining transition rates can be obtained using Equations (7) and (8).

The graph representation of the master equation is shown in Figure 1c. Each pair of vertices is simultaneously connected by two edges, one associated with the cold bath and the other with the hot bath. The topological structure of the graph is very simple as the states 1 and 2 are only coupled with 3, 4, 5 and 6. With this structure, only simple circuits with two or four edges can be found. We have identified 104 circuits, 12 of them being trivial circuits and 92 contributing to the steady state heat currents. The energy exchange between the system and the work source is described by the power $\mathcal{P} = \sum_v \mathcal{P}(C_v)$, being $\mathcal{P}(C_v) = -\dot{Q}_c(C_v) - \dot{Q}_h(C_v)$ the contribution of each circuit.

The simplest circuits are eight two-edge tricycles $C_{ij} = \{i, j, i\}$, where $i = 1, 2$ and $j = 3, 4, 5, 6$. In the following we will assume that the two-edge circuits are oriented choosing $i \rightarrow j$ as the edge corresponding to the cold bath. The affinities can be easily calculated to yield $X^c(\vec{C}_{ij}) = -\hbar(\omega_c + \omega_j - \omega_i)/T_c$ and $X^h(\vec{C}_{ij}) = \hbar(\omega_h + \omega_j - \omega_i)/T_h$. When $g, \lambda \ll \omega_{c,h}$, the leading term in the affinities is proportional to the transition frequencies. The circuit fluxes (12) are given by:

$$I(\vec{C}_{ij}) = D^{-1} \det(-\mathbf{W}|C_{ij}) \left(W_{ji}^c W_{ij}^h - W_{ij}^c W_{ji}^h \right). \quad (29)$$

With this expression, the limit frequency of each circuit can be obtained imposing $I(\vec{C}_{ij}) = 0$ to yield

$$\omega_{c,max}(C_{ij}) = \omega_{c,max} - (\omega_j - \omega_i)\eta_C. \quad (30)$$

When $\omega_{c,max}(C_{ij})$ is approached from below, the circuit reaches the refrigerator Carnot COP ε_C , and from above the engine Carnot efficiency η_C .

We have also identified 96 four-edge circuits $\{i, j, i', j', i\}$: 12 trivial circuits, 60 tricycles ($T_c X^c + T_h X^h \neq 0$) and 24 four-edge circuits associated with heat leaks ($T_c X^c + T_h X^h = 0$). The tricycles can be classified into two different groups, one involving circuits with two edges associated with each bath, for which the affinities are proportional to $2\omega_k + (\omega_j + \omega_{j'})$, and the other with three edges associated to one of the baths, for which $\omega_k + \omega_j - \omega_{j'}$. The limit frequencies for the first group are $\omega_{c,max}(C) = \omega_{c,max} - (\omega_j + \omega_{j'})\eta_C/2$ and for the second are given by Equation (30). The circuits associated with heat leaks have affinities proportional to $\omega_i - \omega_{j'}$ or $\omega_j - \omega_{j'}$. An example is the circuit $C_9 = \{1, 3, 2, 5, 1\}$ shown in Figure 3a for which the affinities are $X^c(\vec{C}_3) = -2\lambda\hbar/T_c$ and $X^h(\vec{C}_3) = 2\lambda\hbar/T_h$.

The optimal coupling constants now satisfy $\gamma_k \ll g, \lambda \ll \omega_c$, as the heat leaks are minimized and the energy flows are mainly determined by the contribution due to the two-edge tricycles. Figure 3b shows the heat current with the cold bath for a significant value of g , where the contribution of the four-edge tricycles becomes relevant. As explained before, for the absorption refrigerator, the device coupled through the wire reaches a larger maximum cooling rate. Although each tricycle can reach the reversible limit, their combination lead again to internal dissipation, now working in the interval $\omega_{c,max} - f(\lambda, g)\eta_C < \omega_c < \omega_{c,max} + f(\lambda, g)\eta_C$, with $f(\lambda, g) = [\lambda + g + (4\lambda^2 + g^2)^{1/2}]/2$, that depends also on g .

We have found that the best choice of circuit representatives between the two-edge tricycles is determined by the ratio g/λ : $C_{1,4}$, $C_{2,5}$, when $g/\lambda < 1$ and $C_{1,6}$, $C_{2,3}$ when $g/\lambda > 1$. For $g \ll \lambda$, the system performance is well described by the uncoupled device. The performance characteristics of the system and its circuit representatives are compared in Figure 3c,d for the two operating modes. Notice that the engine maximum power output is reached at the minimum value of \mathcal{P} . As expected, the circuit representatives provide a more accurate description of the performance than the directly-coupled device. This approximation can be further improved by including a larger number of circuits.

Este documento incorpora firma electrónica, y es copia auténtica de un documento electrónico archivado por la ULL según la Ley 39/2015.
 Su autenticidad puede ser contrastada en la siguiente dirección <https://sede.ull.es/validacion/>

Identificador del documento: 2111210 Código de verificación: lZvvKBaU

Firmado por: Javier Onam González López
 UNIVERSIDAD DE LA LAGUNA

Fecha: 09/09/2019 11:04:42

Daniel Alonso Ramírez
 UNIVERSIDAD DE LA LAGUNA

11/09/2019 14:53:47

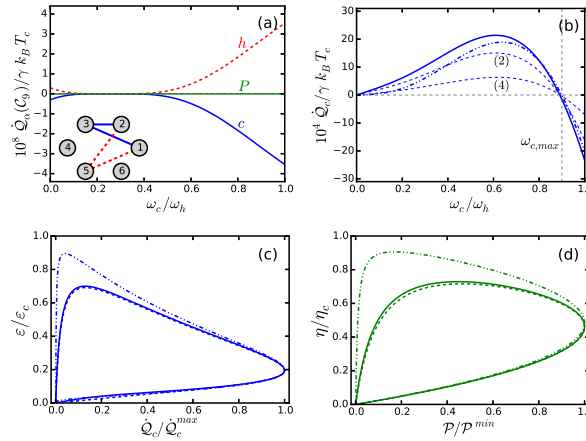


Figure 3. (a) steady state heat currents as a function of the frequency ω_c for the circuit shown in the inset; (b) heat current with the cold bath \dot{Q}_c for the three-level device connected through the two-level wire (solid line) and directly coupled to the classical field (dashed-dotted line). The labeled thin dashed lines show the contribution due to tricycles with two and four edges. The vertical line indicates the frequency $\omega_{c,max}$; (c) performance characteristics for the system when working as a refrigerator ($\omega_c < \omega_{c,max}$) and (d) as an engine ($\omega_c > \omega_{c,max}$) for the case in (b). The dashed lines depict the performance characteristics of the circuit representatives $C_{1,6}$ and $C_{2,3}$. We have fixed $g = 0.25$, $\lambda = 0.05$ and the other parameters are those in Figure 2.

5. Conclusions

In this paper, we have analyzed the irreversible processes in a three-level thermal device coupled with a two-level wire connecting the system to a work bath. The coupling induces heat leaks and internal dissipation that prevents the system from reaching the reversible limit. In addition, if the detuning between the transitions of the three-level device and the two-level wire is too large, the system stops working as an absorption refrigerator as the heat leaks dominate. We found similar results in the analysis of systems in which the wire connects either the cold or the hot bath. The additional irreversible mechanisms are proportional to the coupling constant between the device and the wire. When the wire connects the system with a work source, the coupling induces heat leaks and modifies the frequency interval where internal dissipation appears. The optimal values of the coupling constants are such that $\gamma_\alpha \ll g, \lambda \ll \omega_{2,1}$, which minimize the heat leaks and the interval where the internal dissipation works. The system performance can be well described by just considering two circuit representatives. This description may be improved incorporating additional circuits and renormalizing their contribution to the heat currents [31].

Our results can be generalized to wires composed of a chain of two-level systems. The graph representation of the master equation will have a larger number of vertices and edges, exponentially increasing the number of simple circuits. However, the graph topological structure will be similar. For example, let us consider a chain of n two-level systems connecting the device with a classical periodic field. The corresponding graph resembles the one in Figure 1c, with 2^n states connected to 2^{n+1} states by two edges associated with the cold and the hot baths. Again, the most important contribution to the heat currents comes from the 2^{2n+1} two-edge circuits. Now, the transition rates will depend

on the frequencies $\omega_\alpha + f_{ij}(\lambda, g, n)$ and the affinities X^α of circuits associated with heat leaks will be proportional to f_{ij} . In general, the function f_{ij} , and, therefore, the frequency interval subjected to internal dissipation, increases with n . However, for coupling constants g and λ small enough, the heat leaks can be neglected. This same analysis applies when the system is coupled with a work bath. The only limitation in both cases is that g must be much larger than the coupling constants with the bath γ_α for the master equation to be valid.

The irreversible processes analyzed are the result of the new decay channels due to the additional coupling term. Therefore, they are expected in any quantum device connected through quantum wires to the environments. To avoid them would require reservoir engineering techniques [8] hindered by the complicated system spectrum as the number of states is increased. In this work, we have focused on the stationary regime. Although coherences and populations associated with the system Hamiltonian become decoupled during the evolution, the wire may introduce new effects in the transient regime [34], related to the time-dependent terms in the thermodynamic fluxes. These effects could be explored in future work.

Acknowledgments: We thank A. Ruiz and L. A. Correa for careful reading and commenting on the manuscript. J. Onam González acknowledges a Formación de Profesorado Universitario (FPU) fellowship from the Spanish Ministerio de Educación, Cultura y Deportes (MECD). Financial support by the Spanish Ministerio de Economía y Competitividad (MINECO) (FIS2013-41352-P) and European Cooperation in Science and Technology (COST) Action MP1209 is gratefully acknowledged.

Author Contributions: J. Onam González performed the model calculations. J. Onam González, Daniel Alonso and José P. Palao conceived the study and contributed equally in the mathematical derivations, the discussion of the results and the manuscript writing. All authors have read and approved the final manuscript.

Conflicts of Interest: The authors declare no conflict of interest.

Appendix A

In this appendix, we describe how to obtain all the circuits corresponding to a graph. This simple procedure is illustrated with the three-level system in contact with a cold and a hot unstructured bosonic baths and directly coupled with a periodic classical field. The total Hamiltonian is

$$\hat{H} = \hat{H}_D(t) + \sum_{\alpha=c,h} \hat{H}_{D,\alpha} + \hat{H}_\alpha, \quad (A1)$$

where

$$\hat{H}_D(t) = \omega_c \hbar |2_D\rangle\langle 2_D| + \omega_h \hbar |3_D\rangle\langle 3_D| + \lambda \hbar (|3_D\rangle\langle 2_D| \exp[-i(\omega_h - \omega_c)t] + h.c.). \quad (A2)$$

The bath Hamiltonians \hat{H}_α and the coupling terms $\hat{H}_{D,\alpha}$ are described in Section 3. The quantum master equation for this system can be obtained using the procedure described in Section 4 and the result can be found for example in [1,35]. For convenience, we will use the eigenbasis $|1\rangle \equiv |1_D\rangle$, $|2\rangle \equiv 2^{-1/2}(|3_D\rangle - |2_D\rangle)$ and $|3\rangle \equiv 2^{-1/2}(|3_D\rangle + |2_D\rangle)$ of $\hat{H}_2 = \lambda \hbar (|3_D\rangle\langle 2_D| + |2_D\rangle\langle 3_D|)$. Figure A1a shows a schematic representation of the system transitions assisted by the baths. The non-diagonal elements of the rate matrix \mathbf{W} are $W_{ij} = W_{ij}^c + W_{ij}^h$ with

$$W_{12}^\alpha = \frac{\Gamma_{\omega_\alpha - \lambda}^\alpha}{2}; W_{13}^\alpha = \frac{\Gamma_{\omega_\alpha + \lambda}^\alpha}{2}; W_{21}^\alpha = \frac{\Gamma_{-(\omega_\alpha - \lambda)}^\alpha}{2}; W_{31}^\alpha = \frac{\Gamma_{-(\omega_\alpha + \lambda)}^\alpha}{2}; W_{23}^\alpha = W_{32}^\alpha = 0. \quad (A3)$$

The functions $\Gamma_{\pm\omega}^\alpha$ can be calculated using Equation (4). The graph \mathcal{G} associated with this system have $|V| = 3$ vertices and $|E| = 4$ edges (see Figure A1b).

Este documento incorpora firma electrónica, y es copia auténtica de un documento electrónico archivado por la ULL según la Ley 39/2015.
 Su autenticidad puede ser contrastada en la siguiente dirección <https://sede.ull.es/validacion/>

Identificador del documento: 2111210 Código de verificación: lZvvKBaU

Firmado por: Javier Onam González López
 UNIVERSIDAD DE LA LAGUNA

Fecha: 09/09/2019 11:04:42

Daniel Alonso Ramírez
 UNIVERSIDAD DE LA LAGUNA

11/09/2019 14:53:47

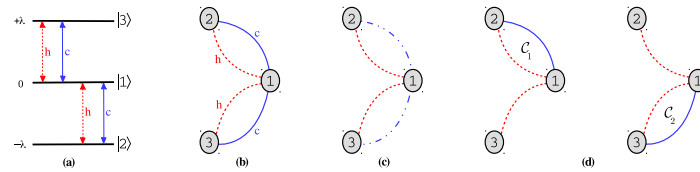


Figure A1. (a) schematic representation of the transitions due to the coupling with the cold and hot baths, labeled by c and h respectively, in a driven three-level system; (b) in the graph \mathcal{G} the vertices represent the three states and the undirected edges represent the transitions connecting them. One of the graph maximal trees \mathcal{T} is shown in (c), for which the chords (dashed-dotted lines) are the edges corresponding to the cold transitions; (d) a set of fundamental circuits $\{C_1, C_2\}$ is then identified by adding each chord to the maximal tree. These circuits are equivalent to the two manifolds operating in the three-level amplifier [1].

The procedure to determine the simple circuits is based on the identification of a maximal tree of \mathcal{G} and its chords. A maximal tree \mathcal{T} is a subgraph with $|V| - 1$ edges connecting all the vertices but without forming any closed path. In principle, many different maximal trees can be found on a given graph, but for this procedure it is sufficient to select any of them as the final result is independent of this choice. A chord of a maximal tree is one of $|E| - |V| + 1$ edges which are not part of it. An example of a maximal tree and its chords is shown in Figure A1c.

A fundamental set of simple circuits [25] can be found adding each chord to the maximal tree, as shown in Figure A1d. The number of fundamental circuits equals the number of chords, $|E| - |V| + 1$. Only for some systems, as our example, the fundamental set contains all the possible simple circuits. Otherwise, the remaining circuits can be obtained by the linear combination of the elements of the fundamental set

$$r_1 C_1 \oplus r_2 C_2 \oplus \dots \oplus r_{|E|-|V|+1} C_{|E|-|V|+1}, \quad (\text{A4})$$

with $r_\lambda = 0$ or 1. The relation $C_\lambda \oplus C_{\lambda'}$ gives a new subgraph that contains all the edges of C_λ and $C_{\lambda'}$ which do not simultaneously belong to C_λ and $C_{\lambda'}$ [25]. The result of each possible linear combination Equation (A4) is considered only when it generates a new simple circuit.

In summary, a simple procedure to obtain the full set of circuits reads as

- (i) Select a maximal tree \mathcal{T} of \mathcal{G} and identify its chords.
- (ii) Find a fundamental set of circuits adding each chord to the maximal tree.
- (iii) Obtain the remaining circuits by the linear combination of the circuits in the fundamental set.

An alternative procedure consists of identifying all the maximal trees of \mathcal{G} and generating the fundamental set of circuits associated with each one. The set of all simple circuits is then the union of all the fundamental sets. For complex graphs, the number of circuits might be very large and more efficient standard algorithms [36] can be used.

References

1. Kosloff, R.; Levy, A. Quantum heat engines and refrigerators: Continuous devices. *Annu. Rev. Phys. Chem.* **2014**, *65*, 365–393.
2. Palao, J.P.; Kosloff, R.; Gordon, J.M. Quantum thermodynamic cooling cycle. *Phys. Rev. E* **2001**, *64*, 056130.
3. Linden N.; Popescu, S.; Skrzypczyk, P. How Small can thermal machines be? The smallest possible refrigerator. *Phys. Rev. Lett.* **2010**, *105*, 130401.
4. Levy, A.; Alicki R.; Kosloff, R. Quantum refrigerators and the third law of thermodynamics. *Phys. Rev. E* **2012**, *85*, 061126.

Este documento incorpora firma electrónica, y es copia auténtica de un documento electrónico archivado por la ULL según la Ley 39/2015.
 Su autenticidad puede ser contrastada en la siguiente dirección <https://sede.ull.es/validacion/>

Identificador del documento: 2111210 Código de verificación: lZvvKBaU

Firmado por: Javier Onam González López
 UNIVERSIDAD DE LA LAGUNA

Fecha: 09/09/2019 11:04:42

Daniel Alonso Ramírez
 UNIVERSIDAD DE LA LAGUNA

11/09/2019 14:53:47

5. Correa, L.A. Multistage quantum absorption heat pumps. *Phys. Rev. E* **2014**, *89*, 042128.
6. Scovil, H.E.D.; Schulz-DuBois, E.O. Three-level masers as heat engines. *Phys. Rev. Lett.* **1959**, *2*, 262–263.
7. Correa, L.A.; Palao, J.P.; Adesso, G.; Alonso, D. Performance bound for quantum absorption refrigerators. *Phys. Rev. E* **2013**, *87*, 042131.
8. Correa, L.A.; Palao, J.P.; Alonso, D. Internal dissipation and heat leaks in quantum thermodynamic cycles. *Phys. Rev. E* **2015**, *92*, 032136.
9. Mari, A.; Eisert, J. Cooling by heating: Very hot thermal light can significantly cool quantum systems. *Phys. Rev. Lett.* **2012**, *108*, 120602.
10. Mitchison, M.T.; Huber, M.; Prior, J.; Woods, M.P.; Plenio, M.B. Autonomous quantum thermal machines in atom-cavity systems. **2016**, arXiv:1603.02082.
11. Leggio, B.; Bellomo, B.; Antezza, M. Quantum thermal machines with single nonequilibrium environments. *Phys. Rev. A* **2015**, *91*, 012117.
12. Chen, Y.X.; Li, S.W. Quantum refrigerator driven by current noise. *Europhys. Lett.* **2012**, *97*, 40003.
13. Venturelli, D.; Fazio, R.; Giovannetti, V. Minimal self-contained refrigerator machine based on four quantum dots. *Phys. Rev. Lett.* **2013**, *110*, 256801.
14. Peng, Z.H.; Liu, Y.; Peltonen, J.T.; Tamamoto, T.; Tsai, J.S.; Astafiev, O. Correlated emission lassing in harmonic oscillators coupled via a single three-level artificial atom. *Phys. Rev. Lett.* **2015**, *115*, 223603.
15. Kosloff, R. Quantum thermodynamics: A dynamical point of view. *Entropy* **2013**, *15*, 2100–2118.
16. Correa, L.A.; Mehboudi, M. Testing a quantum heat pump with a two-level spin. *Entropy* **2016**, *18*, 141.
17. Breuer, H.; Petruccione, F. *The Theory of Open Quantum Systems*; Oxford University Press: Oxford, UK, 2002.
18. Spohn, H. Entropy production for quantum dynamical semigroups. *J. Math. Phys.* **1977**, *19*, 1227–1230.
19. Alicki, R. The quantum open system as a model of the heat engine. *J. Phys. A: Math. Gen.* **1979**, *12*, L103–L107.
20. Levy, A.; Kosloff, R. The local approach to quantum transport may violate the second law of thermodynamics. *Europhys. Lett.* **2014**, *107*, 20004.
21. Van den Broeck, C.; Esposito, M. Ensemble and trajectory thermodynamics: A brief introduction. *Phys. A* **2015**, *418*, 6–16.
22. Hill, T.L. Studies in irreversible thermodynamics IV. Diagrammatic representation of steady state fluxes for unimolecular systems. *J. Theoret. Biol.* **1966**, *10*, 442–459.
23. Kalpazidou, S.L. *Cycle Representation of Markov Processes*; Springer: Berlin, Germany, 2006.
24. Jiang, D.Q.; Qian, M.; Qian, M.P. *Mathematical Theory of Nonequilibrium Steady States*; Springer: Berlin, Germany, 2004.
25. Schnakenberg, J. Network theory of microscopic and macroscopic behaviour of master equation systems. *Rev. Mod. Phys.* **1976**, *48*, 571–585.
26. Andrieux, D.; Gaspard, P. Fluctuation theorem for currents and Schnakenberg network theory. *J. Stat. Phys.* **2007**, *127*, 107–131.
27. Poletini, M. Cycle/cocycle oblique projections on oriented graphs. *Lett. Math. Phys.* **2015**, *105*, 89–107.
28. Altaner, B.; Grosskinsky, S.; Herminghaus, S.; Kathän, L.; Timme, M.; Vollmer, J. Network representations of nonequilibrium steady states: cycle decompositions, symmetries and dominant paths. *Phys. Rev. E* **2012**, *85*, 041133.
29. Moon, J.W. Some determinants and the matrix-tree theorem. *Discret. Math.* **1994**, *124*, 163–171.
30. González, J.O.; Palao, J.P.; Alonso, D. A network description of dissipative effects in thermal machines. 2016, Unpublished work.
31. Knoch, F.; Speck, T. Cycle representatives for the coarse-graining of systems driven into a non-equilibrium steady state. *New J. Phys.* **2015**, *17*, 115004.
32. Alicki, R.; Lidar, D.A.; Zanardi, P. Internal consistency of fault-tolerant quantum error correction in light of rigorous derivations of the quantum Markovian limit. *Phys. Rev. A* **2006**, *73*, 052311.
33. Szczegielski, K.; Gelbwaser-Klimovsky, D.; Alicki, R. Markovian master equation and thermodynamics of a two-level system in a strong laser field. *Phys. Rev. E* **2013**, *87*, 012120.
34. Brask, J.B.; Brunner, N. Small quantum absorption refrigerator in the transient regime: Time scales, enhanced cooling and entanglement. *Phys. Rev. E* **2015**, *92*, 062101.

Este documento incorpora firma electrónica, y es copia auténtica de un documento electrónico archivado por la ULL según la Ley 39/2015.
Su autenticidad puede ser contrastada en la siguiente dirección <https://sede.ull.es/validacion/>

Identificador del documento: 2111210

Código de verificación: lZvvKBaU

Firmado por: Javier Onam González López
UNIVERSIDAD DE LA LAGUNA

Fecha: 09/09/2019 11:04:42

Daniel Alonso Ramírez
UNIVERSIDAD DE LA LAGUNA

11/09/2019 14:53:47

35. Correa, L.A.; Palao, J.P.; Adesso, G.; Alonso, D. Optimal performance of endoreversible quantum refrigerators. *Phys. Rev. E* **2014**, *90*, 062124.
36. Johnson, D.B. Finding all the elementary circuits of a directed graph. *SIAM J. Comput.* **1975**, *4*, 77–84.



© 2016 by the authors; licensee MDPI, Basel, Switzerland. This article is an open access article distributed under the terms and conditions of the Creative Commons Attribution (CC-BY) license (<http://creativecommons.org/licenses/by/4.0/>).

Este documento incorpora firma electrónica, y es copia auténtica de un documento electrónico archivado por la ULL según la Ley 39/2015.
Su autenticidad puede ser contrastada en la siguiente dirección <https://sede.ull.es/validacion/>

Identificador del documento: 2111210 Código de verificación: lZvvKBaU

Firmado por: Javier Onam González López
UNIVERSIDAD DE LA LAGUNA

Fecha: 09/09/2019 11:04:42

Daniel Alonso Ramírez
UNIVERSIDAD DE LA LAGUNA

11/09/2019 14:53:47

5.2 Testing the Validity of the ‘Local’ and ‘Global’ GKLS Master Equations on an Exactly Solvable Model

Open Syst. Inf. Dyn., 24(04):1740010, 2017

J. Onam González, Luis A. Correa, Giorgio Nocerino, José P.
Palao, Daniel Alonso and Gerardo Adesso

Este documento incorpora firma electrónica, y es copia auténtica de un documento electrónico archivado por la ULL según la Ley 39/2015.
Su autenticidad puede ser contrastada en la siguiente dirección <https://sede.ull.es/validacion/>

Identificador del documento: 2111210 Código de verificación: LZvVKBaU

Firmado por: Javier Onam González López
UNIVERSIDAD DE LA LAGUNA

Fecha: 09/09/2019 11:04:42

Daniel Alonso Ramírez
UNIVERSIDAD DE LA LAGUNA

11/09/2019 14:53:47

Testing the Validity of the ‘Local’ and ‘Global’ GKLS Master Equations on an Exactly Solvable Model

J. Onam González^{1,2}, Luis A. Correa², Giorgio Nocerino², José P. Palao¹,
 Daniel Alonso¹, and Gerardo Adesso²

¹*Dpto. de Física and IUdEA: Instituto Universitario de Estudios Avanzados
 Universidad de La Laguna, 38203 Spain*

²*School of Mathematical Sciences and Centre for the Mathematics and Theoretical Physics
 of Quantum Non-Equilibrium Systems
 The University of Nottingham, University Park, Nottingham NG7 2RD, United Kingdom*

(Received: July 22, 2017; Accepted: August 1, 2017; Published: November 30, 2017)

Abstract. When deriving a master equation for a multipartite weakly-interacting open quantum systems, dissipation is often addressed *locally* on each component, i.e. ignoring the coherent couplings, which are later added ‘by hand’. Although simple, the resulting local master equation (LME) is known to be thermodynamically inconsistent. Otherwise, one may always obtain a consistent *global* master equation (GME) by working on the energy basis of the full interacting Hamiltonian. Here, we consider a two-node ‘quantum wire’ connected to two heat baths. The stationary solution of the LME and GME are obtained and benchmarked against the exact result. Importantly, in our model, the validity of the GME is constrained by the underlying secular approximation. Whenever this breaks down (for resonant weakly-coupled nodes), we observe that the LME, in spite of being thermodynamically flawed: (a) predicts the correct steady state, (b) yields with the exact asymptotic heat currents, and (c) reliably reflects the correlations between the nodes. In contrast, the GME fails at all three tasks. Nonetheless, as the inter-node coupling grows, the LME breaks down whilst the GME becomes correct. Hence, the global and local approach may be viewed as *complementary* tools, best suited to different parameter regimes.

Keywords: Open quantum systems; quantum master equations; heat transport; Gaussian states; quantum thermodynamics; quantum correlations.

1. Introduction

The Gorini-Kossakowski-Lindblad-Sudarshan (GKLS) quantum master equation [29, 18] is central in the theory of open quantum systems. It reads

$$\begin{aligned} \frac{d\varrho}{dt} &= \mathcal{L}\varrho = -\frac{i}{\hbar}[\mathbf{H}, \varrho] + \mathcal{D}\varrho \\ &= -\frac{i}{\hbar}[\mathbf{H}, \varrho] + \sum_k \gamma_k \left(A_k \varrho A_k^\dagger - \frac{1}{2} A_k^\dagger A_k \varrho - \frac{1}{2} \varrho A_k^\dagger A_k \right), \end{aligned} \quad (1)$$

1740010-1

Este documento incorpora firma electrónica, y es copia auténtica de un documento electrónico archivado por la ULL según la Ley 39/2015.
 Su autenticidad puede ser contrastada en la siguiente dirección <https://sede.ull.es/validacion/>

Identificador del documento: 2111210 Código de verificación: lZvvKBaU

Firmado por: Javier Onam González López
 UNIVERSIDAD DE LA LAGUNA

Fecha: 09/09/2019 11:04:42

Daniel Alonso Ramírez
 UNIVERSIDAD DE LA LAGUNA

11/09/2019 14:53:47

J. O. González, et al.

and generates a quantum *dynamical semigroup*, i.e. it gives rise to a dynamical map

$$\varrho(t) = \mathcal{V}(t)\varrho(t_0) = e^{\mathcal{L}(t-t_0)}\varrho(t_0)$$

with the semi-group property $\mathcal{V}(t)\mathcal{V}(s) = \mathcal{V}(t+s)$. This type of memoryless or Markovian evolution arises naturally when an open quantum system couples weakly to an environment at inverse-temperature $\beta = (k_B T)^{-1}$, so that the typical relaxation time is by far the largest scale in the problem [5].

Among many others, equation (1) has the following key properties:

- (i) It ensures a *completely positive* dynamics which, in turn, implies that the relative entropy $S(\varrho_1|\varrho_2) := \text{tr}\{\varrho_1(\log \varrho_1 - \log \varrho_2)\}$ between any two states evolving under $\mathcal{V}(t)$ decreases *monotonically* [43, 32], i.e.,

$$\frac{d}{dt}S(\varrho_1(t)|\varrho_2(t)) \leq 0.$$

- (ii) Under mild assumptions, the thermal state $\tau \propto \exp(-\beta\mathbf{H})$ is the *only stationary state* of $\mathcal{V}(t)$, i.e. $\mathcal{L}\tau = 0$ [42]. That is, (1) describes relaxation towards thermal equilibrium.

Interestingly, one may use (1) to model a continuous (quantum) thermodynamic cycle [3, 25]. By coupling the open system (i.e. the *working substance*) to various heat baths at different temperatures and possibly also to a periodic external drive, a stationary non-equilibrium state builds up. The direction of the corresponding steady-state heat currents may be controlled by suitably engineering the spectrum of the working substance. Hence, we can speak of ‘quantum heat engines’ or ‘quantum compression/absorption refrigerators’ [35], which have attracted a lot of attention in recent years [26, 27, 15, 51, 17].

In such quantum heat devices, the stationary incoming heat currents $\{\dot{Q}_\alpha\}$ and the power output $-\mathcal{P}$ are defined as [3]

$$\frac{d}{dt}\text{tr}\{\mathbf{H}\varrho_\infty\} = 0 = \mathcal{P} + \sum_\alpha \dot{Q}_\alpha := \text{tr}\left\{\frac{\partial \mathbf{H}}{\partial t}\varrho_\infty\right\} + \sum_\alpha \text{tr}\{\mathbf{H}\mathcal{D}_\alpha\varrho_\infty\}, \quad (2)$$

where ϱ_∞ is the steady state of the working substance, and \mathcal{D}_α denotes the GKLS dissipation super-operator associated with bath α .

Owing to properties (i) and (ii) above, the stationary heat currents \dot{Q}_α satisfy the relation $\sum_\alpha \dot{Q}_\alpha/T_\alpha \leq 0$, which is the Clausius inequality. In other words, addressing the dynamics of quantum heat devices with GKLS quantum master equations ensures thermodynamic consistency.

When modelling open quantum systems made up of multiple weakly-interacting parts coupled to local environments, it is commonplace to build the corresponding master equation by simply adding the local dissipators for

1740010-2

Este documento incorpora firma electrónica, y es copia auténtica de un documento electrónico archivado por la ULL según la Ley 39/2015.
 Su autenticidad puede ser contrastada en la siguiente dirección <https://sede.ull.es/validacion/>

Identificador del documento: 2111210 Código de verificación: lZvvKBaU

Firmado por: Javier Onam González López
 UNIVERSIDAD DE LA LAGUNA

Fecha: 09/09/2019 11:04:42

Daniel Alonso Ramírez
 UNIVERSIDAD DE LA LAGUNA

11/09/2019 14:53:47

Testing the Validity of the ‘Local’ and ‘Global’ GKLS Master Equations

the relaxation of each individual component (ignoring their coherent interactions). That is, for a multipartite system with Hamiltonian $\mathbf{H} = \sum_j \mathbf{h}_j + k \mathbf{V}$, where \mathbf{V} contains all the internal couplings (of strength k), one would write^a

$$\frac{d\boldsymbol{\rho}}{dt} = -\frac{i}{\hbar}[\mathbf{H}, \boldsymbol{\rho}] + \sum_{\alpha} \mathcal{D}_{\alpha}^{(k=0)} \boldsymbol{\rho}. \quad (3)$$

Although (3) is in GKLS form, property (ii) ceases to hold, as the dissipators $\mathcal{D}_{\alpha}^{(k=0)}$ do not match the Hamiltonian \mathbf{H} , but rather the non-interacting $\sum_j \mathbf{h}_j$. Consequently, describing heat transport with the local master equation (3) may lead to thermodynamic inconsistencies: Heat could, for instance, flow against the temperature gradient [28], or non-vanishing steady-state heat currents could be present even if all reservoirs are set to the same temperature [45].

These observations, strongly advise to follow the standard procedure to consistently obtain the correct global dissipators \mathcal{D}_{α} [5]. However, doing so may become particularly challenging when dealing with large systems, e.g. long harmonic or spin chains. Moreover, in such cases the capital assumption that the dissipation time scale is by far the largest in the problem is likely to break down as the spectrum of the system becomes denser [53]; Equation (1) would then lack a microscopic justification. These difficulties explain the popularity of simple approaches based on weak internal coupling approximations such as equation (3) [53, 46]. In this paper we wish to put such local approaches to the test.

In particular, we choose an exactly solvable model consisting of a two-node harmonic chain weakly coupled on both edges to two heat baths at different temperatures. Our system is set up so that, when the inter-node coupling strength becomes comparable or smaller than the node-baths dissipative couplings, the secular approximation underlying (1) may break down. This allows us to gauge to which extent the local master equation (LME) remains an accurate description. Interestingly, we find that the local approach yields an excellent approximation to the steady state, the stationary heat currents, and the asymptotic quantum and classical correlations, in the regime of parameters in which the global master equation (GME) fails even qualitatively. More generally, it follows that heat conduction through arbitrarily large harmonic chains can be correctly modelled within the local approach always provided that the internal couplings are sufficiently weak. The present work thus adds to the efforts of [40, 11, 53, 44, 41, 45, 28, 46, 38, 10] to clarify the *dos and don'ts* of modelling heat transport through multipartite open quantum systems.

This paper is structured as follows: In Sect. 2.1 we outline the steps of the microscopic derivation of the GKLS quantum master equation. We

^aFor simplicity, we are omitting the Lamb shift (cf. Sect. 2.2).

1740010-3

Este documento incorpora firma electrónica, y es copia auténtica de un documento electrónico archivado por la ULL según la Ley 39/2015.
 Su autenticidad puede ser contrastada en la siguiente dirección <https://sede.ull.es/validacion/>

Identificador del documento: 2111210 Código de verificación: lZvvKBaU

Firmado por: Javier Onam González López
 UNIVERSIDAD DE LA LAGUNA

Fecha: 09/09/2019 11:04:42

Daniel Alonso Ramírez
 UNIVERSIDAD DE LA LAGUNA

11/09/2019 14:53:47

J. O. González, et al.

then proceed to derive and solve such an equation for our specific model in Sect. 2.2. The alternative local master equation is obtained in Sect. 2.3. Before proceeding to benchmark both approaches, in Sect. 3 we sketch how the exact steady-state solution of the system may be obtained by solving the quantum Langevin equations. We then devote Sect. 4 to present and discuss our results. Finally, in Sect. 5 we summarize and draw our conclusions.

2. Deriving Markovian Master Equations

2.1. THE MODEL, THE MARKOVIAN MASTER EQUATION AND ITS STEADY STATE

We will consider a two-node ‘quantum wire’ (see Fig. 1) consisting of mechanically-coupled harmonic oscillators with bare frequencies ω_c and ω_h and coupling strength $k > 0$. Each node will be weakly connected to a bosonic bath, i.e. an infinite collection of uncoupled harmonic modes in thermal equilibrium (at temperatures $T_c < T_h$). The total Hamiltonian may be cast as

$$\begin{aligned} H = & \sum_{\alpha \in \{c,h\}} \left(\frac{\omega_\alpha^2}{2} \mathbf{X}_\alpha^2 + \frac{\mathbf{P}_\alpha^2}{2} \right) + \frac{k}{2} (\mathbf{X}_c - \mathbf{X}_h)^2 \\ & + \sum_{\alpha \in \{c,h\}} \sum_{\mu} \left(\frac{\omega_{\alpha,\mu}^2 m_{\alpha,\mu}}{2} \mathbf{x}_{\alpha,\mu}^2 + \frac{\mathbf{P}_{\alpha,\mu}^2}{2m_{\alpha,\mu}} \right) \\ & - \sum_{\alpha \in \{c,h\}} \mathbf{X}_\alpha \otimes \sum_{\mu} g_{\alpha,\mu} \mathbf{x}_{\alpha,\mu}, \end{aligned} \quad (4)$$

where the masses of the nodes have been set to $m_c = m_h = 1$, and the constants $g_{\alpha,\mu}$ stand for the coupling strength between node α and each of the environmental modes (α, μ) . Also, in all what follows we shall set \hbar and the Boltzmann constant k_B to 1. We will refer to the first three terms in the right-hand side of (4) as the free (system + baths) Hamiltonian $\mathbf{H}_0 = \mathbf{H}_S + \mathbf{H}_B$, as opposed to the last term \mathbf{H}_{int} , which describes the system-baths interaction. For later convenience, we shall also introduce the notation $\mathbf{B}_\alpha := \sum_{\mu} g_{\alpha,\mu} \mathbf{x}_{\alpha,\mu}$.

We will group the system-baths coupling constants in the *spectral density* functions defined as

$$J_\alpha(\omega) := \pi \sum_{\mu} \frac{g_{\alpha,\mu}^2}{2m_\mu \omega_\mu} \delta(\omega - \omega_\mu).$$

In particular, we will choose 1D baths with the Ohmic form

$$J_c(\omega) = J_h(\omega) = \lambda^2 \omega \frac{\Lambda^2}{\omega^2 + \Lambda^2}, \quad (5)$$

1740010-4

Este documento incorpora firma electrónica, y es copia auténtica de un documento electrónico archivado por la ULL según la Ley 39/2015.
 Su autenticidad puede ser contrastada en la siguiente dirección <https://sede.ull.es/validacion/>

Identificador del documento: 2111210 Código de verificación: lZvvKBaU

Firmado por: Javier Onam González López
 UNIVERSIDAD DE LA LAGUNA

Fecha: 09/09/2019 11:04:42

Daniel Alonso Ramírez
 UNIVERSIDAD DE LA LAGUNA

11/09/2019 14:53:47

Testing the Validity of the ‘Local’ and ‘Global’ GKLS Master Equations

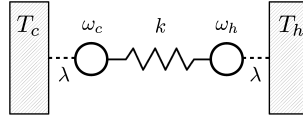


Fig. 1: Schematic representation of the wire. The two harmonic nodes at frequencies ω_c and ω_h are coupled through a spring-like interaction of strength k . Each node is, in turn, dissipatively coupled to a ‘cold’ and ‘hot’ heat bath at temperatures $T_c < T_h$. The dissipation strength λ^2 is assumed sufficiently weak to justify the use of a perturbative master equation up to $\mathcal{O}(\lambda^2)$.

where Λ is a high-frequency cutoff ($\max\{\omega_c, \omega_h\} \ll \Lambda$) and the parameter λ captures the *dissipation strength*. Note that the bath operators \mathbf{B}_α are thus $\mathcal{O}(\lambda)$.

For completeness, we will now briefly sketch a simple procedure to obtain the standard second-order Markovian generator for the reduced dynamics of the system (see [5] for full details). Let us take the Liouville-von Neumann equation in the interaction picture

$$\frac{d\tilde{\rho}(t)}{dt} = -i[\tilde{\mathbf{H}}_{\text{int}}(t), \tilde{\rho}(t)], \quad (6)$$

where $\tilde{\mathbf{H}}_{\text{int}}(t) := e^{i\mathbf{H}_0 t} \mathbf{H}_{\text{int}} e^{-i\mathbf{H}_0 t}$ and $[\cdot, \cdot]$ stands for a commutator. Formally integrating (6) and assuming that the initial condition is such that $\text{tr}\{\tilde{\rho}(0) \tilde{\mathbf{H}}_{\text{int}}\} = 0$ yields the following equation of motion for the system:

$$\frac{d\tilde{\sigma}}{dt} = - \int_0^t ds \text{tr}_B[\tilde{\mathbf{H}}_{\text{int}}(t), [\tilde{\mathbf{H}}_{\text{int}}(s), \tilde{\rho}(s)]]. \quad (7)$$

Here, $\tilde{\sigma} := \text{tr}_B \tilde{\rho}$ and $\text{tr}_B\{\cdot\}$ denotes trace over the baths. We will now assume that the dissipation strength λ is so weak that when starting from a factorized initial condition $\rho_0 := \sigma(0) \otimes \tau_c \otimes \tau_h$ the propagated state $\tilde{\rho}(t) \simeq \tilde{\sigma}(t) \otimes \tau_c \otimes \tau_h$ remains approximately factorized at all times. $\tau_{\alpha \in \{c, h\}}$ are thermal states for the hot and cold bath. We will also replace $\tilde{\sigma}(s)$ inside the integral in (7) by $\tilde{\sigma}(t)$, thus making it time-local. The change of variables $s \rightarrow t - s$ yields the Redfield equation [39, 9]

$$\frac{d\tilde{\sigma}}{dt} \simeq - \int_0^t ds \text{tr}_B[\tilde{\mathbf{H}}_{\text{int}}(t), [\tilde{\mathbf{H}}_{\text{int}}(t-s), \tilde{\sigma}(t) \otimes \tau_c \otimes \tau_h]]. \quad (8)$$

Notice that the resulting state $\rho(t)$ does keep a memory of the initial condition $\rho(0)$ and hence, (8) is non-Markovian. However, provided that the

1740010-5

Este documento incorpora firma electrónica, y es copia auténtica de un documento electrónico archivado por la ULL según la Ley 39/2015.
 Su autenticidad puede ser contrastada en la siguiente dirección <https://sede.ull.es/validacion/>

Identificador del documento: 2111210 Código de verificación: lZvvKBaU

Firmado por: Javier Onam González López
 UNIVERSIDAD DE LA LAGUNA

Fecha: 09/09/2019 11:04:42

Daniel Alonso Ramírez
 UNIVERSIDAD DE LA LAGUNA

11/09/2019 14:53:47

J. O. González, et al.

integrand above decays sufficiently fast, one might set $t \rightarrow \infty$ in the upper limit of integration, which is referred to as Born-Markov approximation. This approximation is justified whenever $\lambda^2 \ll \min\{T, \Lambda\}$.

A further step still remains to be undertaken in order to bring the resulting ‘Markovian Redfield’ master equation to the canonical GKLS form — the secular approximation. Let us examine $\tilde{\mathbf{H}}_{\text{int}}(t)$ more closely. One may always decompose $\mathbf{X}_\alpha = \sum_\omega \mathbf{L}_\alpha^\omega$, where $[\mathbf{H}_S, \mathbf{L}_\alpha^\omega] = -\omega \mathbf{L}_\alpha^\omega$, so that $\tilde{\mathbf{H}}_{\text{int}} = \sum_\omega e^{-i\omega t} \mathbf{L}_\alpha^\omega \otimes \tilde{\mathbf{B}}_\alpha(t)$, with the interaction-picture bath operator $\tilde{\mathbf{B}}_\alpha(t) = e^{i\mathbf{H}_B t} \mathbf{B}_\alpha e^{-i\mathbf{H}_B t}$. Plugging this into (8) leads to

$$\frac{d\tilde{\sigma}}{dt} \simeq \frac{1}{2} \sum_\alpha \sum_{\omega, \omega'} e^{i(\omega' - \omega)t} \gamma_\alpha(\omega) \left(\mathbf{L}_\alpha^\omega \tilde{\sigma} \mathbf{L}_\alpha^{\omega'\dagger} - \mathbf{L}_\alpha^{\omega'\dagger} \mathbf{L}_\alpha^\omega \tilde{\sigma} \right) + \text{h.c.}, \quad (9)$$

where

$$\gamma_\alpha(\omega) = 2 \operatorname{Re} \int_0^\infty ds e^{i\omega s} \operatorname{tr}_B \{ \mathbf{B}_\alpha(t) \mathbf{B}_\alpha(t-s) \}.$$

Note that we are completely ignoring

$$\operatorname{Im} \int_0^\infty ds e^{i\omega s} \operatorname{tr}_B \{ \mathbf{B}_\alpha(t) \mathbf{B}_\alpha(t-s) \},$$

which would eventually lead to a mere shift (of order λ^2) on the energy levels of the Hamiltonian (Lamb shift) [5]. The secular approximation consists in time-averaging of (9) over an interval of the order of the dissipation time $T_D \sim \lambda^{-2}$. All terms with $\omega' \neq \omega$ above can then be discarded provided that they oscillate fast as compared with T_D . Returning to the Schrödinger picture, finally leaves us with the GKLS quantum master equation

$$\begin{aligned} \frac{d\sigma}{dt} &\simeq -i[\mathbf{H}_S, \sigma] + \sum_\alpha \mathcal{D}_\alpha \sigma \\ &= -i[\mathbf{H}_S, \sigma] + \sum_\alpha \sum_\omega \gamma_\alpha(\omega) \left(\mathbf{L}_\alpha^\omega \sigma \mathbf{L}_\alpha^{\omega\dagger} - \frac{1}{2} \{ \mathbf{L}_\alpha^{\omega\dagger} \mathbf{L}_\alpha^\omega, \sigma \}_+ \right), \quad (10) \end{aligned}$$

where $\{ \cdot, \cdot \}_+$ stands for anti-commutator. In the next section, we will concentrate in obtaining the specific form of the operators \mathbf{L}_α^ω for the Hamiltonian in (4).

Because (4) is overall quadratic in position and momenta, the steady state will be Gaussian and thus, fully characterized by its first and second order moments [2]. In fact, one can easily see that $\langle \mathbf{X}_\alpha \rangle = \langle \mathbf{P}_\alpha \rangle = 0$, where $\langle \cdot \rangle$ denotes stationary average. As a result, the steady state will be specified

1740010-6

Este documento incorpora firma electrónica, y es copia auténtica de un documento electrónico archivado por la ULL según la Ley 39/2015.
 Su autenticidad puede ser contrastada en la siguiente dirección <https://sede.ull.es/validacion/>

Identificador del documento: 2111210 Código de verificación: lZvvKBaU

Firmado por: Javier Onam González López
 UNIVERSIDAD DE LA LAGUNA

Fecha: 09/09/2019 11:04:42

Daniel Alonso Ramírez
 UNIVERSIDAD DE LA LAGUNA

11/09/2019 14:53:47

Testing the Validity of the ‘Local’ and ‘Global’ GKLS Master Equations

only by the 4×4 covariance matrix, with elements $[\Gamma]_{kl} := \frac{1}{2} \langle \{ \mathbf{R}_k, \mathbf{R}_l \}_+ \rangle$, with $\vec{\mathbf{R}} = (\mathbf{X}_c, \mathbf{P}_c, \mathbf{X}_h, \mathbf{P}_h)^T$.

Since we wish to calculate the covariances $[\Gamma]_{kl}$ rather than the state σ , it will be more convenient to work with the adjoint master equation [5] which, for an arbitrary system observable in the Heisenberg picture $\mathbf{O}(t)$, reads

$$\begin{aligned} \frac{d\mathbf{O}}{dt} &\simeq i[\mathbf{H}_S, \mathbf{O}] + \sum_{\alpha} \mathcal{D}_{\alpha}^{\dagger} \mathbf{O} \\ &= i[\mathbf{H}_S, \mathbf{O}] + \sum_{\alpha} \sum_{\omega} \gamma_{\alpha}(\omega) \left(\mathbf{L}_{\alpha}^{\omega \dagger} \mathbf{O} \mathbf{L}_{\alpha}^{\omega} - \frac{1}{2} \{ \mathbf{L}_{\alpha}^{\omega \dagger} \mathbf{L}_{\alpha}^{\omega}, \mathbf{O} \}_+ \right). \end{aligned} \quad (11)$$

2.2. THE GLOBAL MASTER EQUATION

The first step to derive consistent $\mathbf{L}_{\alpha}^{\omega}$ operators will be to rotate \mathbf{H}_S into its normal modes. These are

$$\boldsymbol{\eta}_+ = \cos \vartheta \mathbf{X}_c - \sin \vartheta \mathbf{X}_h \quad (12a)$$

$$\boldsymbol{\eta}_- = \sin \vartheta \mathbf{X}_c + \cos \vartheta \mathbf{X}_h, \quad (12b)$$

where the angle ϑ is

$$\cos^2 \vartheta = \frac{-\delta_{\omega}^2 + \sqrt{4k^2 + \delta_{\omega}^4}}{2\sqrt{4k^2 + \delta_{\omega}^4}} \quad (13)$$

and, in turn, $\delta_{\omega}^2 := \omega_h^2 - \omega_c^2$. The corresponding normal-mode frequencies write as

$$\Omega_{\pm}^2 = \frac{1}{2} \left(\omega_c^2 + \omega_h^2 + 2k \pm \sqrt{4k^2 + \delta_{\omega}^4} \right). \quad (14)$$

After this transformation, the Hamiltonian (4) rewrites as

$$\begin{aligned} \mathbf{H} &= \sum_{s \in \{+, -\}} \left(\frac{\Omega_s^2}{2} \boldsymbol{\eta}_s^2 + \frac{\mathbf{\Pi}_s^2}{2} \right) + \mathbf{H}_B - (\cos \vartheta \boldsymbol{\eta}_+ + \sin \vartheta \boldsymbol{\eta}_-) \otimes \mathbf{B}_c \\ &\quad + (\sin \vartheta \boldsymbol{\eta}_+ - \cos \vartheta \boldsymbol{\eta}_-) \otimes \mathbf{B}_h, \end{aligned} \quad (15)$$

where $\mathbf{\Pi}_s = d\boldsymbol{\eta}_s/dt$. By writing $\boldsymbol{\eta}_s = (\mathbf{a}_s + \mathbf{a}_s^{\dagger})/\sqrt{2\Omega_s}$ (with \mathbf{a}_s and \mathbf{a}_s^{\dagger} being annihilation and creation operators on mode Ω_s) one can see that $\mathbf{X}_{\alpha} = \mathbf{L}_{\alpha}^{\Omega_+} + \mathbf{L}_{\alpha}^{\Omega_-} + \text{h.c.}$, where $\mathbf{L}_c^{\Omega_+} := \cos \vartheta \mathbf{a}_+/\sqrt{2\Omega_+}$, $\mathbf{L}_c^{\Omega_-} := \sin \vartheta \mathbf{a}_-/\sqrt{2\Omega_-}$, $\mathbf{L}_h^{\Omega_+} := -\sin \vartheta \mathbf{a}_+/\sqrt{2\Omega_+}$, $\mathbf{L}_h^{\Omega_-} := \cos \vartheta \mathbf{a}_-/\sqrt{2\Omega_-}$, and $\mathbf{L}_{\alpha}^{-\Omega_{\pm}} := (\mathbf{L}_{\alpha}^{\Omega_{\pm}})^{\dagger}$.

Looking back to the right-hand side of (9), we see that there are 16 terms associated with two different open decay channels, oscillating as $e^{i(\omega' - \omega)t}$ at frequencies $|\omega' - \omega| = \{0, 2\Omega_+, 2\Omega_-, \Omega_+ + \Omega_-, \Omega_+ - \Omega_-\}$. Provided that the nodes are sufficiently detuned, i.e. $\delta_{\omega} \gg \lambda^2$, the secular approximation is

1740010-7

Este documento incorpora firma electrónica, y es copia auténtica de un documento electrónico archivado por la ULL según la Ley 39/2015.
 Su autenticidad puede ser contrastada en la siguiente dirección <https://sede.ull.es/validacion/>

Identificador del documento: 2111210 Código de verificación: lZvvKBaU

Firmado por: Javier Onam González López
 UNIVERSIDAD DE LA LAGUNA

Fecha: 09/09/2019 11:04:42

Daniel Alonso Ramírez
 UNIVERSIDAD DE LA LAGUNA

11/09/2019 14:53:47

J. O. González, et al.

guaranteed to be valid for *any* value of the coupling k . However, if $\omega_h - \omega_c$ became comparable or smaller than the dissipation strength λ^2 , there would be no justification to discard the non-secular terms oscillating at $\Omega_+ - \Omega_-$ when k becomes very small. Indeed, defining $R_{\pm} := 2k \pm \sqrt{4k^2 + \delta_{\omega}^4}$ one may write

$$\Omega_+ - \Omega_- = \sqrt{\frac{\omega_c^2 + \omega_h^2}{2}} \left(\sqrt{1 + \frac{R_+}{\omega_c^2 + \omega_h^2}} - \sqrt{1 + \frac{R_-}{\omega_c^2 + \omega_h^2}} \right) \quad (16)$$

whenever $R_{\pm}/(\omega_c^2 + \omega_h^2) \ll 1$, the Taylor expansion $\sqrt{1+x} = 1 + \frac{x}{2} - \frac{x^2}{8} + \dots$ allows to approximate (16) as

$$\Omega_+ - \Omega_- = \sqrt{\frac{4k^2 + \delta_{\omega}^4}{2(\omega_h^2 + \omega_c^2)}} + \mathcal{O}\left(\frac{R_{\pm}^2}{(\omega_c^2 + \omega_h^2)^{3/2}}\right). \quad (17)$$

From (17) it is clear that for the secular approximation to be valid the dissipation rate must be such that

$$\lambda^2 \ll \sqrt{\frac{4k^2 + \delta_{\omega}^4}{2(\omega_h^2 + \omega_c^2)}}, \quad (18)$$

which, in the limit of resonant nodes simplifies to $\lambda^2 \ll k/\omega_c$. Hence, we can anticipate that (10) will fail to describe nearly resonant weakly coupled nodes, which is precisely the regime in which we shall focus our analysis.

The only additional ingredient required to build (11) are the *decay rates* $\gamma_{\alpha}(\pm\Omega_{\pm})$. A direct calculation leads to

$$\gamma_{\alpha}(\omega) = 2J(\omega)[1 + n_{\alpha}(\omega)], \quad (19)$$

where $n_{\alpha}(\omega) := (e^{\omega/T_{\alpha}} - 1)^{-1}$ is the bosonic occupation number for frequency ω at temperature T_{α} . Note that $\gamma_{\alpha}(-\omega) = \exp(-\omega/T_{\alpha})\gamma_{\alpha}(\omega)$. Combining all the above, and after tedious but straightforward algebra, we can obtain a closed set of equations of motion for the covariances^b $\langle \eta_{\pm}^2 \rangle$, $\langle \Pi_{\pm}^2 \rangle$, and $\langle \{\eta_{\pm}, \Pi_{\pm}\}_+ \rangle$. Note that $\langle \cdot \rangle$ denotes here instantaneous average.

$$\frac{d}{dt} \langle \eta_{\pm}^2 \rangle = \Delta_{\pm} \langle \eta_{\pm}^2 \rangle + \langle \{\eta_{\pm}, \Pi_{\pm}\}_+ \rangle + \frac{\Sigma_{\pm}}{2\Omega_{\pm}} \quad (20a)$$

$$\frac{d}{dt} \langle \{\eta_{\pm}, \Pi_{\pm}\}_+ \rangle = 2\langle \Pi_{\pm}^2 \rangle - 2\Omega_{\pm} \langle \eta_{\pm}^2 \rangle + \Delta_{\pm} \langle \{\eta_{\pm}, \Pi_{\pm}\}_+ \rangle \quad (20b)$$

$$\frac{d}{dt} \langle \Pi_{\pm}^2 \rangle = \Delta_{\pm} \langle \Pi_{\pm}^2 \rangle - \Omega_{\pm}^2 \langle \{\eta_{\pm}, \Pi_{\pm}\}_+ \rangle + \frac{\Omega_{\pm}}{2} \Sigma_{\pm}, \quad (20c)$$

^bIt is indeed enough to consider the equations of motion for the mode occupation numbers $\langle \mathbf{a}_{\pm}^{\dagger} \mathbf{a}_{\pm} \rangle$ (which are decoupled), to fully solve the dynamics.

1740010-8

Este documento incorpora firma electrónica, y es copia auténtica de un documento electrónico archivado por la ULL según la Ley 39/2015.
 Su autenticidad puede ser contrastada en la siguiente dirección <https://sede.ull.es/validacion/>

Identificador del documento: 2111210 Código de verificación: lZvvKBaU

Firmado por: Javier Onam González López
 UNIVERSIDAD DE LA LAGUNA

Fecha: 09/09/2019 11:04:42

Daniel Alonso Ramírez
 UNIVERSIDAD DE LA LAGUNA

11/09/2019 14:53:47

Testing the Validity of the ‘Local’ and ‘Global’ GKLS Master Equations

where the following notations have been introduced

$$\Delta_+ := \frac{\cos^2 \vartheta}{2\Omega_+} [\gamma_c(-\Omega_+) - \gamma_c(\Omega_+)] + \frac{\sin^2 \vartheta}{2\Omega_+} [\gamma_h(-\Omega_+) - \gamma_h(\Omega_+)] \quad (21a)$$

$$\Delta_- := \frac{\sin^2 \vartheta}{2\Omega_-} [\gamma_c(-\Omega_-) - \gamma_c(\Omega_-)] + \frac{\cos^2 \vartheta}{2\Omega_-} [\gamma_h(-\Omega_-) - \gamma_h(\Omega_-)] \quad (21b)$$

$$\Sigma_+ := \frac{\cos^2 \vartheta}{2\Omega_+} [\gamma_c(-\Omega_+) + \gamma_c(\Omega_+)] + \frac{\sin^2 \vartheta}{2\Omega_+} [\gamma_h(-\Omega_+) + \gamma_h(\Omega_+)] \quad (21c)$$

$$\Sigma_- := \frac{\sin^2 \vartheta}{2\Omega_-} [\gamma_c(-\Omega_-) + \gamma_c(\Omega_-)] + \frac{\cos^2 \vartheta}{2\Omega_-} [\gamma_h(-\Omega_-) + \gamma_h(\Omega_-)]. \quad (21d)$$

Below, it will be convenient to break down each of these coefficients into the sum of its two constituent terms, as $\Delta_{\pm} := \Delta_{\pm}^c + \Delta_{\pm}^h$ and $\Sigma_{\pm} := \Sigma_{\pm}^c + \Sigma_{\pm}^h$, where e.g. $\Delta_+^c = \cos^2 \vartheta [\gamma_c(-\Omega_+) - \gamma_c(\Omega_+)] / (2\Omega_+)$. The further denotations $\Sigma_{\pm}^{\alpha} = W_{-\Omega_{\pm}}^{\alpha} + W_{\Omega_{\pm}}^{\alpha}$, where e.g. $W_{-\Omega_+}^c = \cos^2 \vartheta \gamma_c(-\Omega_+) / (2\Omega_+)$, will also be employed later on.

The stationary solution to (20) is simply $\langle \boldsymbol{\eta}_{\pm}^2 \rangle = -\Sigma_{\pm} / (2\Delta_{\pm}\Omega_{\pm})$, $\langle \boldsymbol{\Pi}_{\pm} \rangle = -\Omega_{\pm} \Sigma_{\pm} / (2\Delta_{\pm})$, and $\langle \{\boldsymbol{\eta}_{\pm}, \boldsymbol{\Pi}_{\pm}\}_+ \rangle = 0$, so that the asymptotic covariance matrix in the original quadratures reads

$$\Gamma^G = \begin{pmatrix} [\Gamma^G]_{11} & 0 & [\Gamma^G]_{13} & 0 \\ 0 & [\Gamma^G]_{22} & 0 & [\Gamma^G]_{24} \\ [\Gamma^G]_{13} & 0 & [\Gamma^G]_{33} & 0 \\ 0 & [\Gamma^G]_{24} & 0 & [\Gamma^G]_{44} \end{pmatrix}, \quad (22)$$

where $[\Gamma^G]_{11} = \langle \boldsymbol{\eta}_+^2 \rangle \cos^2 \vartheta + \langle \boldsymbol{\eta}_-^2 \rangle \sin^2 \vartheta$, $[\Gamma^G]_{22} = \langle \boldsymbol{\Pi}_+^2 \rangle \cos^2 \vartheta + \langle \boldsymbol{\Pi}_-^2 \rangle \sin^2 \vartheta$, $[\Gamma^G]_{33} = \langle \boldsymbol{\eta}_+^2 \rangle \sin^2 \vartheta + \langle \boldsymbol{\eta}_-^2 \rangle \cos^2 \vartheta$, $[\Gamma^G]_{44} = \langle \boldsymbol{\Pi}_+^2 \rangle \sin^2 \vartheta + \langle \boldsymbol{\Pi}_-^2 \rangle \cos^2 \vartheta$, $[\Gamma^G]_{13} = (\langle \boldsymbol{\eta}_-^2 \rangle - \langle \boldsymbol{\eta}_+^2 \rangle) \sin \vartheta \cos \vartheta$, and $[\Gamma^G]_{24} = (\langle \boldsymbol{\Pi}_-^2 \rangle - \langle \boldsymbol{\Pi}_+^2 \rangle) \sin \vartheta \cos \vartheta$. Finally, the steady-state heat currents can be written as

$$\begin{aligned} \dot{Q}_{\alpha}^G &= \text{tr}\{\mathbf{H}_S \mathcal{D}_{\alpha} \boldsymbol{\sigma}(\infty)\} = \langle \mathcal{D}_{\alpha}^{\dagger} \mathbf{H}_S \rangle \\ &= \frac{1}{2} \sum_{s \in \{+, -\}} [\Delta_s^{\alpha} (\Omega_s^2 \langle \boldsymbol{\eta}_s^2 \rangle + \langle \boldsymbol{\Pi}_s^2 \rangle) + \Omega_s \Sigma_s^{\alpha}]. \end{aligned} \quad (23)$$

Using (21) we can cast (23) as

$$\dot{Q}_h^G = -\dot{Q}_c^G = \sum_{s \in \{+, -\}} \Omega_s \frac{W_{\Omega_s}^c W_{\Omega_s}^h}{\Sigma_s} (e^{-\Omega_s/T_h} - e^{-\Omega_s/T_c}), \quad (24)$$

from where it is clear that $T_h > T_c$ entails $\dot{Q}_h^G = -\dot{Q}_c^G > 0$; that is, heat *always* flows from the hotter bath into the colder one.

1740010-9

Este documento incorpora firma electrónica, y es copia auténtica de un documento electrónico archivado por la ULL según la Ley 39/2015.
 Su autenticidad puede ser contrastada en la siguiente dirección <https://sede.ull.es/validacion/>

Identificador del documento: 2111210 Código de verificación: lZvvKBaU

Firmado por: Javier Onam González López
 UNIVERSIDAD DE LA LAGUNA

Fecha: 09/09/2019 11:04:42

Daniel Alonso Ramírez
 UNIVERSIDAD DE LA LAGUNA

11/09/2019 14:53:47

J. O. González, et al.

2.3. THE LOCAL MASTER EQUATION

Recall from Sect. 1 that, while the *local* master equation looks formally identical to the GME, the choice of operators L_α^ω in the local approach is not consistent with the Hamiltonian H_S . As already advanced and provided that the coupling k is weak, one could derive two independent local dissipators $\mathcal{D}_\alpha^{(k=0)}$, acting on the cold and hot nodes *separately*, to then construct an approximate equation of motion such as

$$\frac{d\sigma}{dt} \simeq -i[H_S, \sigma] + \sum_{\alpha \in \{c, h\}} \mathcal{D}_\alpha^{(k=0)} \sigma,$$

as an alternative to (20). One might argue that this is a convenient strategy whenever finding all energy eigenstates of the full interacting Hamiltonian is hard, as these are required to write the decomposition $\{L_\alpha^\omega\}$ of the system operator coupled to each bath [46]. In our simple example, however, the local approach leads to a more complicated dynamics than the global one — all 10 independent covariances are needed in order to obtain a closed set of equations of motion.

Specifically, within the local approach one decomposes $X_\alpha = L_\alpha^{\omega_\alpha} + L_\alpha^{-\omega_\alpha}$, where $L_\alpha^{\omega_\alpha} := b_\alpha / \sqrt{2\omega_\alpha}$, b_α is an annihilation operator on node ω_α , and $L_\alpha^{-\omega_\alpha} := (L_\alpha^{\omega_\alpha})^\dagger$. The adjoint master equation (11) thus becomes

$$\begin{aligned} \frac{dO}{dt} \simeq & i[H_S, O] + \sum_{\alpha \in \{c, h\}} \left[\frac{\gamma_\alpha(\omega_\alpha)}{2\omega_\alpha} (b_\alpha^\dagger O b_\alpha - \frac{1}{2} \{b_\alpha^\dagger b_\alpha, O\}_+) \right. \\ & \left. + \frac{\gamma_\alpha(-\omega_\alpha)}{2\omega_\alpha} (b_\alpha O b_\alpha^\dagger - \frac{1}{2} \{b_\alpha b_\alpha^\dagger, O\}_+) \right]. \end{aligned} \quad (25)$$

From (25), the equations of motion for the elements of the corresponding covariance matrix Γ^L are found to be

$$\frac{d}{dt} \langle X_\alpha^2 \rangle = \langle \{X_\alpha, P_\alpha\}_+ \rangle + \tilde{\Delta}_\alpha \langle X_\alpha^2 \rangle + \frac{\tilde{\Sigma}_\alpha}{2\omega_\alpha} \quad (26a)$$

$$\frac{d}{dt} \langle P_\alpha^2 \rangle = 2k \langle X_{\bar{\alpha}} P_\alpha \rangle - \nu_\alpha^2 \langle \{X_\alpha, P_\alpha\}_+ \rangle + \tilde{\Delta}_\alpha \langle P_\alpha^2 \rangle + \frac{\omega_\alpha \tilde{\Sigma}_\sigma}{2}, \quad \bar{\alpha} \neq \alpha \quad (26b)$$

$$\begin{aligned} \frac{d}{dt} \langle \{X_\alpha, P_\alpha\}_+ \rangle = & 2 \langle P_\alpha^2 \rangle + \tilde{\Delta}_\alpha \langle \{X_\alpha P_\alpha\}_+ \rangle - 2\nu_\alpha^2 \langle X_\alpha^2 \rangle \\ & + 2k \langle X_\alpha X_{\bar{\alpha}} \rangle, \quad \bar{\alpha} \neq \alpha \end{aligned} \quad (26c)$$

$$\begin{aligned} \frac{d}{dt} \langle X_\alpha P_{\bar{\alpha}} \rangle = & \langle P_\alpha P_{\bar{\alpha}} \rangle + k \langle X_\alpha^2 \rangle + \frac{1}{2} (\tilde{\Delta}_\alpha + \tilde{\Delta}_{\bar{\alpha}}) \langle X_\alpha P_{\bar{\alpha}} \rangle \\ & - \nu_{\bar{\alpha}}^2 \langle X_\alpha X_{\bar{\alpha}} \rangle, \quad \bar{\alpha} \neq \alpha \end{aligned} \quad (26d)$$

$$\frac{d}{dt} \langle X_c X_h \rangle = \langle X_c P_h \rangle + \langle X_h P_c \rangle + \frac{1}{2} (\tilde{\Delta}_c + \tilde{\Delta}_h) \langle X_c X_h \rangle \quad (26e)$$

1740010-10

Este documento incorpora firma electrónica, y es copia auténtica de un documento electrónico archivado por la ULL según la Ley 39/2015.
 Su autenticidad puede ser contrastada en la siguiente dirección <https://sede.ull.es/validacion/>

Identificador del documento: 2111210 Código de verificación: lZvvKBaU

Firmado por: Javier Onam González López
 UNIVERSIDAD DE LA LAGUNA

Fecha: 09/09/2019 11:04:42

Daniel Alonso Ramírez
 UNIVERSIDAD DE LA LAGUNA

11/09/2019 14:53:47

Testing the Validity of the ‘Local’ and ‘Global’ GKLS Master Equations

$$\begin{aligned} \frac{d}{dt} \langle \mathbf{P}_c \mathbf{P}_h \rangle = & \frac{k}{2} (\langle \{\mathbf{X}_h, \mathbf{P}_h\}_+ \rangle + \langle \{\mathbf{X}_c, \mathbf{P}_c\}_+ \rangle) - \nu_c^2 \langle \mathbf{X}_c \mathbf{P}_h \rangle \\ & - \nu_h^2 \langle \mathbf{X}_h \mathbf{P}_c \rangle + \frac{1}{2} (\tilde{\Delta}_c + \tilde{\Delta}_h) \langle \mathbf{P}_c \mathbf{P}_h \rangle, \end{aligned} \quad (26f)$$

where

$$\nu_\alpha^2 := \omega_\alpha^2 + k, \quad \tilde{\Delta}_\alpha := \frac{\gamma_\alpha(-\omega_\alpha) - \gamma_\alpha(\omega_\alpha)}{2\omega_\alpha}, \quad \tilde{\Sigma}_\alpha := \frac{\gamma_\alpha(-\omega_\alpha) + \gamma_\alpha(\omega_\alpha)}{2\omega_\alpha},$$

and the angled brackets denote again instantaneous average. The stationary solution of (26) is cumbersome but the steady-state heat currents can be compactly cast as

$$\dot{Q}_\alpha^L = \frac{\tilde{\Delta}_\alpha}{2} [\omega_\alpha^2 \langle \mathbf{X}_\alpha^2 \rangle + \langle \mathbf{P}_\alpha^2 \rangle + k(\langle \mathbf{X}_\alpha^2 \rangle - \langle \mathbf{X}_\alpha \mathbf{X}_{\bar{\alpha}} \rangle)] + \frac{\tilde{\Sigma}_\alpha}{2} \left(\omega_\alpha + \frac{k}{2\omega_\alpha} \right). \quad (27)$$

As anticipated above and unlike (20), (26) does not necessarily yield a thermodynamically consistent steady state: One could even encounter striking situations for which $\dot{Q}_h^L = -\dot{Q}_c^L < 0$ for $T_h > T_c$ or $\dot{Q}_\alpha^L \neq 0$ for $T_h = T_c$, as illustrated in [28, 45].

2.4. COMMENT ON THE GENERAL VALIDITY OF THE LOCAL APPROACH FOR MODELLING HEAT TRANSPORT UNDER WEAK INTERNAL COUPLING

In spite of its thermodynamic inconsistencies, as it was pointed out in [46] the LME (25) can be formally understood as the lowest order in the perturbative expansion

$$\mathcal{D}_\alpha = \mathcal{D}_\alpha^{(0)} + \mathcal{D}_\alpha^{(1)}k + \mathcal{D}_\alpha^{(2)}k^2 + \dots,$$

where $\mathcal{D}_\alpha^{(0)} = \mathcal{D}_\alpha^{(k=0)}$. The LME (25) would therefore be correct up to $\mathcal{O}(\lambda^2 k)$ and any thermodynamic inconsistency encountered should fall within this ‘error bar’.

Note that the GME is itself a perturbative master equation which neglects corrections of order $\mathcal{O}(\lambda^3)$ and below [14]. However, it is guaranteed to give rise to thermodynamically consistent steady-state heat currents [3, 26], as it enjoys the GKLS form (cf. Sect. 1). Interestingly, it is the secular approximation which endows the GME with thermodynamic consistency: The Markovian Redfield equation (9), i.e. the previous step in the derivation of (10), is known to break positivity [14] and caution must be exercised when using it [24].

Coming back to our problem of describing heat transport in the limit of quasi-resonant weakly-coupled nodes, notice that the secular approximation is not problematic when invoked in the derivation of (25). Indeed, the

1740010-11

Este documento incorpora firma electrónica, y es copia auténtica de un documento electrónico archivado por la ULL según la Ley 39/2015.
 Su autenticidad puede ser contrastada en la siguiente dirección <https://sede.ull.es/validacion/>

Identificador del documento: 2111210 Código de verificación: lZvvKBaU

Firmado por: Javier Onam González López
 UNIVERSIDAD DE LA LAGUNA

Fecha: 09/09/2019 11:04:42

Daniel Alonso Ramírez
 UNIVERSIDAD DE LA LAGUNA

11/09/2019 14:53:47

J. O. González, et al.

operators L_α^ω may be expanded as a power series in k in (9). At the zeroth order in k , each heat bath would contribute to the right-hand side of (9) with one non-oscillatory secular term and two fast-rotating non-secular terms at frequencies $\pm 2\omega_\alpha$. These may be safely averaged out provided that $\omega_\alpha \gg \lambda^2$ and regardless of the detuning between the nodes. Consequently, and unlike (20), the LME should correctly describe the stationary properties of our system when $k/\omega_c \lesssim \lambda^2$.

More generally, one can claim that energy transport through an arbitrarily long harmonic chain is correctly captured by a LME within its range of validity; that is, whenever the inter-node couplings are weak. The claim can be made extensive to heat fluxes on spin chains, which were already addressed in [53] via a perturbative master equation relying on ‘weak internal couplings’, precisely in order to bypass the problems created in the GME by the secular approximation.

Finally, let us note that a natural alternative to the LME in our problem would be to incorporate the problematic decay channel of frequency $\Omega_+ - \Omega_-$ into the GME, thus arriving at a partial Markovian Redfield equation (cf. Appendix). However, scaling up the system in the number of nodes would quickly render this approach too involved to be practical.

3. Exact Non-Equilibrium Steady State

The steady state for an all-linear model can also be found *exactly* by solving the corresponding quantum Langevin equations [19, 52, 4]. In this section, we will limit ourselves to outline the procedure to calculate the stationary covariances for our particular problem, while full details on its application to similar settings can be found in e.g. [30, 8, 47, 48, 49].

To begin with, we must mention that the bare frequencies of the nodes need to be shifted so as to compensate for the distortion caused by the system-baths interactions. This eventually allows to recover the correct high temperature limit [52]. Hence, in the remainder of this section, we shall make the replacement $\omega_\alpha^2 \mapsto \tilde{\omega}_\alpha^2$, where $\tilde{\omega}_\alpha^2 := \omega_\alpha^2 + \sum_\mu g_{\alpha,\mu}^2 / (m_{\alpha,\mu} \omega_{\alpha,\mu}^2)$. For our choice of spectral density (5), the shift amounts simply to $\pi^{-1} \int_0^\infty d\omega J(\omega)/\omega = \lambda^2 \Lambda$.

Starting from (4), one may write the Heisenberg equations of motion for all degrees of freedom. Formally solving for $x_{\alpha,\mu}$ and inserting the result into the equations for X_α yields the quantum Langevin equations

$$\frac{d^2 X_\alpha}{dt^2} + \tilde{\omega}_\alpha^2 X_\alpha + k(X_\alpha - X_{\bar{\alpha}}) - \int_{t_0}^\infty ds \chi_\alpha(t-s) X_\alpha(s) = F_\alpha(t), \quad (28)$$

with $\bar{\alpha} \neq \alpha$. These are the equations of motion for two coupled harmonic oscillators, each of which is perturbed by the noise $F_\alpha(t)$ and relaxes according

1740010-12

Este documento incorpora firma electrónica, y es copia auténtica de un documento electrónico archivado por la ULL según la Ley 39/2015.
 Su autenticidad puede ser contrastada en la siguiente dirección <https://sede.ull.es/validacion/>

Identificador del documento: 2111210 Código de verificación: lZvvKBaU

Firmado por: Javier Onam González López
 UNIVERSIDAD DE LA LAGUNA

Fecha: 09/09/2019 11:04:42

Daniel Alonso Ramírez
 UNIVERSIDAD DE LA LAGUNA

11/09/2019 14:53:47

Testing the Validity of the ‘Local’ and ‘Global’ GKLS Master Equations

to the dissipation kernel $\chi_\alpha(t)$. Specifically, these are defined as

$$\mathbf{F}_\alpha := \sum_\mu g_{\alpha,\mu} \left[\mathbf{x}_{\alpha,\mu}(t_0) \cos \omega_0(t-t_0) + \frac{\mathbf{p}_{\alpha,\mu}(t_0)}{m_{\alpha,\mu}\omega_{\alpha,\mu}} \sin \omega_{\alpha,\mu}(t-t_0) \right] \quad (29a)$$

$$\chi_\alpha(t) := \sum_\mu \frac{g_{\alpha,\mu}^2}{m_{\alpha,\mu}\omega_{\alpha,\mu}} \sin \omega_{\alpha,\mu} t \Theta(t) = \frac{2}{\pi} \Theta(t) \int_0^\infty d\omega J(\omega) \sin \omega t. \quad (29b)$$

The only assumption that we will make in order to find the exact steady state is, once again, that system and baths are initialized in the factorized initial condition $\rho_0 = \sigma(t_0) \otimes \tau_c \otimes \tau_h$. We shall also take $t_0 \rightarrow -\infty$. Let us first concentrate on the (stationary) covariance $\frac{1}{2} \langle \{ \mathbf{X}_\alpha(t), \mathbf{X}_{\alpha'}(t) \}_+ \rangle$, which may be written in terms of the Fourier transform

$$\widehat{\mathbf{X}}_\alpha(\omega) := \int_{-\infty}^\infty dt \mathbf{X}_\alpha(t) e^{i\omega t}$$

as

$$\frac{1}{2} \langle \{ \mathbf{X}_\alpha(t), \mathbf{X}_{\alpha'}(t) \}_+ \rangle = \frac{1}{2} \int_{-\infty}^\infty \frac{d\omega'}{2\pi} \int_{-\infty}^\infty \frac{d\omega''}{2\pi} \langle \{ \widehat{\mathbf{X}}_\alpha(\omega'), \widehat{\mathbf{X}}_{\alpha'}(\omega'') \}_+ \rangle e^{-i(\omega'+\omega'')t}. \quad (30)$$

In turn, $\widehat{\mathbf{X}}_\alpha(\omega)$ can be directly found after Fourier-transforming (28), which yields

$$\begin{aligned} \begin{bmatrix} \widehat{\mathbf{X}}_c \\ \widehat{\mathbf{X}}_h \end{bmatrix} &:= A^{-1} \begin{bmatrix} \widehat{\mathbf{F}}_c \\ \widehat{\mathbf{F}}_h \end{bmatrix} \\ &= \begin{bmatrix} \tilde{\omega}_c^2 - \omega^2 + k - \hat{\chi}_c & -k \\ -k & \tilde{\omega}_h^2 - \omega^2 + k - \hat{\chi}_h \end{bmatrix}^{-1} \begin{bmatrix} \widehat{\mathbf{F}}_c \\ \widehat{\mathbf{F}}_h \end{bmatrix}. \end{aligned} \quad (31)$$

From (29a), one can show that

$$\begin{aligned} \frac{1}{2} \langle \{ \widehat{\mathbf{F}}_\alpha(\omega'), \widehat{\mathbf{F}}_{\alpha'}(\omega'') \}_+ \rangle \\ = 2\pi \delta(\omega' + \omega'') \coth \frac{\omega'}{2T_\alpha} [J(\omega')\Theta(\omega') - J(-\omega')\Theta(-\omega')] \delta_{\alpha,\alpha'}, \end{aligned}$$

where the Dirac delta $\delta(\cdot)$ is not to be confused with the Kronecker delta $\delta_{\alpha,\alpha'}$. Consequently, the integral in (30) for e.g. $\alpha = \alpha' = c$ writes as

$$\begin{aligned} \langle \mathbf{X}_c^2 \rangle &= \int_{-\infty}^\infty \frac{d\omega}{2\pi} \left([A^{-1}(\omega)]_{11} [A^{-1}(-\omega)]_{11} \coth \frac{\omega}{2T_c} J(\omega) \right. \\ &\quad \left. + [A^{-1}(\omega)]_{12} [A^{-1}(-\omega)]_{12} \coth \frac{\omega}{2T_h} J(\omega) \right), \end{aligned} \quad (32)$$

1740010-13

Este documento incorpora firma electrónica, y es copia auténtica de un documento electrónico archivado por la ULL según la Ley 39/2015.
 Su autenticidad puede ser contrastada en la siguiente dirección <https://sede.ull.es/validacion/>

Identificador del documento: 2111210 Código de verificación: lZvvKBaU

Firmado por: Javier Onam González López
 UNIVERSIDAD DE LA LAGUNA

Fecha: 09/09/2019 11:04:42

Daniel Alonso Ramírez
 UNIVERSIDAD DE LA LAGUNA

11/09/2019 14:53:47

J. O. González, et al.

where we are exploiting the fact that our $J(\omega)$ is an odd function. The position-momentum and momentum-momentum covariances are readily obtained as e.g.

$$\begin{aligned} & \frac{1}{2} \langle \{P_\alpha(t'), X_{\alpha'}(t'')\}_+ \rangle \\ &= \frac{1}{2} \int_{-\infty}^{\infty} \frac{d\omega'}{2\pi} \int_{-\infty}^{\infty} \frac{d\omega''}{2\pi} (-i\omega') \langle \{\widehat{X}_\alpha(\omega'), \widehat{X}_{\alpha'}(\omega'')\}_+ \rangle e^{-i(\omega't' + \omega''t'')} . \end{aligned}$$

In order to calculate $\widehat{\chi}_\alpha(\omega)$ it is useful to note that $\text{Im} \widehat{\chi}_\alpha(\omega) = J(\omega)\Theta(\omega) - J(-\omega)\Theta(-\omega)$, and that $\text{Re} \widehat{\chi}_\alpha(\omega)$ and $\text{Im} \widehat{\chi}_\alpha(\omega)$ are related through the Kramers-Kronig relation

$$\text{Re} \widehat{\chi}_\alpha(\omega) = \frac{1}{\pi} \text{P} \int_{-\infty}^{\infty} d\omega' \frac{\text{Im} \widehat{\chi}_\alpha(\omega')}{\omega' - \omega}, \quad (33)$$

where P indicates Cauchy principal value. For our choice of spectral density $\widehat{\chi}_h(\omega) = \widehat{\chi}_c(\omega) = \lambda^2 \Lambda^2 / (\Lambda - i\omega)$ which, combined with (5), (31), and (32), allows us to compute all the elements of the exact steady-state covariance matrix Γ . Finally, following [12, 13], we can cast the exact steady-state heat currents as

$$\dot{Q}_h = -\dot{Q}_c = \frac{k}{2} ([\Gamma]_{14} - [\Gamma]_{23}). \quad (34)$$

Both the steady state covariances and the corresponding heat currents can be seen to perfectly coincide with those obtained from the Markovian Redfield equation derived in the Appendix, always provided that the Born-Markov approximation holds.

4. Discussion

4.1. STEADY STATE AND STATIONARY HEAT CURRENTS

In this section we will compare the steady states and the stationary heat currents predicted by the global, local, and exact approaches. We shall be especially interested in setting up the wire with quasi-resonant nodes ($\delta_\omega \ll \lambda^2$) so as to confirm our intuition that the LME can succeed in describing the system when the GME breaks down (cf. Sect. 2.4).

In order to compare states we will make use of the Uhlmann fidelity, defined as

$$\mathbb{F}(\rho_1, \rho_2) := \left(\text{tr} \sqrt{\sqrt{\rho_1} \rho_2 \sqrt{\rho_1}} \right)^2$$

1740010-14

Este documento incorpora firma electrónica, y es copia auténtica de un documento electrónico archivado por la ULL según la Ley 39/2015.
 Su autenticidad puede ser contrastada en la siguiente dirección <https://sede.ull.es/validacion/>

Identificador del documento: 2111210 Código de verificación: lZvvKBaU

Firmado por: Javier Onam González López
 UNIVERSIDAD DE LA LAGUNA

Fecha: 09/09/2019 11:04:42

Daniel Alonso Ramírez
 UNIVERSIDAD DE LA LAGUNA

11/09/2019 14:53:47

Testing the Validity of the ‘Local’ and ‘Global’ GKLS Master Equations

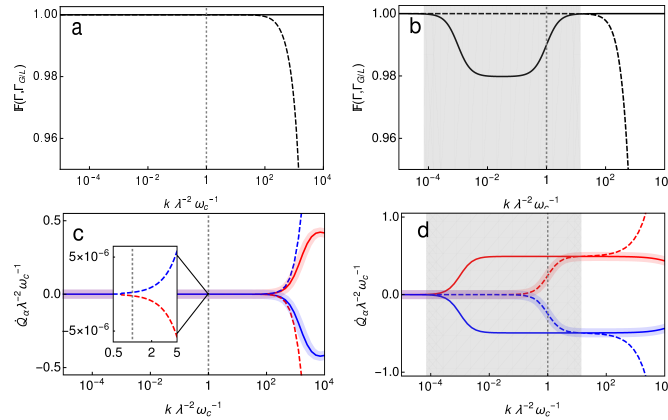


Fig. 2: (Colour online) (top row) Uhlmann fidelity \mathbb{F} between the exact steady state Γ and the approximations Γ^G and Γ^L calculated within the global (solid) and local (dashed) approach, as a function of the coupling k at fixed dissipation strength $\lambda^2 = 10^{-3}$. In (a) frequencies and temperatures were set to $\omega_h = 2$, $\omega_c = 1$, $T_h = 3$, and $T_c = 2$, so that $\delta_\omega \gg \lambda^2$ and the secular approximation is justified. Hence, the global GKLS equation is in perfect agreement with the exact result. The LME starts to break down around $k \sim 0.1$, i.e. when the inter-node coupling becomes comparable to the node frequencies. In (b) the nodes are quasi-resonant ($\omega_c = 1$ and $\delta_\omega^2 = 2 \times 10^{-6}$), while the temperatures are the same as in (a). Due to the breakdown of the secular approximation, the global GKLS equation becomes unreliable. The shaded grey area corresponds to $1 - \mathbb{F}(\Gamma, \Gamma^G) \geq 10^{-4}$. In contrast, the LME remains accurate in that regime of parameters. (bottom row) Stationary incoming heat currents from the hot (red) and cold (blue) baths, as given by the global (thin solid), local (dashed), and exact (thick transparent) approaches. The parameters in (c) are the same as in (a). As can be seen, the LME violates the second law of thermodynamics predicting *reversed* heat currents for all k . Finally, the parameters in (d) are the same as in (b). In the shaded grey region, in which the secular approximation breaks down, the GME greatly overestimates the magnitude of the steady-state heat currents, while the LME perfectly follows the exact result. For all four plots $\Lambda = 10^3$. Recall that we work in units of $m_c = m_h = \hbar = k_B = 1$.

Open Syst. Inf. Dyn. 2017.24. Downloaded from www.worldscientific.com by UNIVERSITY OF NEW ENGLAND on 12/18/17. For personal use only.

1740010-15

Este documento incorpora firma electrónica, y es copia auténtica de un documento electrónico archivado por la ULL según la Ley 39/2015.
 Su autenticidad puede ser contrastada en la siguiente dirección <https://sede.ull.es/validacion/>

Identificador del documento: 2111210 Código de verificación: lZvvKBaU

Firmado por: Javier Onam González López
 UNIVERSIDAD DE LA LAGUNA

Fecha: 09/09/2019 11:04:42

Daniel Alonso Ramírez
 UNIVERSIDAD DE LA LAGUNA

11/09/2019 14:53:47

J. O. González, et al.

for arbitrary ρ_1 and ρ_2 [33]. In the case of two-mode Gaussian states with covariance matrices Γ_1 and Γ_2 and vanishing first order moments the fidelity can be cast as [31]

$$\mathbb{F}(\Gamma_1, \Gamma_2) = \left[(\sqrt{b} + \sqrt{c}) - \sqrt{(\sqrt{b} + \sqrt{c})^2 - a} \right]^{-1}, \quad (35)$$

where $a := \det(\Gamma_1 + \Gamma_2)$, $b := 2^4 \det[(J\Gamma_1)(J\Gamma_2) - \mathbb{I}/4]$,

$$c := 2^4 \det(\Gamma_1 + iJ/2) \det(\Gamma_2 + iJ/2),$$

and $J_{kl} := -i[\mathbf{R}_k, \mathbf{R}_l]$.

As shown in Fig. 2(a), whenever the detuning is large compared with the dissipation strength, both LME and GME are in perfect agreement with the exact solution for most parameters. The local approach only starts to break down when the coupling k becomes comparable or larger than the node frequencies (i.e. $k/\omega_\alpha \gtrsim 0.1\omega_c$, where the extra ω_c has been merely added for dimensional consistency), whereas the global master equation remains correct.

On the contrary, if the detuning is set to $\delta_\omega \ll \lambda^2$, the steady state of the GME can be seen to disagree with the exact solution when the inter-node coupling k/ω_c approaches or falls below the dissipation strength λ^2 (cf. Fig. 3(b)). Recall that this is entirely due to elimination of the non-secular decay channel at frequency $\Omega_+ - \Omega_-$ (cf. Sect. 2.2). Importantly, the LME is still valid so long as $k/\omega_c \ll \omega_c$, *regardless* of the breakdown of the secular approximation. Eventually, as k decreases further, the nodes effectively decouple, and the GME correctly predicts a steady state made up of two uncorrelated thermal modes.

One can also make use of (23), (27), and (34) to compare the steady-state heat currents. Once again, under large detuning δ_ω , both the local and global approach are in good agreement with the exact solution (vanishingly small heat currents), except for when the inter-node coupling becomes comparable to the node frequencies, which invalidates the LME. Interestingly, in Fig. 2(c) we can see that the local approach does indeed violate the second law of thermodynamics by predicting heat transport against the temperature gradient (i.e. $\dot{Q}_h = -\dot{Q}_c < 0$) for any k [28]. The magnitude of this violation, however, loosely falls within the ‘error bars’ $\mathcal{O}(\lambda^2 k)$ [46] of the LME.

On the other hand, Fig. 2(d) shows again a situation in which $\delta_\omega \ll \lambda^2$. Remarkably, we observe that the global approach largely overestimates the magnitude of the steady-state heat currents, where $\mathbb{F}(\Gamma, \Gamma^G)$ falls below 1 (i.e. in the grey area). The LME, however, yields a quantitatively good estimate in all the range of parameters for which it is valid.

We have thus illustrated that the breakdown of the secular approximation may render the predictions of the global master equation *qualitatively* wrong,

1740010-16

Este documento incorpora firma electrónica, y es copia auténtica de un documento electrónico archivado por la ULL según la Ley 39/2015.
 Su autenticidad puede ser contrastada en la siguiente dirección <https://sede.ull.es/validacion/>

Identificador del documento: 2111210 Código de verificación: lZvvKBaU

Firmado por: Javier Onam González López
 UNIVERSIDAD DE LA LAGUNA

Fecha: 09/09/2019 11:04:42

Daniel Alonso Ramírez
 UNIVERSIDAD DE LA LAGUNA

11/09/2019 14:53:47

Testing the Validity of the ‘Local’ and ‘Global’ GKLS Master Equations

while the local approach, in spite of its thermodynamic inconsistency, proves to be an accurate working tool within its range of applicability.

4.2. STEADY-STATE CORRELATIONS

As we shall now see, the GME also fails qualitatively in assessing the node-node correlations (both classical and quantum) when the secular approximation breaks down. This is not the case for the LME.

We measure the total correlations between the ‘cold’ and ‘hot’ nodes of the wire by means of the quantum mutual information $\mathcal{I}(\sigma_{ch}) := S(\sigma_c) + S(\sigma_h) - S(\sigma_{ch})$, where $S(\rho) = -\text{tr}\{\rho \log \rho\}$ is the von Neumann entropy and $\sigma_\alpha := \text{tr}_{\bar{\alpha}} \sigma_{ch}$ stands for the reduced state of node α (the subindices ‘c’ and ‘h’ are added to the stationary state of the wire to emphasize its bipartite nature). The von Neumann entropy of an n -mode Gaussian state can be written as [22]

$$S(\Gamma) = \sum_{j=1}^n \left(\frac{2\nu_j + 1}{2} \log \frac{2\nu_j + 1}{2} + \frac{2\nu_j - 1}{2} \log \frac{2\nu_j - 1}{2} \right), \quad (36)$$

where the ν_j are the n symplectic eigenvalues of the generic $2n \times 2n$ covariance matrix Γ . These can be obtained from the spectrum $\{\pm i\nu_1, \dots, \pm i\nu_n\}$ of $J^{-1}\Gamma$. For Γ to be physical, the symplectic spectrum must satisfy $\nu_j \geq \frac{1}{2}$. In our case, note that e.g. the single-mode covariance matrix Γ_c results from retaining only the first two rows and columns of the two-mode covariance matrix of the full system, i.e. those related to the ‘cold quadratures’ $\{\mathbf{x}_c, \mathbf{p}_c\}$.

As we can see from Fig. 3(a) the inter-node correlations can be both overestimated and underestimated by the global master equation whenever the secular approximation fails. In contrast, the LME assesses \mathcal{I} faithfully. Note from (22) that the stationary covariances $\langle \mathbf{x}_c \mathbf{p}_h \rangle$ and $\langle \mathbf{p}_c \mathbf{x}_h \rangle$ (i.e. Γ_{14} and Γ_{23}) are neglected in the global approach. Indeed, it is easy to see from the corresponding Markovian Redfield equation (cf. Appendix) that these covariances are related to the excluded non-secular term at frequency $\Omega_+ - \Omega_-$. From Fig. 3(b) we observe that the deficit in total quantum correlations predicted by the GME around $k/\omega_c \simeq \lambda^2$ in Fig. 3(a) is precisely due to the fact that

$$[\Gamma^G]_{14} = [\Gamma^G]_{23} = [\Gamma^G]_{32} = [\Gamma^G]_{41} = 0.$$

Notice, comparing again Figs. 3(a) and 3(b), that the peak in the total correlations at lower k is explained by the fact that the GME overestimates $\langle \mathbf{x}_c \mathbf{x}_h \rangle$; once again, within the region in which the secular approximation breaks down.

It is possible to split the total correlations into a *quantum* and a *classical* share (blue dotted and red dashed lines in Fig. 3(a), respectively). We will say

1740010-17

Este documento incorpora firma electrónica, y es copia auténtica de un documento electrónico archivado por la ULL según la Ley 39/2015.
 Su autenticidad puede ser contrastada en la siguiente dirección <https://sede.ull.es/validacion/>

Identificador del documento: 2111210 Código de verificación: lZvvKBaU

Firmado por: Javier Onam González López
 UNIVERSIDAD DE LA LAGUNA

Fecha: 09/09/2019 11:04:42

Daniel Alonso Ramírez
 UNIVERSIDAD DE LA LAGUNA

11/09/2019 14:53:47

J. O. González, et al.

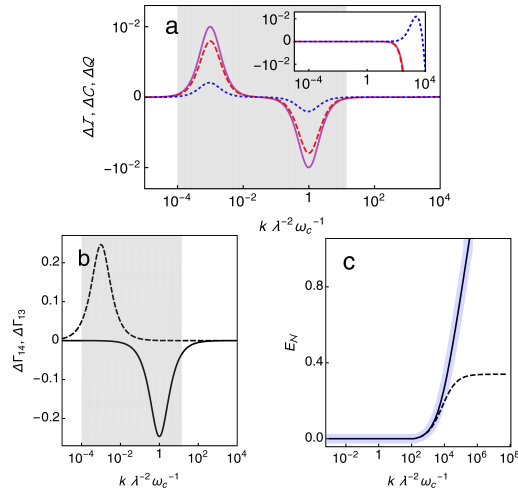


Fig. 3: (Colour online) (a) Excess quantum mutual information $\Delta\mathcal{I} := \mathcal{I}(\Gamma^G) - \mathcal{I}(\Gamma)$ (solid purple), classical correlations $\Delta C^{\leftarrow} := C^{\leftarrow}(\Gamma^G) - C^{\leftarrow}(\Gamma)$ (dashed red), and quantum correlations $\Delta Q^{\leftarrow} = \Delta\mathcal{I} - \Delta C^{\leftarrow}$ (dotted blue), as follows from the comparison of the global approach with the exact solution (see main text for definitions). The inset reproduces the main plot, benchmarking instead the local approach against the exact result. The parameters are the same as in Figs. 2(b) and 2(d), i.e. we work with small detuning. While the LME faithfully captures inter-node correlations in all its range of validity, the GME may both underestimate or overestimate them. In (b) the quantities $\Delta\Gamma_{14} := [\Gamma^G]_{14} - [\Gamma]_{14}$ (solid) and $\Delta\Gamma_{13} := [\Gamma^G]_{13} - [\Gamma]_{13}$ (dashed) are plotted for the same parameters as in (a). We see that the failure of the global approach to correctly assess these covariances ($\langle \mathbf{x}_c \mathbf{p}_h \rangle = -\langle \mathbf{p}_c \mathbf{x}_h \rangle$ and $\langle \mathbf{x}_c \mathbf{x}_h \rangle$) explains the peaks in (a). In (c) we plot the steady state inter-node entanglement, as quantified by the logarithmic negativity $E_{\mathcal{N}}$ within the global (solid black), local (dashed black), and exact (thick transparent blue) approaches. The observation of non-vanishing asymptotic entanglement requires large ratios ω/T_α and very large coupling strengths k . Unfortunately, this prevents entanglement from being observed in the problematic region $k/\omega_c \lesssim \lambda^2$. Interestingly, the LME predicts a saturation of $E_{\mathcal{N}}$ for large k , which is anyway far beyond its range of applicability. In (c) $\omega_c = \omega_h = 10$, $T_c = 1$, $T_h = 2$, $\lambda^2 = 10^{-3}$, and $\Lambda = 10^3$.

1740010-18

77

Este documento incorpora firma electrónica, y es copia auténtica de un documento electrónico archivado por la ULL según la Ley 39/2015.
 Su autenticidad puede ser contrastada en la siguiente dirección <https://sede.ull.es/validacion/>

Identificador del documento: 2111210 Código de verificación: lZvvKBaU

Firmado por: Javier Onam González López
 UNIVERSIDAD DE LA LAGUNA

Fecha: 09/09/2019 11:04:42

Daniel Alonso Ramírez
 UNIVERSIDAD DE LA LAGUNA

11/09/2019 14:53:47

Testing the Validity of the ‘Local’ and ‘Global’ GKLS Master Equations

that a bipartite quantum state ρ_{AB} has quantum correlations with respect to B if there exists no local measurement on B that leaves the marginal of A unperturbed. This notion of *quantumness* of correlations is captured by the discord [34, 20]

$$\mathcal{Q}^-(\rho_{AB}) := S(\rho_B) - \left[S(\rho_{AB}) - \inf_{\{\Pi_j^B\}} \sum_j p_j S(\rho_{A|j}) \right].$$

Given a complete set of projectors $\{\Pi_j^B\}$ on B , $\rho_{A|j} := \text{tr}_B\{\Pi_j^B \rho_{AB} \Pi_j^B\}$ denotes the post-measurement marginal of A conditioned on the outcome j , occurring with probability $p_j = \text{tr}\{\Pi_j^B \rho_{AB}\}$. Note that discord is not symmetric, i.e. the quantumness of correlations as revealed by measurements on B need not coincide with the quantumness of correlations as revealed by measurements on A .

Note as well that, due to the explicit minimization over all local measurements on B , the evaluation of \mathcal{Q}^- is often very challenging. Luckily, restricting the optimization to the set of Gaussian positive operator valued measurements makes it possible to obtain a closed formula for two-mode Gaussian states (see [1, 16, 36] for full details). The difference between the total correlations and the quantum discord is referred to as classical correlations

$$\mathcal{C}^-(\rho_{AB}) := \mathcal{I}(\rho_{AB}) - \mathcal{Q}^-(\rho_{AB}).$$

As shown in Fig. 3(a), both quantum and classical correlations behave very similarly to the mutual information within the global approach. This is not the case, however, for the LME (cf. inset in Fig. 3(a)): at large coupling strengths (i.e. beyond its range of validity) the local approach may overestimate the amount of quantum correlations present between the nodes, although at sufficiently large couplings, all correlations are largely underestimated.

Finally, we may want to look at the inter-node *entanglement* [23]. Entanglement is a somewhat stronger form of quantum correlation since a state can display non-zero discord and yet be unentangled, but not the other way around. In the case of two-mode Gaussian states, quantum entanglement can be gauged by the logarithmic negativity $E_{\mathcal{N}}$, which writes as [50, 37]

$$E_{\mathcal{N}}(\Gamma) := \sum_j \max\{0, -\log(2\tilde{\nu}_j)\}, \quad (37)$$

where $\tilde{\nu}_j$ are the symplectic eigenvalues of the *partially-transposed* covariance matrix $\tilde{\Gamma}$. This is obtained from Γ by simply changing the sign of all covariances involving e.g. the momentum p_c and either of the ‘hot’ quadratures.

The buildup of steady-state entanglement requires much larger inter-node coupling k and large ratios ω_α/T_α as shown in Fig. 3(c). While there is no

1740010-19

Este documento incorpora firma electrónica, y es copia auténtica de un documento electrónico archivado por la ULL según la Ley 39/2015.
 Su autenticidad puede ser contrastada en la siguiente dirección <https://sede.ull.es/validacion/>

Identificador del documento: 2111210 Código de verificación: lZvvKBaU

Firmado por: Javier Onam González López
 UNIVERSIDAD DE LA LAGUNA

Fecha: 09/09/2019 11:04:42

Daniel Alonso Ramírez
 UNIVERSIDAD DE LA LAGUNA

11/09/2019 14:53:47

J. O. González, et al.

reason for the GME not to accurately capture the entanglement as $k \rightarrow \infty$, the LME wrongly predicts a saturation in the stationary logarithmic negativity in that limit. One can obtain the correct scaling of entanglement at strong coupling from the GME which, for resonant nodes, simplifies to

$$E_{\mathcal{N}}(\Gamma) \xrightarrow{k \rightarrow \infty} \frac{1}{4} \log \frac{2k(1 - e^{\omega/T_c})^2(1 - e^{\omega/T_h})^2}{(1 - e^{2\omega/T})^2 \omega^2} \quad (38)$$

$$\text{with } \bar{T} := \left(\frac{T_c^{-1} + T_h^{-1}}{2} \right)^{-1}.$$

5. Conclusions

We have studied a simple model for heat transport between two heat baths at different temperatures when weakly connected through a two-node quantum wire. Due to the weak dissipative wire-baths coupling, it is possible to address the problem via second-order Markovian quantum master equations. In particular, we consistently derived the GKLS master equation via a *global* treatment of dissipation, and found its steady state, the stationary heat currents through the wire, and the asymptotic inter-node quantum and classical correlations. For comparison, we adopted the popular *local* approach, which addresses dissipation on each node individually (i.e. ignoring the effects of the inter-node coupling). Since our model is linear, its steady state can be obtained *exactly* by resorting to quantum Langevin equations. This provided us with means to quantitatively compare the performance of the global and the local approaches.

As expected, we found that the local approach is only valid when the internal coupling between the nodes of the wire is weak. Furthermore, as previously noted, we observed that the local approach does break the second law of thermodynamics [28], although any violations can be bounded with suitably-defined error bars within its range of applicability [46].

Interestingly, our setup allows us to consider very weak internal couplings, comparable with the dissipation strength. In this regime, the crucial secular approximation breaks down if, in addition, the nodes are nearly resonant. As a result, the predictions of the global master GME become qualitatively wrong — the magnitude of the stationary heat currents is largely overestimated, and key features of the correlation-sharing structure are not captured by the GME. On the contrary, the LME does accurately describe the stationary properties of the wire. This agrees with previous observations on the complementarity of GME and LME when describing dynamics [40]. More generally, the usage of the local approach in the treatment of heat transport through arbitrarily long harmonic or spin chains [53] may be justified provided that the internal couplings are weak enough, and always keeping in

1740010-20

Este documento incorpora firma electrónica, y es copia auténtica de un documento electrónico archivado por la ULL según la Ley 39/2015.
 Su autenticidad puede ser contrastada en la siguiente dirección <https://sede.ull.es/validacion/>

Identificador del documento: 2111210 Código de verificación: lZvvKBaU

Firmado por: Javier Onam González López
 UNIVERSIDAD DE LA LAGUNA

Fecha: 09/09/2019 11:04:42

Daniel Alonso Ramírez
 UNIVERSIDAD DE LA LAGUNA

11/09/2019 14:53:47

Testing the Validity of the ‘Local’ and ‘Global’ GKLS Master Equations

mind that the predictions of the LME should be accompanied by the corresponding error estimates [46].

In spite of these encouraging observations, the local approach should not be used lightly, especially in quantum thermodynamics. Even though the LME may be an excellent working tool that even outperforms the canonical global GKLS master equation in certain regimes, it might as well lead to qualitatively wrong conclusions, *a priori* within its range of applicability. For instance, it has been shown that a local modelling of quantum thermodynamic cycles completely fails to account for heat leaks and internal dissipation effects [6, 7] that can become dominant in the operation of the device in question. As a result, e.g. intrinsically irreversible models may be wrongly classified as *endoreversible*. This is a reminder that perturbative equations of motion for open quantum systems must always be handled with care.

Note added: During the preparation of this manuscript we became aware of the related work by Patrick P. Hofer *et al.* [21], where local and global approaches are compared in a quantum heat engine model.

Acknowledgements

The authors gratefully acknowledge A. Levy, Nahuel Freitas and Karen V. Hovhannisyan for helpful comments. This project was funded by the Spanish MECD (FPU14/06222), the Spanish MINECO (FIS2013-41352-P), the European Research Council under the StG GQCOP (Grant No. 637352), and the COST Action MP1209: “Thermodynamics in the quantum regime”.

Appendix: The *Partial* Markovian Redfield Master Equation

In order to compensate for the deficiencies of the GME one may simply take into consideration the problematic non-secular term corresponding to the $\Omega_+ - \Omega_-$ channel. Equations (9) and (11) would then need to be combined as

$$\begin{aligned} \frac{dO}{dt} \simeq & i[H_S, O] + \sum_{\alpha \in \{c, h\}} \sum_{\omega \in \{\pm\Omega_{\pm}\}} \gamma_{\alpha}(\omega) \left(L_{\alpha}^{\omega \dagger} O L_{\alpha}^{\omega} - \frac{1}{2} \{ L_{\alpha}^{\omega \dagger} L_{\alpha}^{\omega}, O \}_+ \right) \\ & + \frac{1}{2} \sum_{\alpha \in \{c, h\}} \gamma_{\alpha}(\Omega_+) \left(L_{\alpha}^{\Omega_+ \dagger} O L_{\alpha}^{\Omega_+} - O L_{\alpha}^{\Omega_+ \dagger} L_{\alpha}^{\Omega_+} + L_{\alpha}^{\Omega_+ \dagger} O L_{\alpha}^{\Omega_-} - L_{\alpha}^{\Omega_+ \dagger} L_{\alpha}^{\Omega_-} O \right) \\ & + \frac{1}{2} \sum_{\alpha \in \{c, h\}} \gamma_{\alpha}(-\Omega_+) \left(L_{\alpha}^{\Omega_-} O L_{\alpha}^{\Omega_+ \dagger} - O L_{\alpha}^{\Omega_-} L_{\alpha}^{\Omega_+ \dagger} + L_{\alpha}^{\Omega_+} O L_{\alpha}^{\Omega_- \dagger} - L_{\alpha}^{\Omega_+} L_{\alpha}^{\Omega_- \dagger} O \right) \end{aligned}$$

1740010-21

Este documento incorpora firma electrónica, y es copia auténtica de un documento electrónico archivado por la ULL según la Ley 39/2015.
 Su autenticidad puede ser contrastada en la siguiente dirección <https://sede.ull.es/validacion/>

Identificador del documento: 2111210 Código de verificación: lZvvKBaU

Firmado por: Javier Onam González López
 UNIVERSIDAD DE LA LAGUNA

Fecha: 09/09/2019 11:04:42

Daniel Alonso Ramírez
 UNIVERSIDAD DE LA LAGUNA

11/09/2019 14:53:47

J. O. González, et al.

$$\begin{aligned}
 & + \frac{1}{2} \sum_{\alpha \in \{c, h\}} \gamma_{\alpha}(\Omega_{-}) \left(\mathbf{L}_{\alpha}^{\Omega_{+} \dagger} \mathbf{O} \mathbf{L}_{\alpha}^{\Omega_{-}} - \mathbf{O} \mathbf{L}_{\alpha}^{\Omega_{+} \dagger} \mathbf{L}_{\alpha}^{\Omega_{-}} + \mathbf{L}_{\alpha}^{\Omega_{-} \dagger} \mathbf{O} \mathbf{L}_{\alpha}^{\Omega_{+}} - \mathbf{L}_{\alpha}^{\Omega_{-} \dagger} \mathbf{L}_{\alpha}^{\Omega_{+}} \mathbf{O} \right) \\
 & + \frac{1}{2} \sum_{\alpha \in \{c, h\}} \gamma_{\alpha}(-\Omega_{-}) \left(\mathbf{L}_{\alpha}^{\Omega_{+}} \mathbf{O} \mathbf{L}_{\alpha}^{\Omega_{-} \dagger} - \mathbf{O} \mathbf{L}_{\alpha}^{\Omega_{+}} \mathbf{L}_{\alpha}^{\Omega_{-} \dagger} + \mathbf{L}_{\alpha}^{\Omega_{-}} \mathbf{O} \mathbf{L}_{\alpha}^{\Omega_{+} \dagger} - \mathbf{L}_{\alpha}^{\Omega_{-}} \mathbf{L}_{\alpha}^{\Omega_{+} \dagger} \mathbf{O} \right),
 \end{aligned} \tag{39}$$

where the operators $\mathbf{L}_{\alpha}^{\omega}$ are those defined in Sect. 2.2.

In principle, a full set of ten dynamical variables would be necessary to obtain all steady-state covariances. We shall choose $\mathbf{D}_{\pm\pm} := i(\mathbf{a}_{\pm}^{\dagger} \mathbf{a}_{\pm}^{\dagger} - \mathbf{a}_{\pm} \mathbf{a}_{\pm})$, $\mathbf{S}_{\pm\pm} := \mathbf{a}_{\pm}^{\dagger} \mathbf{a}_{\pm}^{\dagger} + \mathbf{a}_{\pm} \mathbf{a}_{\pm}$, $\mathbf{D}_{+-} := i(\mathbf{a}_{+}^{\dagger} \mathbf{a}_{-}^{\dagger} - \mathbf{a}_{+} \mathbf{a}_{-})$, $\mathbf{S}_{+-} := \mathbf{a}_{+}^{\dagger} \mathbf{a}_{-}^{\dagger} + \mathbf{a}_{+} \mathbf{a}_{-}$, $\mathbf{d}_{+-} := i(\mathbf{a}_{+}^{\dagger} \mathbf{a}_{-} - \mathbf{a}_{+} \mathbf{a}_{-}^{\dagger})$, $\mathbf{s}_{+-} := \mathbf{a}_{+}^{\dagger} \mathbf{a}_{-} + \mathbf{a}_{+} \mathbf{a}_{-}^{\dagger}$, and $\mathbf{n}_{\pm} := \mathbf{a}_{\pm}^{\dagger} \mathbf{a}_{\pm}$. As it turns out, the stationary averages of the first six variables vanish (i.e. $\langle \mathbf{D}_{\pm\pm} \rangle = \langle \mathbf{S}_{\pm\pm} \rangle = \langle \mathbf{D}_{+-} \rangle = \langle \mathbf{S}_{+-} \rangle = 0$), so that we are left with only four relevant observables. The corresponding equations of motion write as $d\mathbf{j}/dt = B\mathbf{j} + b$, where $\mathbf{j} = (\mathbf{n}_{+}, \mathbf{n}_{-}, \mathbf{d}_{+-}, \mathbf{s}_{+-})^T$, the non-zero elements of b are given by

$$[b]_1 = W_{-\Omega_{+}}^c + W_{-\Omega_{+}}^h, \tag{40a}$$

$$[b]_2 = W_{-\Omega_{-}}^c + W_{-\Omega_{-}}^h, \tag{40b}$$

$$\begin{aligned}
 [b]_4 &= \sqrt{\frac{\Omega_{+}}{\Omega_{-}}} (W_{-\Omega_{+}}^c \tan \vartheta - W_{-\Omega_{+}}^h \cot \vartheta) \\
 &+ \sqrt{\frac{\Omega_{-}}{\Omega_{+}}} (W_{-\Omega_{-}}^c \cot \vartheta - W_{-\Omega_{-}}^h \tan \vartheta),
 \end{aligned} \tag{40c}$$

and the coefficients of the matrix B read

$$[B]_{11} = W_{-\Omega_{+}}^c + W_{-\Omega_{+}}^h - W_{\Omega_{+}}^c - W_{\Omega_{+}}^h,$$

$$[B]_{14} = \frac{1}{2}[B]_{42} = \frac{1}{2} \sqrt{\frac{\Omega_{-}}{\Omega_{+}}} ([W_{-\Omega_{-}}^c - W_{\Omega_{-}}^c] \cot \vartheta - [W_{-\Omega_{-}}^h - W_{\Omega_{-}}^h] \tan \vartheta),$$

$$[B]_{22} = W_{-\Omega_{-}}^c + W_{-\Omega_{-}}^h - W_{\Omega_{-}}^c - W_{\Omega_{-}}^h,$$

$$[B]_{24} = \frac{1}{2}[B]_{41} = \frac{1}{2} \sqrt{\frac{\Omega_{+}}{\Omega_{-}}} ([W_{-\Omega_{+}}^c - W_{\Omega_{+}}^c] \tan \vartheta - [W_{-\Omega_{+}}^h - W_{\Omega_{+}}^h] \cot \vartheta),$$

$$[B]_{33} = [B]_{44}$$

$$= \frac{1}{2} (W_{-\Omega_{-}}^c + W_{\Omega_{+}}^c + W_{-\Omega_{-}}^h + W_{\Omega_{+}}^h - W_{\Omega_{-}}^c - W_{\Omega_{+}}^c - W_{\Omega_{-}}^h - W_{\Omega_{+}}^h),$$

$$[B]_{34} = -[B]_{43} = \Omega_{-} - \Omega_{+}.$$

All the remaining coefficients vanish.

1740010-22

Este documento incorpora firma electrónica, y es copia auténtica de un documento electrónico archivado por la ULL según la Ley 39/2015.
 Su autenticidad puede ser contrastada en la siguiente dirección <https://sede.ull.es/validacion/>

Identificador del documento: 2111210 Código de verificación: lZvvKBaU

Firmado por: Javier Onam González López
 UNIVERSIDAD DE LA LAGUNA

Fecha: 09/09/2019 11:04:42

Daniel Alonso Ramírez
 UNIVERSIDAD DE LA LAGUNA

11/09/2019 14:53:47

Testing the Validity of the ‘Local’ and ‘Global’ GKLS Master Equations

The non-zero elements of the steady-state covariance matrix $\{\Gamma^R\}$ in the basis of the normal modes $\{\eta_-, \Pi_-, \eta_+, \Pi_+\}$ are

$$\begin{aligned} [\Gamma^R]_{11} &= \frac{1}{\Omega_-} \left(\frac{1}{2} + \langle n_- \rangle \right), & [\Gamma^R]_{22} &= \Omega_- \left(\frac{1}{2} + \langle n_- \rangle \right), \\ [\Gamma^R]_{33} &= \frac{1}{\Omega_+} \left(\frac{1}{2} + \langle n_+ \rangle \right), & [\Gamma^R]_{44} &= \Omega_+ \left(\frac{1}{2} + \langle n_+ \rangle \right), \\ [\Gamma^R]_{13} &= [\Gamma^R]_{31} = \frac{\langle s_{+-} \rangle}{2\sqrt{\Omega_+ \Omega_-}}, & [\Gamma^R]_{14} &= [\Gamma^R]_{41} = -\frac{\langle d_{+-} \rangle}{2} \sqrt{\frac{\Omega_-}{\Omega_+}}, \\ [\Gamma^R]_{23} &= [\Gamma^R]_{32} = \frac{\langle d_{+-} \rangle}{2} \sqrt{\frac{\Omega_+}{\Omega_-}}, & [\Gamma^R]_{24} &= [\Gamma^R]_{42} = \frac{\langle s_{+-} \rangle}{2} \sqrt{\Omega_+ \Omega_-}. \end{aligned} \quad (41)$$

Just like in (22), this can be rotated into the original quadratures by applying the suitable rotation matrix as defined in (12) and (13).

Finally, the steady state heat currents obtained from the stationary solution of (39) can be cast as

$$\begin{aligned} \dot{Q}_c^R &= -\dot{Q}_h^R = \Omega_+ \left[W_{\Omega_+}^c \langle n_+ \rangle - W_{-\Omega_+}^c (1 + \langle n_+ \rangle) \right] \\ &+ \Omega_- \left[W_{\Omega_-}^c \langle n_- \rangle - W_{-\Omega_-}^c (1 + \langle n_- \rangle) \right] \\ &+ \frac{1}{2} \sqrt{\Omega_+ \Omega_-} \langle s_{+-} \rangle \left[(W_{\Omega_-}^c - W_{-\Omega_-}^c) \cot \vartheta + (W_{\Omega_+}^c - W_{-\Omega_+}^c) \tan \vartheta \right]. \end{aligned}$$

Bibliography

- [1] G. Adesso and A. Datta, Phys. Rev. Lett. **105**, 30501 (2010).
- [2] G. Adesso, S. Ragy, and A. R. Lee, Open Sys. Information Dyn. **21**, 1440001 (2014).
- [3] R. Alicki, J. Phys. A **12**, L 103 (1979).
- [4] D. Boyanovsky and D. Jasnow, preprint arXiv:1707.04135.
- [5] H.-P. Breuer and F. Petruccione, *The Theory of Open Quantum Systems*, Oxford University Press, 2002.
- [6] L. A. Correa, J. P. Palao, G. Adesso, and D. Alonso, Phys. Rev. E **87**, 042131 (2013).
- [7] L. A. Correa, J. P. Palao, and D. Alonso, Phys. Rev. E **92**, 032136 (2015).
- [8] L. A. Correa, A. A. Valido, and D. Alonso, Phys. Rev. A **86**, 012110 (2012).
- [9] I. de Vega and D. Alonso, Rev. Mod. Phys. **89**, 015001 (2017).
- [10] G. L. Deçordi, and A. Vidiella-Barranco, Opt. Commun. **387**, 366–376 (2017).
- [11] C. Fleming, N. I. Cummings, C. Anastopoulos, and B. L. Hu, J. Phys. A: Math. Theor. **43**, 405304 (2010).
- [12] N. Freitas and J. P. Paz, Phys. Rev. E **90**, 042128 (2014).
- [13] N. Freitas and J. P. Paz, Phys. Rev. E **95**, 012146 (2017).
- [14] P. Gaspard and M. Nagaoka, J. Chem. Phys. **111**, 5668 (1999).

1740010-23

Este documento incorpora firma electrónica, y es copia auténtica de un documento electrónico archivado por la ULL según la Ley 39/2015.
 Su autenticidad puede ser contrastada en la siguiente dirección <https://sede.ull.es/validacion/>

Identificador del documento: 2111210 Código de verificación: lZvvKBaU

Firmado por: Javier Onam González López
 UNIVERSIDAD DE LA LAGUNA

Fecha: 09/09/2019 11:04:42

Daniel Alonso Ramírez
 UNIVERSIDAD DE LA LAGUNA

11/09/2019 14:53:47

J. O. González, et al.

- [15] D. Gelbwaser-Klimovsky, W. Niedenzu, and G. Kurizki, *Adv. At. Mol. Opt. Phys.* **64**, 329 (2015).
- [16] P. Giorda and M. G. A. Paris, *Phys. Rev. Lett.* **105**, 020503 (2010).
- [17] J. Goold, M. Huber, A. Riera, L. del Rio, and P. Skrzypczyk, *J. Phys. A: Math. Theor.* **49**, 143001 (2016).
- [18] V. Gorini, A. Kossakowski, and E. Sudarshan, *J. Math. Phys.* **17**, 821 (1976).
- [19] H. Grabert, U. Weiss, and P. Talkner, *Z. Phys. B* **55**, 87 (1984).
- [20] L. Henderson and V. Vedral, *J. Phys. A: Math. Gen.* **34**, 6899 (2001).
- [21] P. P. Hofer, M. Perarnau-Llobet, L. D. M. Miranda, G. Haack, R. Silva, J. Bohr Brask, and N. Brunner, preprint, arXiv:1707.09211 (2017).
- [22] A. S. Holevo and R. F. Werner, *Phys. Rev. A* **63**, 032312 (2001).
- [23] R. Horodecki, P. Horodecki, M. Horodecki, and K. Horodecki, *Rev. Mod. Phys.* **81**, 865 (2009).
- [24] J. Jeske, D. J. Ing, M. B. Plenio, S. F. Huelga, and J. H. Cole, *J. Chem. Phys.* **142**, 064104 (2015).
- [25] R. Kosloff, *J. Chem. Phys.* **80**, 1625 (1984).
- [26] R. Kosloff, *Entropy* **15**(6), 2100 (2013).
- [27] R. Kosloff and A. Levy, *Annu. Rev. Phys. Chem.* **65**, 365 (2014).
- [28] A. Levy and R. Kosloff, *Europhys. Lett.* **107**, 20004 (2014).
- [29] G. Lindblad, *Commun. Math. Phys.* **48**, 119 (1976).
- [30] M. Ludwig, K. Hammerer, and F. Marquardt, *Phys. Rev. A* **82**, 012333 (2010).
- [31] P. Marian and T. A. Marian, *Phys. Rev. A* **86**, 022340 (2012).
- [32] A. Müller-Hermes and D. Reeb, *Ann. Henri Poincaré* **18**, 1777 (2017).
- [33] M. A. Nielsen and I. L. Chuang, *Quantum Computation and Quantum Information*, Cambridge University Press, 2000.
- [34] H. Ollivier and W. H. Zurek, *Phys. Rev. Lett.* **88**, 017901 (2001).
- [35] J. P. Palao, R. Kosloff, and J. M. Gordon, *Phys. Rev. E* **64**, 056130 (2001).
- [36] S. Pirandola, G. Spedalieri, S. L. Braunstein, N. J. Cerf, and S. Lloyd, *Phys. Rev. Lett.* **113**, 140405 (2014).
- [37] M. B. Plenio, *Phys. Rev. Lett.* **95**, 090503 (2005).
- [38] A. Purkayastha, A. Dhar, and M. Kulkarni, *Phys. Rev. A* **93**, 062114 (2016).
- [39] A. G. Redfield, *IBM J. Res. Dev.* **1**, 19 (1957).
- [40] A. Rivas, A. D. K. Plato, S. F. Huelga, and M. B. Plenio, *New J. Phys.* **12**, 113032 (2010).
- [41] J. P. Santos, and G. T. Landi, *Phys. Rev. E* **94**, 062143 (2016).
- [42] H. Spohn, *Lett. Math. Phys.* **2**, 33 (1977).
- [43] H. Spohn, *J. Math. Phys.* **19**, 1227 (1978).
- [44] T. M. Stace, A. C. Doherty, and D. J. Reilly, *Phys. Rev. Lett.* **111**, 180602 (2013).
- [45] J. T. Stockburger and T. Motz, *Fortschr. Phys.*, 1–7 (2016)
[DOI 10.1002/prop.201600067].
- [46] A. Trushechkin and I. Volovich, *Europhys. Lett.* **113**, 30005 (2016).
- [47] A. A. Valido, D. Alonso, and S. Kohler, *Phys. Rev. A* **88**, 042303 (2013).
- [48] A. A. Valido, L. A. Correa, and D. Alonso, *Phys. Rev. A* **88**, 012309 (2013).

1740010-24

Este documento incorpora firma electrónica, y es copia auténtica de un documento electrónico archivado por la ULL según la Ley 39/2015.
Su autenticidad puede ser contrastada en la siguiente dirección <https://sede.ull.es/validacion/>

Identificador del documento: 2111210 Código de verificación: lZvvKBaU

Firmado por: Javier Onam González López
UNIVERSIDAD DE LA LAGUNA

Fecha: 09/09/2019 11:04:42

Daniel Alonso Ramírez
UNIVERSIDAD DE LA LAGUNA

11/09/2019 14:53:47

Testing the Validity of the 'Local' and 'Global' GKLS Master Equations

- [49] A. A. Valido, A. Ruiz, and D. Alonso, Phys. Rev. E **91**, 062123 (2015).
- [50] G. Vidal and R. F. Werner, Phys. Rev. A **65**, 032314 (2002).
- [51] S. Vinjanampathy and J. Anders, Contemp. Phys. **57**, 545 (2016).
- [52] U. Weiss, *Quantum Dissipative Systems*, vol. 13, World Scientific Pub. Co Inc., 2008.
- [53] H. Wichterich, M. J. Henrich, H.-P. Breuer, J. Gemmer, and M. Michel, Phys. Rev. E **76**, 031115 (2007).

Open Syst. Inf. Dyn. 2017.24. Downloaded from www.worldscientific.com
by UNIVERSITY OF NEW ENGLAND on 12/18/17. For personal use only.

1740010-25

84

Este documento incorpora firma electrónica, y es copia auténtica de un documento electrónico archivado por la ULL según la Ley 39/2015.
Su autenticidad puede ser contrastada en la siguiente dirección <https://sede.ull.es/validacion/>

Identificador del documento: 2111210 Código de verificación: lZvvKBaU

Firmado por: Javier Onam González López
UNIVERSIDAD DE LA LAGUNA

Fecha: 09/09/2019 11:04:42

Daniel Alonso Ramírez
UNIVERSIDAD DE LA LAGUNA

11/09/2019 14:53:47

5.3 Relation between topology and heat currents in multilevel absorption machines

New J. Phys., 19(11):113037, 2017

J. Onam González, José P. Palao and Daniel Alonso

Este documento incorpora firma electrónica, y es copia auténtica de un documento electrónico archivado por la ULL según la Ley 39/2015.
Su autenticidad puede ser contrastada en la siguiente dirección <https://sede.ull.es/validacion/>

Identificador del documento: 2111210 Código de verificación: lZvvKBaU

Firmado por: Javier Onam González López
UNIVERSIDAD DE LA LAGUNA

Fecha: 09/09/2019 11:04:42

Daniel Alonso Ramírez
UNIVERSIDAD DE LA LAGUNA

11/09/2019 14:53:47

PAPER • OPEN ACCESS

Relation between topology and heat currents in
multilevel absorption machines

To cite this article: J Onam González *et al* 2017 *New J. Phys.* **19** 113037

View the [article online](#) for updates and enhancements.

Related content

- [Markovian master equations for quantum thermal machines: local vs global approach](#)
Patrick P Hofer, Marti Perarnau-Llobet, L David M Miranda *et al.*
- [Qubit absorption refrigerator at strong coupling](#)
Anqi Mu, Bijay Kumar Agarwalla, Gernot Schaller *et al.*
- [Nonequilibrium thermodynamics in the strong coupling and non-Markovian regime based on a reaction coordinate mapping](#)
Philipp Strasberg, Gernot Schaller, Neill Lambert *et al.*

This content was downloaded from IP address 193.145.124.213 on 08/01/2018 at 12:05

Este documento incorpora firma electrónica, y es copia auténtica de un documento electrónico archivado por la ULL según la Ley 39/2015.
Su autenticidad puede ser contrastada en la siguiente dirección <https://sede.ull.es/validacion/>

Identificador del documento: 2111210 Código de verificación: lZvvKBaU

Firmado por: Javier Onam González López
UNIVERSIDAD DE LA LAGUNA

Fecha: 09/09/2019 11:04:42

Daniel Alonso Ramírez
UNIVERSIDAD DE LA LAGUNA

11/09/2019 14:53:47



PAPER

OPEN ACCESS

RECEIVED
16 April 2017

REVISED
31 July 2017

ACCEPTED FOR PUBLICATION
15 August 2017

PUBLISHED
24 November 2017

Original content from this work may be used under the terms of the Creative Commons Attribution 3.0 licence.

Any further distribution of this work must maintain attribution to the author(s) and the title of the work, journal citation and DOI.



Relation between topology and heat currents in multilevel absorption machines

J Onam González, José P Palao and Daniel Alonso

Departamento de Física and IUdEA, Universidad de La Laguna, La Laguna E-38204, Spain

E-mail: dalonso@ull.es

Keywords: quantum thermodynamics, absorption devices, Hill theory

Abstract

The steady state heat currents of continuous absorption machines can be decomposed into thermodynamically consistent contributions, each of them associated with a circuit in the graph representing the master equation of the thermal device. We employ this tool to study the functioning of absorption refrigerators and heat transformers with an increasing number of active levels. Interestingly, such an analysis is independent of the particular physical implementation (classical or quantum) of the device. We provide new insights into the understanding of scaling up thermal devices concerning both the performance and the magnitude of the heat currents. Indeed, it is shown that the performance of a multilevel machine is smaller or equal than the corresponding to the largest circuit contribution. Besides, the magnitude of the heat currents is well-described by a purely topological parameter which in general increases with the connectivity of the graph. Therefore, we conclude that for a fixed number of levels, the best of all different constructions of absorption machines is the one whose associated graph is as connected as possible, with the condition that the performance of all the contributing circuits is equal.

1. Introduction

Continuous quantum absorption machines [1] are multilevel systems connected to several thermal baths at different temperatures. Their autonomous functioning can be rigorously described by using the theory of open quantum systems [2]. Some basic models such as the three-level [3, 4], the two-qubit [5] and the three-qubit [4, 6] absorption refrigerators have been widely employed in establishing fundamental relations in quantum thermodynamics [7]. Besides, several experimental proposals have been put forward, for example those based on nano-mechanical oscillators or atoms interacting with optical resonators [8, 9], atoms interacting with nonequilibrium electromagnetic fields [10], superconducting quantum interference devices [11, 12], and quantum dots [13]. Further, an experimental realization of a quantum absorption refrigerator has been recently reported [14].

The dynamics of quantum machines is described by a master equation when the coupling with the baths is weak enough. Along this paper we consider in addition systems for which two states with the same energy cannot be connected to a third one through the same bath. This assumption greatly simplifies the quantum master equation as the population and coherence dynamics are decoupled in the system energy eigenbasis [2], and will be referred in the following as the PCD condition. It guarantees the thermodynamic consistency of the models [15, 16], which may be broken when some uncontrolled approximations are introduced [17]. Under this assumption coherences decay with time and are irrelevant in the steady state functioning of the device, contrary, for example, to externally driven devices [18] and systems including matter currents [19], where they may play an important role on the thermodynamic properties. When the PCD condition holds, the populations follow a continuous time Markov master equation [20], given in terms of the rates for the transitions between states, which are always allowed in both directions. In this case a thermal device implemented in a quantum system can be described within the framework of stochastic thermodynamics [21–23].

© 2017 IOP Publishing Ltd and Deutsche Physikalische Gesellschaft

Este documento incorpora firma electrónica, y es copia auténtica de un documento electrónico archivado por la ULL según la Ley 39/2015.
Su autenticidad puede ser contrastada en la siguiente dirección <https://sede.ull.es/validacion/>

Identificador del documento: 2111210

Código de verificación: lZvvKBaU

Firmado por: Javier Onam González López
UNIVERSIDAD DE LA LAGUNA

Fecha: 09/09/2019 11:04:42

Daniel Alonso Ramírez
UNIVERSIDAD DE LA LAGUNA

11/09/2019 14:53:47

The analysis of the thermodynamic quantities can be realized at different levels of description [24]. From a macroscopic point of view, where the relevant quantities are the bath temperatures and the physical (total) heat currents, to a microscopic description that considers in addition the device structure. This latter perspective is more and more relevant as the advance of the experimental techniques allows for the design and the manipulation of the device. A prominent tool for this microscopic analysis is graph theory, where the stochastic master equation for the populations is represented by a graph. Schnakenberg theory [25] is a popular approach that gives a decomposition of the total entropy production based on a set of fundamental circuits in the graph. Basically, Schnakenberg applies Kirchhoff's current laws to reduce the number of terms appearing in the entropy production, which may be highly beneficial for optimization procedures. It has been used for example in linear irreversible thermodynamics [26] and in the study of steady-state fluctuation theorems [27, 28]. This method does not intend to associate an entropy production with each circuit. In particular, the attempt to interpret individually each term in the decomposition may lead to apparent negative entropy productions, although this problem can be avoided by a convenient choice of the fundamental circuits [29–31]. However, it has been shown that the diagnosis of the machine performance greatly benefits from considering the thermodynamic analysis of not only the fundamental but all the possible circuits in the graph [32–34]. A convenient approach is then Hill theory [35]. Schnakenberg and Hill theory assign the same affinity to each circuit, but the latter considers all the possible circuits and leads to thermodynamically consistent entropy productions. Both methods coincide when the fundamental set of circuits contains all the possible ones.

In this paper we use Hill theory to fully characterize the two relevant quantities in the study of continuous absorption devices: the steady state heat currents and performance. Our aim is to find out under what conditions these quantities are as large as possible, i.e. what is the best construction of multilevel machines. Graph theory allows us to answer this key question from a very general perspective, looking only at the topological structure of the graph. Although we are motivated by the study of quantum models and in the following we will assume the PCD condition, our analysis also applies to classical stochastic models, including mesoscopic systems where the relevant degrees of freedom are identified by a coarse graining procedure [36, 37]. In fact, the main advantage of this approach is that many properties of a device can be inferred from its graph representation irrespectively of its underlying, microscopic or mesoscopic, quantum or classical, realization.

It has been shown that systems with degenerate energy levels and driven by an external field may present a linear increment of the heat currents with the number of states [38, 39]. Furthermore, two-stroke models in the quasi-equilibrium regime show an improvement in the performance with the number of levels [40]. However, using a particular construction of continuous absorption devices by merging three-level systems, Correa [41] found no changes in the performance and a fast saturation in the magnitude of the heat currents as the number of levels increases. Thus the question arises whether this limitation may be overcome by different designs of the absorption device.

We are interested in continuous machines that either extract energy from the coldest bath (refrigerators) or inject energy to the hottest bath (heat transformers). We do not consider devices designed for complicated tasks involving more than one target bath, although our procedure could also be applied to such systems. The best refrigerators and heat transformers should generally provide the largest possible heat currents and be also able of reaching the reversible limit for a particular set of the parameters. In order to identify them, we first justify that a machine coupled to three baths is capable of achieving the same currents than more complicated devices which consider additional heat reservoirs. As multilevel machines are composed by multiple circuits, our next step is to identify the optimal circuit to be used as building block. In general the magnitude of the heat currents increases with the transitions rates for any circuit. Hence, to elucidate the role of the circuit structure in the currents we set the rates to fixed values. Moreover, this condition avoids processes which prevents the machine from reaching the reversible limit when considering multiple circuits. The following step is to determine the graph structure leading to the largest heat currents considering optimal blocks. Finally, we relax the condition of fixed rates to improve the scaling of the currents with the number of levels without introducing harmful processes as heat leaks.

The paper is organized as follows: in section 2 we motivate the generic nature of our work by describing two different models of absorption devices which are represented by the same four-state graph. The master equation for all the quantum models used as illustration of the general results can be obtained using appendix A with the Hamiltonians provided in appendix B. We also introduce in section 2 the essential concepts of graph theory needed to characterize the heat currents associated with a circuit inside a general graph. This result allows us to relate each circuit to a thermodynamic mechanism and classify it attending to its contribution to the overall functioning of a device coupled to three baths. Although we have used previously the circuit decomposition in a different context, the analysis of the irreversible mechanisms arising in thermal devices indirectly connected to environments [34], we provide now a derivation of it using Hill theory in appendix C. The differences between Hill and Schnakenberg decompositions are discussed and worked out for the four-state graph in appendices D and E. In section 3 we analyze multilevel machines represented by a graph circuit. Explicit expressions for the

Este documento incorpora firma electrónica, y es copia auténtica de un documento electrónico archivado por la ULL según la Ley 39/2015.
Su autenticidad puede ser contrastada en la siguiente dirección <https://sede.ull.es/validacion/>

Identificador del documento: 2111210

Código de verificación: lZvvKBaU

Firmado por: Javier Onam González López
UNIVERSIDAD DE LA LAGUNA

Fecha: 09/09/2019 11:04:42

Daniel Alonso Ramírez
UNIVERSIDAD DE LA LAGUNA

11/09/2019 14:53:47

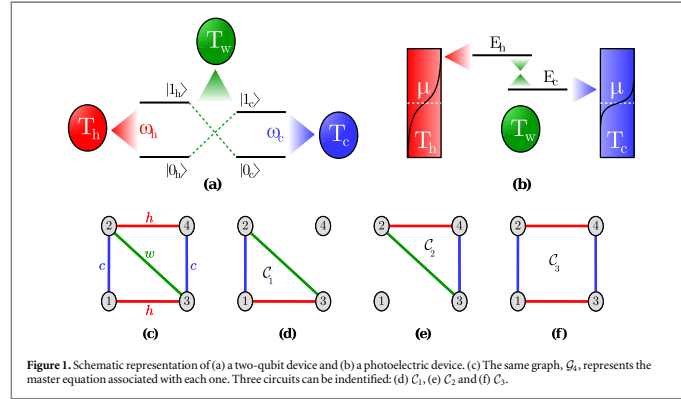


Figure 1. Schematic representation of (a) a two-qubit device and (b) a photoelectric device. (c) The same graph, G_4 , represents the master equation associated with each one. Three circuits can be identified: (d) C_1 , (e) C_2 and (f) C_3 .

scaling of the heat currents with the number of levels in the high and low temperature limits are provided in appendix F. Machines represented by graphs with multiple circuits are studied in section 4. A simple example to illustrate the relation between the heat currents and the graph connectivity is presented in appendix G. We draw our conclusions in section 5.

2. Motivation and background

We will motivate our approach by first considering two different models of absorption devices, both connected to three reservoirs at temperatures T_c (cold), T_h (hot) and T_w (referred in the following as the temperature of the work bath, in analogy with devices driven by an external field), with $T_c < T_h < T_w$. Depending on internal parameters, the devices can either work as heat transformers, transferring energy from the hot to the work bath, or as refrigerators, extracting energy from the cold bath assisted by the work bath. The first model is the two-qubit device [5] shown in figure 1 (a). Each qubit is connected to a bosonic heat bath at temperatures T_c and T_h . The interaction between them is mediated by another bath at temperature T_w . The state of this machine can be expanded in the product state basis $|1\rangle \equiv |0_h 0_c\rangle$, $|2\rangle \equiv |0_h 1_c\rangle$, $|3\rangle \equiv |1_h 0_c\rangle$ and $|4\rangle \equiv |1_h 1_c\rangle$, with energies $E_1 = 0$, $E_2 = \hbar\omega_c$, $E_3 = \hbar\omega_h$ and $E_4 = \hbar(\omega_c + \omega_h)$. When the system is weakly coupled to the reservoirs, the dynamics of the populations is described by a master equation

$$\frac{d}{dt} p_i(t) = \sum_{j=1}^4 (W_{ij}^c + W_{ij}^w + W_{ij}^h) p_j(t), \quad (1)$$

where p_i are the populations, $W_{ij}^\alpha \geq 0$ the transition rates associated with the coupling with the bath α , and $W_{ii}^\alpha = -\sum_{j \neq i} W_{ij}^\alpha$. For our purpose now is only important that the non-zero rates associated with the cold bath correspond to transitions $1 \leftrightarrow 2$, $3 \leftrightarrow 4$, with the hot bath to $1 \leftrightarrow 3$, $2 \leftrightarrow 4$, and with the work bath to $2 \leftrightarrow 3$.

The second model is a photoelectric device [32, 42–44] composed of two single-level, spinless quantum dots with energies E_c and E_h that can be both occupied at the same time. Each dot is connected to a metal electrode with chemical potential $\mu < E_c < E_h$ and temperatures T_c and T_h , see figure 1 (b). We choose the same chemical potential in order to avoid introducing mechanical work and assume that neither the temperatures nor the chemical potential are modified by the interchange of electrons through the quantum dots. The system states are $1 \equiv 0_h 0_c$, $2 \equiv 0_h 1_c$, $3 \equiv 1_h 0_c$ and $4 \equiv 1_h 1_c$, with energies $E_1 = 0$, $E_2 = E_h$, $E_3 = E_c$ and $E_4 = E_c + E_h$, where now 0_h and 1_h are the number of electrons in the dot. Transitions between the two dots are supported by an additional radiation source (for example the Sun in photovoltaic models [32, 44]) at an effective temperature T_w . Considering a weak coupling with the electrodes and a negligible line broadening of the energy levels, the device dynamics can be described by a stochastic master equation [45] in the form (1), but with transition rates determined by the particularities of the physical model under consideration. In the case of the absorption device with bosonic baths the rates are proportional to Planck distributions, while for the photoelectric device they are proportional to Fermi functions.

Este documento incorpora firma electrónica, y es copia auténtica de un documento electrónico archivado por la ULL según la Ley 39/2015.
 Su autenticidad puede ser contrastada en la siguiente dirección <https://sede.ull.es/validacion/>

Identificador del documento: 2111210

Código de verificación: lZvvKBaU

Firmado por: Javier Onam González López
 UNIVERSIDAD DE LA LAGUNA

Fecha: 09/09/2019 11:04:42

Daniel Alonso Ramírez
 UNIVERSIDAD DE LA LAGUNA

11/09/2019 14:53:47

The relevant point for our analysis is that since the master equations have the same structure, the devices share several thermodynamic properties that stem directly from it. The different physics involved in each case is only reflected in the particular values of the transition rates. The master equation may be represented by a network, a weighted and labeled multi-digraph. However, as transition between states are always allowed in both directions, we will use a simpler representation consisting in a labeled graph, with vertices associated with the system states and undirected edges with the transitions [25, 35]. When necessary, an arbitrary orientation can be assigned to the graph and a weight to each edge, given by the corresponding transition rate. For example, the representation of (1), denoted in the following by \mathcal{G}_α , is shown in figure 1(c). The circuits of \mathcal{G}_α , defined as a cyclic sequence of distinct edges, are displayed in figures 1(d)–(f). Circuits C_1 and C_2 participate in different processes depending on their two possible orientations, referred as cycles. For example the cycle $\vec{C}_1 \equiv \{1, 2, 3, 1\}$ absorbs energy from the cold and work baths that is rejected to the hot bath, whereas the opposite cycle $-\vec{C}_1 \equiv \{1, 3, 2, 1\}$ absorbs energy from the hot bath and rejects it to the cold and work baths. In both processes there is a net exchange of energy with the three baths.

The circuit C_3 involves only two baths (cold and hot) and in our models does not lead to any net exchange of energy. This is a consequence of having the same energy gap for transitions assisted by the same bath. However, in more general setups with different transition energies, $E_{34} = E_{12} + \Delta$ and $E_{24} = E_{13} + \Delta$ with $E_{ij} = E_i - E_j$, there is a heat leak which increases with the energy shift Δ [33].

The overall physical heat currents \dot{Q}_α and the performance of the device are then the result of the interplay of the different mechanisms related to each circuit. In spite of the simplicity of the previous qualitative interpretation, the microscopic currents $\dot{q}_\alpha(C_i)$ corresponding to each circuit in the graph are not straightforwardly obtained from the physical currents. We introduce below the concepts of graph theory needed to characterize them.

2.1. Graph, circuits and steady state heat currents

For simplicity we consider systems with N states of energies E_i , $1 \leq i \leq N$, represented by a connected graph and coupled with thermal baths. The generalization for systems exchanging particles without involving any mechanical work, as the absorption device of figure 1(b), is straightforward. The system transitions may be coupled to one or several independent heat baths, each one in equilibrium at temperature T_α , $1 \leq \alpha \leq R$. The system evolution is described by a master equation

$$\frac{d}{dt} p_i(t) = \sum_{j=1}^N \sum_{\alpha=1}^R W_{ij}^\alpha p_j(t), \quad (2)$$

where p_i is the normalized probability distribution to be in the state i , $W_{ij}^\alpha \geq 0$ is the transition rate from the state j to the state i due to the coupling with the bath α , and

$$W_{ii}^\alpha = -\sum_{j \neq i} W_{ij}^\alpha. \quad (3)$$

The transition matrix W , with elements $W_{ij} = \sum_{\alpha=1}^R W_{ij}^\alpha$, is singular, which guarantees the existence of a non-trivial steady state solution of (2) and the conservation of the normalization. In addition, we assume that

$$\frac{W_{ji}^\alpha}{W_{ij}^\alpha} = \exp\left[\frac{E_{ji}}{k_B T_\alpha}\right], \quad (4)$$

where k_B is the Boltzmann constant. If the transition rates W_{ij}^α for $j > i$ are known, the remaining rates can be determined by using (3) and (4).

The master equation (2) is represented by a graph $\mathcal{G}(N, U)$ composed of N vertices and U undirected edges. Let \vec{x}_e be an edge in the graph, $1 \leq e \leq U$. In the following \vec{x}_e will denote an edge oriented from vertex i_e to j_e , whereas $-\vec{x}_e$ connects j_e to i_e in both cases due to the coupling with the bath α_e . Oriented edges are related to rate coefficients by $W(\vec{x}_e) = W_{i_e j_e}^{\alpha_e}$ and $W(-\vec{x}_e) = W_{j_e i_e}^{\alpha_e}$. An algebraic value \mathcal{A} may be assigned to any oriented subgraph $\vec{\mathcal{G}}_s$ of \mathcal{G} , composed of $s \leq U$ oriented edges \vec{x}_e [25],

$$\mathcal{A}(\vec{\mathcal{G}}_s) = \prod_{\alpha=1}^R \mathcal{A}^\alpha(\vec{\mathcal{G}}_s), \quad (5)$$

where, if the subgraph involves edges associated with the bath α ,

$$\mathcal{A}^\alpha(\vec{\mathcal{G}}_s) = \prod_{e \in s, \alpha} W(\vec{x}_e), \quad (6)$$

with $\prod_{e \in s, \alpha}$ the product over all the directed edges of $\vec{\mathcal{G}}_s$ corresponding to this bath, and otherwise $\mathcal{A}^\alpha(\vec{\mathcal{G}}_s) = 1$.

Both $\mathcal{A}(\vec{\mathcal{G}}_s)$ and $\mathcal{A}^\alpha(\vec{\mathcal{G}}_s)$ are positive real numbers. A maximal tree T^μ , $1 \leq \mu \leq N_T$, is a subgraph of \mathcal{G} containing $N - 1$ edges without forming any closed path. The oriented subgraph \vec{T}_i^μ is a maximal tree in which

Este documento incorpora firma electrónica, y es copia auténtica de un documento electrónico archivado por la ULL según la Ley 39/2015.
 Su autenticidad puede ser contrastada en la siguiente dirección <https://sede.ull.es/validacion/>

Identificador del documento: 2111210

Código de verificación: lZvvKBaU

Firmado por: Javier Onam González López
 UNIVERSIDAD DE LA LAGUNA

Fecha: 09/09/2019 11:04:42

Daniel Alonso Ramírez
 UNIVERSIDAD DE LA LAGUNA

11/09/2019 14:53:47

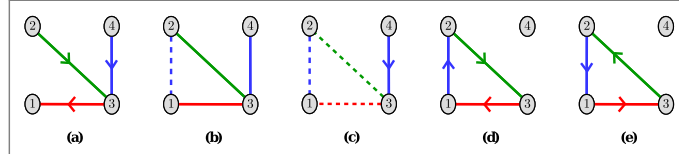


Figure 2. (a) A maximal tree T^1 of G_k oriented towards the vertex 1 is denoted by \vec{T}_1^1 . (b) When adding the chord x_ν (dashed line) to T^1 , the circuit C_ν is obtained. (c) Removing the circuit (dashed line) and orienting the remaining edges towards it, the forest \vec{F}_1^β is found. The cycles \vec{C}_1 and $-\vec{C}_1$ are shown in (d) and (e).

all the edges are directed towards the vertex i . A chord of a maximal tree is one of the $U - N + 1$ edges that are not part of it. The subgraph obtained when a chord is added to a maximal tree has only a circuit C_ν , $1 \leq \nu \leq N_C$. When removing the circuit from the previous subgraph, a collection of edges remains. Orienting them towards the circuit, a forest \vec{F}_1^β is found. The index β indicates that for a given circuit different forests can be found, resulting from different maximal trees. The number of maximal trees (N_T), circuits (N_C) and forests depend on the topological structure of the graph \mathcal{G} . Each circuit C_ν may be oriented in one of the two possible directions, leading to the cycles \vec{C}_ν and $-\vec{C}_\nu$. Some examples are shown in figure 2. In appendix C we use Hill theory to show that the steady state heat current associated with a circuit is given by

$$\dot{q}_\alpha(C_\nu) = -T_\alpha D(\mathcal{G})^{-1} \det(-\mathbf{W}|C_\nu) [\mathcal{A}(\vec{C}_\nu) - \mathcal{A}(-\vec{C}_\nu)] X^\alpha(\vec{C}_\nu). \quad (7)$$

The factor D is calculated using

$$D(\mathcal{G}) = \sum_{i=1}^N \sum_{\mu=1}^{N_C} \mathcal{A}(\vec{T}_i^\mu) = |\det(\vec{\mathbf{W}})|. \quad (8)$$

The quantity $D(\mathcal{G}) > 0$ increases with the complexity (both the number of vertices and edges). It is a factor which reduces the population in a circuit and therefore the corresponding heat currents when considering machines with an increasing number of them. The matrix $\vec{\mathbf{W}}$ is obtained from the transition matrix \mathbf{W} by replacing the elements of an arbitrary row by ones, whereas the matrix $(-\mathbf{W}|C_\nu)$ is obtained by removing from $-\mathbf{W}$ all the rows and columns corresponding to the vertices of the circuit. Indeed, $\det(-\mathbf{W}|C_\nu)$ is the sum of the forests of C_ν and can be thought of as an 'injection of population' through edges not belonging to it.

We have also introduced the cycle affinity associated with the bath α ,

$$X^\alpha(\vec{C}_\nu) = k_B \ln \left(\frac{\mathcal{A}^\alpha(\vec{C}_\nu)}{\mathcal{A}^\alpha(-\vec{C}_\nu)} \right), \quad (9)$$

and then the total cycle affinity is

$$X(\vec{C}_\nu) = \sum_{\alpha=1}^R X^\alpha(\vec{C}_\nu) = k_B \ln \left(\frac{\mathcal{A}(\vec{C}_\nu)}{\mathcal{A}(-\vec{C}_\nu)} \right), \quad (10)$$

The quantity $-T_\alpha X^\alpha(\vec{C}_\nu)$ is just the net amount of energy interchanged between the bath α and the system when performing the cycle \vec{C}_ν . Notice that $X^\alpha(-\vec{C}_\nu) = -X^\alpha(\vec{C}_\nu)$ and hence each cycle is related to a process where some energy is either absorbed from or rejected to the bath. The circuit heat current (7) can be viewed as the result of the competition between the two cycles, described by $-T_\alpha [\mathcal{A}(\vec{C}_\nu) - \mathcal{A}(-\vec{C}_\nu)] X^\alpha(\vec{C}_\nu)$, weighted by how the circuit is immersed in the graph, which is contained in $D(\mathcal{G})^{-1} \det(-\mathbf{W}|C_\nu)$.

As a consequence of (4)

$$\sum_{\alpha=1}^R T_\alpha X^\alpha(\vec{C}_\nu) = 0, \quad (11)$$

reflecting that the net energy exchanged by the system with the baths along a complete cycle is zero. Using it the following relation is found,

$$\sum_{\alpha=1}^R \dot{q}_\alpha(C_\nu) = 0, \quad (12)$$

and since the only contribution to the steady state entropy production is due to finite-rate heat transfer effects, the circuit entropy production is

Este documento incorpora firma electrónica, y es copia auténtica de un documento electrónico archivado por la ULL según la Ley 39/2015.
 Su autenticidad puede ser contrastada en la siguiente dirección <https://sede.ull.es/validacion/>

Identificador del documento: 2111210

Código de verificación: lZvvKBaU

Firmado por: Javier Onam González López
 UNIVERSIDAD DE LA LAGUNA

Fecha: 09/09/2019 11:04:42

Daniel Alonso Ramírez
 UNIVERSIDAD DE LA LAGUNA

11/09/2019 14:53:47

$$\dot{s}(C_v) = - \sum_{\alpha=1}^R \frac{\dot{q}_\alpha(C_v)}{T_\alpha} \geq 0, \quad (13)$$

where the inequality is shown in appendix C. These two last equations assure the consistency of the circuit heat currents and the entropy production with the first and second laws of thermodynamics. Finally, the total entropy production is given by $\dot{S} = \sum_{v=1}^{N_c} \dot{s}(C_v)$ and the physical heat currents by $\dot{Q}_\alpha = \sum_{v=1}^{N_c} \dot{q}_\alpha(C_v)$. They can be directly obtained from the transition rates by using (7), without determining the steady state populations. As an illustration of the circuit decomposition, the heat currents for the graph \mathcal{G}_4 are worked out in appendix D. Let us remind that other decompositions of \dot{S} are possible and we briefly discuss them in appendix E.

The circuit heat currents (7) are homogeneous functions of degree 1 with respect to the transition rates, that is

$$W_{ij}^\alpha \rightarrow \sigma W_{ij}^\alpha; \quad \dot{q}_\alpha(C_v) \rightarrow \sigma \dot{q}_\alpha(C_v); \quad \dot{Q}_\alpha \rightarrow \sigma \dot{Q}_\alpha, \quad (14)$$

with $\sigma > 0$. Therefore, the currents can be always modified by changing the rates, provided that the assumptions to obtain the master equation remain valid. This property emphasizes the importance of the graph topology.

2.2. Classification of circuits

The contribution of each circuit C_v to the physical heat currents can be classified attending to their non-zero affinities X^α :

- (i) $X^\alpha(\vec{C}_v) = 0$ for all the baths. These circuits will be referred as trivial circuits, as they do not contribute neither to the steady state heat currents nor to the entropy production.
- (ii) Condition (11) prevents any circuit from having only a non-zero affinity X^α .
- (iii) $X^\alpha(\vec{C}_v) \neq 0$ only for two baths, $\alpha = \alpha_1, \alpha_2$. Then there is only a net energy transfer between them, although other baths could participate in the cycle. Using (12) and (13), the following condition is found

$$\dot{q}_{\alpha_1}(C_v) \left(\frac{1}{T_{\alpha_2}} - \frac{1}{T_{\alpha_1}} \right) \geq 0. \quad (15)$$

Taking $T_{\alpha_1} < T_{\alpha_2}$, the heat currents verify $\dot{q}_{\alpha_2}(C_v) > 0$ and $\dot{q}_{\alpha_1}(C_v) < 0$. Therefore the net heat current associated with these circuits always flows from the higher temperature bath to the lower temperature one. In the context of refrigerators and heat transformers these circuits are related to heat leaks that decrease the performance [33, 34].

- (iv) $X^\alpha(\vec{C}_v) \neq 0$ for three baths, $\alpha = \alpha_1, \alpha_2, \alpha_3$. They will be referred as three-bath circuits in the following. Equation (11) implies that, given a circuit orientation, two of the affinities and their corresponding heat currents must have the same sign. Considering $\text{sgn}(X^{\alpha_1}) = \text{sgn}(X^{\alpha_2}) = -\text{sgn}(X^{\alpha_3})$ and using again (12) and (13), we obtain

$$\dot{q}_{\alpha_1}(C_v) \left(\frac{1}{T_{\alpha_3}} - \frac{1}{T_{\alpha_1}} \right) + \dot{q}_{\alpha_2}(C_v) \left(\frac{1}{T_{\alpha_3}} - \frac{1}{T_{\alpha_2}} \right) \geq 0. \quad (16)$$

The formalism applies also to circuits with non-zero affinities associated with more than three baths, but they are not relevant for our analysis.

2.3. Circuits in refrigerators and heat transformers

For simplicity we discuss now refrigerators, but the results are also valid for heat transformers. In general, the environment may be composed by the target coldest bath, a collection of sink baths with temperatures $\{T_{h,i}\}$ (where the surplus energy is rejected) and work baths with temperatures $\{T_{w,i}\}$ (supplying energy to complete the cycles). Let $\{X^{\alpha,i}\}$ be the affinities of a particular circuit. Equation (7) implies that we can always find a hot and a work bath with temperatures and affinities given by $T_h, X^h \equiv \sum_i T_{w,i} X^{\alpha,i}$ ($\alpha = h, w$), such that tuning their rate values (14) we obtain the same or larger heat currents than in the original system. Therefore we focus in the following on circuits and thermal machines coupled to three thermal baths with temperatures $T_c < T_h < T_w$.

In the construction of the device we do not consider circuits with two edges associated with different baths connecting the same vertices, as it would lead directly to heat leaks (iii). To perform useful tasks we must include three-bath circuits (iv), which can be classified as:

- (a) $\alpha_1 = h$ and $\alpha_2 = w$, which leads to $\dot{q}_h(C_v), \dot{q}_w(C_v) > 0$ and $\dot{q}_c(C_v) < 0$.

Este documento incorpora firma electrónica, y es copia auténtica de un documento electrónico archivado por la ULL según la Ley 39/2015.
 Su autenticidad puede ser contrastada en la siguiente dirección <https://sede.ull.es/validacion/>

Identificador del documento: 2111210 Código de verificación: lZvvKBaU

Firmado por: Javier Onam González López
 UNIVERSIDAD DE LA LAGUNA

Fecha: 09/09/2019 11:04:42

Daniel Alonso Ramírez
 UNIVERSIDAD DE LA LAGUNA

11/09/2019 14:53:47

(b) $\alpha_1 = c$ and $\alpha_2 = h$, giving now $\dot{q}_c(C_v)$, $\dot{q}_h(C_v) < 0$ and $\dot{q}_w(C_v) > 0$.

(c) $\alpha_1 = c$ and $\alpha_2 = w$, for which

$$\text{sgn}[X^c(\vec{C}_v)] = \text{sgn}[X^w(\vec{C}_v)] = -\text{sgn}[X^h(\vec{C}_v)]. \quad (17)$$

In cases (a) and (b) heat is simply transferred from the work to the cold bath, whereas the hot bath absorbs or gives up some energy. In (c) two different directions for the heat currents are possible: $\dot{q}_c(C_v) > 0$, $\dot{q}_h(C_v) > 0$ and $\dot{q}_w(C_v) > 0$, $\dot{q}_h(C_v) < 0$, $\dot{q}_w(C_v) < 0$, which correspond to the conditions for the heat currents in heat transformers and refrigerators respectively. Therefore equation (17) settles the condition for the affinities in useful circuits. The particular working mode will depend on the system parameters.

3. Thermal machines represented by a circuit graph

In this section we analyze thermal machines that are represented by a circuit graph, $\mathcal{G} = \mathcal{C}^N$, with $N \geq 3$ states (vertices) and $U = N$ undirected edges. We consider useful three-bath circuits for which (17) holds. Along this section we shall make explicit the circuit length (the number of states or edges) by the superscript N . In this case the physical and circuit heat currents coincide. From (10) we obtain $\mathcal{A}(-\vec{C}^N) = \mathcal{A}(\vec{C}^N) \exp[-X(\vec{C}^N)/k_B]$, and then the physical heat currents are given by

$$\dot{Q}_\alpha = \dot{q}_\alpha(C^N) = -T_\alpha \mathcal{R}(\vec{C}^N) \{1 - \exp[-X(\vec{C}^N)/k_B]\} X^\alpha(\vec{C}^N), \quad (18)$$

where

$$\mathcal{R}(\vec{C}^N) = D(\mathcal{C}^N)^{-1} \mathcal{A}(\vec{C}^N). \quad (19)$$

Notice that the dependence on the arrangement of the edges in the circuit is contained in $\mathcal{R}(\vec{C}^N)$ and the currents vanish for $X(\vec{C}^N) = 0$. Using (11), the circuit affinity is rewritten as

$$X(\vec{C}^N) = \left(1 - \frac{T_c}{T_w}\right) X^c(\vec{C}^N) + \left(1 - \frac{T_h}{T_w}\right) X^h(\vec{C}^N). \quad (20)$$

The device operating mode depends only on the parameter $x = -(T_c X^c)/(T_h X^h)$, $0 \leq x \leq 1$, which is independent of the particular circuit orientation, and for $X(\vec{C}^N) = 0$ results in

$$x_r = \frac{T_c(T_w - T_h)}{T_h(T_w - T_c)}. \quad (21)$$

When $x < x_r$, the device operates as an absorption refrigerator whose coefficient of performance is

$$\varepsilon = \frac{\dot{Q}_c}{\dot{Q}_w} = \frac{x}{1 - x}. \quad (22)$$

The coefficient of performance reaches the Carnot value $\varepsilon_C = T_c(T_w - T_h)/[T_w(T_h - T_c)]$ when x approaches to x_r from below but at vanishing heat currents ($X(\vec{C}^N) = 0$). When $x > x_r$, the machine operates as a heat transformer with efficiency

$$\eta = \frac{-\dot{Q}_w}{\dot{Q}_h} = 1 - x, \quad (23)$$

reaching the Carnot value $\eta_C = T_w(T_h - T_c)/[T_h(T_w - T_c)]$ when x approaches to x_r from above. In consequence, the device performance depends only on the circuit affinities $X^\alpha(\vec{C}^N)$, irrespective of the value $\mathcal{R}(\vec{C}^N)$, and they may be suitably tuned to reach the reversible limit for any graph circuit.

3.1. Circuit structure, performance and heat currents

In the following and without loss of generality, we choose a circuit orientation such that $X(\vec{C}^N) > 0$. The affinities and the algebraic value $\mathcal{A}(\vec{C}^N)$ depend only on the number of edges and their associated transitions rates. In particular, $\mathcal{A}(\vec{C}^N)$ is the product of N transition rates. However, the factor D depends also on the arrangement of the edges through the oriented maximal trees in (8). The $N_T = N$ maximal trees are obtained by removing in each case one of the edges in the circuit. We denote by T^j the maximal tree obtained by removing the edge starting in the state j . The term $D(\mathcal{C}^N)$ is the sum of N^2 terms $\mathcal{A}(\vec{T}^j)$, each one composed of the product of $N - 1$ transition rates.

Este documento incorpora firma electrónica, y es copia auténtica de un documento electrónico archivado por la ULL según la Ley 39/2015.
Su autenticidad puede ser contrastada en la siguiente dirección <https://sede.ull.es/validacion/>

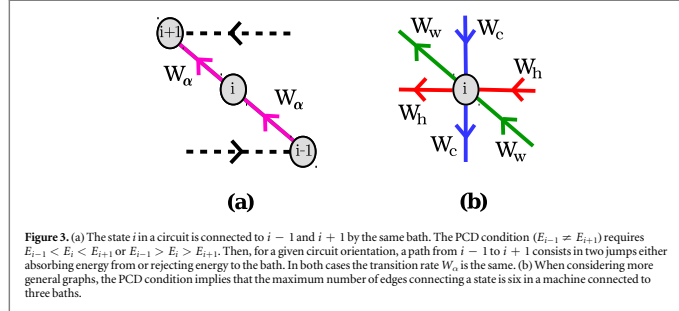
Identificador del documento: 2111210 Código de verificación: lZvvKBaU

Firmado por: Javier Onam González López
UNIVERSIDAD DE LA LAGUNA

Fecha: 09/09/2019 11:04:42

Daniel Alonso Ramírez
UNIVERSIDAD DE LA LAGUNA

11/09/2019 14:53:47



3.1.1. Dependence on the transition rates

From the previous results for \mathcal{A} and D and after a straightforward calculation, the heat currents are bounded by

$$|\dot{Q}_\alpha| < T_\alpha W_m X^\alpha(\vec{C}^N), \quad (24)$$

where W_m is the minimum rate in $\mathcal{A}(\vec{C}^N)$. As intuitively expected, increasing the lowest rates may result in larger heat currents for any circuit. The remaining question is then what kind of circuit shows the largest heat currents for a set of fixed transition rates. In order to answer it, we assume in the following that the available resource in the machine design is a set of three undirected edges with fixed transitions rates, W_α and $W_{-\alpha}$, associated the first with energy transfer to and the second with energy absorption from the bath $\alpha = c, w, h$. This construction can always overcome complicated ones with more than three edges using a proper scaling of the rates, see (14). Besides, it implies fixed energy gaps $|E_{ij}| \equiv E_i$ for transitions assisted by the same bath and:

- (i) When two edges, x_{i-1} and x_i , connecting the state i are associated with the same bath, then $W(\vec{x}_{i-1}) = W(\vec{x}_i)$ for any of the two cycles as a consequence of the PCD condition, see figure 3(a).
- (ii) The minimum number of edges required to construct a useful three-bath circuit is three, therefore $E_c + E_w = E_h$ as a result of (11) and (17). For simplicity we take $E_c \neq E_w$.

Considering these points, any circuit must be constructed adding either two-edge sets $\{\alpha\alpha\}$, with $\alpha = c, w, h$, or three-edge sets $\{cwh\}$ to guarantee that the change of energy of the system in a complete cycle is zero. We denote by $m = m_c + m_w + m_h$ the number of two-edge sets in a circuit. Each one of them contributes with the product $W_{-\alpha}W_\alpha$ to the algebraic value $\mathcal{A}(\vec{C}^N)$, independently of the circuit orientation. Circuits constructed only by adding two-edge sets ($N = 2m$) are trivial circuits, $X^\alpha(\vec{C}^{2m}) = 0$. The $n = n_+ + n_-$ three-edge sets $\{cwh\}$ in a circuit contribute either with the product $W_{-c}W_{-w}W_h$ (sets n_+) or $W_cW_wW_{-h}$ (sets n_-) to $\mathcal{A}(\vec{C}^N)$. Notice that when changing the circuit orientation to $-\vec{C}$, n_+ and n_- are interchanged. The smallest useful circuit is a triangle denoted by \mathcal{C}^3 , see for example figures 1(d) and (e). Large circuits \mathcal{C}^N with $N = 3n + 2m$ states are obtained adding additional two and three-edges sets to \mathcal{C}^3 . Their smallest instances are shown in figures 4(a) and (d).

3.1.2. Circuit affinities and $\mathcal{R}(\vec{C}^N)$

The circuit affinities are given by $X^\alpha(\vec{C}^N) = (n_+ - n_-)X^\alpha(\vec{C}^3)$ for a proper choice of the cycles. Both \mathcal{C}^N and \mathcal{C}^3 have the same value of the parameter x , provided that $n_+ - n_- \neq 0$, and then the performance of the circuit \mathcal{C}^N , given by (22) or (23), is necessarily equal to the performance of \mathcal{C}^3 . In other words, for a fixed set of transition rates the circuit performance is independent of the number of edges.

The remaining question is whether larger circuits result in an increment of the magnitude of the heat currents with respect to \mathcal{C}^3 . As $X^\alpha(\vec{C}^N)$ increases at most linearly with N , the term depending on the affinities in (18) increases at most as N^2 , but only when $NX(\vec{C}^3)/k_B$ remains small. However, the increment of the affinities with the number of states is compensated by the factor $\mathcal{R}(\vec{C}^N)$. As the number of terms in D grows quadratically with N , one would expect that in most cases $\mathcal{R}(\vec{C}^N)$ decreases when adding new states and edges to the circuit. In fact, numerical evidence indicates that when adding two and three-edges sets to a circuit, $\mathcal{R}(\vec{C}^N)$ decreases equal

Este documento incorpora firma electrónica, y es copia auténtica de un documento electrónico archivado por la ULL según la Ley 39/2015.
 Su autenticidad puede ser contrastada en la siguiente dirección <https://sede.ull.es/validacion/>

Identificador del documento: 2111210

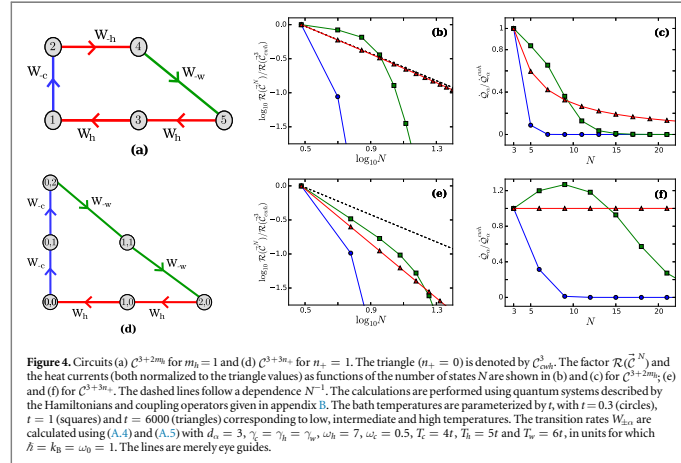
Código de verificación: lZvvKBaU

Firmado por: Javier Onam González López
 UNIVERSIDAD DE LA LAGUNA

Fecha: 09/09/2019 11:04:42

Daniel Alonso Ramírez
 UNIVERSIDAD DE LA LAGUNA

11/09/2019 14:53:47



or faster than N^{-z} , with $z \geq 1$ for large enough N , see for example figures 4(b) and (e). Notice that we do not claim that $\mathcal{R}(C^N) < \mathcal{R}(C^{N'})$ for arbitrary values of N and N' subjected to the condition $N' > N$. Our statement only applies to the construction where the circuit $C^{N'}$ is obtained by adding two-edge and three-edge sets to C^3 , while keeping the edges and the orientation of the latter. Explicit expressions for $\mathcal{R}(C^N)$ in the high and low temperature limits supporting this result are given in appendix F.

We have shown that typically the affinity term in (18) depends linearly on N whereas $\mathcal{R}(C^N)$ decreases faster than N^{-1} , and therefore in most cases the heat currents will decrease when adding additional edges to C^3 , see figures 4(c) and (f). An increment in the heat currents may be obtained at some extent by adding some three-edge sets when $z < 2$ while the circuit affinity remains small enough to grow quadratically with the number of states, as shown in figure 4(f) for intermediate temperatures. This improvement, although modest, may be relevant in situations where the heat currents are intrinsically small. Intuitively, increasing the circuit size implies the addition of states with larger energies and small populations except for specific values of the parameters. This small population makes harder closing the cycles and then effectively reduces the heat currents. Thus, the triangle C^3 is in general the optimal choice as building block for multilevel devices.

3.2. The triangle C^3

There are only two possible configurations of the triangle C^3 compatible with condition (17): C_{cwh}^3 , shown in figure 1(d), and C_{wch}^3 , where the cold and work edges are interchanged. This machine is one of the reference models used in quantum thermodynamics and it has been studied in both the *cwh* [1, 3, 4] and *wch* [23] configurations. Since $X^{\alpha}(C_{\text{cwh}}^3) = X^{\alpha}(C_{\text{wch}}^3)$ for a proper orientation, the circuits show the same thermodynamic performance. Notice that $A(C_{\text{cwh}}^3) = A(C_{\text{wch}}^3)$ but $D(C_{\text{cwh}}^3) \neq D(C_{\text{wch}}^3)$. Using (18), the heat currents are related by

$$\frac{\dot{Q}_{\alpha}^{\text{wch}}}{\dot{Q}_{\alpha}^{\text{cwh}}} = \frac{D(C_{\text{cwh}}^3)}{D(C_{\text{wch}}^3)}. \quad (25)$$

For high temperatures, $\gamma_{\alpha} \equiv \exp[-E_{\alpha}/(k_B T_{\alpha})] \approx 1$, the arrangement of the edges in the circuit is irrelevant and $\dot{Q}_{\alpha}^{\text{wch}}/\dot{Q}_{\alpha}^{\text{cwh}} \approx 1$. A different picture appears at low temperatures, $\gamma_{\alpha} \ll 1$,

$$\frac{\dot{Q}_{\alpha}^{\text{wch}}}{\dot{Q}_{\alpha}^{\text{cwh}}} \approx \frac{W_c W_h + W_c W_w}{W_c W_w + W_w W_h}. \quad (26)$$

For $W_c < W_w$, the ratio $\dot{Q}_\alpha^{wch} / \dot{Q}_\alpha^{chw} < 1$ and for $W_c > W_w$, $\dot{Q}_\alpha^{wch} / \dot{Q}_\alpha^{chw} > 1$. Then the most favorable configuration corresponds to the lowest transition rate being associated with transitions from the ground state, by far the most populated in the low temperature limit.

4. Thermal machines represented by a graph with multiple circuits

We study now multilevel absorption machines with multiple circuits. We start by analyzing the relation between the heat currents and the performance of a circuit C_ν in an arbitrary graph \mathcal{G} , and the corresponding quantities for the (isolated) graph circuit C_ν^{iso} . To this end, we rewrite (7) as

$$\dot{q}_\alpha(C_\nu) = D(\mathcal{G})^{-1} \det(-\mathbf{W}(C_\nu)D(C_\nu^{iso})) \dot{q}_\alpha(C_\nu^{iso}). \quad (27)$$

Using this expression we find:

- (i) $|\dot{q}_\alpha(C_\nu)| < |\dot{q}_\alpha(C_\nu^{iso})|$.
- (ii) $\varepsilon(C_\nu) = \dot{q}_c(C_\nu) / \dot{q}_w(C_\nu) = \varepsilon(C_\nu^{iso})$ and $\eta(C_\nu) = -\dot{q}_c(C_\nu) / \dot{q}_h(C_\nu) = \eta(C_\nu^{iso})$.

The first result indicates that the magnitude of the heat currents associated with a circuit in a graph is always smaller than the one corresponding to the isolated circuit. It follows from (8) by noticing that the product between a term in the forest $\det(-\mathbf{W}(C_\nu))$ and a term of $D(C_\nu^{iso})$ gives the algebraic value of one of the oriented maximal trees of \mathcal{G} . Therefore $\det(-\mathbf{W}(C_\nu)D(C_\nu^{iso})) = \sum_{\mu=1}^{N_c} \sum_{i \in \nu} \mathcal{A}(\vec{T}_i^\mu)$, with $\sum_{i \in \nu}$ the summation over all the vertices of C_ν , and being the number of maximal trees involved $N_c^\mu \leq N_T$. The second result derives directly from (22) and (23) and indicates that the circuit performance is not modified when the circuit is included in an arbitrary graph.

4.1. General bound for the performance

A consequence of (ii) is that the device performance cannot exceed the corresponding to the circuit with the best performance. For example, let us consider a device working as an absorption refrigerator, \dot{Q}_c and $\dot{Q}_w > 0$. The coefficient of performance is given by

$$\varepsilon = \sum_{\nu=1}^{N_c} \frac{\dot{q}_w(C_\nu)}{\dot{Q}_w} \varepsilon(C_\nu) - \sum_{\nu=N_c+1}^{N_c} \frac{|\dot{q}_c(C_\nu)|}{\dot{Q}_w}, \quad (28)$$

where $\dot{q}_c(C_\nu)$ is positive for the N_c' circuits contributing to the cooling cycle, and negative for the $N_c'' - N_c'$ 'counter-contributing' circuits, corresponding for example to heat leaks and circuits with finite counter-currents which flow in directions against the operation mode [33, 34]. The $N_c - N_c''$ trivial circuits are irrelevant in this discussion. In consequence, denoting by $\varepsilon(C_\nu)_{\max}$ the largest performance of a circuit in the graph,

$$\varepsilon \leq \varepsilon(C_\nu)_{\max}, \quad (29)$$

and the equality, $\varepsilon = \varepsilon(C_\nu)_{\max}$, is reached when $N_c'' - N_c' = 0$ and $\varepsilon(C_\nu) = \varepsilon(C_\nu)_{\max}$ for all the circuits. In particular, $\varepsilon = \varepsilon_C$ only if all of them achieve the Carnot performance for the same value of the affinity. A similar analysis applies to the device working as a heat transformer. Therefore, with regard to the performance, optimal multilevel machines are represented by graphs without 'counter-contributing' circuits. We will impose this condition in the design of the optimal graph.

4.2. Graph topology and heat currents

The magnitude of the physical heat currents is determined by the graph topology and the value of the transition rates. We first explore the graph topology of an arbitrary graph with the only restriction that two vertices can be connected by just one edge (see section 2.3).

In general $\dot{Q}_\alpha = \sum_{\nu=1}^{N_c} \dot{q}_\alpha(C_\nu)$ increases with the number of positive contributing circuits $N_c' \leq N_c$, which operate in the same way as the entire device. However, this increment may be hindered by the unavoidable decrease in $D(\mathcal{G})^{-1} \det(-\mathbf{W}(C_\nu))$ when adding new states and edges to a graph. The factor D is the sum of NN_T terms. For circuits of length L , $\det(-\mathbf{W}(C_\nu))$ is the sum of $\det(\tilde{\mathbf{A}}(C_\nu^L))$ terms. In this expression the submatrix $\tilde{\mathbf{A}}(C_\nu^L)$ is obtained by removing from $\tilde{\mathbf{A}}$ all the rows and columns corresponding to the vertices of the circuit C_ν^L . The matrix $\tilde{\mathbf{A}}$ is calculated by replacing the diagonal elements a_{ii} of the adjacency matrix \mathbf{A} (see for example [46]) by the vertex degree of the corresponding state i . The non diagonal elements are $a_{ij} = 1$ when states i and j are connected by an edge, and $a_{ij} = 0$ otherwise. Therefore, when attending to the number of terms, the magnitude of the heat currents resulting from the positive contributions of $N_c' \leq N_c$ circuits of length L is related to the topological parameter

Este documento incorpora firma electrónica, y es copia auténtica de un documento electrónico archivado por la ULL según la Ley 39/2015.
 Su autenticidad puede ser contrastada en la siguiente dirección <https://sede.ull.es/validacion/>

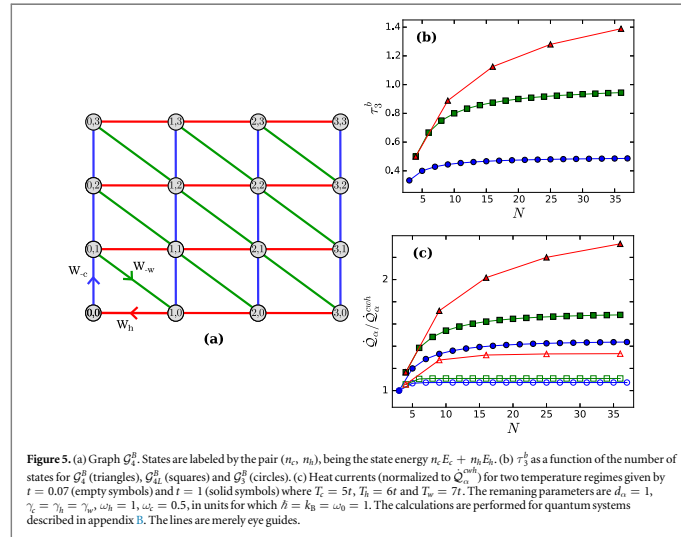
Identificador del documento: 2111210 Código de verificación: lZvvKBaU

Firmado por: Javier Onam González López
 UNIVERSIDAD DE LA LAGUNA

Fecha: 09/09/2019 11:04:42

Daniel Alonso Ramírez
 UNIVERSIDAD DE LA LAGUNA

11/09/2019 14:53:47



$$\tau_L \equiv \frac{1}{N} \sum_{\nu=1}^{N_L} \lambda(C_\nu^L) < \tau_L^t \equiv \frac{N_L}{N}, \quad (30)$$

where $\lambda(C_\nu^L) \equiv \det(\tilde{\mathbf{A}}(C_\nu^L)/N_T)$, with $N_T^{-1} \leq \lambda(C_\nu^L) < 1$. The ratio λ may depend on the position of the circuit in the graph and in general $\lambda(C_\nu^L) < \lambda(C_\nu^L)$ when $L' > L$. Although τ_L can be readily calculated, we found that the upper bound τ_L^t incorporates the relevant information about the graph topology. In particular, it makes clear the relevance of the graph connectivity: favorable graphs consist in as many small positive contributing circuits as possible (that is, avoiding heat leaks and another negative contributions), built with the smallest possible number of states, implying a large graph connectivity. This dependence on the graph topology is weighted by the transition rates. For high temperatures all circuits participate in the heat currents. However, only small circuits including the ground state will contribute significantly in the low temperature regime, independently of the total number of circuits in the graph.

4.2.1. Graphs constructed by merging triangles

The optimal choice for the building block is the triangle, the smallest possible contributing circuit as described before. We consider that all the triangles have fixed energy gaps for transitions assisted by the same bath. This is a necessary condition to achieve the maximal possible connectivity because otherwise adjacent triangles cannot share any edge. In order to analyze the dependence on the graph topology we consider now the more restrictive condition of fixed transition rates for each bath. This assumption will be relaxed latter. Moreover, we assume the PCD condition, that implies now that the maximum vertex degree in the graph is six, i.e. each state may be connected at most to another six ones, see figure 3(b). As a consequence, all the constructed graphs are planar and τ_3^B incorporates the relevant topological information. The number triangles is easily accessible by using the adjacency matrix, $N_3 = \text{Tr}\{\mathbf{A}^3\}/6$, where $\text{Tr}\{\}$ denotes the trace.

The graph with the largest connectivity compatible with our restrictions is denoted by G_4^B . It is constructed using B units of two triangles sharing one edge, for example one associated with the work bath, see figure 5(a). We consider square graphs with 1, 4, 9, ... units, being the smallest instance $G_4^{B=1} \equiv G_4$. By construction, the two configurations of the triangle, cwh and wch , are present. Besides, many other circuits can be identified. For example $\{(0, 0), (0, 1), (1, 1), (2, 0), (1, 0), (0, 0)\}$ is a circuit C^{3+2m_h} with $m_h = 1$, and $\{(0, 0), (0, 1), (0, 2), (1, 1), (2, 0), (1, 0), (0, 0)\}$ a circuit C^{3+3m_h} with $m_h = 1$. All of them follow the same operation mode. There are also many trivial circuits, for example $\{(0, 0), (0, 1), (1, 1), (1, 0), (0, 0)\}$. This construction is optimal with respect to

Este documento incorpora firma electrónica, y es copia auténtica de un documento electrónico archivado por la ULL según la Ley 39/2015.
 Su autenticidad puede ser contrastada en la siguiente dirección <https://sede.ull.es/validacion/>

Identificador del documento: 2111210

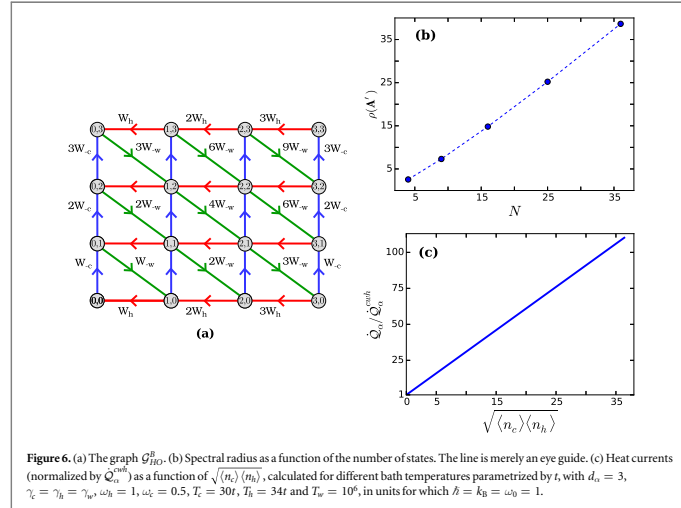
Código de verificación: lZvvKBaU

Firmado por: Javier Onam González López
 UNIVERSIDAD DE LA LAGUNA

Fecha: 09/09/2019 11:04:42

Daniel Alonso Ramírez
 UNIVERSIDAD DE LA LAGUNA

11/09/2019 14:53:47



the performance because it can attain the reversible limit as there are not ‘counter-contributing’ circuit, see the discussion for \mathcal{C}_3 in section 2.

We also consider two subgraphs of \mathcal{G}_4^B for comparison purposes. The first one is a row of this units, denoted by \mathcal{G}_{4L}^B , which represents the absorption device studied in [41]. The second one is obtained considering only a row and removing the upper hot edges. We use this graph, denoted by \mathcal{G}_3^B , to compare τ_3^B with other measure of the graph connectivity in appendix G.

Figure 5(b) shows the parameter τ_3^B for $\mathcal{G}_4^B, \mathcal{G}_{4L}^B$ and \mathcal{G}_3^B , considering only complete units in each case. For a given number of states, larger values of τ_3^B correspond to larger number of circuits and therefore to a larger connectivity. When the number of states increases the parameter τ_3^B saturates to a different constant value in each case. This is reflected in the physical heat currents shown in figure 5(c) for different bath temperatures. This saturation is due to the difficulty of exploring big circuits or those which are distant from the ground state in complex graphs. The simple picture based on the parameter τ_3^B is weighted by the transition rates. For decreasing bath temperatures, all the currents converge to the same result, independently of the number of circuits, since only the triangle including the ground state contributes significantly to them.

In summary, given a set of transition rates and a number of levels, the best topology corresponds to the most connected planar graph \mathcal{G}_4^B . This construction only contains trivial and positive contributing circuits and provides in general the largest heat currents for fixed rates.

4.3. Transition rates and heat currents

We have shown that for fixed transition rates the heat currents saturate to a constant value when increasing the number of states. To overcome this limitation, we now consider a graph with the optimal topology given by \mathcal{G}_4^B and relax the condition on the rates but keeping fixed energy gaps. The circuit affinities and then the performance are not modified. Considering (4), all the transition rates must be taken as $sW_{\pm, \alpha}$ with $s \geq 1$, and $W_{\pm, \alpha}$ the smallest rate. As discussed for circuit graphs, increasing s will lead to larger heat currents.

In particular, we analyze the construction shown in figure 6(a), denoted by \mathcal{G}_{HO}^B , which has a simple physical implementation as discussed below. Seeking a measure of the graph connectivity when the transition rates increase with s , and in analogy with the adjacency matrix, we define \mathbf{A}' with elements $a'_{ij} = s$ when states i and j are adjacent with transition rates $sW_{\pm, \alpha}$, and we denote its spectral radius as $\rho(\mathbf{A}')$, see appendix G. When incorporating additional building units into the graph, the spectral radius defined in this way increases nearly linearly with the number of states, see figure 6(b).

The graph G_{HO}^B , allowing an infinity number of building blocks, represents the master equation of a device composed of two harmonic oscillators [5]. Each oscillator is connected to a thermal bath at temperatures T_c and T_h . The coupling operators are $\hat{S}_c = \hat{a}_c$ and $\hat{S}_h = \hat{a}_h$ (see appendix A), being \hat{a}_α the annihilation operator of the oscillator coupled to the bath α . A third bath at temperature T_w is coupled to the system through the operator $\hat{S}_w = \hat{a}_c^\dagger \hat{a}_h$. For simplicity we assume a very large value of T_w , a regime for which the heat currents can be easily calculated. Figure 6(c) shows the heat currents as a function of $\sqrt{\langle n_c \rangle \langle n_h \rangle}$, which gives a rough estimation of the number of states populated and then of the effective graph size, calculated for increasing bath temperatures. In this expression $\langle n_\alpha \rangle$ is the average number of excitations in the oscillator $\alpha = c, h$. When the temperature increases, larger areas of the graph are populated involving a larger number of circuits, which results in an increment of the magnitude of the heat currents. This example illustrates that given a machine with the optimal topology, the rates can always be carefully designed to achieve larger currents without diminishing the performance.

5. Conclusions

We have determined the steady state heat currents associated with all possible circuits in the graph representing the master equation of multilevel continuous absorption machines. Each circuit is related to a thermodynamically consistent mechanism in the device functioning. Although the number of circuits may be very large when increasingly complex graphs are considered, efficient standard algorithms, which scale as $N_C(N + 2U)$ [47], can be used for determining them. For example, in the graphs studied in previous sections U increases linearly and N_C quadratically with the number of states and the computational cost scales as N^3 . The main result of the decomposition is an equation for the circuit heat currents depending only on the transition rates, without any prior knowledge of the steady state populations. This expression allows us to analyze the two relevant quantities for refrigerators and heat transformer, the magnitude of the physical heat currents and the performance. We focus on devices coupled to three baths, since they can provide the same currents than more complicated setups.

In order to elucidate the role of the graph topology in the thermodynamic properties, we have analyzed machines constructed by a fixed set of transition rates. In devices represented by a single graph circuit, the performance depends only on the circuit affinities, which can be tuned to reach the reversible limit, and the magnitude of the heat currents decreases in general with the number of states. Then the simplest graph, a triangle, leads to the largest heat currents in most cases and is the proper building block for optimal multilevel machines.

When considering generic devices, we have found that the performance of the device cannot exceed the corresponding to the circuit with maximum performance. Besides the magnitude of the heat currents is described by a topological parameter that increases with the graph connectivity. As a consequence, if the construction of larger graphs including additional circuits presents a limited connectivity, then the magnitude of the resulting physical heat currents saturates to a constant value, which is different for different constructions. We use triangles with fixed energy gaps for transitions assisted by the same bath to construct the graph with the largest possible connectivity, denoted by G_4^B . This is a planar graph containing neither heat leaks nor 'counter-contributing' circuits.

The assumption of a fixed set of transition rates can be relaxed. We give the necessary condition to improve the currents without modifying the performance. We provide an example using a system of harmonic oscillators. In this case the magnitude of the heat currents increases almost linearly with the effective size of the graph, determined by the achievable range of temperatures. An interesting question is whether there are other physical feasible implementations leading to a faster than linear dependence of the currents on the number of states.

The circuit decomposition could be employed in other different scenarios, from the study of heat transport through quantum wires to the analysis of machines designed for complicated tasks involving more than three baths. Besides, our formalism also applies to the case of reservoirs exchanging both energy and particles with the system, and even to periodically driven machines. The only condition required is that the population and coherence dynamics are decoupled in a certain basis. However, this is not always possible, as for example in weakly driven systems. Finally, it is worth mentioning that the study of four-stroke many-particle thermal machines has recently been addressed in [48]; the analysis of their continuous counterparts is another interesting issue we can explore in the future by using the circuit decomposition. We expect these findings will help in the experimental design of absorption devices.

Acknowledgments

We thank L Correa and A Ruiz for useful discussions. J Onam González acknowledges a Formación de Profesorado Universitario (FPU) fellowship from the Spanish Ministerio de Educación, Cultura y Deportes (MECD). Financial support by the Spanish Ministerio de Economía y Competitividad (MINECO) (FIS2013-

Este documento incorpora firma electrónica, y es copia auténtica de un documento electrónico archivado por la ULL según la Ley 39/2015.
 Su autenticidad puede ser contrastada en la siguiente dirección <https://sede.ull.es/validacion/>

Identificador del documento: 2111210

Código de verificación: lZvvKBaU

Firmado por: Javier Onam González López
 UNIVERSIDAD DE LA LAGUNA

Fecha: 09/09/2019 11:04:42

Daniel Alonso Ramírez
 UNIVERSIDAD DE LA LAGUNA

11/09/2019 14:53:47

41352-P) and European Cooperation in Science and Technology (COST) Action MP1209 is gratefully acknowledged.

Appendix A. Transition rates for quantum systems weakly coupled with thermal baths

In this appendix we describe how to calculate the transition rates W_{ij}^{α} in the master equation (2) for a quantum system with Hamiltonian $\hat{H}_S = \sum_{i=1}^N \hbar \omega_i |i\rangle \langle i|$, and coupled with R bosonic baths at temperatures T_{α} . We assume that the PCD condition holds. The total Hamiltonian reads

$$\hat{H} = \hat{H}_S + \sum_{\alpha=1}^R (\hat{H}_{S,\alpha} + \hat{H}_{\alpha}), \quad (\text{A.1})$$

where \hat{H}_{α} are the bath Hamiltonians and the coupling terms are given by

$$\hat{H}_{S,\alpha} = \hbar \sqrt{\gamma_{\alpha}} (\hat{S}_{\alpha} + \hat{S}_{\alpha}^{\dagger}) \otimes \hat{B}_{\alpha}, \quad (\text{A.2})$$

with \hat{S}_{α} and \hat{B}_{α} a system and a bath operator respectively. The rates γ_{α} determine the time scale of the system relaxation dynamics. Finally, the system operators in the coupling terms are

$$\hat{S}_{\alpha} = \sum_{i=1}^N \sum_{j>i}^N c_{ij}^{\alpha} |i\rangle \langle j|. \quad (\text{A.3})$$

We consider the following assumptions: the system is weakly coupled with the environments, $\hbar \gamma_{\alpha} \ll k_B T_{\alpha}$, and $\gamma_{\alpha} \ll |\omega_{ij} - \omega_j|$, with $\omega_{ij} \neq \omega_j$ and $\omega_{ij} = \omega_j - \omega_i$. Then the Born–Markov and the rotating wave approximation applies and the master equation for the populations of the eigenstates of \hat{H}_S [2] is given by (2) with transition rates ($i < j$)

$$W_{ij}^{\alpha} = \gamma_{\alpha} |c_{ij}^{\alpha}|^2 \Gamma_{\omega_{ij}}^{\alpha}. \quad (\text{A.4})$$

The functions Γ^{α} only depend on bath operators

$$\Gamma_{\omega}^{\alpha} = 2\Re \left\{ \int_0^{\infty} dt \exp(i\omega t) \text{Tr}_{\alpha} [\hat{B}_{\alpha}(t) \hat{B}_{\alpha} \hat{\rho}_{\alpha}] \right\}, \quad (\text{A.5})$$

where $\hat{B}_{\alpha}(t) = \exp(i\hat{H}_{\alpha}t/\hbar) \hat{B}_{\alpha} \exp(-i\hat{H}_{\alpha}t/\hbar)$ and $\hat{\rho}_{\alpha}$ denotes the bath thermal state. We will consider bosonic baths of physical dimensions d_{α} and coupling operators $\hat{B}_{\alpha} \propto \sum_{\mu} \sqrt{\omega_{\mu}} (\hat{b}_{\mu}^{\alpha} + \hat{b}_{\mu}^{\alpha\dagger})$. The summation is over all the bath modes of frequencies ω_{μ} and annihilation operators \hat{b}_{μ}^{α} . With this choice the rates Γ_{ω}^{α} are [2]

$$\begin{aligned} \Gamma_{\omega}^{\alpha} &= (\omega/\omega_0)^{d_{\alpha}} [N^{\alpha}(\omega) + 1], \\ \Gamma_{-\omega}^{\alpha} &= \Gamma_{\omega}^{\alpha} \exp(-\omega\hbar/k_B T_{\alpha}), \end{aligned} \quad (\text{A.6})$$

with $N^{\alpha}(\omega) = [\exp(\omega\hbar/k_B T_{\alpha}) - 1]^{-1}$. The frequency ω_0 depends on the physical realization of the coupling with the bath. The condition (3) derives now directly from the conservation of the normalization of the system density matrix. Besides, the Kubo–Martin–Schwinger relation in (A.6) implies (4).

Appendix B. Quantum implementation of the graphs

We introduce here a possible quantum physical realization of the graphs described in the main text by specifying their Hamiltonians and coupling operators. Considering bosonic heat baths, the results of appendix A can be used to obtain the corresponding transition rates. In all cases $\omega_c + \omega_w = \omega_h$.

(i) \mathcal{G}_4 .

$$\hat{H}_S = \hbar [\omega_c |2\rangle \langle 2| + \omega_h |3\rangle \langle 3| + (\omega_h + \omega'_c) |4\rangle \langle 4|], \quad (\text{B.1})$$

and $\hat{S}_c = |1\rangle \langle 2| + |3\rangle \langle 4|$, $\hat{S}_w = |2\rangle \langle 3|$, $\hat{S}_h = |1\rangle \langle 3| + |2\rangle \langle 4|$. The two-qubit model [5] corresponds to $\omega'_c = \omega_c$.

(ii) \mathcal{C}_{cwh} .

$$\hat{H}_S = \hbar (\omega_c |2\rangle \langle 2| + \omega_h |3\rangle \langle 3|), \quad (\text{B.2})$$

and $\hat{S}_c = |1\rangle \langle 2|$, $\hat{S}_w = |2\rangle \langle 3|$, $\hat{S}_h = |1\rangle \langle 3|$.

Este documento incorpora firma electrónica, y es copia auténtica de un documento electrónico archivado por la ULL según la Ley 39/2015.
 Su autenticidad puede ser contrastada en la siguiente dirección <https://sede.ull.es/validacion/>

Identificador del documento: 2111210

Código de verificación: lZvvKBaU

Firmado por: Javier Onam González López
 UNIVERSIDAD DE LA LAGUNA

Fecha: 09/09/2019 11:04:42

Daniel Alonso Ramírez
 UNIVERSIDAD DE LA LAGUNA

11/09/2019 14:53:47

(iii) \mathcal{C}_{weh}^3 .

$$\hat{H}_S = \hbar (\omega_w |2\rangle \langle 2| + \omega_h |3\rangle \langle 3|), \quad (B.3)$$

and $\hat{S}_w = |1\rangle \langle 2|$, $\hat{S}_c = |2\rangle \langle 3|$, $\hat{S}_h = |1\rangle \langle 3|$.

(iv) \mathcal{C}^{3+2m_h} .

$$\hat{H}_S = \sum_{n=1}^{m_h+1} n \hbar \omega_h |2n+1\rangle \langle 2n+1| + \hbar [(n-1)\omega_h + \omega_c] |2n\rangle \langle 2n|, \quad (B.4)$$

and $\hat{S}_c = |1\rangle \langle 2|$, $\hat{S}_w = |3+2m_h-1\rangle \langle 3+2m_h|$, $\hat{S}_h = \sum_{n=1}^{2m_h+1} |n\rangle \langle n+2|$.

(v) \mathcal{C}^{3+3n_+} .

$$\hat{H}_S = \sum_{n_h=0}^{n_++1} \sum_{n_c=0}^{n_+-n_h+1} \hbar [n_h \omega_h + n_c \omega_c] |n_h, n_c\rangle \langle n_h, n_c|, \quad (B.5)$$

and $\hat{S}_c = \sum_{n_c=0}^{n_+} |0, n_c\rangle \langle 0, n_c+1|$,

$\hat{S}_w = \sum_{n_h=0}^{n_+} |n_h, n_+ - n_h + 1\rangle \langle n_h + 1, n_+ - n_h|$, $\hat{S}_h = \sum_{n_h=0}^{n_+} |n_h, 0\rangle \langle n_h + 1, 0|$.

(vi) \mathcal{G}_3^B .

$$\hat{H}_S = \sum_{n=1}^{(N-1)/2} n \hbar \omega_h |2n+1\rangle \langle 2n+1| + \hbar [(n-1)\omega_h + \omega_c] |2n\rangle \langle 2n|, \quad (B.6)$$

and $\hat{S}_c = \sum_{n=1}^{(N-1)/2} |2n-1\rangle \langle 2n|$, $\hat{S}_w = \sum_{n=1}^{(N-1)/2} |2n\rangle \langle 2n+1|$, $\hat{S}_h = \sum_{n=1}^{(N-1)/2} |2n-1\rangle \langle 2n+1|$.

(vii) \mathcal{G}_4^B .

$$\hat{H}_S = \sum_{n_h=0}^{\sqrt{N}-1} \sum_{n_c=0}^{\sqrt{N}-1} [n_h \omega_h + n_c \omega_c] |n_h, n_c\rangle \langle n_h, n_c|, \quad (B.7)$$

and

$$\begin{aligned} \hat{S}_c &= \sum_{n_h=0}^{\sqrt{N}-1} \sum_{n_c=0}^{\sqrt{N}-2} f(n_c) |n_h, n_c\rangle \langle n_h, n_c+1|, \\ \hat{S}_w &= \sum_{n_h=1}^{\sqrt{N}-1} \sum_{n_c=0}^{\sqrt{N}-2} g(n_h, n_c) |n_h-1, n_c+1\rangle \langle n_h, n_c|, \\ \hat{S}_h &= \sum_{n_h=0}^{\sqrt{N}-2} \sum_{n_c=0}^{\sqrt{N}-1} f(n_h) |n_h, n_c\rangle \langle n_h+1, n_c|, \end{aligned} \quad (B.8)$$

with $f, g = 1$. The Hamiltonian and coupling operators for \mathcal{G}_{HO}^B are recuperated for an infinity number of states N , $f(n_c) = \sqrt{n_c+1}$, and $g(n_h, n_c) = \sqrt{n_h(n_c+1)}$.

Appendix C. Hill theory and the steady state heat currents

We apply Hill theory [35] to obtain (7). The starting point is the steady state probability of finding the system in the state i [25, 35]

$$P_i^s = D(\mathcal{G})^{-1} \sum_{\mu=1}^{N_r} \mathcal{A}(\vec{T}_i^\mu), \quad (C.1)$$

with D given by (8). Introducing the steady state fluxes along a directed edge

$$J(\vec{x}_e) = W_{i_k i_l}^{\alpha_e} P_{i_k}^s - W_{i_l i_k}^{\alpha_e} P_{i_l}^s, \quad (C.2)$$

and the corresponding affinities

$$X(\vec{x}_e) = k_B \ln \left(\frac{W_{i_k i_l}^{\alpha_e} P_{i_k}^s}{W_{i_l i_k}^{\alpha_e} P_{i_l}^s} \right), \quad (C.3)$$

Este documento incorpora firma electrónica, y es copia auténtica de un documento electrónico archivado por la ULL según la Ley 39/2015.
 Su autenticidad puede ser contrastada en la siguiente dirección <https://sede.ull.es/validacion/>

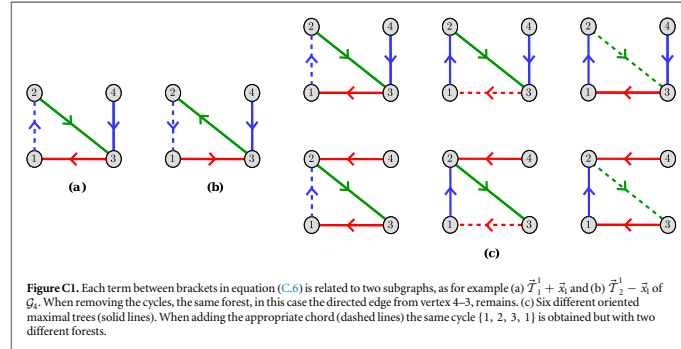
Identificador del documento: 2111210 Código de verificación: lZvvKBaU

Firmado por: Javier Onam González López
 UNIVERSIDAD DE LA LAGUNA

Fecha: 09/09/2019 11:04:42

Daniel Alonso Ramírez
 UNIVERSIDAD DE LA LAGUNA

11/09/2019 14:53:47



the total steady state entropy production is given by [22, 25]

$$\dot{S} = \sum_{e=1}^U J(\vec{x}_e) X(\vec{x}_e), \quad (C.4)$$

where the orientation of each edge is arbitrary. Introducing the populations in the product between fluxes and affinities

$$J(\vec{x}_e) X(\vec{x}_e) = D(\mathcal{G})^{-1} \sum_{\mu \in M_e} [W_{i_k i_l}^{\alpha_\mu} \mathcal{A}(\vec{T}_i^\mu) - W_{i_l i_k}^{\alpha_\mu} \mathcal{A}(\vec{T}_i^\mu)] X(\vec{x}_e), \quad (C.5)$$

where $\sum_{\mu \in M_e}$ denotes the summation only over the maximal trees for which x_e is a chord, since otherwise the term between brackets is zero. The product $W_{i_k i_l}^{\alpha_\mu} \mathcal{A}(\vec{T}_i^\mu)$ is no more than the algebraic value \mathcal{A} of the oriented subgraph $\vec{T}_i^\mu + \vec{x}_e$, composed of the maximal tree \vec{T}_i^μ and its chord \vec{x}_e . Then the entropy production (C.4) can be written as

$$\dot{S} = D(\mathcal{G})^{-1} \sum_{e=1}^U \sum_{\mu \in M_e} [\mathcal{A}(\vec{T}_i^\mu + \vec{x}_e) - \mathcal{A}(\vec{T}_i^\mu - \vec{x}_e)] X(\vec{x}_e). \quad (C.6)$$

Each term between brackets is only related to a circuit oriented in the two possible directions, \vec{C}_ν and $-\vec{C}_\nu$, associated with $\vec{T}_i^\mu + \vec{x}_e$ and $\vec{T}_i^\mu - \vec{x}_e$ respectively. When removing these two cycles from the corresponding subgraphs, the same forest \vec{T}_i^β remains, see for example figures C1 (a) and (b). Using this result and the properties of \mathcal{A} , each term in (C.6) can be written as $\mathcal{A}(\vec{T}_i^\beta) [\mathcal{A}(\vec{C}_\nu) - \mathcal{A}(-\vec{C}_\nu)] X(\vec{x}_e)$. The number of such terms with the same forest \vec{T}_i^β equals the number of edges of the circuit C_ν , as shown in figure C1 (c). Next we introduce the cycle affinity (10), $X(\vec{C}_\nu) = \sum_{e \in \nu} X(\vec{x}_e)$ with $\sum_{e \in \nu}$ the summation over all edges of \vec{C}_ν , to obtain

$$\dot{S} = D(\mathcal{G})^{-1} \sum_{\nu=1}^{N_c} \sum_{\beta \in \nu} \mathcal{A}(\vec{T}_i^\beta) [\mathcal{A}(\vec{C}_\nu) - \mathcal{A}(-\vec{C}_\nu)] X(\vec{C}_\nu), \quad (C.7)$$

where $\sum_{\beta \in \nu}$ denotes the summation over all the different forests associated with C_ν . This expression can be further simplified applying the matrix-tree theorem [49], $\sum_{\beta \in \nu} \mathcal{A}(\vec{T}_i^\beta) = \det(-\mathbf{W}|C_\nu)$. The flux associated with each cycle is

$$I(\vec{C}_\nu) = D(\mathcal{G})^{-1} \det(-\mathbf{W}|C_\nu) [\mathcal{A}(\vec{C}_\nu) - \mathcal{A}(-\vec{C}_\nu)]. \quad (C.8)$$

Considering that the cycle affinity and flux are odd functions, $X(-\vec{C}_\nu) = -X(\vec{C}_\nu)$ and $I(-\vec{C}_\nu) = -I(\vec{C}_\nu)$, we can define without any ambiguity the entropy production in the steady state corresponding to each circuit as

$$\dot{s}(C_\nu) = I(\vec{C}_\nu) X(\vec{C}_\nu) \geq 0, \quad (C.9)$$

where the last inequality results from $D(\mathcal{G})^{-1} > 0$, $\det(-\mathbf{W}|C_\nu) > 0$ and $[\mathcal{A}(\vec{C}_\nu) - \mathcal{A}(-\vec{C}_\nu)] \ln[\mathcal{A}(\vec{C}_\nu)/\mathcal{A}(-\vec{C}_\nu)] \geq 0$. Since the only contribution to the steady state entropy production is due to finite-rate heat transfer effects, we use (C.9) to identify the circuit heat currents (7).

Este documento incorpora firma electrónica, y es copia auténtica de un documento electrónico archivado por la ULL según la Ley 39/2015.
 Su autenticidad puede ser contrastada en la siguiente dirección <https://sede.ull.es/validacion/>

Identificador del documento: 2111210

Código de verificación: lZvvKBaU

Firmado por: Javier Onam González López
 UNIVERSIDAD DE LA LAGUNA

Fecha: 09/09/2019 11:04:42

Daniel Alonso Ramírez
 UNIVERSIDAD DE LA LAGUNA

11/09/2019 14:53:47

Appendix D. Circuit decomposition of the four-state model

Here we work out the circuit decomposition of \mathcal{G}_4 . Now we only assume $E_1 < E_2 < E_3 < E_4$, the consistency relation $E_{23} = E_{24} - E_{43} = E_{13} - E_{12}$ and the condition (4). The transition matrix for the four-state model is given by

$$\mathbf{W} = \begin{pmatrix} W_{11} & W_{12}^c & W_{13}^h & 0 \\ W_{21}^c & W_{22} & W_{23}^w & W_{24}^h \\ W_{31}^h & W_{32}^w & W_{33} & W_{34}^c \\ 0 & W_{42}^h & W_{43}^c & W_{44} \end{pmatrix}, \quad (\text{D.1})$$

with diagonal elements $W_{11} = -W_{21}^c - W_{31}^h$, $W_{22} = -W_{12}^c - W_{32}^w - W_{42}^h$, $W_{33} = -W_{13}^h - W_{23}^w - W_{43}^c$ and $W_{44} = -W_{24}^h - W_{34}^c$.

We denote by \vec{C}_1 the cycle $\{1, 2, 3, 1\}$, see figure 1(d), for which using (5) we obtain $\mathcal{A}(\vec{C}_1) = W_{21}^c$, $\mathcal{A}^w(\vec{C}_1) = W_{32}^w$, and $\mathcal{A}^h(\vec{C}_1) = W_{13}^h$. Then $\mathcal{A}(\vec{C}_1) = W_{21}^c W_{32}^w W_{13}^h$ and $\mathcal{A}(-\vec{C}_1) = W_{12}^c W_{23}^w W_{31}^h$. The cycle affinities associated with each bath (9) are $X^c(\vec{C}_1) = E_{21}/T_c$, $X^w(\vec{C}_1) = E_{32}/T_w$, and $X^h(\vec{C}_1) = E_{13}/T_h$, where $E_{ij} = E_j - E_i$. The contribution of the forests is $\det(-\mathbf{W}|C_1) = W_{24}^h + W_{34}^c$, from which the cycle flux is given by

$$I(\vec{C}_1) = D(\mathcal{G}_4)^{-1}(W_{24}^h + W_{34}^c)(W_{21}^c W_{32}^w W_{13}^h - W_{12}^c W_{23}^w W_{31}^h), \quad (\text{D.2})$$

where $D(\mathcal{G}_4)$ is determined by using (8). Then the circuit heat currents are $\dot{q}_c(C_1) = E_{12}I(\vec{C}_1)$, $\dot{q}_w(C_1) = E_{23}I(\vec{C}_1)$ and $\dot{q}_h(C_1) = E_{31}I(\vec{C}_1)$. The consistency of the circuit currents with the first law $\dot{q}_c(C_1) + \dot{q}_w(C_1) + \dot{q}_h(C_1) = 0$ follows from $E_{12} + E_{23} + E_{31} = 0$. The cycle affinity (10) is $X(\vec{C}_1) = E_{21}/T_c + E_{32}/T_w + E_{13}/T_h$ from which the circuit entropy production can be determined with (C.9). A similar procedure can be used in order to obtain the quantities associated with the circuit C_2 .

For the circuit C_3 we denote by \vec{C}_3 the cycle $\{1, 2, 4, 3, 1\}$. Now $\mathcal{A}(\vec{C}_3) = W_{21}^c W_{34}^c$, $\mathcal{A}^w(\vec{C}_3) = 1$ (there is not any edge associated with the work bath) and $\mathcal{A}^h(\vec{C}_3) = W_{12}^c W_{13}^h$, $\mathcal{A}(\vec{C}_3) = W_{21}^c W_{34}^c W_{12}^c W_{13}^h$ and $\mathcal{A}(-\vec{C}_3) = W_{12}^c W_{43}^c W_{24}^h W_{31}^h$. The cycle affinities associated with each bath are $X^c(\vec{C}_3) = (E_{34} - E_{12})/T_c$, $X^w(\vec{C}_3) = 0$ and $X^h(\vec{C}_3) = (E_{13} - E_{24})/T_h$. Notice that $(E_{13} - E_{24}) = -(E_{34} - E_{12})$. When the transition energies are equal, $E_{34} = E_{12}$ and $E_{24} = E_{13}$, all the affinities are zero. The circuit C_3 involves all the graph vertices and therefore there is not any forest associated with it. Then $(-\mathbf{W}|C_3)$ is an empty matrix and $\det(-\mathbf{W}|C_3) = 1$. The cycle flux is given by

$$I(\vec{C}_3) = D(\mathcal{G}_4)^{-1}(W_{21}^c W_{34}^c W_{12}^c W_{13}^h - W_{12}^c W_{43}^c W_{24}^h W_{31}^h), \quad (\text{D.3})$$

and the circuit heat currents by $\dot{q}_c(C_3) = (E_{43} - E_{21})I(\vec{C}_3)$, $\dot{q}_w(C_3) = 0$ and $\dot{q}_h(C_3) = (E_{31} - E_{42})I(\vec{C}_3)$.

Appendix E. Other decompositions of the entropy production

There are several possible decompositions of the steady state entropy production in terms of circuits. Schnakenberg [25] designed a method based on the identification of a set of $U - N + 1$ fundamental circuits. The circuits are determined by choosing an arbitrary maximal tree and adding each one of its chords. Taking a particular orientation for the circuits, a set of fundamental cycles is found. The total steady state entropy production is then $\dot{S} = \sum_{c=1}^{U-N+1} J(\vec{x}_c) X(\vec{C}_c)$, where \vec{x}_c is the chord giving the circuit C_c , and $J(\vec{x}_c)$ is the corresponding flux. The previous decomposition is simple and specially relevant when $U - N$ is small. However, it is not unique, since it depends on the choice of the maximal tree, and some terms in the sum may be not positive definite, which discards a possible consistent thermodynamic interpretation of each circuit contribution. Besides the evaluation of $J(\vec{x}_c)$ requires the calculation of the steady state populations.

As an example we apply Schnakenberg method to the four-state model. The procedure requires an arbitrary set of fundamental circuits of the graph \mathcal{G}_4 . We choose the maximal tree shown in figure 2(a), which has two chords, $\{1, 2\}$ and $\{2, 4\}$. By adding the chord $\{1, 2\}$ the circuit C_1 is obtained. Choosing an arbitrary orientation, for example \vec{C}_1 as in figure 2(d), the directed chord \vec{x}_1 goes from states 1 to 2. In this decomposition the flux associated with each cycle is taken as the corresponding to the directed chord (C.2), $J(\vec{x}_1) = W_{21}^c p_1^c - W_{12}^c p_2^c$. The cycle affinity is defined by (10) and was calculated in appendix D, $X(\vec{C}_1) = E_{21}/T_c + E_{32}/T_w + E_{13}/T_h$. When adding the chord $\{2, 4\}$ we obtain the circuit C_2 . Choosing the orientation $\{2, 3, 4, 2\}$, the directed chord \vec{x}_2 goes from states 4 to 2. The flux is $J(\vec{x}_2) = W_{34}^c p_4^c - W_{43}^c p_2^c$ and the affinity $X(\vec{C}_2) = E_{43}/T_c + E_{32}/T_w + E_{24}/T_h$. Then the entropy production is

Este documento incorpora firma electrónica, y es copia auténtica de un documento electrónico archivado por la ULL según la Ley 39/2015.
 Su autenticidad puede ser contrastada en la siguiente dirección <https://sede.ull.es/validacion/>

Identificador del documento: 2111210 Código de verificación: lZvvKBaU

Firmado por: Javier Onam González López
 UNIVERSIDAD DE LA LAGUNA

Fecha: 09/09/2019 11:04:42

Daniel Alonso Ramírez
 UNIVERSIDAD DE LA LAGUNA

11/09/2019 14:53:47

$$\dot{S} = J(\vec{x}_1)X(\vec{C}_1) + J(\vec{x}_2)X(\vec{C}_2). \quad (E.1)$$

The cycles $\{\vec{C}_1, \vec{C}_2\}$ are the elements of one of the possible fundamental sets of \mathcal{G}_4 . Notice that for our choice the circuit C_3 is not involved.

A related decomposition is obtained by the algorithm of Kalpazidou [29, 30]. For systems showing dynamical reversibility the algorithm leads to a Schnakenberg decomposition with a clever choice of the fundamental set of cycles, such that all the terms in the sum are positive. Therefore a positive entropy production can be assigned to each cycle, which is required in many applications [50, 51]. The algorithm is based on choosing an orientation for the graph such that all the fluxes (C.2) for the directed edges are positive. Next a cycle is identified and the entropy production $J_{\min}(\vec{x}_v)X(\vec{C}_v) > 0$ is assigned to it, where $J_{\min}(\vec{x}_v)$ is the smallest flux associated with an edge of \vec{C}_v . Then $J_{\min}(\vec{x}_v)$ is subtracted to each flux in the cycle to obtain a new flux field and the process is repeated for new cycles until a fundamental set is completed [50, 51]. For example, let us assume parameter values for which the two triangles of the four-state model work as refrigerators. Then the fluxes along $\vec{x}_1, \vec{x}_2, \vec{x}_3$ (from 3 to 4), \vec{x}_4 (from 3 to 1) and \vec{x}_5 (from 2 to 3) are positive. With this orientation only the cycles \vec{C}_1 and \vec{C}_2 appear in the directed graph and the entropy production can be written as (E.1), where the two terms are guaranteed to be positive. If we modify the system parameters such that the circuit C_2 works as a heat transformer but the overall device remains working as a refrigerator, the total entropy production can still be determined using (E.1), but the positivity of each term is not guaranteed. Now the fluxes are positive along the edges $\vec{x}_1, -\vec{x}_2, -\vec{x}_3, \vec{x}_4$ and \vec{x}_5 . Only the cycles \vec{C}_1 and \vec{C}_3 remain with this graph orientation and the algorithm of Kalpazidou leads to

$$\dot{S} = J(\vec{x}_5)X(\vec{C}_1) + J(-\vec{x}_2)X(\vec{C}_3). \quad (E.2)$$

However, in this expression the contribution of each mechanism, refrigerator (C_1), heat transformer (C_2) and heat leak (C_3) could not be isolated.

Appendix F. $\mathcal{R}(\vec{C}^N)$ in the high and low temperature limits

In the high temperature limit, $y_\alpha \equiv \exp[-E_\alpha/(k_B T_\alpha)] \approx 1$, the transition rates satisfy $W_{-\alpha} \approx W_\alpha$, leading to vanishing affinities and heat currents. Now $\mathcal{A}(\vec{T}_i^j)$ is in a good approximation independent of the orientation, what considerably facilitates the calculations to obtain

$$\mathcal{R}(\vec{C}^N) \approx \left[N \left(\frac{r_c}{W_c} + \frac{r_h}{W_h} + \frac{r_w}{W_w} \right) \right]^{-1}, \quad (F.1)$$

with $r_\alpha = n + m_\alpha$ and $r_c + r_w + r_h = N$. In this limit $\mathcal{R}(\vec{C}^N)$ decreases quadratically ($z = 2$) with N , except when one or two of the terms r_α/W_α are much larger than the others and r_α remains constant when increasing N , which can only happen adding two-edge sets. In this limit $\mathcal{R}(\vec{C}^N)$ decreases as N^{-1} for small enough values of N .

In the low temperature limit, $y_\alpha \ll 1$ and $W_{-\alpha} \ll W_\alpha$. Again this limit implies vanishing heat currents. The cycle algebraic value is proportional to the small factors y_α , $\mathcal{A}(\vec{C}^N) \propto \prod_\alpha y_\alpha^{u_\alpha + u'_\alpha}$, where u_α and u'_α are the number of $W_{-\alpha}$ transitions before and after the highest-energy state respectively. Besides, the largest contributions to D comes from two terms that include the lowest number of rates $W_{-\alpha}$, $\mathcal{A}(\vec{T}_1^{h-1})$ and $\mathcal{A}(\vec{T}_1^h)$, being $i = 1$ the ground state and $j = h$ the highest-energy state. Both terms are proportional to $\prod_\alpha y_\alpha^{f_\alpha + u'_\alpha}$, where f_α is the number of W_α transitions before the highest-energy state in $\mathcal{A}(\vec{C}^N)$. Necessarily $u_\alpha - f_\alpha$ is positive, increases with N and then $\mathcal{R}(\vec{C}^N)$ decreases exponentially when adding new states to the circuit. For example, $\mathcal{R}(\vec{C}^N) \propto \prod_\alpha \exp[-u_\alpha E_\alpha / (k_B T_\alpha)]$ when $f_\alpha = 0$. Examples of these behaviors are given in figures 4(b) and (e).

Appendix G. Heat currents and spectral radius of \mathcal{G}_3^B

The simple topological structure of \mathcal{G}_3^B , see figure G1(a), allows for the direct identification of all the $N_T = 3^N$ maximal trees. Then

$$\det(-\mathbf{W}|C_\alpha)D(C_3) = \sum_{\mu=1}^{N_T} \sum_{i=2\mu-1}^{2\mu+1} \mathcal{A}(\vec{T}_i^\mu). \quad (G.1)$$

Este documento incorpora firma electrónica, y es copia auténtica de un documento electrónico archivado por la ULL según la Ley 39/2015.
 Su autenticidad puede ser contrastada en la siguiente dirección <https://sede.ull.es/validacion/>

Identificador del documento: 2111210

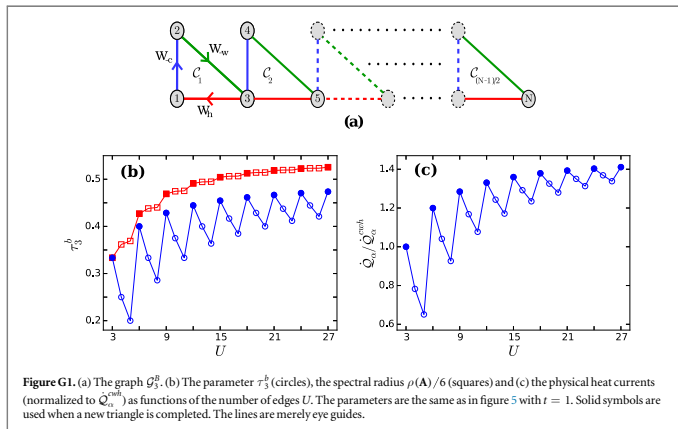
Código de verificación: lZvvKBaU

Firmado por: Javier Onam González López
 UNIVERSIDAD DE LA LAGUNA

Fecha: 09/09/2019 11:04:42

Daniel Alonso Ramírez
 UNIVERSIDAD DE LA LAGUNA

11/09/2019 14:53:47



Using this result the physical heat currents are given by

$$\mathcal{Q}_\alpha = \left[1 + \frac{\sum_{\mu=1}^{N_t} \sum_{i=1}^{N_c-1} \mathcal{A}(\mathcal{T}_{2i+1}^\mu)}{\sum_{\mu=1}^{N_t} \sum_{i=1}^N \mathcal{A}(\mathcal{T}_i^\mu)} \right] \mathcal{Q}_\alpha^{\text{wh}} \equiv K \mathcal{Q}_\alpha^{\text{wh}}, \quad (\text{G.2})$$

where $1 \leq K \leq 2$ and $K = 3N_c / (2N_c + 1)$ in the high temperature limit.

For this graph $\lambda(C_i) = \frac{1}{3}$ and $\tau_3 = \tau_3^h/3$. The parameter τ_3^h as a function of the number of edges is shown in figure G1(b). The spectral radius $\rho(\mathbf{A})$, defined as the largest eigenvalue of the adjacency matrix of the unweighted graph [52], is also shown. The spectral radius is a measure of the graph connectivity which increases monotonically with the number of edges. However, it does not reflect the decrease in the heat currents each time a pendant edge is added to the graph, see figure G1(c). An increment in the total heat currents is only found when a new triangle is completed, saturating to a constant value when the addition of new circuits does not improve significantly the graph connectivity. This behavior is well described by τ_3^h .

References

- [1] Kosloff R and Levy A 2014 Quantum heat engines and refrigerators: continuous devices *Annu. Rev. Phys. Chem.* **65** 365–93
- [2] Breuer H and Petruccione F 2002 *The Theory of Open Quantum Systems* (New York: Oxford University Press)
- [3] Palao J P, Kosloff R and Gordon J M 2001 Quantum thermodynamic cooling cycle *Phys. Rev. E* **64** 056130
- [4] Linden N, Popescu S and Skrzypczyk P 2010 How small can thermal machines be? The smallest possible refrigerator *Phys. Rev. Lett.* **105** 130401
- [5] Levy A, Alicki R and Kosloff R 2012 Quantum refrigerators and the third law of thermodynamics *Phys. Rev. E* **85** 061126
- [6] Correa L A, Palao J P, Adesso G and Alonso D 2013 Performance bound for quantum absorption refrigerators *Phys. Rev. E* **87** 042131
- [7] Kosloff R 2013 Quantum thermodynamics: a dynamical point of view *Entropy* **15** 2100–18
- [8] Mari A and Eisert J 2012 Cooling by heating: very hot thermal light can significantly cool quantum systems *Phys. Rev. Lett.* **108** 120602
- [9] Mitchison M T, Huber M, Prior J, Woods M P and Plenio M B 2016 Realising a quantum absorption refrigerator with an atom-cavity system *Quantum Sci. Technol.* **1** 015001
- [10] Leggio B, Bellomo B and Antezza M 2015 Quantum thermal machines with single nonequilibrium environments *Phys. Rev. A* **91** 012117
- [11] Hofer P, Perarnau-Llobet M, Bohr Brask J, Silva R, Huber M and Brunner N 2016 Autonomous quantum refrigerator in a circuit QED architecture based on a Josephson junction *Phys. Rev. B* **94** 235420
- [12] Chen Y X and Li S W 2012 Quantum refrigerator driven by current noise *Europhys. Lett.* **97** 40003
- [13] Venturelli D, Fazio R and Giovannetti V 2013 Minimal self-contained refrigerator machine based on four quantum dots *Phys. Rev. Lett.* **110** 256801
- [14] Maslennikov G, Ding S, Hablützel R, Gan J, Roulet A, Nimmrichter S, Dai J, Scarani V and Matsukevich D 2017 Quantum absorption refrigerator with trapped ions arXiv:1702.08672
- [15] Spohn H 1977 Entropy production for quantum dynamical semigroups *J. Math. Phys.* **19** 1227–30
- [16] Alicki R 1979 The quantum open system as a model of the heat engine *J. Phys. A: Math. Gen.* **12** L103–7
- [17] Levy A and Kosloff R 2014 The local approach to quantum transport may violate the second law of thermodynamics *Europhys. Lett.* **107** 20004

Este documento incorpora firma electrónica, y es copia auténtica de un documento electrónico archivado por la ULL según la Ley 39/2015.
 Su autenticidad puede ser contrastada en la siguiente dirección <https://sede.ull.es/validacion/>

Identificador del documento: 2111210

Código de verificación: lZvvKBaU

Firmado por: Javier Onam González López
 UNIVERSIDAD DE LA LAGUNA

Fecha: 09/09/2019 11:04:42

Daniel Alonso Ramírez
 UNIVERSIDAD DE LA LAGUNA

11/09/2019 14:53:47

- [18] Uzdin R, Levy A and Kosloff R 2015 Equivalence of quantum heat machines, and quantum-thermodynamic signatures *Phys. Rev. X* **5** 031044
- [19] Cuetara G B, Esposito M and Schaller G 2016 Quantum thermodynamics with degenerate eigenstate coherences *Entropy* **18** 447
- [20] Gardiner C W 1985 *Handbook of Stochastic Methods* (Berlin: Springer)
- [21] Seifert U 2012 Stochastic thermodynamics, fluctuations theorems and molecular machines *Rep. Prog. Phys.* **75** 126001
- [22] Van den Broeck C and Esposito M 2015 Ensemble and trajectory thermodynamics: a brief introduction *Physica A* **418** 6–16
- [23] Esposito M, Lindenberg K and Van den Broeck C 2009 Universality of efficiency at maximum power *Phys. Rev. Lett.* **102** 130602
- [24] Polettini M, Bulnes-Cuetara G and Esposito M 2016 Conservation laws and symmetries in stochastic thermodynamics *Phys. Rev. E* **94** 052117
- [25] Schnakenberg J 1976 Network theory of microscopic and macroscopic behavior of master equation systems *Rev. Mod. Phys.* **48** 571–85
- [26] Yamamoto S, Sosome I, Shiraishi N and Sagawa T 2016 Linear irreversible thermodynamics and Onsager reciprocity for information-driven engines *Phys. Rev. E* **94** 052121
- [27] Andrieux D and Gaspard P 2007 Fluctuation theorem for currents and Schnakenberg network theory *J. Stat. Phys.* **127** 107–31
- [28] Rahav S and Jarzynski C 2013 Nonequilibrium fluctuation theorems from equilibrium fluctuations *New J. Phys.* **15** 125029
- [29] MacQueen J 1981 Circuit processes *Ann. Probab.* **9** 604–10
- [30] Kalpaizidou S L 2006 *Cycle Representation of Markov Processes* (Berlin: Springer)
- [31] Jiang D Q, Qian M and Qian M P 2004 *Mathematical Theory of Nonequilibrium Steady States* (Berlin: Springer)
- [32] Einax M and Nitzan A 2014 Network analysis of photovoltaic energy conversion *J. Phys. Chem. C* **118** 27226–34
- [33] Correa L A, Palao J P and Alonso D 2015 Internal dissipation and heat leaks in quantum thermodynamic cycles *Phys. Rev. E* **92** 032136
- [34] González J O, Alonso D A and Palao J P 2016 Performance of continuous quantum thermal devices indirectly connected to environments *Entropy* **18** 166
- [35] Hill T L 1966 Studies in irreversible thermodynamics: IV. Diagrammatic representation of steady state fluxes for unimolecular systems *J. Theor. Biol.* **10** 442–59
- [36] Esposito M 2012 Stochastic thermodynamics under coarse graining *Phys. Rev. E* **85** 041125
- [37] Altaner B and Vollmer J 2012 Fluctuation-preserving coarse graining for biochemical systems *Phys. Rev. Lett.* **108** 228101
- [38] Gelbwaser-Klimovsky D, Niedenzu W, Brumer P and Kurizki G 2015 Power enhancement of heat engines via correlated thermalization in a three-level working fluid *Sci. Rep.* **5** 14413
- [39] Niedenzu W, Gelbwaser-Klimovsky D and Kurizki G 2015 Performance limits of multilevel and multipartite quantum heat machines *Phys. Rev. E* **92** 042123
- [40] Silva R, Manzano G, Skrzypczyk P and Brunner N 2016 Performance of autonomous quantum thermal machines: Hilbert space dimension as a thermodynamical resource *Phys. Rev. E* **94** 032120
- [41] Correa L A 2014 Multistage quantum absorption heat pumps *Phys. Rev. E* **89** 042128
- [42] Esposito M, Lindenberg K and Van den Broeck C 2009 Thermoelectric efficiency at maximum power in a quantum dot *Europhys. Lett.* **85** 60010
- [43] Cleuren B, Rutten B and Van den Broeck C 2012 Cooling by heating: refrigeration powered by photons *Phys. Rev. Lett.* **108** 120603
- [44] Li C, Zhang Y, Wang J and He J 2013 Performance characteristics and optimal analysis of a nanosized quantum dot photoelectric refrigerator *Phys. Rev. E* **88** 062120
- [45] Averin D V, Korotkov A N and Likharev K K 1991 Theory of single-electron charging of quantum wells and dots *Phys. Rev. B* **44** 6199–211
- [46] Foulds L R 1992 *Graph Theory Applications* (New York: Springer)
- [47] Johnson D B 1975 Finding all the elementary circuits of a directed graph *SIAM J. Comput.* **4** 77–84
- [48] Jaramillo J, Beau M and del Campo A 2016 Quantum supremacy of many-particle thermal machines *New J. Phys.* **18** 075019
- [49] Moon J W 1994 Some determinants and the matrix-tree theorem *Discrete Math.* **124** 163–71
- [50] Altaner B, Grosskinsky S, Herminghaus S, Kathan L, Timme M and Vollmer J 2012 Network representations of nonequilibrium steady states: cycle decompositions, symmetries and dominant paths *Phys. Rev. E* **85** 041133
- [51] Knoch F and Speck T 2015 Cycle representatives for the coarse-graining of systems driven into a non-equilibrium steady state *New J. Phys.* **17** 115004
- [52] Wilson R J and Beineke L W (ed) 1979 *Applications of Graph Theory* (New York: Academic)

Este documento incorpora firma electrónica, y es copia auténtica de un documento electrónico archivado por la ULL según la Ley 39/2015.
Su autenticidad puede ser contrastada en la siguiente dirección <https://sede.ull.es/validacion/>

Identificador del documento: 2111210

Código de verificación: lZvvKBaU

Firmado por: Javier Onam González López
UNIVERSIDAD DE LA LAGUNA

Fecha: 09/09/2019 11:04:42

Daniel Alonso Ramírez
UNIVERSIDAD DE LA LAGUNA

11/09/2019 14:53:47

5.4 Classical emulation of quantum-coherent thermal machines

Phys. Rev. E, 99:062102, 2019.

J. Onam González, José P. Palao, Daniel Alonso and Luis A. Correa

Este documento incorpora firma electrónica, y es copia auténtica de un documento electrónico archivado por la ULL según la Ley 39/2015.
Su autenticidad puede ser contrastada en la siguiente dirección <https://sede.ull.es/validacion/>

Identificador del documento: 2111210 Código de verificación: lZvvKBaU

Firmado por: Javier Onam González López
UNIVERSIDAD DE LA LAGUNA

Fecha: 09/09/2019 11:04:42

Daniel Alonso Ramírez
UNIVERSIDAD DE LA LAGUNA

11/09/2019 14:53:47

Classical emulation of quantum-coherent thermal machines


J. Onam González,^{1,2,*} José P. Palao,^{1,2,†} Daniel Alonso,^{1,2,‡} and Luis A. Correa^{3,4,§}

¹Departamento de Física, Universidad de La Laguna, La Laguna 38204, Spain

²IUJEA, Universidad de La Laguna, La Laguna 38204, Spain

³School of Mathematical Sciences and CQNE, The University of Nottingham, University Park, Nottingham NG7 2RD, United Kingdom

⁴Kavli Institute for Theoretical Physics University of California, Santa Barbara, CA 93106, USA

 (Received 6 November 2018; revised manuscript received 8 February 2019; published 3 June 2019)

The performance enhancements observed in various models of continuous quantum thermal machines have been linked to the buildup of coherences in a preferred basis. But is this connection always an evidence of “quantum-thermodynamic supremacy”? By force of example, we show that this is not the case. In particular, we compare a power-driven three-level continuous quantum refrigerator with a four-level combined cycle, partly driven by power and partly by heat. We focus on the weak driving regime and find the four-level model to be superior since it can operate in parameter regimes in which the three-level model cannot and it may exhibit a larger cooling rate and, simultaneously, a better coefficient of performance. Furthermore, we find that the improvement in the cooling rate matches the increase in the stationary quantum coherences *exactly*. Crucially, though, we also show that the thermodynamic variables for both models follow from a classical representation based on graph theory. This implies that we can build incoherent stochastic-thermodynamic models with the same steady-state operation or, equivalently, that both coherent refrigerators can be emulated classically. More generally, we prove this for *any* N -level weakly driven device with a “cyclic” pattern of transitions. Therefore, even if coherence is present in a specific quantum thermal machine, it is often not essential to replicate the underlying energy conversion process.

DOI: 10.1103/PhysRevE.99.062102

I. INTRODUCTION

Quantum thermodynamics studies the emergence of thermodynamic behavior in individual quantum systems [1]. Over the past few years, the field has developed very rapidly [2–6] and yet key recurring questions remain unanswered: What is *quantum* in quantum thermodynamics? Can quantum heat devices exploit *quantumness* to outperform their classical counterparts?

Quantum thermal machines are the workhorse of quantum thermodynamics. Very generally, these consist of an individual system S which can couple to heat baths at different temperatures and, possibly, is also subject to dynamical control by an external field. After a transient, S reaches a nonequilibrium steady state characterized by certain rates of energy exchange with the heat baths. The direction of these energy fluxes can be chosen by engineering S , which may result in, e.g., a heat engine [7] or a refrigerator [8]. Considerable efforts have been devoted to optimize these devices [9–22] and to understand whether genuinely *quantum* features play an active role in their operation [23–42].

One might say that a thermal machine is *quantum* provided that S has a discrete spectrum. In fact, the energy filtering allowed by such discreteness can be said to be

advantageous, since it enables continuous energy conversion at the (reversible) Carnot limit of maximum efficiency [13,16,43]. Similarly, energy quantization in multistroke thermodynamic cycles can give rise to experimentally testable nonclassical effects [42]. In most cases, however, it is attributes such as entanglement or coherence which are regarded as the hallmark of genuine quantumness.

In particular, quantum coherence [44,45] has often been seen as a potential resource, since it can influence the thermodynamically relevant quantities, such heat and work, of open systems [46]. It has been argued, for instance, that radiatively and noise-induced coherences [23–26] might enhance the operation of quantum heat engines [31,34,38] and heat-driven quantum refrigerators [39–41]. However, it is not clear whether they are truly *instrumental* [18,19,39,41], since similar effects can be obtained from stochastic-thermodynamic models [47–50], i.e., classical incoherent systems whose dynamics is governed by balance equations concerning *only* the populations in some relevant basis (usually, the energy basis).

A possible approach to elucidate the role of quantum coherence in any given model is to add dephasing, thus making it fully incoherent (or classical) [22,30,41]. An ensuing reduction in performance would be an evidence of the usefulness of coherence in quantum thermodynamics. Furthermore, if the ultimate limits on the performance of incoherent thermal machines can be established, then coherences would become *thermodynamically* detectable—one would simply need to search for violations of such bounds [22,51].

In this paper we adopt a much more stringent operational definition for “quantumness”: *No thermal machine*

*jgonzall@ull.es

†jppalao@ull.edu.es

‡dalonso@ull.edu.es

§luis.correa@nottingham.ac.uk

Este documento incorpora firma electrónica, y es copia auténtica de un documento electrónico archivado por la ULL según la Ley 39/2015.
Su autenticidad puede ser contrastada en la siguiente dirección <https://sede.ull.es/validacion/>

Identificador del documento: 2111210

Código de verificación: lZvvKBaU

Firmado por: Javier Onam González López
UNIVERSIDAD DE LA LAGUNA

Fecha: 09/09/2019 11:04:42

Daniel Alonso Ramírez
UNIVERSIDAD DE LA LAGUNA

11/09/2019 14:53:47

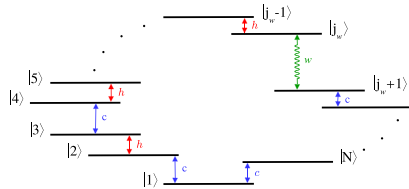


FIG. 1. Energy-level diagram for a generic N -level cyclic thermal machine. The labeled red and blue arrows denote transitions mediated by dissipative interactions with the hot and cold bath, respectively. Their distribution is arbitrary. The periodic field coupling energy levels $|j_w\rangle$ and $|j_w + 1\rangle$ is indicated by the wobbly green arrow.

should be classified as quantum if its thermodynamically relevant quantities can be replicated exactly by an incoherent emulator.¹ More precisely, the emulator should be a classical dissipative system operating between the same heat baths and with the same frequency gaps and number of discrete states. Interestingly, we will show that the currents of many continuous quantum-coherent devices are thermodynamically indistinguishable from those of their “classical emulators”.

If it exists, such emulator needs not be related to the coherent device of interest by the mere addition of dephasing—it can be a different model so long as it remains incoherent at all times and that, once in the stationary regime, it exchanges energy with its surroundings at the same rates as the original machine. In particular, the transient dynamics of the coherent model can be very different from that of its emulator. In the steady state, however, it must be impossible to tell one from the other by only looking at heat fluxes and power.

For simplicity, we focus on periodically driven continuous refrigerators with a “cyclic” scheme of transitions (see Fig. 1), although, as we shall point out, our results apply to devices with more complex transition patterns. Specifically, “continuous” thermal machines [3] are models in which the working substance S couples *simultaneously* to a cold bath at temperature T_c , a hot bath at $T_h > T_c$, and a classical field.² Since the driving field is periodic, we must think of the steady state of the machine as a “limit cycle” where all thermodynamic variables are evaluated as time averages. Concretely, a quantum refrigerator can drive heat transport against the temperature gradient in a suitable parameter range, or “cooling window.” We work in the limit of *very weak* driving, which allows us to derive a “local” master equation for S [52]. We show that stationary quantum coherence is not

¹Note that throughout this paper, we only require the emulator to replicate the *averaged* heat flows, but we make no mention to their fluctuations. The emulability of higher-order moments of the fluxes is an interesting point that certainly deserves separate analysis.

²In an absorption refrigerator the driving is replaced by thermal coupling to a “work bath” at temperature $T_w > T_h$, which drives the cooling process.

only present in all these models but, in fact, it is *essential* for the energy-conversion process to take place. Strikingly, however, our main result is that the steady-state operation of any such quantum-coherent N -level machine admits a classical representation based on graph theory [49,53–56]. It follows that an incoherent device can always be built such that its steady-state thermodynamic variables coincide with those of the original model. Hence, this entire family of quantum-coherent thermal machines can be emulated classically. The design of such emulator is reminiscent of the mapping of the limit cycle of a periodically driven classical system to a nonequilibrium steady state [57]. We want to stress that, from now on, we focus exclusively on the steady-state operation of continuous quantum heat devices. In particular, this leaves out all “reciprocating” machines. We note, however, that the latter reduce to the former in the limit of “weak action” [30].

As an illustration, we consider the paradigmatic power-driven three-level refrigerator [8,9,58], which we use as a benchmark for a novel four-level hybrid device, driven by a mixture of heat and work. Concretely, we show that our new model may have a wider cooling window, larger cooling power, and larger coefficient of performance. We also show that the energy-conversion rate in both models is proportional to their steady-state coherence. As a result, the excess coherence of the four-level model relative to the benchmark matches exactly the cooling enhancement. It would thus seem that quantum coherence is necessary for continuous refrigeration in the weak driving limit and that the improved cooling performance of the four-level model can be fully attributed to its larger steady-state coherence. If so, observing a non-vanishing “cooling rate” in either device or certifying that the cooling rate of the four-level model is indeed larger than that of the benchmark would be unmistakable signatures of *quantumness*. Crucially, both coherent devices are cyclic and weakly driven and, as such, they cannot be distinguished from their *classical* analogues in a black-box scenario. Therefore, quantum features might not only be present, but even be intimately related to the thermodynamic variables of quantum thermal machines under study and still, there may be nothing necessarily quantum about their operation. We remark, however, that the thermodynamic equivalence between the continuous thermal machine and its emulator only holds in the steady state. Importantly, we shall also see that the graph theory analysis is a convenient and powerful tool [55,56] to obtain accurate approximations for the nontrivial steady-state heat currents of these devices.

The paper is organized as follows: In Sec. II we introduce our central model of weakly and periodically driven N -level “cyclic” refrigerator. Its steady-state classical emulator is constructed in Sec. III. Some basic concepts of graph theory are also introduced at this point. In particular, we show that the emulator is a single-circuit graph whose heat currents, power, and coefficient of performance may be obtained in a thermodynamically consistent way. The generalization to more complex transition schemes is also discussed at this point. Using the graph-theoretical toolbox, we then analyze, in Sec. IV, our four-level device and the three-level benchmark. We thus arrive to analytical expressions indicating improvements in the steady-state functioning of the four-level model in a suitable regime. Finally, in Sec. V, we discuss

Este documento incorpora firma electrónica, y es copia auténtica de un documento electrónico archivado por la ULL según la Ley 39/2015.
 Su autenticidad puede ser contrastada en la siguiente dirección <https://sede.ull.es/validacion/>

Identificador del documento: 2111210

Código de verificación: lZvvKBaU

Firmado por: Javier Onam González López
 UNIVERSIDAD DE LA LAGUNA

Fecha: 09/09/2019 11:04:42

Daniel Alonso Ramírez
 UNIVERSIDAD DE LA LAGUNA

11/09/2019 14:53:47

the implications of our results, summarize, and draw our conclusions.

II. CYCLIC THERMAL MACHINES

A. The system Hamiltonian

We start by introducing the general model for a coherent cyclic thermal machine (see Fig. 1). The Hamiltonian for the system or *working substance* S is composed of two terms: a bare (time-independent) Hamiltonian \hat{H}_0 and a time-dependent contribution $\hat{H}_d(t)$ which describes the coupling to a sinusoidal driving field. That is,

$$\hat{H}_s(t) = \hat{H}_0 + \hat{H}_d(t), \quad (1a)$$

$$\hat{H}_0 = \sum_{i=1}^N E_i |i\rangle\langle i|, \quad (1b)$$

$$\hat{H}_d(t) = 2\hbar\lambda |j_w\rangle\langle j_w + 1| \cos \omega_{j_w} t + \text{H.c.}, \quad (1c)$$

where \hbar is the reduced Planck constant and λ controls the strength of the interaction with the field. E_i and $|i\rangle$ are, respectively, the energies and eigenstates of the bare Hamiltonian. In particular, the driving connects the bare energy states $|j_w\rangle$ and $|j_w + 1\rangle$. For simplicity, we assume a *resonant* coupling, i.e., $\omega_{j_w} := (E_{j_w+1} - E_{j_w})/\hbar$, which is optimal from a thermodynamic viewpoint. The generalization to the nonresonant case is, nevertheless, straightforward.

The hot and cold bath can be cast as infinite collections of independent bosonic modes with a well-defined temperature. Their Hamiltonians read

$$\hat{H}_\alpha = \hbar \sum_{\mu} \omega_{\mu,\alpha} \hat{b}_{\mu,\alpha}^\dagger \hat{b}_{\mu,\alpha}, \quad \alpha \in \{c, h\}, \quad (2)$$

with $\hat{b}_{\mu,\alpha}^\dagger$ and $\hat{b}_{\mu,\alpha}$ being the bosonic creation and annihilation operators of the mode at frequency $\omega_{\mu,\alpha}$ in bath $\alpha \in \{c, h\}$. For the system-baths couplings, we adopt the general form $\hat{H}_{s-\alpha} = \hat{X}_\alpha \otimes \hat{B}_\alpha$, where

$$\hat{X}_\alpha = \sum_{i \in \mathbf{R}_\alpha} |i\rangle\langle i+1| + \text{H.c.}, \quad (3a)$$

$$\hat{B}_\alpha = \hbar \sqrt{\gamma_\alpha} \sum_{\mu} g_{\mu,\alpha} (\hat{b}_{\mu,\alpha} + \hat{b}_{\mu,\alpha}^\dagger). \quad (3b)$$

Here $g_{\mu,\alpha} \propto \sqrt{\omega_{\mu,\alpha}}$ and γ_α is the *dissipation rate* for bath α . \mathbf{R}_α stands for the labels of the eigenstates $|i\rangle$ dissipatively coupled to $|i+1\rangle$ through the interaction with bath α . For instance, in Fig. 1, $\mathbf{R}_c = \{1, 3, \dots, j_w + 1, \dots, N\}$ and $\mathbf{R}_h = \{2, 4, \dots, j_w - 1, \dots\}$. Notice that *all* levels $|i\rangle$ are thermally coupled to $|i+1\rangle$ (provided that $i \neq j_w$) via either the hot or the cold bath. In particular, the N th level couples to $i = 1$, hence closing the cycle. Without loss of generality, we consider that all transitions related to the same bath have different energy gaps, i.e., $|\omega_k| \neq |\omega_l|$ for $k, l \in \mathbf{R}_\alpha$ ($k \neq l$). This technical assumption simplifies the master equation but does not restrict the physics of the problem. The full Hamiltonian of the setup is thus

$$\hat{H} = \hat{H}_s + \sum_{\alpha} \hat{H}_{s-\alpha} + \hat{H}_\alpha. \quad (4)$$

Although we consider a cyclic scheme of transitions, our formalism applies to more general quantum-coherent heat devices. Namely, equivalent results can be easily found for nondegenerate systems with various nonconsecutive driven transitions. Likewise, one could include parasitic loops to the design. As an illustration, we analyze a model including an extra hot transition between $|j_w\rangle$ and $|j_w + 1\rangle$ in the Appendix below.

B. The local master equation for weak driving

When deriving an effective equation of motion for the system, it is important to consider the various timescales involved [59]. Namely, the bath correlation time τ_B , the intrinsic timescale of the bare system τ_0 , the relaxation timescale τ_R , and the typical time associated with the interaction of the bare system with the external field τ_{s-d} . These are

$$\tau_B \simeq \max\{\hbar/(k_B T_c), \hbar/(k_B T_h)\} = \hbar/(k_B T_c), \quad (5a)$$

$$\tau_0 \simeq \max\{|\pm \omega_k \mp \omega_l|^{-1}, |2\omega_k|^{-1}\}, \quad (k \neq l), \quad (5b)$$

$$\tau_R \simeq \gamma_\alpha^{-1}, \quad \alpha \in \{c, h\}, \quad (5c)$$

$$\tau_{s-d} \simeq \lambda^{-1}. \quad (5d)$$

For a moment, let us switch off the time-dependent term $\hat{H}_d(t)$ and discuss the usual weak-coupling Markovian master equation, i.e., the Gorini-Kossakowski-Lindblad-Sudarshan (GKLS) equation [60,61]. Its microscopic derivation relies on the Born-Markov and secular approximations, which hold whenever $\tau_B \ll \tau_R$ and $\tau_0 \ll \tau_R$. It can be written as

$$\frac{d\hat{\rho}_s}{dt} = -\frac{i}{\hbar} [\hat{H}_0, \hat{\rho}_s] + (\mathcal{L}_c + \mathcal{L}_h) \hat{\rho}_s, \quad (6)$$

where $\hat{\rho}_s$ is the reduced state of the N -level system. Crucially, due to the underlying Born approximation of weak dissipation, Eq. (6) is correct only to $\mathcal{O}(\max\{\gamma_c, \gamma_h\})$.

The action of the superoperator \mathcal{L}_α is given by

$$\mathcal{L}_\alpha \hat{\rho}_s = \sum_{i \in \mathbf{R}_\alpha} \Gamma_{\omega_i}^\alpha \left(\hat{A}_i \hat{\rho}_s \hat{A}_i^\dagger - \frac{1}{2} \{ \hat{A}_i^\dagger \hat{A}_i, \hat{\rho}_s \}_+ \right) + \Gamma_{-\omega_i}^\alpha \left(\hat{A}_i^\dagger \hat{\rho}_s \hat{A}_i - \frac{1}{2} \{ \hat{A}_i \hat{A}_i^\dagger, \hat{\rho}_s \}_+ \right). \quad (7)$$

Here $\hat{A}_i = |i\rangle\langle i+1|$ and the notation $\{\cdot, \cdot\}_+$ stands for anticommutator. The “jump” operators \hat{A}_i are such that $\hat{X}_\alpha = \sum_{i \in \mathbf{R}_\alpha} (\hat{A}_i + \hat{A}_i^\dagger)$ and $[\hat{H}_0, \hat{A}_i] = -\omega_i \hat{A}_i$. As a result, the operators \hat{X}_α in the interaction picture with respect to \hat{H}_0 read

$$e^{i\hat{H}_0 t/\hbar} \hat{X}_\alpha e^{-i\hat{H}_0 t/\hbar} = \sum_{i \in \mathbf{R}_\alpha} e^{-i\omega_i t} \hat{A}_i. \quad (8)$$

This identity is a key step in the derivation of Eq. (6) [59].

If we now switch $\hat{H}_d(t)$ back on, then we will need to change the propagator in Eq. (8) over to the time-ordered exponential

$$\hat{U}_s(t) = \mathcal{T} \exp \left\{ -i\hbar^{-1} \int_0^t dt' [\hat{H}_0 + \hat{H}_d(t')] \right\}. \quad (9)$$

When deriving a GKLS master equation for such a periodically driven system one also looks for a different

062102-3

Este documento incorpora firma electrónica, y es copia auténtica de un documento electrónico archivado por la ULL según la Ley 39/2015.
 Su autenticidad puede ser contrastada en la siguiente dirección <https://sede.ull.es/validacion/>

Identificador del documento: 2111210

Código de verificación: lZvvKBaU

Firmado por: Javier Onam González López
 UNIVERSIDAD DE LA LAGUNA

Fecha: 09/09/2019 11:04:42

Daniel Alonso Ramírez
 UNIVERSIDAD DE LA LAGUNA

11/09/2019 14:53:47

decomposition on the right-hand side of Eq. (8) [16,62,63]. Namely,

$$\hat{U}_s^\dagger(t) \hat{X}_\alpha \hat{U}_s(t) = \sum_{q \in \mathbb{Z}} \sum_{\{\omega\}} e^{-i(\omega+q\omega_{j_w})t} \hat{A}_1^{(q)}. \quad (10)$$

We will skip all the technical details and limit ourselves to note that if, in addition to $\tau_B \ll \tau_R$ and $\tau_0 \ll \tau_R$, we make the *weak driving* assumption of $\tau_R \ll \tau_{s-d}$, Eq. (10) can be cast as

$$\begin{aligned} \hat{U}_s^\dagger(t) \hat{X}_\alpha \hat{U}_s(t) &= e^{i\hat{H}_0 t/\hbar} \hat{X}_\alpha e^{-i\hat{H}_0 t/\hbar} + \mathcal{O}(\lambda) \\ &= \sum_{i \in \mathbb{R}_\alpha} e^{-i\omega_i t} \hat{A}_i + \mathcal{O}(\lambda). \end{aligned} \quad (11)$$

This is due to the fact that \hat{H}_d is $\mathcal{O}(\lambda)$ while \hat{H}_0 is $\mathcal{O}(1)$. Exploiting Eq. (11) and following the exact same standard steps that lead to Eq. (6), one can easily see that the master equation

$$\frac{d\hat{\rho}_s}{dt} = -\frac{i}{\hbar} [\hat{H}_0 + \hat{H}_d(t), \hat{\rho}_s] + (\mathcal{L}_c + \mathcal{L}_h) \hat{\rho}_s \quad (12)$$

would hold up to $\mathcal{O}(\lambda \max\{\gamma_c, \gamma_h\})$.

Effectively, Eq. (12) assumes that the dissipation is entirely decoupled from the intrinsic dynamics of S , which includes the driving. This is reminiscent of the “local” master equations which are customarily used when dealing with weakly interacting multipartite open quantum systems [52,64,65]. We want to emphasize that, just like we have done here, *it is very important to establish precisely the range of validity of such local equations* [66] since using them inconsistently can lead to violations of the laws of thermodynamics [67,68].

It is convenient to move into the rotating frame $\hat{\rho}_s \mapsto e^{i\hat{H}_0 t/\hbar} \hat{\rho}_s e^{-i\hat{H}_0 t/\hbar} := \hat{\sigma}_s$ in order to remove the explicit time dependence on the right-hand side of Eq. (12) and simplify the calculations. This gives

$$\frac{d\hat{\sigma}_s}{dt} = -\frac{i}{\hbar} [\hat{H}_d, \hat{\sigma}_s] + (\mathcal{L}_c + \mathcal{L}_h) \hat{\sigma}_s, \quad (13)$$

where the Hamiltonian $\hat{H}_d(t)$ in the rotating frame is given by

$$\hat{H}_d \simeq \hbar\lambda (j_w) (j_w + 1) + \text{H.c.} \quad (14)$$

Here we have neglected two fast-rotating terms, with frequencies $\pm 2\omega_{j_w}$. This is consistent with our weak driving approximation $\tau_{s-d} \gg \tau_R$, as all quantities here have been time averaged over one period of the driving field.

The “decay rates” Γ_ω^α from Eq. (7) are the only missing pieces to proceed to calculate the thermodynamic variables in the nonequilibrium steady state of S . These are

$$\Gamma_\omega^\alpha = 2 \text{Re} \int_0^\infty dr e^{i\omega t} \text{Tr} \{ \hat{B}_\alpha(t) \hat{B}_\alpha(t-r) \hat{\rho}_\alpha \}, \quad (15)$$

where the operator $\hat{\rho}_\alpha$ represents the thermal state of bath α . Assuming d_α -dimensional baths with an infinite cutoff frequency, the decay rates become [59]

$$\Gamma_\omega^\alpha = \gamma_\alpha (\omega/\omega_0)^{d_\alpha} [1 - \exp(-\hbar\omega/k_B T_\alpha)]^{-1}, \quad (16a)$$

$$\Gamma_{-\omega}^\alpha = \exp(-\hbar\omega/k_B T_\alpha) \Gamma_\omega^\alpha, \quad (16b)$$

062102-4

with $\omega > 0$. In our model, ω_0 depends on the physical realization of the system-bath coupling. $d_\alpha = 1$ would correspond to Ohmic dissipation and $d_\alpha = \{2, 3\}$, to the super-Ohmic case.

C. Heat currents, power, and performance

As it is standard in quantum thermodynamics, we will use the master equation (13) to break down the average energy change of the bare system $\frac{d}{dt} \langle E \rangle(t) = \text{tr} \{ \hat{H}_0 \frac{d}{dt} \hat{\sigma}_s(t) \}$ into “heat” and “power” contributions [i.e., $\frac{d}{dt} \langle E \rangle(t) = \sum_\alpha \dot{\mathcal{Q}}_\alpha(t) + \mathcal{P}(t)$]. These can be defined as [30]

$$\dot{\mathcal{Q}}_\alpha(t) := \text{tr} \{ \hat{H}_0 \mathcal{L}_\alpha \hat{\sigma}_s(t) \}, \quad (17a)$$

$$\mathcal{P}(t) := -i \hbar^{-1} \text{tr} \{ \hat{H}_0 [\hat{h}_d, \hat{\sigma}_s(t)] \}. \quad (17b)$$

In the long-time limit, $\frac{d}{dt} \langle E \rangle \xrightarrow{t \rightarrow \infty} 0$, and we will denote the corresponding steady-state heat currents and stationary power input by $\dot{\mathcal{Q}}_\alpha$ and \mathcal{P} , respectively. In particular, from Eqs. (7) and (17) it can be shown that [69,70]

$$\dot{\mathcal{Q}}_c + \dot{\mathcal{Q}}_h + \mathcal{P} = 0, \quad (18a)$$

$$\frac{\dot{\mathcal{Q}}_c}{T_c} + \frac{\dot{\mathcal{Q}}_h}{T_h} \leq 0, \quad (18b)$$

which amount to the first and second laws of thermodynamics. It is important to note that the strict negativity of Eq. (18b) follows directly from the geometric properties of the dynamics generated by the local dissipators \mathcal{L}_α [70]. Working with any other reference frame to quantify energy exchanges in Eqs. (17), such as, e.g., $\hat{H}_0 + \hat{h}_d$, would lead to undesirable violations of the second law [67]. We thus see that the choice of the eigenstates of the bare Hamiltonian as preferred basis has a sound thermodynamic justification.

Using Eqs. (1b), (7), (14), and (17), we find for our cyclic N -level model

$$\dot{\mathcal{Q}}_\alpha = \sum_{i \in \mathbb{R}_\alpha} (E_{i+1} - E_i) J_i, \quad (19a)$$

$$\mathcal{P} = 2\hbar\lambda \omega_{j_w} \text{Im} (j_w \hat{\sigma}_s(\infty) j_w + 1), \quad (19b)$$

where $J_i = \Gamma_{-\omega_i}^\alpha p_i^{(\infty)} - \Gamma_{\omega_i}^\alpha p_{i+1}^{(\infty)}$ is the net stationary transition rate from $|i\rangle$ to $|i+1\rangle$ and $p_i^{(\infty)} := \langle i | \hat{\sigma}_s(\infty) | i \rangle$. The superindex α_i stands for the bath associated with the dissipative transition $|i\rangle \leftrightarrow |i+1\rangle$. Crucially, Eq. (19b) implies that vanishing stationary quantum coherence results in vanishing power consumption ($\mathcal{P} = 0$) and, hence, no refrigeration (see also, e.g., Ref. [3]). In fact, as we shall see below, $\dot{\mathcal{Q}}_\alpha = 0$ in absence of coherence. Therefore, our cyclic model in Fig. 1 is *inherently quantum* since it requires nonzero coherences to operate.

D. Steady-state populations and coherence

The key to understand why our weakly driven cyclic devices can be emulated classically resides in the interplay between populations and coherence in the eigenbasis $\{|i\rangle\}_{i=1}^N$ of the bare Hamiltonian \hat{H}_0 . In this representation, Eq. (13)

Este documento incorpora firma electrónica, y es copia auténtica de un documento electrónico archivado por la ULL según la Ley 39/2015.
Su autenticidad puede ser contrastada en la siguiente dirección <https://sede.ull.es/validacion/>

Identificador del documento: 2111210

Código de verificación: lZvvKBaU

Firmado por: Javier Onam González López
UNIVERSIDAD DE LA LAGUNA

Fecha: 09/09/2019 11:04:42

Daniel Alonso Ramírez
UNIVERSIDAD DE LA LAGUNA

11/09/2019 14:53:47

reads:

$$\frac{dp_i}{dt} = \Gamma_{-\omega_{i-1}}^{\alpha_{i-1}} p_{i-1} - (\Gamma_{\omega_{i-1}}^{\alpha_{i-1}} + \Gamma_{-\omega_i}^{\alpha_i}) p_i + \Gamma_{\omega_i}^{\alpha_i} p_{i+1}, \quad (20a)$$

$$\frac{dp_{j_w}}{dt} = \Gamma_{-\omega_{j_w-1}}^{\alpha_{j_w-1}} p_{j_w-1} - \Gamma_{\omega_{j_w-1}}^{\alpha_{j_w-1}} p_{j_w} - 2\lambda \text{Im} \langle j_w | \hat{\sigma}_s | j_w + 1 \rangle, \quad (20b)$$

$$\frac{dp_{j_w+1}}{dt} = \Gamma_{\omega_{j_w+1}}^{\alpha_{j_w+1}} p_{j_w+2} - \Gamma_{-\omega_{j_w+1}}^{\alpha_{j_w+1}} p_{j_w+1} + 2\lambda \text{Im} \langle j_w | \hat{\sigma}_s | j_w + 1 \rangle, \quad (20c)$$

for $i \neq \{j_w, j_w + 1\}$. Note that we have omitted the time labels in $p_k = \langle k | \hat{\sigma}_s(t) | k \rangle$ for brevity. Importantly, the populations of the pair of levels coupled to the driving field do depend on the coherence between them. In turn, this coherence evolves as

$$\frac{d}{dt} \langle j_w | \hat{\sigma}_s | j_w + 1 \rangle = -\frac{1}{2} (\Gamma_{\omega_{j_w-1}}^{\alpha_{j_w-1}} + \Gamma_{-\omega_{j_w+1}}^{\alpha_{j_w+1}}) \langle j_w | \hat{\sigma}_s | j_w + 1 \rangle - i\lambda (p_{j_w+1} - p_{j_w}). \quad (21)$$

Hence, the steady-state coherence (i.e., $\frac{d}{dt} \langle j_w | \hat{\sigma}_s | j_w + 1 \rangle_{\infty} := 0$) in the subspace spanned by $|j_w\rangle$ and $|j_w + 1\rangle$ is given in terms of the steady-state populations *only*. Namely, as

$$\langle j_w | \hat{\sigma}_s | j_w + 1 \rangle_{\infty} = i \frac{2\lambda [p_{j_w}^{(\infty)} - p_{j_w+1}^{(\infty)}]}{\Gamma_{\omega_{j_w-1}}^{\alpha_{j_w-1}} + \Gamma_{-\omega_{j_w+1}}^{\alpha_{j_w+1}}}. \quad (22)$$

Inserting Eq. (22) into (20) and imposing $\frac{d}{dt} p_k^{(\infty)} = 0$ yields a linear system of equations for the N stationary populations $\mathbf{p}_{\infty} := [p_1^{(\infty)}, p_2^{(\infty)}, \dots, p_N^{(\infty)}]^T$. This can be cast as $\mathbf{W} \mathbf{p}_{\infty} = 0$, where the nonzero elements of the “matrix of rates” \mathbf{W} are

$$\begin{aligned} W_{i,i+1} &= \Gamma_{\omega_i}^{\alpha_i}, & W_{i+1,i} &= \Gamma_{-\omega_i}^{\alpha_i}, \\ W_{i,i-1} &= \Gamma_{-\omega_{i-1}}^{\alpha_{i-1}}, & W_{i-1,i} &= \Gamma_{\omega_{i-1}}^{\alpha_{i-1}}, \\ W_{i,i} &= -(\Gamma_{\omega_{i-1}}^{\alpha_{i-1}} + \Gamma_{-\omega_i}^{\alpha_i}), \end{aligned} \quad (23)$$

for $i \neq \{j_w, j_w + 1\}$, and

$$\begin{aligned} W_{j_w, j_w+1} &= W_{j_w+1, j_w} = 4\lambda^2 [\Gamma_{\omega_{j_w-1}}^{\alpha_{j_w-1}} + \Gamma_{-\omega_{j_w+1}}^{\alpha_{j_w+1}}]^{-1}, \\ W_{j_w, j_w} &= -(\Gamma_{\omega_{j_w-1}}^{\alpha_{j_w-1}} + W_{j_w, j_w+1}), \\ W_{j_w+1, j_w+1} &= -(\Gamma_{-\omega_{j_w+1}}^{\alpha_{j_w+1}} + W_{j_w, j_w+1}). \end{aligned} \quad (24)$$

Note that even if $\mathbf{W} \mathbf{p}_{\infty} = 0$ (together with the normalization condition) determines the stationary populations of our model, Eqs. (20) certainly differ from

$$\frac{d\mathbf{q}(t)}{dt} = \mathbf{W} \mathbf{q}(t). \quad (25)$$

That is, the $\mathbf{q}(t)$ defined by Eq. (25) converges to \mathbf{p}_{∞} asymptotically but it does not coincide with $[p_1(t), \dots, p_N(t)]^T$ at any finite time. Nonetheless, as we shall argue below, a classical system S' made up of N discrete states evolving as per Eq. (25) can emulate the steady-state energy conversion process of the quantum-coherent system S . Note that a similar trick has been used in Ref. [39], for an absorption refrigerator model where coherences appear accidentally, due to degeneracy. In contrast, as argued in Sec. II C, the quantum coherence in our model is *instrumental* for its operation.

Remarkably, an equation similar to (25) can be found for an arbitrary choice of basis. Crucially, however, the physically motivated choice of the eigenbasis of \hat{H}_0 ensures the positivity of all nondiagonal rates in \mathbf{W} , that they obey detailed balance relations [cf. Eqs. (26)], and the structure of Eq. (19a). All these are necessary conditions for building a classical emulator for the energy-conversion process, as we show below.

III. CLASSICAL EMULATORS

A. General properties

Let us now discuss in detail the properties of the emulator S' as defined by Eq. (25). First, note that (25) is a proper balance equation since: (i) the nondiagonal elements of \mathbf{W} are positive, (ii) the pairs $\{W_{i,i+1}, W_{i+1,i}\}$ satisfy the detailed balance relations [cf. Eqs. (16b), (23), and (24)]

$$\frac{W_{i+1,i}}{W_{i,i+1}} = \exp\left(-\frac{\hbar\omega_i}{k_B T_{\alpha_i}}\right), \quad (i \neq j_w), \quad (26a)$$

$$\frac{W_{j_w+1, j_w}}{W_{j_w, j_w+1}} = 1, \quad (26b)$$

and (iii) the sum over columns in \mathbf{W} is zero (i.e., $W_{i,k} = -\sum_{j \neq k} W_{j,k}$), reflecting the conservation of probability. This also implies that \mathbf{W} is singular and that \mathbf{p}_{∞} is given by its nonvanishing off-diagonal elements.

Notice as well that rates like $\{W_{i,i+1}, W_{i+1,i}\}_{i \neq j_w}$ in Eq. (26) can always be attributed to excitation/relaxation processes (across a gap $\hbar\omega_i$) mediated by a heat bath at temperature T_{α_i} . On the contrary, $\{W_{j_w, j_w+1}, W_{j_w+1, j_w}\}$ indicate saturation. Therefore, one possible physical implementation of S' would be an N -state quantum system connected via suitably chosen coupling strengths to a hot and a cold bath as well as to a work repository, such as an infinite-temperature heat bath. Indeed, looking back at Eqs. (23), we see that the rates for the dissipative interactions in S' are identical to those in S . However, according to Eq. (24), the coupling to the driving is much smaller in the emulator than in the original quantum-coherent model. Hence, S' is *not* the result of dephasing the N -level cyclic machine, but a different device.

At this point, we still need to show that the steady-state energy fluxes of our emulator actually coincide with Eqs. (19). To do so, we now build a classical representation of S' based on graph theory. Importantly, this also serves as the generic physical embodiment for the emulator.

B. Graph representation and thermodynamic variables

Using graph theory for the thermodynamic analysis of a system described by a set of rate equations has two major advantages: First, it provides a clear interpretation of the underlying energy conversion mechanisms [55] and, second,

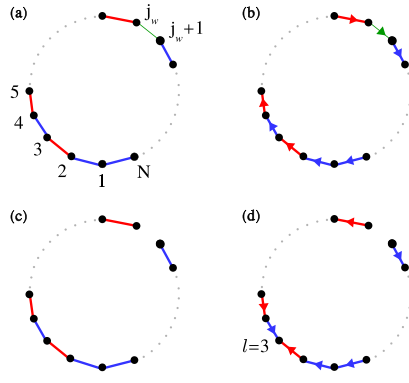


FIG. 2. (a) The circuit graph \mathcal{C}_N is a classical emulator for the steady state of the N -level quantum-coherent device of Fig. 1. The blue edges are associated with dissipative transitions mediated by the cold bath. Similarly, the red edges and the green edge relate to the hot bath and the external driving. (b) When orienting the edges of \mathcal{C}_N clockwise, the cycle $\vec{\mathcal{C}}_N$ is obtained. (c) Removing the edge $(j_w, j_w + 1)$ from \mathcal{C}_N yields the maximal tree $\vec{\mathcal{T}}_{j_w}$. (d) Orienting $\vec{\mathcal{T}}_{j_w}$ toward, e.g., vertex $l = 3$ gives the oriented maximal tree $\vec{\mathcal{T}}_{j_w}^l$.

it allows for the calculation of the thermodynamic variables directly from the matrix of rates [53]. In fact, the graph itself also follows from \mathbf{W} —each state $k = 1, 2, \dots, N$ becomes a “vertex” and each pair of nonvanishing rates $\{W_{k,l}, W_{l,k}\}_{k \neq l}$ becomes an “undirected edge” (k, l) connecting k and l . Specifically, this mapping would take Eq. (25) into the “circuit graph” \mathcal{C}_N depicted in Fig. 2(a). We can thus think of S as a classical device transitioning cyclically between N states.

Now that we have a physical picture in mind, we show that such classical emulator is thermodynamically equivalent to the coherent N -level machine, once in its steady state. Specifically, we focus on rewriting the thermodynamic variables of S [cf. Eqs. (19)] in terms of elements of S' . To that end, some graph objects need to be introduced. For instance, the undirected graph \mathcal{C}_N may be oriented (or directed) either clockwise or anticlockwise, leading to the “cycles” $\vec{\mathcal{C}}_N$ and $-\vec{\mathcal{C}}_N$, respectively [see Fig. 2(b)]. We may want to eliminate an edge from \mathcal{C}_N , e.g., $(k, k + 1)$; the resulting undirected graph would be the “maximal tree” $\vec{\mathcal{T}}_k$ [see Fig. 2(c)]. Maximal trees can also be oriented toward a vertex, e.g., l ; the corresponding graph would then be denoted by $\vec{\mathcal{T}}_k^l$ [see Fig. 2(d)]. Finally, if the edge (k, l) is directed, e.g., from vertex k to vertex l , then we may pair it with the transition rate $W_{k,l}$. Similarly, any directed subgraph $\vec{\mathcal{G}}$, for example the cycle $\vec{\mathcal{C}}_N$ or the oriented maximal tree $\vec{\mathcal{T}}_k^l$, can be assigned a numeric value $\mathcal{A}(\vec{\mathcal{G}})$ given by the product of the transition rates of its directed edges. In particular, $\mathcal{A}(\vec{\mathcal{C}}_N) = \prod_{n=1}^N W_{n+1,n}$, $\mathcal{A}(-\vec{\mathcal{C}}_N) = \prod_{n=1}^N W_{n,n+1}$ and

$$\mathcal{A}(\vec{\mathcal{T}}_k^l) = \begin{cases} \prod_{n=1}^{l-1} W_{n+1,n} \prod_{n=l+1}^k W_{n-1,n} \prod_{n=k+1}^N W_{n+1,n} & l < k \\ \prod_{n=1}^{k-1} W_{n+1,n} \prod_{n=k+1}^{l-1} W_{n+1,n} \prod_{n=l}^N W_{n,n+1} & l > k + 1 \\ \prod_{n=1}^{k-1} W_{n+1,n} \prod_{n=k+1}^N W_{n+1,n} & l = k \\ \prod_{n=1}^{k-1} W_{n+1,n} \prod_{n=k+1}^N W_{n,n+1} & l = k + 1 \end{cases}, \quad (27)$$

where $W_{N,N+1} \equiv W_{N,1}$ and $W_{N+1,N} \equiv W_{1,N}$.

Our aim is to cast \mathcal{Q}_α and \mathcal{P} solely as functions of graph objects referring to \mathcal{C}_N . Let us start by noting that, the steady-state populations $p_i^{(\infty)}$ of S can be written as [54]

$$p_i^{(\infty)} = \mathcal{D}(\mathcal{C}_N)^{-1} \sum_{k=1}^N \mathcal{A}(\vec{\mathcal{T}}_k^i), \quad (28)$$

since, by definition, they coincide with those of S' . Here $\mathcal{D}(\mathcal{C}_N) = \sum_{k=1}^N \sum_{l=1}^N \mathcal{A}(\vec{\mathcal{T}}_k^l)$. Introducing Eq. (28) in the definition of J_i [see text below Eqs. (19)], we get

$$J_i = \mathcal{D}(\mathcal{C}_N)^{-1} \sum_{k=1}^N [W_{i+1,i} \mathcal{A}(\vec{\mathcal{T}}_k^i) - W_{i,i+1} \mathcal{A}(\vec{\mathcal{T}}_k^{i+1})]. \quad (29)$$

The bracketed term in Eq. (29) turns out to be $[\mathcal{A}(\vec{\mathcal{C}}_N) - \mathcal{A}(-\vec{\mathcal{C}}_N)] \delta_{ki}$ [56], where δ_{ki} stands for the Kronecker delta.

Therefore J_i does not depend on i

$$J_i = \mathcal{D}(\mathcal{C}_N)^{-1} [\mathcal{A}(\vec{\mathcal{C}}_N) - \mathcal{A}(-\vec{\mathcal{C}}_N)] := J. \quad (30)$$

That is, in the steady state, the system exchanges energy with both baths and the driving field, with the same flux [54]. This “tight-coupling” condition between thermodynamic fluxes [13] implies that our N -level device is “endoreversible” [16] and, hence, that it can operate in the reversible limit of maximum energy efficiency [28].

As a result, Eq. (19a) becomes $\mathcal{Q}_\alpha = J \sum_{i \in \mathcal{R}_\alpha} (E_{i+1} - E_i)$. Using (23) and (26a), we can see that

$$\sum_{i \in \mathcal{R}_\alpha} (E_{i+1} - E_i) = -T_\alpha k_B \ln \frac{\mathcal{A}^\alpha(\vec{\mathcal{C}}_N)}{\mathcal{A}^\alpha(-\vec{\mathcal{C}}_N)} := -T_\alpha \mathcal{X}^\alpha(\vec{\mathcal{C}}_N), \quad (31)$$

where $\mathcal{A}^\alpha(\pm \vec{\mathcal{C}}_N)$ is the product of the rates of the directed edges in $\pm \vec{\mathcal{C}}_N$ associated with bath α only. Combining Eqs. (30) and (31), we can finally express the steady-state heat

currents $\dot{\mathcal{Q}}_\alpha$ of the quantum-coherent N -level device S as:

$$\dot{\mathcal{Q}}_\alpha = \frac{-T_\alpha \mathcal{X}^\alpha(\vec{C}_N)}{\mathcal{D}(C_N)} [\mathcal{A}(\vec{C}_N) - \mathcal{A}(-\vec{C}_N)] \equiv \dot{\mathcal{Q}}_\alpha(C_N). \quad (32)$$

On the other hand, the power is easily calculated from energy conservation [cf. Eq. (18a)]. Remarkably, the right-hand side of Eq. (32) coincides with the steady-state heat currents of the circuit graph in Fig. 2(a), i.e., $\dot{\mathcal{Q}}_\alpha \equiv \dot{\mathcal{Q}}_\alpha(C_N)$ [53]. Note that this is far from trivial, since (32) refers to S , even if written in terms of graph objects related to S' . Therefore, we have shown that the N -level refrigerator and its classical emulator exhibit the same stationary heat currents and power consumption and are thus *thermodynamically indistinguishable*. This is our main result. Note that the significance of Eq. (32) is not just that our model is classically emulable, but that it is *classically emulable in spite of requiring quantum coherence to operate* (cf. Sec. II C).

C. Performance optimization of the thermal machine

The graph-theoretic expression (32) for the circuit currents of the classical emulator can also prove useful in the performance optimization of our quantum-coherent thermal machines S [56]. For instance, from the bracketed factor we see that the *asymmetry* in the stationary rates associated with opposite cycles is crucial in increasing the energy-conversion rate. On the other hand, the number of positive terms in the denominator scales as $\mathcal{D}(C_N) \sim N^2$, leading to vanishing currents. Therefore, larger energy-conversion rates are generally obtained in small few-level devices [17] featuring the largest possible asymmetry between opposite cycles.

Let us now focus on the refrigerator operation mode (i.e., $\dot{\mathcal{Q}}_c > 0$, $\dot{\mathcal{Q}}_h < 0$, and $\dot{\mathcal{P}} > 0$). Besides maximizing the cooling rate $\dot{\mathcal{Q}}_c$, it is of practical interest to operate at large “coefficient of performance” (COP) \mathcal{E} , i.e., at large cooling per unit of supplied power. In particular, the COP writes as

$$\mathcal{E} := \mathcal{E}(C_N) = \frac{\dot{\mathcal{Q}}_c(C_N)}{\dot{\mathcal{P}}(C_N)} = \frac{-T_c \mathcal{X}^c(\vec{C}_N)}{T_c \mathcal{X}^c(\vec{C}_N) + T_h \mathcal{X}^h(\vec{C}_N)}. \quad (33)$$

As a consequence of the second law [cf. Eq. (18b)], $\mathcal{E}(C_N)$ is upper bounded by the Carnot COP (\mathcal{E}_C),

$$\mathcal{E}(C_N) \leq \mathcal{E}_C = \frac{T_c}{T_h - T_c}. \quad (34)$$

This limit would be saturated when $\mathcal{X}^h(C_N) = -\mathcal{X}^c(C_N)$.³

Since the coupling to the driving field sets the smallest energy scale in our problem, the corresponding transition rate normally satisfies $W_{j_w, j_w+1} \ll W_{i, i+1}$, $\forall i \neq j_w$, unless some ω_i becomes very small. In turn, recalling the definition of

³In Sec. III B we noted that a quantum thermal machine obeying Eqs. (20) and (21) is endoreversible and, therefore, capable of operating at the reversible limit of Eq. (34). Recall, however, that the underlying quantum master equation (12) is based on a *local approximation*. A more accurate master equation—nonperturbative in the driving strength—can, nevertheless, be obtained using Floquet theory [16,62,63]. Importantly, this would introduce internal dissipation [20] neglected in Eq. (12), thus keeping the refrigerator from ever becoming Carnot efficient [16,28].

an oriented maximal tree \vec{T}_k^l [see Fig. 2(d)], this implies $\{\mathcal{A}(\vec{T}_k^l)\}_{k \neq j_w} \ll \{\mathcal{A}(\vec{T}_{j_w}^l)\}$ for $l \in \{1, \dots, N\}$, since the latter do not contain the small factors $W_{j_w, j_w+1} = W_{j_w+1, j_w}$, and allows for a convenient simplification of $\mathcal{D}(C_N)$ that we shall use below. Namely,

$$\mathcal{D}(C_N) = \left[\frac{\sum_{k \neq j_w} \sum_{l=1}^N \mathcal{A}(\vec{T}_k^l)}{\sum_{l=1}^N \mathcal{A}(\vec{T}_{j_w}^l)} + 1 \right] \sum_{l=1}^N \mathcal{A}(\vec{T}_{j_w}^l) \approx \sum_{l=1}^N \mathcal{A}(\vec{T}_{j_w}^l). \quad (35)$$

IV. EXAMPLE: POWER ENHANCEMENT IN A COHERENT FOUR-LEVEL HYBRID REFRIGERATOR

In this section we apply the above to a concrete example. Namely, we solve for the steady state of two models of quantum refrigerator and find that one of them is more energy efficient and cools at a larger rate than the other *provided its steady-state coherence is also larger*. Moreover, the quantitative improvement in the cooling rate matches exactly the increase in steady-state coherence. As suggestive as this observation may seem, we then move on to show that quantum coherence is not indispensable to achieve such performance enhancement. We do so precisely by building classical emulators for both quantum-coherent models and observing that the exact same performance enhancement is possible within a fully classical stochastic-thermodynamic picture.

A. Performance advantage

Let us start by considering the three-level model depicted in Fig. 3(a). As we can see, this simple design consists of three states $\{|1\rangle, |2\rangle, |3\rangle\}$, with energies $\{0, \hbar\omega_c, \hbar\omega_h\}$ connected through dissipative interactions with a cold and a hot bath (transitions $|1\rangle \leftrightarrow |2\rangle$ and $|1\rangle \leftrightarrow |3\rangle$, respectively), and the action of a weak driving field (transition $|2\rangle \leftrightarrow |3\rangle$).

It is then straightforward to find the steady-state $\hat{\sigma}_i(\infty)$ for the corresponding master equation (13), and use Eqs. (17) to compute the stationary heat currents $\dot{\mathcal{Q}}_\alpha^{(3)}$ and power consumption $\dot{\mathcal{P}}^{(3)}$. It can be seen that the tight-coupling condition introduced in Sec. III B also applies to this case so that the coefficient of performance writes as

$$\mathcal{E}_3 := \frac{\dot{\mathcal{Q}}_c^{(3)}}{\dot{\mathcal{P}}^{(3)}} = \frac{\omega_c}{\omega_w}, \quad (36)$$

where $\omega_w := \omega_h - \omega_c$.

We note that, when operating as a refrigerator, the three-level device uses the hot bath as a mere entropy sink; i.e., any excess heat is simply dumped into the hot bath and never reused. Interestingly, in order to improve the COP of actual (absorption) refrigerators it is commonplace to harness regenerative heat exchange in double-stage configurations. These recover waste heat from condensation to increase the evaporation rate of refrigerant [71]. Taking inspiration from thermal engineering, we thus add a fourth level $|4\rangle$ with energy $\hbar(\omega_h + \epsilon)$ as a stepping stone between $|2\rangle$ and $|3\rangle$. As shown in Fig. 3(b), we propose to use the external field only to drive the transition $|2\rangle \leftrightarrow |4\rangle$, with gap $\hbar(\omega_w + \epsilon)$. In order

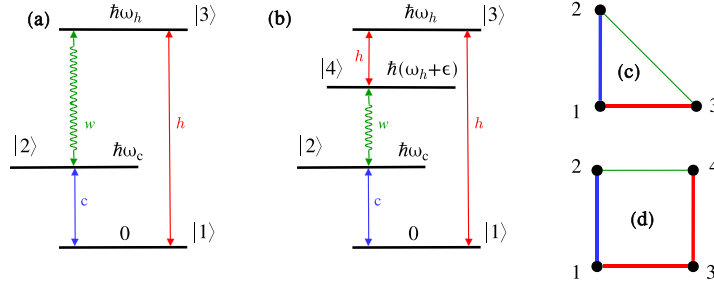


FIG. 3. (a) Three-level model. The system S consists of three levels with energies $(0, \hbar\omega_c, \hbar\omega_h)$, such that $0 < \omega_c < \omega_h$. The dissipative transitions tagged c and h are mediated by a cold (blue arrow) and a hot bath (red arrow), respectively. The transition w is driven by an external sinusoidal field (curly green arrow). (b) Four-level model. An extra level with energy $\hbar(\omega_h + \epsilon)$ is added to the three-level scheme. Note that ϵ can be positive or negative. The driving is now applied to the transition $|2\rangle \leftrightarrow |4\rangle$ and the new dissipative transition $|4\rangle \leftrightarrow |3\rangle$, due to the hot bath, is added to close the thermodynamic cooling cycle. The circuit graphs associated with the three and four-level models are depicted in panels (c) and (d), respectively. The thick blue (red) lines stand for dissipative transitions via the cold (hot) baths and the thin green lines, for the coupling to the driving.

to close the thermodynamic cooling cycle, we put the hot bath to good use and connect dissipatively levels $|4\rangle$ and $|3\rangle$. This results in another tightly coupled quantum refrigerator, with COP

$$\mathcal{E}_3 := \frac{\dot{\mathcal{Q}}_c^{(4)}}{\dot{\mathcal{P}}^{(4)}} = \frac{\omega_c}{\omega_w + \epsilon}. \quad (37)$$

This is *larger* than \mathcal{E}_3 whenever $\epsilon < 0$, as intended. For comparison, recall that quantum absorption refrigerators [58] entirely replace the driving by a dissipative coupling to a third bath at temperature $T_w > T_h$. Our combined-cycle four-level model is therefore a hybrid design of independent interest, as it is partly driven by power and partly, by recovered waste heat.

B. Power enhancement and quantum coherence

Even if the combined-cycle four-level refrigerator is more energy efficient than its power-driven three-level counterpart, we do not know yet whether it can also cool at a faster rate. To see this, let us define the figure of merit $\mathcal{R} := \dot{\mathcal{Q}}_c^{(4)}/\dot{\mathcal{Q}}_c^{(3)}$. From Eqs. (18a) and (19), it follows that

$$\mathcal{R} = \frac{C_i[\hat{\sigma}_s^{(4)}(\infty)]}{C_i[\hat{\sigma}_s^{(3)}(\infty)]}, \quad (38)$$

where $C_i[\hat{\sigma}_s^{(N)}(\infty)] = \text{Im}(j_w|\hat{\sigma}_s^{(N)}(\infty)\langle j_w + 1|)$ stands for the l_1 norm of coherence [44,45] in the stationary state $\hat{\sigma}_s^{(N)}(\infty)$ of the N -level thermal machine. This is a *bona fide* quantifier of the amount of coherence involved in the steady-state operation of the device. An enhancement in the cooling rate translates into $\mathcal{R} > 1$ and hence, is only possible if the steady state $\hat{\sigma}_s^{(4)}(\infty)$ of the four-level device contains more quantum coherence than $\hat{\sigma}_s^{(3)}(\infty)$. As it turns out, it is rather easy to find parameter ranges in which $\mathcal{R} > 1$, as shown in Figs. 4(a) and 4(b). Importantly, it is even possible to find parameters for which $\mathcal{E}_4 > \mathcal{E}_3$ and $\dot{\mathcal{Q}}_c^{(4)} > \dot{\mathcal{Q}}_c^{(3)}$ simultaneously.

C. Power enhancement without quantum coherence

Both the three- and four-level refrigerators are cyclic non-degenerate heat devices and hence classically emulable. In particular, the emulator for the three-level model is the triangle \mathcal{C}_3 depicted in Fig. 3(c) while the steady state of the hybrid four-level refrigerator is emulated by the square graph \mathcal{C}_4 of Fig. 3(d). In spite of the fact that there exist quantum coherent implementations of these energy-conversion cycles for which $\mathcal{R} > 1 \Leftrightarrow C_i[\hat{\sigma}_s^{(4)}(\infty)] > C_i[\hat{\sigma}_s^{(3)}(\infty)]$, it would be wrong to claim that quantumness is *necessary* for such performance boost—the corresponding emulators also satisfy $\dot{\mathcal{Q}}_c(\mathcal{C}_4) = \dot{\mathcal{Q}}_c^{(4)} > \dot{\mathcal{Q}}_c(\mathcal{C}_3) = \dot{\mathcal{Q}}_c^{(3)}$ and yet have no coherence.

D. Analytical insights from graph theory

1. Cooling rate

Using Eqs. (26a) and (31)–(33), we readily find that

$$\dot{\mathcal{Q}}_c(\mathcal{C}_3) = \hbar\omega_c \frac{A(\mathcal{C}_3)}{D(\mathcal{C}_3)} [1 - \exp(X_c - X_h)], \quad (39a)$$

$$\dot{\mathcal{Q}}_c(\mathcal{C}_4) = \hbar\omega_c \frac{A(\mathcal{C}_4)}{D(\mathcal{C}_4)} [1 - \exp(X_c - X_h - X_\epsilon)]. \quad (39b)$$

The quantities $X_c := \hbar\omega_c/k_B T_c$, $X_h := \hbar\omega_h/k_B T_h$, and $X_\epsilon := \hbar\epsilon/k_B T_h$ are “thermodynamic forces” associated with the cold and hot baths. Note that their difference encodes the *asymmetry* between the two possible orientations of the graphs.

2. Performance enhancement

A manageable analytical approximation for the figure of merit $\mathcal{R} = \dot{\mathcal{Q}}_c(\mathcal{C}_4)/\dot{\mathcal{Q}}_c(\mathcal{C}_3)$ can be obtained by combining Eqs. (23), (24), (39a), and (39b) with the assumption that the smallest transition rate is the one related to the driving field

062102-8

Este documento incorpora firma electrónica, y es copia auténtica de un documento electrónico archivado por la ULL según la Ley 39/2015.
Su autenticidad puede ser contrastada en la siguiente dirección <https://sede.ull.es/validacion/>

Identificador del documento: 2111210

Código de verificación: lZvvKBaU

Firmado por: Javier Onam González López
UNIVERSIDAD DE LA LAGUNA

Fecha: 09/09/2019 11:04:42

Daniel Alonso Ramírez
UNIVERSIDAD DE LA LAGUNA

11/09/2019 14:53:47

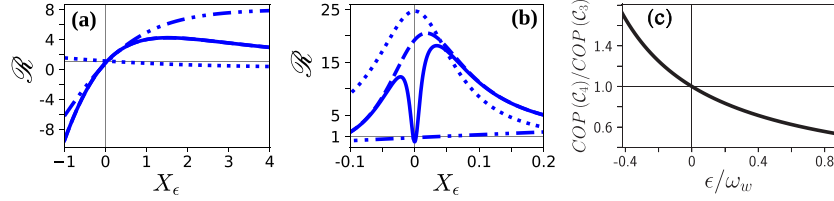


FIG. 4. (a) Performance ratio $\mathcal{R} = \mathcal{Q}_c(C_4)/\mathcal{Q}_c(C_3)$ (solid line) as a function of the thermodynamic force X_ϵ . We also plot the approximation AD from Eq. (40a) (dashed line) and the factors A (dotted line) and D (dot-dashed line). In this case, the solid and dashed lines are indistinguishable at the scale of the figure. We have chosen one-dimensional baths $d_c = d_h = 1$, $\omega_c = 1$, $\omega_h = 0.3$, $\lambda = 10^{-8}$, $\gamma_c = \gamma_h = 10^{-6}$, $T_c = 1.5$, and $T_h = 3$ ($\hbar = k_B = 1$). Importantly, as discussed in Sec. IV B, \mathcal{R} coincides with the ratio of stationary coherence of the four-level model and the benchmark, measured by the l_1 norm. (b) Same as in (a) for three-dimensional baths ($d_c = d_h = 3$). The rest of parameters remain unchanged. (c) Ratio between the COPs of C_3 and C_4 versus ϵ . Note that, for $\epsilon < 0$, the four-level device can simultaneously achieve larger cooling power and COP. All parameters are the same as in (b).

[i.e., Eq. (35)]. This gives

$$\mathcal{R} \simeq AD, \quad (40a)$$

$$A := \frac{1 + \exp(X_c) + \exp(X_c - X_h)}{1 + \exp(X_c) + \exp(X_c - X_h) + \exp(X_c - X_h - X_\epsilon)} \times \frac{1 - \exp(X_c - X_h - X_\epsilon)}{1 - \exp(X_c - X_h)}, \quad (40b)$$

$$D := \frac{\Gamma_{\omega_c}^c + \Gamma_{\omega_h}^h}{\Gamma_{\omega_c}^c + \Gamma_{\omega_h}^h}. \quad (40c)$$

As we can see, the factor A depends exclusively on the thermodynamic forces X_c , X_h , and X_ϵ . Its second term describes the ratio between the cycles asymmetries. The new thermodynamic force allows for an additional control on the asymmetry of the four-level refrigerator, thus favoring the cooling cycle for $X_\epsilon > 0$. In contrast, the quantity D is purely dissipative; it encodes the ratio between the rates associated with the driving field Eq. (24). Importantly, small ϵ in the four-level model can increase D . The choice of spectral density for the system-bath interactions (i.e., the dimensionality or ‘‘Ohmicity’’ of the baths) can lead to a sufficiently large D so that the product $\mathcal{R} = AD > 1$ for $\epsilon < 0$. Thus, factorizing \mathcal{R} as in Eqs. (40) provides insights into the competing physical mechanisms responsible for the cooling power enhancements in the four-level device.

Figure 4(a) illustrates how the approximation (40a) may hold almost exactly; namely, we work with one-dimensional baths ($d_c = d_h = 1$) at moderate to large temperatures ($k_B T_u / \hbar \omega_u \gtrsim 1$). In this range of parameters, A is the main contribution to the enhancement of \mathcal{Q}_c , so that \mathcal{R} is nearly insensitive to changes in the dissipation strengths.

On the contrary, when taking three-dimensional baths ($d_c = d_h = 3$), the frequency dependence of the transition rates is largely accentuated. At small ϵ the rate $W_{2,4}$ ceases to be the smallest in C_4 , which invalidates Eqs. (40) [see

Fig. 4(b)].⁴ In this case, the behavior of \mathcal{R} is dominated by D and grows almost linearly with γ_h . Similar disagreements between \mathcal{R} and the approximate formula Eq. (40) can be observed in the low-temperature regime.

As shown in Fig. 4(b), the hybrid four-level design can operate at much larger energy-conversion rates than the power-driven benchmark. Indeed, for the arbitrarily chosen parameters in the figure, $\mathcal{Q}_c(C_4)$ can outperform $\mathcal{Q}_c(C_3)$ by an order of magnitude at appropriate values of ϵ . Such enhancement may be classically interpreted solely in terms of the asymmetry A and the dissipation factor D , without resorting to the buildup of quantum coherence. Importantly, such qualitative understanding follows directly from the classical emulation of the model, which allows us to study the emulator in place of the original quantum-coherent device.

3. Coefficient of performance and cooling window

The COPs of C_3 and C_4 are related through

$$\mathcal{E}(C_4)/\mathcal{E}(C_3) = (1 + \epsilon/\omega_w)^{-1}. \quad (41)$$

As already mentioned, $\epsilon < 0$ results in an increase of the energetic performance of the four-level machine due to the lower power consumption [see Fig. 4(c)]. Interestingly, the ratio \mathcal{R} can be larger than one for $\epsilon < 0$, which entails a *simultaneous power and efficiency enhancement*. For instance, comparing Figs. 4(b) and 4(c), we observe increased power by a factor of 10 together with a 10% improvement in energy efficiency.

On the other hand, the operation mode—heat engine or refrigerator—depends on the specific parameters of the models. In particular, to achieve cooling action in the three-level benchmark we must have $\mathcal{Q}_c(C_3) > 0$. According to Eq. (39a),

⁴Recall that for Eq. (12) to be valid, we must have $2\epsilon \gg \gamma_h$, as required by the underlying secular approximation $\tau_0 \ll \tau_R$ [cf. Eq. (5)]. The solid lines in Figs. 4 are mere guides to the eye, which smoothly interpolate between points well within the range of validity of the master equation.

this implies $X_c - X_h < 0$ or, equivalently,

$$\omega_c < \omega_{c,\text{rev}} := \omega_h T_c / T_h. \quad (42)$$

Taking a fixed ω_h , the range of values $\omega_c < \omega_{c,\text{rev}}$ is thus referred to as *cooling window*. On the other hand, from Eq. (39b) we can see that cooling is possible on C_4 if

$$\omega_c < (\omega_h + \epsilon) T_c / T_h. \quad (43)$$

Hence, whenever $\epsilon > 0$ the cooling window of the four-level model is *wider* than that of the benchmark for the *same* parameters ω_h , T_c , λ , γ_a , and d_a . Conversely, if we were interested in building a quantum heat engine, then a negative ϵ [as depicted in Fig. 3(b)] would broaden the operation range.

V. CONCLUSIONS

We have analyzed periodically driven thermal machines weakly coupled to an external field and characterized by a *cyclic* sequence of transitions. We have proposed an approach to build fully *incoherent* classical emulators for this family of *quantum-coherent* heat devices, which exhibit the exact same thermodynamic operation in the long-time limit. In particular, we exploit the fact that the steady state of this type of coherent thermal machines coincides with that of some stochastic-thermodynamic model with the same number of states dissipatively connected via thermal coupling to the same heat baths and obeying consistent rate equations.

We have then shown how the performance of a three-level quantum-coherent refrigerator may be significantly improved by driving it with a combination of waste heat and external power—both the energy efficiency and the cooling rate can be boosted in this way. In particular, we have shown that the cooling enhancement is identical to the increase in stationary quantum coherence, when comparing our hybrid model with an equivalent benchmark solely driven by power. In spite of the close connection between the observed effects and the buildup of additional quantum coherence, we remark that these cannot be seen as unmistakable signatures of quantumness since our model belongs to the aforementioned family of “classically emulable” thermal machines.

In fact, the possibility to emulate classically a quantum heat device goes far beyond the cyclic and weakly driven models discussed here. For instance, in the opposite limit of *strong* periodic driving (i.e., $\tau_d \ll \tau_R$) one can always resort to Floquet theory to map the steady-state operation of the machine into a fully incoherent stochastic-thermodynamic process in some relevant rotating frame [16,62,63]. Graph theory can be then directly applied for a complete thermodynamic analysis [55]. Note that this holds for *any* periodically driven model and not just for those with a cyclic transition pattern. Similarly, *all* heat-driven (or “absorption”) thermal machines with nondegenerate energy spectra are incoherent in their energy basis and thus classically emulable in the weak-coupling limit [56]. Furthermore, the equivalence between multistroke and continuous heat devices in the small action limit [30] provides a means to generalize our “classical simulability” argument to *reciprocating* quantum thermodynamic cycles.

In this paper, we have thus extended the applicability of Hill theory [53,54] to enable the graph-based analysis of a whole class of quantum-coherent thermal devices. We have

also put forward a hybrid energy conversion model of independent interest, which exploits heat recovery for improved operation. More importantly, we have neatly illustrated why extra care must be taken when linking quantum effects and enhanced thermodynamic performance. This becomes especially delicate in, e.g., biological systems [72], in which the details of the underlying physical model are not fully known.

It is conceivable that the steady state of some continuous quantum thermal machines might not be classically emulable—for our arguments to hold, the resulting equations of motion [analogous to our Eq. (25)] must also be proper balance equations with positive transition rates and a clear interpretation in terms of probability currents. Since the positivity of the rates is model dependent, the search for classical emulators of more complicated devices, including consecutive driven transitions and degenerate states, might pave the way toward *genuinely quantum* energy-conversion processes with no classical analog. This interesting open question will be the subject of future work.

ACKNOWLEDGMENTS

We gratefully acknowledge financial support by the Spanish MINECO (Grant No. FIS2017-82855-P), the European Research Council (StG QCCOP Grant No. 637352), and the U.S. National Science Foundation under Grant No. NSF PHY1748958. J.O.G. acknowledges an FPU fellowship from the Spanish MECED. L.A.C. thanks the Kavli Institute for Theoretical Physics for their warm hospitality during the program “Thermodynamics of quantum systems: Measurement, engines, and control.”

APPENDIX: A MODEL WITH HEAT LEAKS

We consider here the model depicted in Fig. 1 when adding an extra hot transition between the levels $|j_w\rangle$ and $|j_w + 1\rangle$. The populations of such device fulfill Eq. (20a) and

$$\begin{aligned} \frac{dp_{j_w}}{dt} &= \Gamma_{-\omega_{j_w-1}}^{\alpha_{j_w-1}} p_{j_w-1} - \Gamma_{\omega_{j_w-1}}^{\alpha_{j_w-1}} p_{j_w} \\ &\quad - 2\lambda \text{Im} \langle j_w | \hat{\sigma}_s | j_w + 1 \rangle + J_{j_w, j_w+1}, \\ \frac{dp_{j_w+1}}{dt} &= \Gamma_{\omega_{j_w+1}}^{\alpha_{j_w+1}} p_{j_w+2} - \Gamma_{-\omega_{j_w+1}}^{\alpha_{j_w+1}} p_{j_w+1} \\ &\quad + 2\lambda \text{Im} \langle j_w | \hat{\sigma}_s | j_w + 1 \rangle - J_{j_w, j_w+1}, \end{aligned} \quad (A1)$$

where

$$J_{j_w, j_w+1} = \Gamma_{\omega_{j_w}}^h p_{j_w+1} - \Gamma_{-\omega_{j_w}}^h p_{j_w} \quad (A2)$$

is the flux from the state $|j_w\rangle$ to $|j_w + 1\rangle$. This new flux is the responsible for the emergence of an additional term in the nondiagonal rates

$$W_{j_w, j_w+1} = 4\lambda^2 \left[\Gamma_{\omega_{j_w-1}}^{\alpha_{j_w-1}} + \Gamma_{-\omega_{j_w+1}}^{\alpha_{j_w+1}} \right]^{-1} + \Gamma_{\omega_{j_w}}^h, \quad (A3)$$

$$W_{j_w+1, j_w} = 4\lambda^2 \left[\Gamma_{\omega_{j_w-1}}^{\alpha_{j_w-1}} + \Gamma_{-\omega_{j_w+1}}^{\alpha_{j_w+1}} \right]^{-1} + \Gamma_{-\omega_{j_w}}^h. \quad (A4)$$

The functions $\Gamma_{\omega_{j_w}}^h$ and $\Gamma_{-\omega_{j_w}}^h$ are always positive and fulfill a detailed balance relation at temperature T_h and frequency

062102-10

Este documento incorpora firma electrónica, y es copia auténtica de un documento electrónico archivado por la ULL según la Ley 39/2015.
 Su autenticidad puede ser contrastada en la siguiente dirección <https://sede.ull.es/validacion/>

Identificador del documento: 2111210

Código de verificación: lZvvKBaU

Firmado por: Javier Onam González López
 UNIVERSIDAD DE LA LAGUNA

Fecha: 09/09/2019 11:04:42

Daniel Alonso Ramírez
 UNIVERSIDAD DE LA LAGUNA

11/09/2019 14:53:47

ω_{j_w} . The other nondiagonal rates remain the same following Eq. (23). The resulting matrix of rates allows for the definition of a graph representation; therefore, a classical emulator can be assigned also to this model.

Such emulator is defined by a graph \mathcal{G} with three circuits: the original circuit C_N , a two-edge circuit C_2 —with vertices j_w and $j_w + 1$ —corresponding to power dissipation into the hot bath, and a N -edge circuit C'_N , where the work edge is replaced by the new hot edge, related to a heat leak from the hot to the cold bath. The heat currents and power of these circuits can be obtained by following the techniques explained in Refs. [55] and [56]. The total heat currents are then the sum of the following three thermodynamically consistent

contributions

$$\begin{aligned}\dot{\mathcal{Q}}_\alpha(C_N) &= \frac{-T_\alpha \mathcal{X}^\alpha(\vec{C}_N)}{\mathcal{D}(\mathcal{G})} [\mathcal{A}(\vec{C}_N) - \mathcal{A}(-\vec{C}_N)], \\ \dot{\mathcal{Q}}_\alpha(C_2) &= \frac{-T_\alpha \mathcal{X}^\alpha(\vec{C}_2) \det(-\mathbf{W}|C_2)}{\mathcal{D}(\mathcal{G})} [\mathcal{A}(\vec{C}_2) - \mathcal{A}(-\vec{C}_2)], \\ \dot{\mathcal{Q}}_\alpha(C'_N) &= \frac{-T_\alpha \mathcal{X}^\alpha(\vec{C}'_N)}{\mathcal{D}(\mathcal{G})} [\mathcal{A}(\vec{C}'_N) - \mathcal{A}(-\vec{C}'_N)],\end{aligned}\quad (\text{A5})$$

where $\mathcal{D}(\mathcal{G})$ is calculated by considering all the maximal trees of the graph containing the three circuits. Besides the matrix $\mathbf{W}|C_2$ is obtained from the matrix of rates by removing the rows and columns corresponding to the vertices of C_2 .

- [1] *Thermodynamics in the Quantum Regime*, edited by F. Binder, L. A. Correa, C. Gogolin, J. Anders, and G. Adesso, Fundamental Theories of Physics (Springer, Berlin, 2018).
- [2] R. Kosloff, Quantum thermodynamics: A dynamical viewpoint, *Entropy* **15**, 2100 (2013).
- [3] R. Kosloff and A. Levy, Quantum heat engines and refrigerators: Continuous devices, *Annu. Rev. Phys. Chem.* **65**, 365 (2014).
- [4] D. Gelbwaser-Klimovsky, W. Niedenzu, and G. Kurizki, Thermodynamics of quantum systems under dynamical control, *Adv. At. Mol. Opt. Phys.* **64**, 329 (2015).
- [5] J. Goolid, M. Huber, A. Riera, L. del Rio, and P. Skrzypczyk, The role of quantum information in thermodynamics—A topical review, *J. Phys. A: Math. Theor.* **49**, 143001 (2016).
- [6] S. Vinjanampathy and J. Anders, Quantum thermodynamics, *Contemp. Phys.* **57**, 545 (2016).
- [7] H. E. D. Scovil and E. O. Schulz-DuBois, Three-Level Masers as Heat Engines, *Phys. Rev. Lett.* **2**, 262 (1959).
- [8] J. E. Geusic, E. O. Schulz-DuBois, R. W. De Grasse, and H. E. D. Scovil, Three level spin refrigeration and maser action at 1500 mc/sec, *J. Appl. Phys.* **30**, 1113 (1959).
- [9] E. Geva and R. Kosloff, The quantum heat engine and heat pump: An irreversible thermodynamic analysis of the three-level amplifier, *J. Chem. Phys.* **104**, 7681 (1996).
- [10] T. Feldmann and R. Kosloff, Performance of discrete heat engines and heat pumps in finite time, *Phys. Rev. E* **61**, 4774 (2000).
- [11] T. Feldmann and R. Kosloff, Quantum lubrication: Suppression of friction in a first-principles four-stroke heat engine, *Phys. Rev. E* **73**, 025107(R) (2006).
- [12] Y. Rezek and R. Kosloff, Irreversible performance of a quantum harmonic heat engine, *New J. Phys.* **8**, 83 (2006).
- [13] M. Esposito, K. Lindenberg, and C. Van den Broeck, Universality of Efficiency at Maximum Power, *Phys. Rev. Lett.* **102**, 130602 (2009).
- [14] C. Creatore, M. A. Parker, S. Emmott, and A. W. Chin, Efficient Biologically Inspired Photocell Enhanced by Delocalized Quantum States, *Phys. Rev. Lett.* **111**, 253601 (2013).
- [15] L. A. Correa, J. P. Palao, D. Alonso, and G. Adesso, Quantum-enhanced absorption refrigerators, *Sci. Rep.* **4**, 3949 (2014).
- [16] L. A. Correa, J. P. Palao, G. Adesso, and D. Alonso, Optimal performance of endoreversible quantum refrigerators, *Phys. Rev. E* **90**, 062124 (2014).
- [17] L. A. Correa, Multistage quantum absorption heat pumps, *Phys. Rev. E* **89**, 042128 (2014).
- [18] D. Gelbwaser-Klimovsky, W. Niedenzu, P. Brumer, and G. Kurizki, Power enhancement of heat engines via correlated thermalization in a three-level “working fluid,” *Sci. Rep.* **5**, 14413 (2015).
- [19] W. Niedenzu, D. Gelbwaser-Klimovsky, and G. Kurizki, Performance limits of multilevel and multipartite quantum heat machines, *Phys. Rev. E* **92**, 042123 (2015).
- [20] L. A. Correa, J. P. Palao, and D. Alonso, Internal dissipation and heat leaks in quantum thermodynamic cycles, *Phys. Rev. E* **92**, 032136 (2015).
- [21] J. P. Palao, L. A. Correa, G. Adesso, and D. Alonso, Efficiency of inefficient endoreversible thermal machines, *Braz. J. Phys.* **46**, 282 (2016).
- [22] R. Uzdin, A. Levy, and R. Kosloff, Quantum heat machines equivalence, work extraction beyond markovianity, and strong coupling via heat exchangers, *Entropy* **18**, 124 (2016).
- [23] M. O. Scully, M. S. Zubairy, G. S. Agarwal, and H. Walther, Extracting work from a single heat bath via vanishing quantum coherence, *Science* **299**, 862 (2003).
- [24] M. O. Scully, Quantum Photocell: Using Quantum Coherence to Reduce Radiative Recombination and Increase Efficiency, *Phys. Rev. Lett.* **104**, 207701 (2010).
- [25] M. O. Scully, K. R. Chapin, K. E. Dorfman, M. B. Kim, and A. Svidzinsky, Quantum heat engine power can be increased by noise-induced coherence, *Proc. Natl. Acad. Sci. USA* **108**, 15097 (2011).
- [26] A. A. Svidzinsky, K. E. Dorfman, and M. O. Scully, Enhancing photovoltaic power by fano-induced coherence, *Phys. Rev. A* **84**, 053818 (2011).
- [27] T. Feldmann and R. Kosloff, Short time cycles of purely quantum refrigerators, *Phys. Rev. E* **85**, 051114 (2012).
- [28] L. A. Correa, J. P. Palao, G. Adesso, and D. Alonso, Performance bound for quantum absorption refrigerators, *Phys. Rev. E* **87**, 042131 (2013).
- [29] N. Brunner, M. Huber, N. Linden, S. Popescu, R. Silva, and P. Skrzypczyk, Entanglement enhances cooling in microscopic quantum refrigerators, *Phys. Rev. E* **89**, 032115 (2014).

062102-11

Este documento incorpora firma electrónica, y es copia auténtica de un documento electrónico archivado por la ULL según la Ley 39/2015.
 Su autenticidad puede ser contrastada en la siguiente dirección <https://sede.ull.es/validacion/>

Identificador del documento: 2111210

Código de verificación: lZvvKBaU

Firmado por: Javier Onam González López
 UNIVERSIDAD DE LA LAGUNA

Fecha: 09/09/2019 11:04:42

Daniel Alonso Ramírez
 UNIVERSIDAD DE LA LAGUNA

11/09/2019 14:53:47

- [30] R. Uzdin, A. Levy, and R. Kosloff, Equivalence of Quantum Heat Machines, and Quantum-Thermodynamic Signatures, *Phys. Rev. X* **5**, 031044 (2015).
- [31] N. Killoran, S. F. Huelga, and M. B. Plenio, Enhancing light-harvesting power with coherent vibrational interactions: A quantum heat engine picture, *J. Chem. Phys.* **143**, 155102 (2015).
- [32] J. B. Brask and N. Brunner, Small quantum absorption refrigerator in the transient regime: Time scales, enhanced cooling, and entanglement, *Phys. Rev. E* **92**, 062101 (2015).
- [33] M. T. Mitchison, M. P. Woods, J. Prior, and M. Huber, Coherence-assisted single-shot cooling by quantum absorption refrigerators, *New J. Phys.* **17**, 115013 (2015).
- [34] D. Xu, C. Wang, Y. Zhao, and J. Cao, Polarization effects on the performance of light-harvesting systems: A quantum heat engine perspective, *New J. Phys.* **18**, 023003 (2016).
- [35] R. Silva, G. Manzano, P. Skrzypczyk, and N. Brunner, Performance of autonomous quantum thermal machines: Hilbert space dimension as a thermodynamical resource, *Phys. Rev. E* **94**, 032120 (2016).
- [36] A. Friedenberger and E. Lutz, When is a quantum heat engine quantum? *Europhys. Lett.* **120**, 10002 (2017).
- [37] P. Grangier and A. Auffèves, What is quantum in quantum randomness? *Philos. Trans. R. Soc. A* **376**, 20170322 (2018).
- [38] K. E. Dorfman, D. Xu, and J. Cao, Efficiency at maximum power of a laser quantum heat engine enhanced by noise-induced coherence, *Phys. Rev. E* **97**, 042120 (2018).
- [39] V. Holubeč and T. Novotný, Effects of noise-induced coherence on the performance of quantum absorption refrigerators, *J. Low Temp. Phys.* **192**, 147 (2018).
- [40] J.-Y. Du and F.-L. Zhang, Nonequilibrium quantum absorption refrigerator, *New J. Phys.* **20**, 063005 (2018).
- [41] M. Kilgour and D. Segal, Coherence and decoherence in quantum absorption refrigerators, *Phys. Rev. E* **98**, 012117 (2018).
- [42] D. Gelbwaser-Klimovsky, A. Bylinskii, D. Gangloff, R. Islam, A. Aspuru-Guzik, and V. Vuletic, Single-Atom Heat Machines Enabled by Energy Quantization, *Phys. Rev. Lett.* **120**, 170601 (2018).
- [43] J. E. Geusic, E. O. Schulz-DuBios, and H. E. D. Scovil, Quantum equivalent of the Carnot cycle, *Phys. Rev.* **156**, 343 (1967).
- [44] T. Baumgratz, M. Cramer, and M. B. Plenio, Quantifying Coherence, *Phys. Rev. Lett.* **113**, 140401 (2014).
- [45] A. Streltsov, G. Adesso, and M. B. Plenio, Colloquium: Quantum coherence as a resource, *Rev. Mod. Phys.* **89**, 041003 (2017).
- [46] G. Bulnes Cuetara, M. Esposito, and G. Schaller, Quantum thermodynamics with degenerate eigenstate coherences, *Entropy* **18**, 447 (2016).
- [47] U. Seifert, Stochastic thermodynamics, fluctuation theorems and molecular machines, *Rep. Prog. Phys.* **75**, 126001 (2012).
- [48] C. Van den Broeck and M. Esposito, Ensemble and trajectory thermodynamics: A brief introduction, *Phys. A* **418**, 6 (2015).
- [49] M. Poletini, G. Bulnes-Cuetara, and M. Esposito, Conservation laws and symmetries in stochastic thermodynamics, *Phys. Rev. E* **94**, 052117 (2016).
- [50] S. Nimmrichter, J. Dai, A. Roulet, and V. Scarani, Quantum and classical dynamics of a three-mode absorption refrigerator, *Quantum* **1**, 37 (2017).
- [51] J. Klatzow, J. N. Becker, P. M. Ledingham, C. Weinzetl, K. T. Kaczmarek, D. J. Saunders, J. Nunn, I. A. Walmsley, R. Uzdin, and E. Poem, Experimental Demonstration of Quantum Effects in the Operation of Microscopic Heat Engines, *Phys. Rev. Lett.* **122**, 110601 (2019).
- [52] J. O. González, L. A. Correa, G. Nocerino, J. P. Palao, D. Alonso, and G. Adesso, Testing the validity of the 'local' and 'global' GKLS master equations on an exactly solvable model, *Open Syst. Inf. Dyn.* **24**, 1740010 (2017).
- [53] T. L. Hill, Studies in irreversible thermodynamics. IV. Diagrammatic representation of steady state fluxes for unimolecular systems, *J. Theor. Biol.* **10**, 442 (1966).
- [54] J. Schnakenberg, Network theory of microscopic and macroscopic behavior of master equation systems, *Rev. Mod. Phys.* **48**, 571 (1976).
- [55] J. O. González, D. Alonso, and J. P. Palao, Performance of continuous quantum thermal devices indirectly connected to environments, *Entropy* **18**, 166 (2016).
- [56] J. O. González, J. P. Palao, and D. Alonso, Relation between topology and heat currents in multilevel absorption machines, *New J. Phys.* **19**, 113037 (2017).
- [57] O. Raz, Y. Subaşı, and C. Jarzynski, Mimicking Nonequilibrium Steady states with Time-Periodic Driving, *Phys. Rev. X* **6**, 021022 (2016).
- [58] J. P. Palao, R. Kosloff, and J. M. Gordon, Quantum thermodynamic cooling cycle, *Phys. Rev. E* **64**, 056130 (2001).
- [59] H. Breuer and F. Petruccione, *The Theory of Open Quantum Systems* (Oxford University Press, New York, 2002).
- [60] V. Gorini, A. Kossakowski, and E. Sudarshan, Completely positive dynamical semigroups of n-level systems, *J. Math. Phys.* **17**, 821 (1976).
- [61] G. Lindblad, On the generators of quantum dynamical semigroups, *Commun. Math. Phys.* **48**, 119 (1976).
- [62] R. Alicki, D. Gelbwaser-Klimovsky, and G. Kurizki, Periodically driven quantum open systems: Tutorial, [arXiv:1205.4552](https://arxiv.org/abs/1205.4552).
- [63] K. Szczygielski, On the application of Floquet theorem in development of time-dependent Lindbladians, *J. Math. Phys.* **55**, 083506 (2014).
- [64] H. Wichterich, M. J. Henrich, H.-P. Breuer, J. Gemmer, and M. Michel, Modeling heat transport through completely positive maps, *Phys. Rev. E* **76**, 031115 (2007).
- [65] P. P. Hofer, M. Perarnau-Llobet, L. D. M. Miranda, G. Haack, R. Silva, J. B. Brask, and N. Brunner, Markovian master equations for quantum thermal machines: Local versus global approach, *New J. Phys.* **19**, 123037 (2017).
- [66] A. Trushechkin and I. Volovich, Perturbative treatment of inter-site couplings in the local description of open quantum networks, *Europhys. Lett.* **113**, 30005 (2016).
- [67] A. Levy and R. Kosloff, The local approach to quantum transport may violate the second law of thermodynamics, *Europhys. Lett.* **107**, 20004 (2014).
- [68] J. T. Stockburger and T. Motz, Thermodynamic deficiencies of some simple Lindblad operators, *Fortschr. Phys.* **65**, 1600067 (2017).
- [69] R. Alicki, The quantum open system as a model of the heat engine, *J. Phys. A* **12**, L103 (1979).

062102-12

Este documento incorpora firma electrónica, y es copia auténtica de un documento electrónico archivado por la ULL según la Ley 39/2015.
Su autenticidad puede ser contrastada en la siguiente dirección <https://sede.ull.es/validacion/>

Identificador del documento: 2111210

Código de verificación: lZvvKBaU

Firmado por: Javier Onam González López
UNIVERSIDAD DE LA LAGUNA

Fecha: 09/09/2019 11:04:42

Daniel Alonso Ramírez
UNIVERSIDAD DE LA LAGUNA

11/09/2019 14:53:47

CLASSICAL EMULATION OF QUANTUM-COHERENT ...

PHYSICAL REVIEW E 99, 062102 (2019)

[70] H. Spohn, Entropy production for quantum dynamical semi-groups, *J. Math. Phys.* **19**, 1227 (1978).
[71] J. M. Gordon and K. C. Ng, *Cool Thermodynamics* (Cambridge International Science Publishing, Cambridge, 2000).

[72] G. S. Engel, T. R. Calhoun, E. L. Read, T.-K. Ahn, T. Mančal, Y.-C. Cheng, R. E. Blankenship, and G. R. Fleming, Evidence for wavelike energy transfer through quantum coherence in photosynthetic systems, *Nature* **446**, 782 (2007).

062102-13

120

Este documento incorpora firma electrónica, y es copia auténtica de un documento electrónico archivado por la ULL según la Ley 39/2015.
Su autenticidad puede ser contrastada en la siguiente dirección <https://sede.ull.es/validacion/>

Identificador del documento: 2111210 Código de verificación: lZvvKBaU

Firmado por: Javier Onam González López
UNIVERSIDAD DE LA LAGUNA

Fecha: 09/09/2019 11:04:42

Daniel Alonso Ramírez
UNIVERSIDAD DE LA LAGUNA

11/09/2019 14:53:47

Appendix A

Master equations

In this appendix we summarize how to obtain the Redfield [80], Global (or Secular) [4] and Local [81] master equations. The formalism can be used to study both absorption and periodically driven devices. We consider a general scheme with a quantum system S whose Hamiltonian $\hat{H}_S = \hat{H}_S^0 + \hat{H}_S^w(t)$ may be time dependent. The term $\hat{H}_S^w(t)$ that describes the interaction with a laser field can be written as

$$\hat{H}_S^w(t) = \hbar \lambda [\hat{O}_S e^{i\omega_L t} + \hat{O}_S^\dagger e^{-i\omega_L t}], \quad (\text{A.1})$$

with $\hat{O}_S = \sum_{n,m} |n\rangle\langle m|$ a system operator describing the transitions $|m\rangle \rightarrow |n\rangle$ coupled to the field. In the case of absorption devices $\lambda = 0$ and, hence, $\hat{H}_S = \hat{H}_S^0$ is time independent. Besides, S is coupled to a set of independent baths $B \equiv \{B_\alpha\}$ whose Hamiltonians \hat{H}_{B_α} are given by (2.1). The interaction between S and each bath B_α is described by the Hamiltonian $\hat{H}_{SB_\alpha} = \hat{A}^\alpha \otimes \hat{B}^\alpha$, where \hat{B}^α is expressed in (2.5). We denote $\hat{H}_B = \sum_\alpha \hat{H}_{B_\alpha}$ and $\hat{H}_I = \sum_\alpha \hat{H}_{SB_\alpha}$. The total Hamiltonian of the device is $\hat{H} = \hat{H}_S + \hat{H}_B + \hat{H}_I$.

In the following, we consider two main restrictions. First, we assume that the interaction \hat{H}_I is so weak that the influence of S on the baths is negligible. Hence, the characteristic time of the interaction $\tau_{SB} \sim \gamma_\alpha^{-1}$ is much larger than the time scale of the baths $\tau_B \sim \frac{\hbar}{k_B T_\alpha}$ or, equivalently, $\gamma_\alpha \ll \frac{k_B T_\alpha}{\hbar}$. Thus, master equations can be derived by using a reduced description of the system in this weak coupling regime. Second, we assume that the evolution operator of the system can be written as

$$\hat{U}_S(t) = e^{-i\hat{A}_1 t/\hbar} e^{-i\hat{A}_2 t/\hbar}, \quad (\text{A.2})$$

with \hat{A}_1 and \hat{A}_2 hermitian operators such that $[\hat{A}_1, \hat{H}_S^0] = 0$. Such evolution operator fulfills

$$i\hbar \frac{d}{dt} \hat{U}_S(t) = (\hat{H}_S^0 + \hat{H}_S^w(t)) \hat{U}_S(t). \quad (\text{A.3})$$

Este documento incorpora firma electrónica, y es copia auténtica de un documento electrónico archivado por la ULL según la Ley 39/2015.
 Su autenticidad puede ser contrastada en la siguiente dirección <https://sede.ull.es/validacion/>

Identificador del documento: 2111210

Código de verificación: lZvvKBaU

Firmado por: Javier Onam González López
 UNIVERSIDAD DE LA LAGUNA

Fecha: 09/09/2019 11:04:42

Daniel Alonso Ramírez
 UNIVERSIDAD DE LA LAGUNA

11/09/2019 14:53:47

Equation (A.2) is valid for any absorption device as long as $e^{-i\hat{A}_1 t/\hbar} = \mathbb{I}$ and $\hat{A}_2 = \hat{H}_S^0$, where \mathbb{I} is the identity operator. However, Eq. (A.2) is only applicable for some instances of periodically driven machines.

A.1 Redfield master equation

Let us start by considering the interaction picture von Neumann equation [4]

$$\frac{d\hat{\sigma}(t)}{dt} = -\frac{i}{\hbar}[\hat{H}_I(t), \hat{\sigma}(t)], \quad (\text{A.4})$$

where $\hat{\sigma}$ is the interaction picture density matrix corresponding to the whole machine (system and baths) and

$$\hat{H}_I(t) = \sum_{\alpha} \hat{U}_S^{\dagger}(t) \hat{A}^{\alpha} \hat{U}_S(t) \otimes e^{i\hat{H}_{B\alpha} t/\hbar} \hat{B}^{\alpha} e^{-i\hat{H}_{B\alpha} t/\hbar} \equiv \sum_{\alpha} \hat{A}^{\alpha}(t) \otimes \hat{B}^{\alpha}(t). \quad (\text{A.5})$$

Integrating both sides of Eq. (A.4), we get

$$\hat{\sigma}(t) = \hat{\sigma}(0) - \frac{i}{\hbar} \int_0^t d\tau [\hat{H}_I(\tau), \hat{\sigma}(\tau)]. \quad (\text{A.6})$$

Inserting Eq. (A.6) into Eq. (A.4) leads to

$$\frac{d\hat{\sigma}(t)}{dt} = -\frac{i}{\hbar}[\hat{H}_I(t), \hat{\sigma}(0)] - \frac{1}{\hbar^2} \int_0^t d\tau [\hat{H}_I(t), [\hat{H}_I(\tau), \hat{\sigma}(\tau)]]. \quad (\text{A.7})$$

We take trace over the baths in Eq (A.7) to find

$$\begin{aligned} \text{Tr}_B \left\{ \frac{d\hat{\sigma}(t)}{dt} \right\} &= \frac{d}{dt} \text{Tr}_B \{ \hat{\sigma}(t) \} \equiv \frac{d\hat{\sigma}_S(t)}{dt} \\ &= -\frac{1}{\hbar^2} \int_0^t d\tau \text{Tr}_B \{ [\hat{H}_I(t), [\hat{H}_I(\tau), \hat{\sigma}(\tau)]] \}, \end{aligned} \quad (\text{A.8})$$

where we have assumed

$$\text{Tr}_B \{ [\hat{H}_I(t), \hat{\sigma}(0)] \} = 0. \quad (\text{A.9})$$

Note that $\hat{\sigma}_S(t)$ is the interaction picture reduced density matrix of the system. In the limit of weak coupling with the baths, the Born approximation holds and the total state is a product state of the form [4]

$$\hat{\sigma}(t) = \hat{\sigma}_S(t) \otimes \hat{\sigma}_B, \quad (\text{A.10})$$

Este documento incorpora firma electrónica, y es copia auténtica de un documento electrónico archivado por la ULL según la Ley 39/2015.
 Su autenticidad puede ser contrastada en la siguiente dirección <https://sede.ull.es/validacion/>

Identificador del documento: 2111210 Código de verificación: lZvvKBaU

Firmado por: Javier Onam González López
 UNIVERSIDAD DE LA LAGUNA

Fecha: 09/09/2019 11:04:42

Daniel Alonso Ramírez
 UNIVERSIDAD DE LA LAGUNA

11/09/2019 14:53:47

where $\hat{\sigma}_B = \bigotimes_{\alpha} \hat{\sigma}_{B_{\alpha}} = \bigotimes_{\alpha} \exp(-\hat{H}_{B_{\alpha}}/k_B T_{\alpha}) [\text{Tr}\{\exp(-\hat{H}_{B_{\alpha}}/k_B T_{\alpha})\}]^{-1}$ is a product of Gibbs states with well defined temperatures. Considering Eqs. (A.5), (2.1), (2.5) and (A.10), the assumption (A.9) is valid. Inserting Eq. (A.10) in Eq. (A.8) we obtain

$$\frac{d\hat{\sigma}_S(t)}{dt} = -\frac{1}{\hbar^2} \int_0^t d\tau \text{Tr}_B\{[\hat{H}_I(t), [\hat{H}_I(\tau), \hat{\sigma}_S(\tau) \otimes \hat{\sigma}_B]]\}. \quad (\text{A.11})$$

In order to proceed further we perform a Markovian approximation. Thus, we can replace $\hat{\sigma}_S(\tau)$ by $\hat{\sigma}_S(t)$ in the integrand of Eq. (A.11). After some algebra we get

$$\frac{d\hat{\sigma}_S(t)}{dt} = -\frac{1}{\hbar^2} \int_0^t d\tau \text{Tr}_B\{[\hat{H}_I(t), [\hat{H}_I(t-\tau), \hat{\sigma}_S(t) \otimes \hat{\sigma}_B]]\}. \quad (\text{A.12})$$

Using (A.5), the integrand of the previous equation can be written as

$$\begin{aligned} & \text{Tr}_B\{[\hat{H}_I(t), [\hat{H}_I(t-\tau), \hat{\sigma}_S(t) \otimes \hat{\sigma}_B]]\} = \\ & \sum_{\alpha} [-\hat{A}^{\alpha}(t-\tau)\hat{\sigma}_S(t)\hat{A}^{\alpha}(t) + \hat{A}^{\alpha}(t)\hat{A}^{\alpha}(t-\tau)\hat{\sigma}_S(t)] \langle \hat{B}^{\alpha}(\tau)\hat{B}^{\alpha} \rangle + h.c., \end{aligned} \quad (\text{A.13})$$

with *h.c.* denoting the hermitian conjugate. We have defined the reservoir correlation functions $\langle \hat{B}_{\alpha}(\tau)\hat{B}_{\alpha} \rangle = \text{Tr}_{B_{\alpha}}\{\hat{\sigma}_{B_{\alpha}}\hat{B}_{\alpha}(\tau)\hat{B}_{\alpha}\}$. To obtain (A.13) we have used the fact that $\hat{\sigma}_{B_{\alpha}}$ is a stationary state of $\hat{H}_{B_{\alpha}}$. In the weak coupling limit, the integrand (A.13) decays fast enough to set the upper limit $t \rightarrow \infty$. Thus, Eq. (A.12) can be expressed as

$$\begin{aligned} \frac{d\hat{\sigma}_S(t)}{dt} = \frac{1}{\hbar^2} \sum_{\alpha} \int_0^{\infty} d\tau [\hat{A}^{\alpha}(t-\tau)\hat{\sigma}_S(t)\hat{A}^{\alpha}(t) \\ - \hat{A}^{\alpha}(t)\hat{A}^{\alpha}(t-\tau)\hat{\sigma}_S(t)] \langle \hat{B}^{\alpha}(\tau)\hat{B}^{\alpha} \rangle + h.c. \end{aligned} \quad (\text{A.14})$$

This equation can be greatly simplified if we decompose the interaction picture system operators $\hat{A}^{\alpha}(t)$ into their Fourier components $\hat{A}_{\omega}^{\alpha}$

$$\hat{A}^{\alpha}(t) = \hat{U}_S^{\dagger}(t)\hat{A}^{\alpha}\hat{U}_S(t) = \sum_{\omega} \hat{A}_{\omega}^{\alpha} e^{-i\omega t} = \sum_{\omega} \hat{A}_{\omega}^{\alpha\dagger} e^{i\omega t}. \quad (\text{A.15})$$

Inserting the Fourier decomposition in (A.14), we find

$$\frac{d\hat{\sigma}_S(t)}{dt} = \sum_{\alpha} \sum_{\omega, \omega'} e^{i(\omega' - \omega)t} C_{\omega}^{\alpha} [\hat{A}_{\omega}^{\alpha}\hat{\sigma}_S(t)\hat{A}_{\omega'}^{\alpha\dagger} - \hat{A}_{\omega'}^{\alpha\dagger}\hat{A}_{\omega}^{\alpha}\hat{\sigma}_S(t)] + h.c., \quad (\text{A.16})$$

Este documento incorpora firma electrónica, y es copia auténtica de un documento electrónico archivado por la ULL según la Ley 39/2015.
Su autenticidad puede ser contrastada en la siguiente dirección <https://sede.ull.es/validacion/>

Identificador del documento: 2111210 Código de verificación: lZvvKBaU

Firmado por: Javier Onam González López
UNIVERSIDAD DE LA LAGUNA

Fecha: 09/09/2019 11:04:42

Daniel Alonso Ramírez
UNIVERSIDAD DE LA LAGUNA

11/09/2019 14:53:47

with $C_\omega^\alpha = \int_0^\infty d\tau e^{i\omega\tau} \langle \hat{B}^\alpha(\tau) \hat{B}^\alpha \rangle \equiv \frac{1}{2} \Gamma_\omega^\alpha + i\delta_\omega^\alpha$. The imaginary part δ_ω^α is associated with small Lamb shifts in the energy levels. We will neglect them in the following. For our choice of bosonic baths with coupling operators (2.5), the functions Γ_ω^α are given by Eq. (2.11). The expression (A.16) is called the interaction picture Markovian Redfield master equation.

Finally, we can remove the time dependence in Eq. (A.16) by choosing an adequate rotating frame. The density matrix in such a frame is $\hat{\rho}_S = e^{-i\hat{A}_2 t/\hbar} \hat{\sigma}_S e^{i\hat{A}_2 t/\hbar}$. The corresponding Redfield master equation reads

$$\frac{d\hat{\rho}_S(t)}{dt} = -\frac{i}{\hbar} [\hat{A}_2, \hat{\rho}_S(t)] + \sum_\alpha \mathcal{R}_\alpha \{\hat{\rho}_S(t)\}, \quad (\text{A.17})$$

where the super-operators $\mathcal{R}_\alpha \{\hat{\rho}_S(t)\}$ are

$$\mathcal{R}_\alpha \{\hat{\rho}_S(t)\} = \sum_{\omega, \omega'} C_\omega^\alpha [\hat{A}_\omega^\alpha \hat{\rho}_S(t) \hat{A}_{\omega'}^{\alpha\dagger} - \hat{A}_{\omega'}^{\alpha\dagger} \hat{A}_\omega^\alpha \hat{\rho}_S(t)] + h.c.. \quad (\text{A.18})$$

A.1.1 Energy currents

Both heat currents and power can be defined by using the master equation (A.17). Namely, the time evolution of the mean energy of the system reads

$$\frac{d}{dt} \text{Tr} \{ \hat{H}_S(t) \hat{\sigma}_S(t) \} = \frac{d}{dt} \text{Tr} \{ (\hat{A}_1 + \hat{A}_2) \hat{\rho}_S(t) \} = P(t) + \sum_\alpha \dot{Q}_\alpha(t), \quad (\text{A.19})$$

with

$$P(t) = -\frac{i}{\hbar} \text{Tr} \{ \hat{A}_1 [\hat{A}_2, \hat{\rho}_S(t)] \} \quad (\text{A.20})$$

the power performed by the field and

$$\dot{Q}_\alpha(t) = \text{Tr} \{ (\hat{A}_1 + \hat{A}_2) \mathcal{R}_\alpha \{\hat{\rho}_S(t)\} \} \quad (\text{A.21})$$

the heat current from B_α into S . In the steady state $P + \sum_\alpha \dot{Q}_\alpha = 0$, where $P(t \rightarrow \infty) \equiv P$ and $\dot{Q}_\alpha(t \rightarrow \infty) \equiv \dot{Q}_\alpha$ are the stationary power and heat currents.

A note of precaution should be stated at this point. Complete positivity and thermodynamic consistency are not ensured within the Redfield approach. However, when performing extra assumptions, it leads to consistent approaches as discussed below. It is worth to point out that complete positivity depends only on the specific structure of the master equation, while thermodynamic consistency is also dependent on the definition chosen for the energy currents.

Este documento incorpora firma electrónica, y es copia auténtica de un documento electrónico archivado por la ULL según la Ley 39/2015.
 Su autenticidad puede ser contrastada en la siguiente dirección <https://sede.ull.es/validacion/>

Identificador del documento: 2111210 Código de verificación: lZvvKBaU

Firmado por: Javier Onam González López
 UNIVERSIDAD DE LA LAGUNA

Fecha: 09/09/2019 11:04:42

Daniel Alonso Ramírez
 UNIVERSIDAD DE LA LAGUNA

11/09/2019 14:53:47

A.2 Global master equation

A rotating wave approximation brings Eq. (A.17) into secular form. Specifically, we consider that the intrinsic time of the system $\tau_S \sim |\omega - \omega'|^{-1}$ ($\omega \neq \omega'$) is much smaller than the scale of its interaction with the baths $\tau_{SB} \sim \gamma_\alpha^{-1}$, i. e. $\gamma_\alpha \ll |\omega - \omega'|$. Thus, neglecting the terms such that $\omega \neq \omega'$ in (A.18) leads to

$$\frac{d\hat{\rho}_S(t)}{dt} = -\frac{i}{\hbar}[\hat{A}_2, \hat{\rho}_S] + \sum_{\alpha} \mathcal{L}_{\alpha}\{\hat{\rho}_S(t)\}, \quad (\text{A.22})$$

where the Lindblad super-operators characterizing the influence of B_{α} on S are

$$\mathcal{L}_{\alpha}\{\hat{\rho}_S(t)\} = \sum_{\omega} \Gamma_{\omega}^{\alpha} \left(\hat{A}_{\omega}^{\alpha} \hat{\rho}_S(t) \hat{A}_{\omega}^{\alpha\dagger} - \frac{1}{2} \hat{A}_{\omega}^{\alpha\dagger} \hat{A}_{\omega}^{\alpha} \hat{\rho}_S(t) - \frac{1}{2} \hat{\rho}_S(t) \hat{A}_{\omega}^{\alpha\dagger} \hat{A}_{\omega}^{\alpha} \right). \quad (\text{A.23})$$

The expression (A.22) is known as the Global or Secular master equation. Within this secular approach, the power and heat currents are obtained from (A.20) and (A.21) replacing $\mathcal{R}_{\alpha}\{\hat{\rho}_S(t)\}$ by $\mathcal{L}_{\alpha}\{\hat{\rho}_S(t)\}$. The structure of the Lindblad super-operators guarantees thermodynamic consistency when considering these definitions for the currents [67, 66, 9, 12].

A.3 Local master equation

In the case of periodically driven devices, the time scale of the laser plays a central role $\tau_S^w \sim \lambda^{-1}$. When $\tau_S^w \ll \tau_{SB}$ a global equation provides a good description of the functioning of the device. However, when $\tau_S^w \gg \tau_{SB}$ or equivalently $\lambda \ll \gamma_{\alpha}$, it is necessary to employ a Redfield approach since the rotating wave approximation is not well justified. Interestingly, we have another option to study the machine behavior within this weak driving regime. Such approach is based on a Local master equation of the form

$$\frac{d\hat{\rho}_S(t)}{dt} = -\frac{i}{\hbar}[\hat{A}_2, \hat{\rho}_S] + \sum_{\alpha} \mathcal{L}_{\alpha}^0\{\hat{\rho}_S(t)\}. \quad (\text{A.24})$$

The Lindblad super-operators $\mathcal{L}_{\alpha}^0\{\hat{\rho}_S(t)\}$ are obtained by considering an expansion of $\mathcal{L}_{\alpha}\{\hat{\rho}_S(t)\}$ in the variable λ and keeping the leading terms. When such leading terms are all of order λ^0 , the local super-operator \mathcal{L}_{α}^0 are given by (A.23) but considering the following Fourier components

$$e^{i\hat{H}_S^0 t/\hbar} \hat{A}^{\alpha} e^{-i\hat{H}_S^0 t/\hbar} = \sum_{\omega} \hat{A}_{\omega}^{\alpha} e^{-i\omega t} = \sum_{\omega} \hat{A}_{\omega}^{\alpha\dagger} e^{i\omega t}. \quad (\text{A.25})$$

Este documento incorpora firma electrónica, y es copia auténtica de un documento electrónico archivado por la ULL según la Ley 39/2015.
 Su autenticidad puede ser contrastada en la siguiente dirección <https://sede.ull.es/validacion/>

Identificador del documento: 2111210 Código de verificación: lZvvKBaU

Firmado por: Javier Onam González López
 UNIVERSIDAD DE LA LAGUNA

Fecha: 09/09/2019 11:04:42

Daniel Alonso Ramírez
 UNIVERSIDAD DE LA LAGUNA

11/09/2019 14:53:47

The power and currents within this approach are [58, 82]

$$P(t) = -\frac{i}{\hbar} \text{Tr}\{\hat{H}_S^0 [\hat{A}_2, \hat{\rho}_S]\} \quad (\text{A.26})$$

and

$$\dot{Q}_\alpha(t) = \text{Tr}\{\hat{H}_S^0 \mathcal{L}_\alpha^0\{\hat{\rho}_S(t)\}\}. \quad (\text{A.27})$$

It is important to stress that this definition of the currents provides a thermodynamically consistent description when considering periodically driven devices. However, the local approach may lead to violations of the Second Law of Thermodynamics when dealing with absorption machines [83].

Este documento incorpora firma electrónica, y es copia auténtica de un documento electrónico archivado por la ULL según la Ley 39/2015.
Su autenticidad puede ser contrastada en la siguiente dirección <https://sede.ull.es/validacion/>

Identificador del documento: 2111210 Código de verificación: lZvvKBaU

Firmado por: Javier Onam González López
UNIVERSIDAD DE LA LAGUNA

Fecha: 09/09/2019 11:04:42

Daniel Alonso Ramírez
UNIVERSIDAD DE LA LAGUNA

11/09/2019 14:53:47

Bibliography

- [1] Felix Binder, Luis A. Correa, Christian Gogolin, Janet Anders, and Gerardo Adesso, editors. *Thermodynamics in the quantum regime*. Fundamental Theories of Physics. Springer, 2018.
- [2] Sai Vinjanampathy and Janet Anders. Quantum thermodynamics. *Contemp. Phys.*, 57(4):545–579, 2016.
- [3] John Goold, Marcus Huber, Arnau Riera, Lídia del Rio, and Paul Skrzypczyk. The role of quantum information in thermodynamics—a topical review. *Journal of Physics A: Mathematical and Theoretical*, 49(14):143001, feb 2016.
- [4] H.P. Breuer and F. Petruccione. *The Theory of Open Quantum Systems*. Oxford University Press, USA, 2002.
- [5] Inés de Vega and Daniel Alonso. Dynamics of non-markovian open quantum systems. *Rev. Mod. Phys.*, 89:015001, Jan 2017.
- [6] Ronnie Kosloff. Quantum thermodynamics and open-systems modeling. *The Journal of Chemical Physics*, 150(20):204105, May 2019.
- [7] Ronnie Kosloff. Quantum thermodynamics: A dynamical viewpoint. *Entropy*, 15(6):2100–2128, 2013.
- [8] Amikam Levy, Robert Alicki, and Ronnie Kosloff. Quantum refrigerators and the third law of thermodynamics. *Physical Review E*, 85(6), June 2012.
- [9] Herbert Spohn. Entropy production for quantum dynamical semigroups. *Journal of Mathematical Physics*, 19(5):1227–1230, May 1978.
- [10] Nahuel Freitas and Juan Pablo Paz. Fundamental limits for cooling of linear quantum refrigerators. *Physical Review E*, 95(1), January 2017.

Este documento incorpora firma electrónica, y es copia auténtica de un documento electrónico archivado por la ULL según la Ley 39/2015.
Su autenticidad puede ser contrastada en la siguiente dirección <https://sede.ull.es/validacion/>

Identificador del documento: 2111210 Código de verificación: lZvvKBaU

Firmado por: Javier Onam González López
UNIVERSIDAD DE LA LAGUNA

Fecha: 09/09/2019 11:04:42

Daniel Alonso Ramírez
UNIVERSIDAD DE LA LAGUNA

11/09/2019 14:53:47

- [11] H. E. D. Scovil and E. O. Schulz-DuBois. Three-level masers as heat engines. *Physical Review Letters*, 2(6):262–263, March 1959.
- [12] R Alicki. The quantum open system as a model of the heat engine. *Journal of Physics A: Mathematical and General*, 12(5):L103–L107, may 1979.
- [13] Ronnie Kosloff. A quantum mechanical open system as a model of a heat engine. *The Journal of Chemical Physics*, 80(4):1625–1631, February 1984.
- [14] Ronnie Kosloff and Amikam Levy. Quantum Heat Engines and Refrigerators: Continuous Devices. *Annual Rev. Phys. Chem.*, 65:365, 2014.
- [15] Eitan Geva and Ronnie Kosloff. A quantum-mechanical heat engine operating in finite time. a model consisting of spin-1/2 systems as the working fluid. *The Journal of Chemical Physics*, 96(4):3054–3067, February 1992.
- [16] Eitan Geva and Ronnie Kosloff. On the classical limit of quantum thermodynamics in finite time. *The Journal of Chemical Physics*, 97(6):4398–4412, September 1992.
- [17] Tova Feldmann, Eitan Geva, Ronnie Kosloff, and Peter Salamon. Heat engines in finite time governed by master equations. *American Journal of Physics*, 64(4):485–492, April 1996.
- [18] Tova Feldmann and Ronnie Kosloff. Performance of discrete heat engines and heat pumps in finite time. *Physical Review E*, 61(5):4774–4790, May 2000.
- [19] Ronnie Kosloff and Tova Feldmann. Discrete four-stroke quantum heat engine exploring the origin of friction. *Physical Review E*, 65(5), May 2002.
- [20] Ronnie Kosloff and Yair Rezek. The quantum harmonic Otto cycle. *Entropy*, 19(4):136, March 2017.
- [21] J. Rosnagel, S. T. Dawkins, K. N. Tolazzi, O. Abah, E. Lutz, F. Schmidt-Kaler, and K. Singer. A single-atom heat engine. *Science*, 352(6283):325–329, April 2016.
- [22] H. T. Quan, Yu xi Liu, C. P. Sun, and Franco Nori. Quantum thermodynamic cycles and quantum heat engines. *Physical Review E*, 76(3), September 2007.

Este documento incorpora firma electrónica, y es copia auténtica de un documento electrónico archivado por la ULL según la Ley 39/2015.
Su autenticidad puede ser contrastada en la siguiente dirección <https://sede.ull.es/validacion/>

Identificador del documento: 2111210 Código de verificación: lZvvKBaU

Firmado por: Javier Onam González López
UNIVERSIDAD DE LA LAGUNA

Fecha: 09/09/2019 11:04:42

Daniel Alonso Ramírez
UNIVERSIDAD DE LA LAGUNA

11/09/2019 14:53:47

- [23] Armen E. Allahverdyan, Ramandeep S. Johal, and Guenter Mahler. Work extremum principle: Structure and function of quantum heat engines. *Physical Review E*, 77(4), April 2008.
- [24] Ralph Silva, Gonzalo Manzano, Paul Skrzypczyk, and Nicolas Brunner. Performance of autonomous quantum thermal machines: Hilbert space dimension as a thermodynamical resource. *Phys. Rev. E*, 94:032120, Sep 2016.
- [25] Yi-Xin Chen and Sheng-Wen Li. Quantum refrigerator driven by current noise. *EPL (Europhysics Letters)*, 97(4):40003, February 2012.
- [26] Davide Venturelli, Rosario Fazio, and Vittorio Giovannetti. Minimal self-contained quantum refrigeration machine based on four quantum dots. *Physical Review Letters*, 110(25), June 2013.
- [27] Mark T Mitchison, Marcus Huber, Javier Prior, Mischa P Woods, and Martin B Plenio. Realising a quantum absorption refrigerator with an atom-cavity system. *Quantum Science and Technology*, 1(1):015001, mar 2016.
- [28] Patrick P. Hofer, Martí Perarnau-Llobet, Jonatan Bohr Brask, Ralph Silva, Marcus Huber, and Nicolas Brunner. Autonomous quantum refrigerator in a circuit qed architecture based on a josephson junction. *Phys. Rev. B*, 94:235420, Dec 2016.
- [29] Gleb Maslennikov, Shiqian Ding, Roland Häublützel, Jaren Gan, Alexandre Roulet, Stefan Nimmrichter, Jibo Dai, Valerio Scarani, and Dzmitry Matsukevich. Quantum absorption refrigerator with trapped ions. *Nature Communications*, 10(1), January 2019.
- [30] José P. Palao, Ronnie Kosloff, and Jeffrey M. Gordon. Quantum thermodynamic cooling cycle. *Phys. Rev. E*, 64:056130, Oct 2001.
- [31] Noah Linden, Sandu Popescu, and Paul Skrzypczyk. How small can thermal machines be? the smallest possible refrigerator. *Phys. Rev. Lett.*, 105:130401, Sep 2010.
- [32] Amikam Levy and Ronnie Kosloff. Quantum absorption refrigerator. *Physical Review Letters*, 108(7), February 2012.
- [33] Eitan Geva and Ronnie Kosloff. The quantum heat engine and heat pump: An irreversible thermodynamic analysis of the three-level amplifier. *The Journal of Chemical Physics*, 104(19):7681–7699, May 1996.

Este documento incorpora firma electrónica, y es copia auténtica de un documento electrónico archivado por la ULL según la Ley 39/2015.
Su autenticidad puede ser contrastada en la siguiente dirección <https://sede.ull.es/validacion/>

Identificador del documento: 2111210 Código de verificación: lZvvKBaU

Firmado por: Javier Onam González López
UNIVERSIDAD DE LA LAGUNA

Fecha: 09/09/2019 11:04:42

Daniel Alonso Ramírez
UNIVERSIDAD DE LA LAGUNA

11/09/2019 14:53:47

- [34] Ronnie Kosloff, Eitan Geva, and Jeffrey M. Gordon. Quantum refrigerators in quest of the absolute zero. *Journal of Applied Physics*, 87(11):8093–8097, June 2000.
- [35] Jürgen Schnakenberg. Network theory of microscopic and macroscopic behavior of master equation systems. *Rev. Mod. Phys.*, 48(4):571, 1976.
- [36] Terrell L Hill. Studies in irreversible thermodynamics iv. diagrammatic representation of steady state fluxes for unimolecular systems. *J. Theoret. Biol.*, 10(3):442, 1966.
- [37] Sophia L. Kalpazidou. *Cycle Representations of Markov Processes*, volume 28. 01 1995.
- [38] David Andrieux and Pierre Gaspard. Fluctuation theorem for currents and schnakenberg network theory. *Journal of Statistical Physics*, 127(1):107–131, Apr 2007.
- [39] B. Altaner, S. Grosskinsky, S. Herminghaus, L. Katthän, M. Timme, and J. Vollmer. Network representations of nonequilibrium steady states: Cycle decompositions, symmetries, and dominant paths. *Physical Review E*, 85(4), April 2012.
- [40] J Onam González, Daniel Alonso, and José P Palao. Performance of continuous quantum thermal devices indirectly connected to environments. *Entropy*, 18(5):166, 2016.
- [41] Luis A. Correa, José P. Palao, Gerardo Adesso, and Daniel Alonso. Optimal performance of endoreversible quantum refrigerators. *Physical Review E*, 90(6), December 2014.
- [42] J Onam González, José P Palao, and Daniel Alonso. Relation between topology and heat currents in multilevel absorption machines. *New J. Phys.*, 19(11):113037, 2017.
- [43] José P. Palao, Luis A. Correa, Gerardo Adesso, and Daniel Alonso. Efficiency of inefficient endoreversible thermal machines. *Brazilian Journal of Physics*, 46(3):282–287, January 2016.
- [44] X. L. Huang, Tao Wang, and X. X. Yi. Effects of reservoir squeezing on quantum systems and work extraction. *Phys. Rev. E*, 86:051105, Nov 2012.

Este documento incorpora firma electrónica, y es copia auténtica de un documento electrónico archivado por la ULL según la Ley 39/2015.
Su autenticidad puede ser contrastada en la siguiente dirección <https://sede.ull.es/validacion/>

Identificador del documento: 2111210 Código de verificación: lZvvKBaU

Firmado por: Javier Onam González López
UNIVERSIDAD DE LA LAGUNA

Fecha: 09/09/2019 11:04:42

Daniel Alonso Ramírez
UNIVERSIDAD DE LA LAGUNA

11/09/2019 14:53:47

- [45] Obinna Abah and Eric Lutz. Efficiency of heat engines coupled to nonequilibrium reservoirs. *EPL (Europhysics Letters)*, 106(2):20001, April 2014.
- [46] Bruno Leggio, Bruno Bellomo, and Mauro Antezza. Quantum thermal machines with single nonequilibrium environments. *Phys. Rev. A*, 91:012117, Jan 2015.
- [47] Luis A. Correa, José P. Palao, Daniel Alonso, and Gerardo Adesso. Quantum-enhanced absorption refrigerators. *Scientific Reports*, 4(1), February 2014.
- [48] Jan Klaers, Stefan Faelt, Atac Imamoglu, and Emre Togan. Squeezed thermal reservoirs as a resource for a nanomechanical engine beyond the carnot limit. *Physical Review X*, 7(3), September 2017.
- [49] Bijay Kumar Agarwalla, Jian-Hua Jiang, and Dvira Segal. Quantum efficiency bound for continuous heat engines coupled to noncanonical reservoirs. *Physical Review B*, 96(10), September 2017.
- [50] Luis A. Correa. Multistage quantum absorption heat pumps. *Phys. Rev. E*, 89:042128, Apr 2014.
- [51] Wolfgang Niedenzu, David Gelbwaser-Klimovsky, and Gershon Kurizki. Performance limits of multilevel and multipartite quantum heat machines. *Phys. Rev. E*, 92:042123, Oct 2015.
- [52] P. Gaspard and M. Nagaoka. Slippage of initial conditions for the redfield master equation. *The Journal of Chemical Physics*, 111(13):5668–5675, October 1999.
- [53] J Onam González, Luis A Correa, Giorgio Nocerino, José P Palao, Daniel Alonso, and Gerardo Adesso. Testing the validity of the local and global master equations on an exactly solvable model. *Open Syst. Inf. Dyn.*, 24(04):1740010, 2017.
- [54] Patrick P Hofer, Martí Perarnau-Llobet, L David M Miranda, Géraldine Haack, Ralph Silva, Jonatan Bohr Brask, and Nicolas Brunner. Markovian master equations for quantum thermal machines: local versus global approach. *New Journal of Physics*, 19(12):123037, dec 2017.
- [55] M. O. Scully. Extracting work from a single heat bath via vanishing quantum coherence. *Science*, 299(5608):862–864, January 2003.

Este documento incorpora firma electrónica, y es copia auténtica de un documento electrónico archivado por la ULL según la Ley 39/2015.
Su autenticidad puede ser contrastada en la siguiente dirección <https://sede.ull.es/validacion/>

Identificador del documento: 2111210 Código de verificación: lZvvKBaU

Firmado por: Javier Onam González López
UNIVERSIDAD DE LA LAGUNA

Fecha: 09/09/2019 11:04:42

Daniel Alonso Ramírez
UNIVERSIDAD DE LA LAGUNA

11/09/2019 14:53:47

- [56] Anatoly A. Svidzinsky, Konstantin E. Dorfman, and Marlan O. Scully. Enhancing photovoltaic power by fano-induced coherence. *Phys. Rev. A*, 84:053818, Nov 2011.
- [57] Nicolas Brunner, Marcus Huber, Noah Linden, Sandu Popescu, Ralph Silva, and Paul Skrzypczyk. Entanglement enhances cooling in microscopic quantum refrigerators. *Physical Review E*, 89(3), March 2014.
- [58] Raam Uzdin, Amikam Levy, and Ronnie Kosloff. Equivalence of quantum heat machines, and quantum-thermodynamic signatures. *Phys. Rev. X*, 5:031044, Sep 2015.
- [59] David Gelbwaser-Klimovsky, Wolfgang Niedenzu, Paul Brumer, and Gershon Kurizki. Power enhancement of heat engines via correlated thermalization in a three-level “working fluid”. *Scientific Reports*, 5(1), September 2015.
- [60] Pietro Liuzzo-Scorpo, Luis Correa, Rebecca Schmidt, and Gerardo Adesso. Thermodynamics of quantum feedback cooling. *Entropy*, 18(2):48, February 2016.
- [61] Alexander Friedenberger and Eric Lutz. When is a quantum heat engine quantum? *EPL (Europhysics Letters)*, 120(1):10002, October 2017.
- [62] Konstantin E. Dorfman, Dazhi Xu, and Jianshu Cao. Efficiency at maximum power of a laser quantum heat engine enhanced by noise-induced coherence. *Physical Review E*, 97(4), April 2018.
- [63] James Klatzow, Jonas N. Becker, Patrick M. Ledingham, Christian Weinzetl, Krzysztof T. Kaczmarek, Dylan J. Saunders, Joshua Nunn, Ian A. Walmsley, Raam Uzdin, and Eilon Poem. Experimental demonstration of quantum effects in the operation of microscopic heat engines. *Physical Review Letters*, 122(11), March 2019.
- [64] Udo Seifert. Stochastic thermodynamics, fluctuation theorems and molecular machines. *Reports on Progress in Physics*, 75(12):126001, nov 2012.
- [65] Massimiliano Esposito. Stochastic thermodynamics under coarse graining. *Phys. Rev. E*, 85:041125, Apr 2012.
- [66] G. Lindblad. On the generators of quantum dynamical semigroups. *Comm. Math. Phys.*, 48(2):119–130, 1976.

Este documento incorpora firma electrónica, y es copia auténtica de un documento electrónico archivado por la ULL según la Ley 39/2015.
Su autenticidad puede ser contrastada en la siguiente dirección <https://sede.ull.es/validacion/>

Identificador del documento: 2111210 Código de verificación: lZvvKBaU

Firmado por: Javier Onam González López
UNIVERSIDAD DE LA LAGUNA

Fecha: 09/09/2019 11:04:42

Daniel Alonso Ramírez
UNIVERSIDAD DE LA LAGUNA

11/09/2019 14:53:47

- [67] Vittorio Gorini. Completely positive dynamical semigroups of n-level systems. *Journal of Mathematical Physics*, 17(5):821, 1976.
- [68] M. Esposito, K. Lindenberg, and C. Van den Broeck. Thermoelectric efficiency at maximum power in a quantum dot. *EPL (Europhysics Letters)*, 85(6):60010, March 2009.
- [69] B. Cleuren, B. Rutten, and C. Van den Broeck. Cooling by heating: Refrigeration powered by photons. *Physical Review Letters*, 108(12), March 2012.
- [70] Cong Li, Yanchao Zhang, Jianhui Wang, and Jizhou He. Performance characteristics and optimal analysis of a nanosized quantum dot photoelectric refrigerator. *Physical Review E*, 88(6), December 2013.
- [71] Mario Einax and Abraham Nitzan. Network analysis of photovoltaic energy conversion. *The Journal of Physical Chemistry C*, 118(47):27226–27234, November 2014.
- [72] C. Van den Broeck and M. Esposito. Ensemble and trajectory thermodynamics: A brief introduction. *Physica A: Statistical Mechanics and its Applications*, 418:6–16, January 2015.
- [73] Donald B. Johnson. Finding all the elementary circuits of a directed graph. *SIAM Journal on Computing*, 4(1):77–84, March 1975.
- [74] Luis A. Correa, José P. Palao, and Daniel Alonso. Internal dissipation and heat leaks in quantum thermodynamic cycles. *Physical Review E*, 92(3), September 2015.
- [75] J. E. Geusic, E. O. Schulz-Du Bois, R. W. De Grasse, and H. E. D. Scovil. Three level spin refrigeration and maser action at 1500 mc/sec. *Journal of Applied Physics*, 30(7):1113–1114, July 1959.
- [76] Krzysztof Szczygielski. On the application of floquet theorem in development of time-dependent lindbladians. *Journal of Mathematical Physics*, 55(8):083506, August 2014.
- [77] Krzysztof Szczygielski, David Gelbwaser-Klimovsky, and Robert Alicki. Markovian master equation and thermodynamics of a two-level system in a strong laser field. *Phys. Rev. E*, 87:012120, Jan 2013.

Este documento incorpora firma electrónica, y es copia auténtica de un documento electrónico archivado por la ULL según la Ley 39/2015.
Su autenticidad puede ser contrastada en la siguiente dirección <https://sede.ull.es/validacion/>

Identificador del documento: 2111210 Código de verificación: lZvvKBaU

Firmado por: Javier Onam González López
UNIVERSIDAD DE LA LAGUNA

Fecha: 09/09/2019 11:04:42

Daniel Alonso Ramírez
UNIVERSIDAD DE LA LAGUNA

11/09/2019 14:53:47

- [78] Archak Purkayastha, Abhishek Dhar, and Manas Kulkarni. Out-of-equilibrium open quantum systems: A comparison of approximate quantum master equation approaches with exact results. *Phys. Rev. A*, 93:062114, Jun 2016.
- [79] Michael Kilgour and Dvira Segal. Coherence and decoherence in quantum absorption refrigerators. *Phys. Rev. E*, 98:012117, Jul 2018.
- [80] A. G. Redfield. On the theory of relaxation processes. *IBM Journal of Research and Development*, 1(1):19–31, January 1957.
- [81] A. S. Trushechkin and I. V. Volovich. Perturbative treatment of inter-site couplings in the local description of open quantum networks. *EPL (Europhysics Letters)*, 113(3):30005, feb 2016.
- [82] J. Onam González, José P. Palao, Daniel Alonso, and Luis A. Correa. Classical emulation of quantum-coherent thermal machines. *Phys. Rev. E*, 99:062102, Jun 2019.
- [83] Amikam Levy and Ronnie Kosloff. The local approach to quantum transport may violate the second law of thermodynamics. *EPL (Europhysics Letters)*, 107(2):20004, jul 2014.

Este documento incorpora firma electrónica, y es copia auténtica de un documento electrónico archivado por la ULL según la Ley 39/2015.
Su autenticidad puede ser contrastada en la siguiente dirección <https://sede.ull.es/validacion/>

Identificador del documento: 2111210 Código de verificación: lZvvKBaU

Firmado por: Javier Onam González López
UNIVERSIDAD DE LA LAGUNA

Fecha: 09/09/2019 11:04:42

Daniel Alonso Ramírez
UNIVERSIDAD DE LA LAGUNA

11/09/2019 14:53:47